STEADY – STATE STABILITY OF A TRANSMISSION SYSTEM WITH CONTROLLED SYNCHRONOUS CONDENSERS AT THE SECTIONALIZING SUBSTATION*

N.I. SOKOLOV

(Received 11 June 1956)

One of the first (chronologically) methods suggested for improving the transmitting capacity of long transmission lines was their sub-division into sections and the erection of synchronous condensers in the intermediate sub-stations. The original publication of this method, subsequently known as Baun's circuit took place in 1921 [1]. The basic assumption was that the stability of each section of the line could be considered as independent of that of the other sections.

Further experimental and theoretical work on the subject revealed that the increase of the transmitting capacity has to be bought by particularly high rating of the synchronous condensers [2]. It was mainly due to the fact that on transmission lines with synchronous condensers were not actually erected.

In 1937 S.A. Lebedev [3] showed that in the presence of an automatic regulation of the excitation it is basically possible to reduce the rating of the intermediate synchronous condensers to economically justifiable values. Analogous calculations were also carried out for the case of synchronous condensers fitted with compounding-gear [7].

The necessary kVA for intermediate synchronous condensers are determined by the requirement of keeping the voltage at the ends of each section constant when the limiting power is transmitted over the line. The latter will be greater, the greater the active power transmitted through the line in comparison with the natural power of the line. When the natural power is transmitted, the synchronous condensers work on no-load.

However, the usual excitation regulators (electronic regulator of the All-Union Electrotechnical Institute, compounding-gear with corrector, etc), cannot assure constancy of the voltage at a given point when angle swings occur, since in this case large amplification factors and high-speed action are required. The best to be obtained from ordinary excitation regulators is the constancy of the e.m.f.

* *Elektrichestvo*, No. 5, 25 – 30, 1957 [Reprint Order No. EL 18].

behind the transient reactance of the generator. The limiting transmitting capacity is in this case considerably smaller.

S.A. Lebedev's investigations demonstrated the possibility of a transmission through a sectionalized line of large powers with intermediate synchronous condensers of relatively small rating if sensitive automatic high-speed excitation regulators are used, and if their regulation is controlled by derivatives of the controlled quantity. The introduction of the first derivative of the voltage enabled the limit of the constancy of the e.m.f. behind the transient reactance to be surpassed and constancy of the voltage at the generator terminals approached.

The investigations of the stability of the synchronous condensers referred to dealt only with an idealized regulation without considering the transient processes in the generators and the time lags in the excitors and regulators. Yet they were still the first to reveal the real possibility of a very considerable increase of the transmitting capacity of transmission systems.

Up to the present time there were not regulators perfect enough to permit a regulation according to the deviation of the controlled quantity and its derivatives. The regulators used by S.A. Lebedev in 1937 in his laboratory experiments were imperfect and that was why his experiments did not yield realistic results.

In recent years comprehensive investigations into the stability of synchronous generators working on long transmission lines were carried out and regulators designed of equality assuring during the transient process not only constancy, but even an increase of the flux-linkages of the rotor without provoking hunting phenomena. These regulators may maintain the voltage at given system points constant, thereby considerably improving the steady-state stability of the transmission systems. They are now known as strong-action regulators and usually respond not only to a deviation, but also on the first and second derivatives of the deviation. The strong-action regulators were investigated theoretically and on electric models [4] and [5], and were tested under operating conditions.

Investigations and tests of strong-action regulators on the generators showed that they are likewise useful for synchronous condensers erected in the sectionalizing sub-stations. However this calls for an additional theoretical clarification of the effect of the transient processes in the generator on the regulation of the synchronous condenser, the combined regulation of generators and synchronous condensers, and furthermore, an investigation of the stability of the regulation with unchanged coefficients of the regulation and changes of the loading of the line within a wide range; also, the possibility of increasing the transmitted power with a minimum rating of the synchronous condensers and of their concentration in one sectionalizing substation should be examined.

All these problems were theoretically investigated in the Central Electrotechnical Research Laboratory of the Ministry of Power Stations.

The investigations of the effect of intermediate synchronous condensers on system stability were based on the method of small oscillations; simplified equations of the synchronous machines (without transformer e.m.f's) were used and the resistances in the stator circuits were neglected. Since the relation between the electro-magnetic torques of the machines and the angles between the e.m.f.'s is non-linear, the equations were linearized in the range of small deviations.

Let subscript 1 denote quantities referring to the sending-end station, subscript 2 those referring to the receiving system, 3 those referring to the sectionalizing substation. Let us, furthermore, consider the power of the receiving system as infinite. The equations of motion may then be written for every station (not considering mechanical friction and the effect of damping) as follows:

$$\Delta P + T_{j_1} p^2 \delta_{12} = 0;\ \Delta P_3 + T_{j_3} p^2 \Delta \delta_{32} = 0;$$
$$p^2 \delta_1 = p^2 \delta_{12};\ p^2 \delta_3 = p^2 \delta_{32} \tag{1}$$

The deviations of the powers are a function of the relative angles and e.m.f.'s of the generators (cf. appendix) and may be expressed linearly by the partial derivatives with respect to the corresponding variables. Using also the expressions of the deviations of the torques by the deviations of the synchronous and transient e.m.f.'s and introducing the well-known relationship between them, viz

$$\Delta E_{dc_1} = \Delta E_{d_1} + T_{d_1}\, pE'_{d_1}$$
$$\Delta E_{dc_3} = \Delta E_{d_3} + T_{d_3}\, pE'_{d_3} \tag{2}$$

We get the characteristic equation of the system of the three stations, not considering the regulation, viz

$$Q_1 Q_4 - Q_2 Q_3 = 0 \tag{3}$$

where Q_1, Q_2, Q_3, Q_4 are third order polynomials depending on the parameters of the transmission system as well as on the power transmitted or the angle

To consider the regulation of the excitation of the generators of the sending-end station and the synchronous condensors we introduce into the equations the transmission functions of the regulators: the characteristic equation of the system then takes the following form:

$$\left[Q_1 + \frac{M(p)_1}{Z(p)_1}\right]\left[Q_4 + \frac{M(p)_3}{Z(p)_3}\right] - Q_2 Q_3 = 0 \tag{4}$$

It is clear that in such a relatively complicated system (of three stations) the coefficients of the characteristic equation will have a very involved structure and their investigation in a general form will therefore be laborious. The problem can, however, be greatly simplified by substituting numerical values into the initial expressions. The result is still of a sufficiently general character to enable the analysis of a number of cases important for the practice to be carried out.

In considering actual transmission systems it is convenient to plot the ranges of stability vs. two variable coefficients of regulation, for example, the coefficients

for the first and second derivatives. The other coefficients remain fixed. The method of graphing these ranges from the characteristic equation is not described here because it is sufficiently well-known [8].

For the generator as well as for the synchronous condenser the analysis was carried out for regulation according to the angle between the e.m.f. of the generator and the voltage of the receiving system; the coefficients of the regulation according to deviation were chosen on the condition of the constancy of the voltage at the h.v. busbars of the sending-end station and sectionalizing substation. The regulation based on the angle was adopted only for convenience of the analysis. We may state that with a correct choice of the coefficients, regulation based on current, voltage or on both combined, leads to the same limit of the power transmitted as a regulation based on the angle. The theoretical analysis showed that by a close regulation on generators and synchronous condensers the limit of the power transmitted may be considerably increased, i.e. up to the ;ower limit of the weakest section. For example, the limit of the power transmitted through the line Kuibyshev Hydro-Electric Power Station – Moscow, may be increased to 1800 MW when the condensers are placed in the central sub-station, without the use of longitudinal compensation. The angle between the vectors of the e.m.f. of the sending-end station and the voltage of the receiving system goes in this case up to 150°. We note that the theoretical limit of the transmitted power without intermediate synchronous condensers and without longitudinal compensation, but with close regulation on the generators of the Kuibyshev H.E.S., is 1150 – 1200 MW.

The limit of the transmitted power could be further increased and the angle brought up to 180° if the location of the central substation could be chosen from the condition of equality of the angles between the voltage vectors of the busbars of the sending-end station and the intermediate sub-station, and also at the intermediate sub-station and the receiving end. In our consideration of the case we adopted the location of the sub-station foreseen in the project of the transmission system.

The ranges of stability for various angles between the vectors of the e.m.f. of the sending-end station and the voltage of the receiving system are in a concentrical position (Fig.1). This fact indicates that there is no necessity for altering the coefficients of the regulation when the transmitted power varies. The investigation also showed that regulation according to derivatives need only be used on the synchronous condensers, whereas on the generators it is sufficient to regulate according to the deviation without any stabilizing gear. Comparison of Fig.1 and 2 shows that use of regulation according to derivatives also on the generators leads only to a displacement of the stability range which may be useful in certain operational circumstances.

We see from the Table, the data of which were obtained without considering the shunting reactors, that the kVAr of the synchronous condensers required for keeping the voltage at the 400 kV busbars of the intermediate sub-station constant,

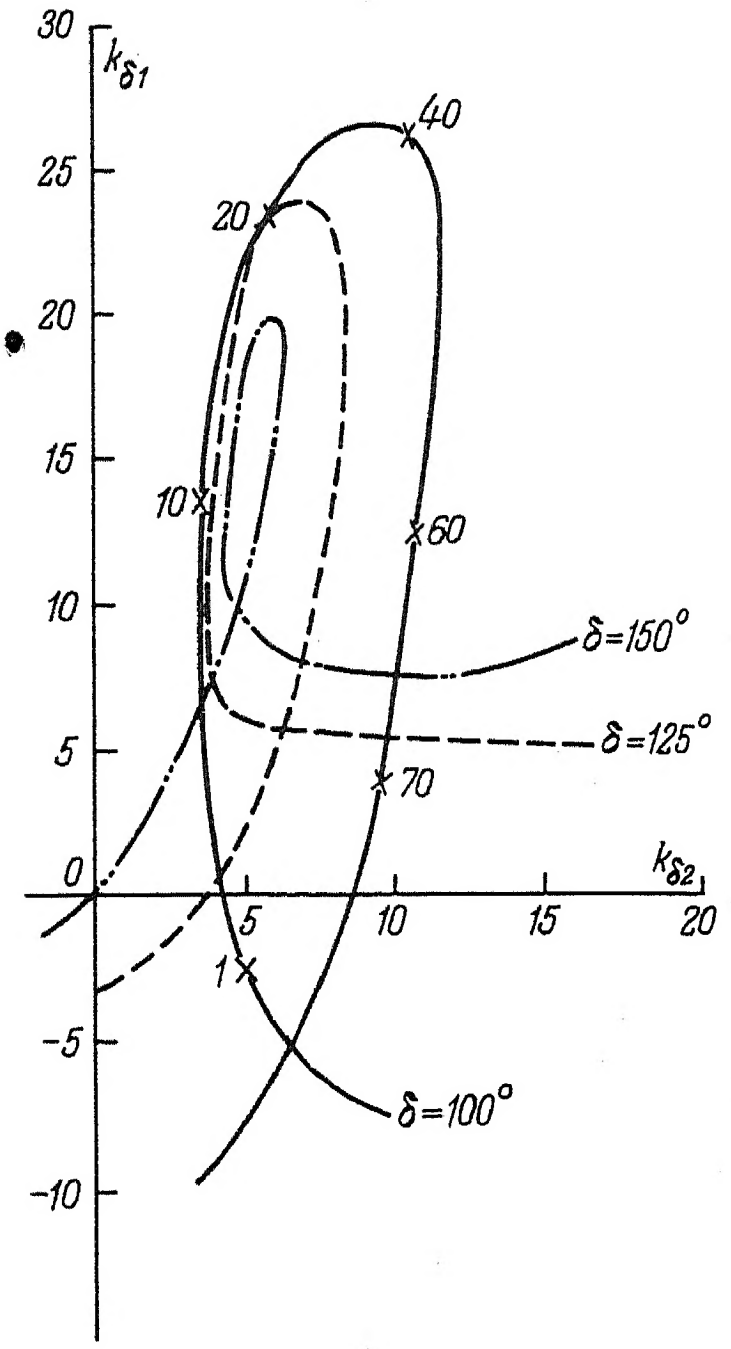

FIG.1. Stability ranges at angles $\delta = 100^0$, 125^0 and 150^0 and control (regulation) on the generators only from deviation and on the synchronous condensers according to deviations of the angle and its two derivatives.

The figures against the points of the curves indicate $2\pi\omega$, where ω is the frequency of the free oscillations.

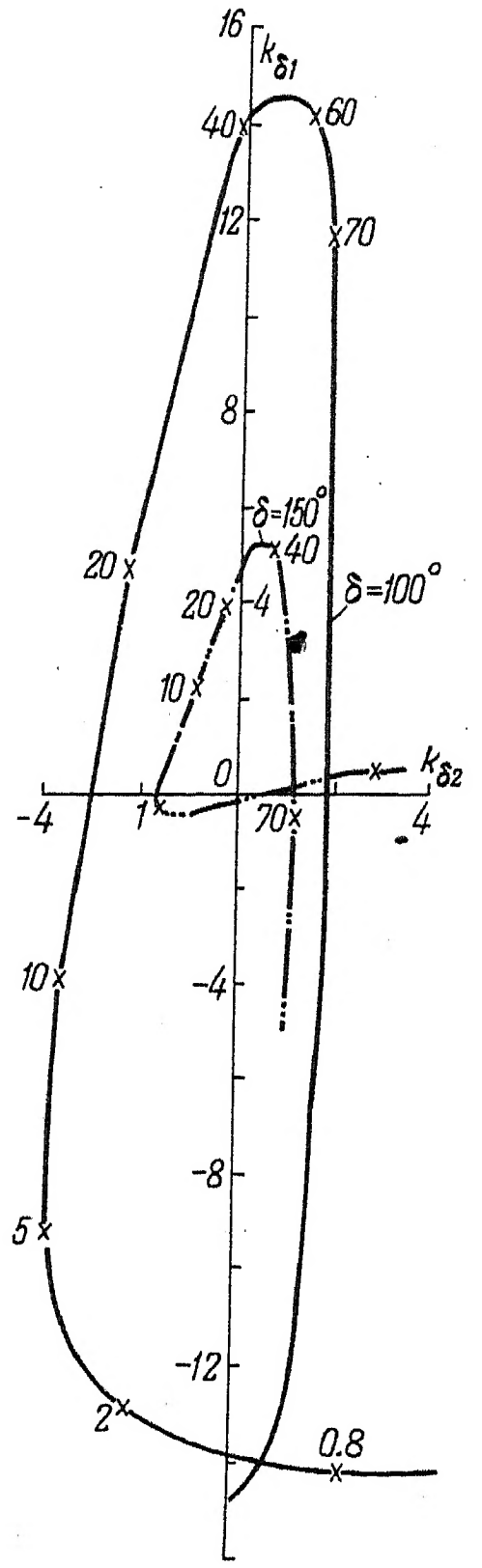

FIG.2. Stability ranges for angles $\delta = 100^0$, 150^0 and regulation according to derivatives on generators and synchronous condensers.

The coefficients of regulation on the generators are assumed to be constants, viz. $k\delta_0 = 1; k\delta_1 = 3; k\delta_2 = 2$.

TABLE 1

Angle	100^0	120^0	150^0
Power transmitted through the line MW.....	1300	1600	1800
Required rating of the synchronous condensers MVA	225	525	1425

depend to great extent on the power transmitted through the line. It is clear that with 750 MW installed power of the synchronous condensers and

without longitudinal compensation the system can continuously transmit 1600—1650 MW. After faults in the system short-time transmission of 1800 MW is possible when the synchronous condensers work with 100 per cent overload. Considering that a synchronous condenser works under normal conditions almost on no-load, the duration of this overloading should not exceed 1 min. This time will be sufficient to permit the automatic load-shedding devices to reduce the loading of the system to the permissible limit.

The investigation of the characteristic equation also showed that in the absence of an excitation control of generators on synchronous condensers the latter will produce practically no increase of the transmitting capacity of the line, even if their rating is fairly high (750 MW).

The use of a strong-action excitation control makes great demands on the high-speed action of regulators and excitors. If the time constant of the exciter exceeds 0.1 sec, the efficiency of the control is already considerably reduced. The use of a rigid feedback comprises the excitor enabling the time constant to be appreciably reduced, if the latter is mainly due to the parameters of the excitor winding itself. Time lags introduced by eddy currents in the massive poles, and also by currents passing through the auxiliary windings placed on these poles cannot be eliminated.

An increase of the mechanical time constant of the synchronous condensers has a beneficial effect on the stability at small deviations, N.A. Kachanova [7] has shown that an increase of the mechanical time constant is very useful in the case of large disturbances.

The results of the theoretical investigations were corroborated by tests on the model of the Central Electrotechnical Research Laboratory of the Ministry of Power Stations in the Karamyshev H.E.5 [6].

For the model tests two hydrogenerators of the station, of ratings 1360 kW (1700 kVA) and an artificial line consisting of four reactors, capacitors and resistors, were used. The circuit of the model (Fig.3) permits the parameters of the system to be altered within certain limits.

The time constant of the rotor and the mechanical constant of the generators of the Karamyshev station differ from the corresponding constants of the generators of the Kuibyshev. For this reason the results of the experimental investigation are more useful in a qualitative than in a quantitative respect.

The model circuit was so assembled that one of the generators of the Karamyshev's H.E.S. represented the sending-end station and the second the synchronous condenser. Corresponded to the actual line, the place of erection of the synchronous condenser would not coincide with the mid-point of the line, and its position on the line model was somewhat less favourable.

Both generators were provided with regulators of the Central Electrotechnical Research Laboratory enabling regulation to be carried out either according to the

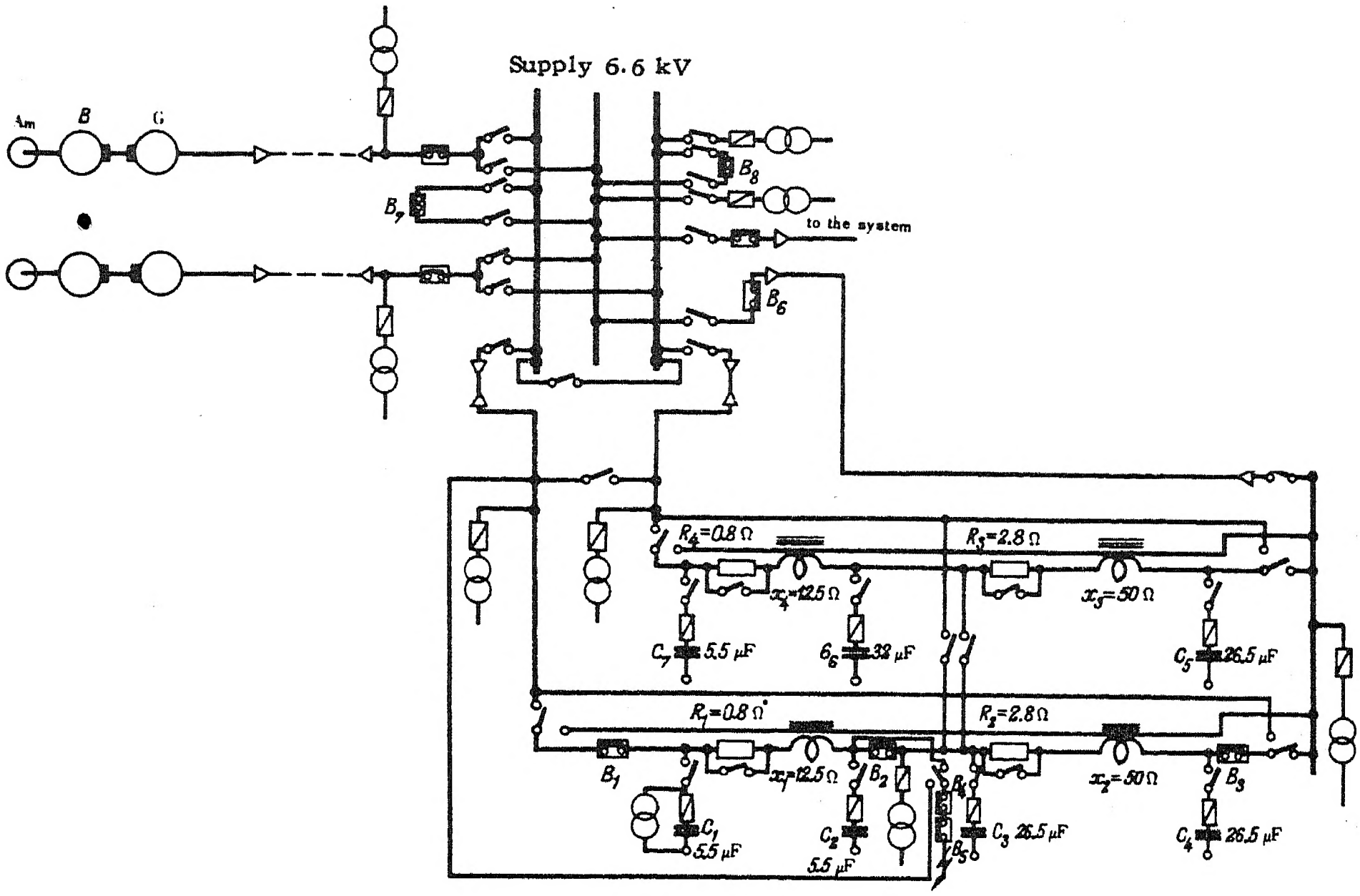

FIG.3. Diagram of the model on the Karamyshev HES. Am – angle-measuring machine; B – exciter; G – generator.

angle and its derivatives, or according to voltage and the derivatives of the angle. In the first tests the generator was regulated according to the angle and its derivatives, the condenser during one test series according to the angle and its derivatives, and during other tests, according to the voltage and the derivatives of the angle relative to the receiving end. The latter method of regulation was found to be more favourable in the practice, since it led to a higher limit of the transmitted power. This is explained by the fact that with an invariable coefficient of regulation according to the angle the relationship between the voltage in the sectionalizing sub-station and the angle is non-linear owing to which the voltage varied considerably at load changes and loss of stability of the section of the transmission line sometimes occurred. The maximum angle that could be obtained in steady operation was 145°; in this case, the angle between the voltage vectors at the ends of the section was almost 90°. A further increase of the load resulted in loss of stability due to the stability limit of the section being exceeded. The character of this loss of stability was a vehement increase of the angle not preceded by any hunting phenomena.

When the intermediate synchronous condenser was regulated according to the voltage variations and to the derivatives of the angle, and the generator only according to variations of the angle, practically the same results were obtained.

Conclusions

The limit of the power transmitted over long transmission lines can be efficiently increased by the use of synchronous condensers erected in sectionalizing sub-stations; their use is particularly indicated where it is necessary to tap off power at points along the line. In this case the use of synchronous condensers will not involve any complications of the lay-out of the sub-stations and in most cases not even the installation of additional transformers.

The points of erection of the synchronous condensers along the line and their rating are determined by technical and economic considerations.

Sub-stations may consume kVAr, thereby reducing, or even eliminating the need for shunting reactors.

Appendix

Characteristic equation of a transmission system with synchronous condensers in one sectionalizing substation. The power of the generating station may be expressed in the following way by the generator e.m.f.'s and the angles between the e.m.f. vectors:

$$\left.\begin{aligned} P_1 &= \frac{E_{q1}E_{q2}}{x_{12}}\sin\delta_{12} + \frac{E_{q1}E_{q3}}{x_{13}}\sin\delta_{13};\\ P_2 &= \frac{E_{q2}E_{q1}}{x_{12}}\sin\delta_{21} + \frac{E_{q2}E_{q3}}{x_{32}}\sin\delta_{23};\\ P_3 &= \frac{E_{q3}E_{q1}}{x_{31}}\sin\delta_{31} + \frac{E_{q3}E_{q2}}{x_{32}}\sin\delta_{32};\\ \delta_{12} &= -\delta_{21};\quad \delta_{13} = -\delta_{31};\quad \delta_{13} = \delta_{12} - \delta_{32}. \end{aligned}\right\} \qquad (A,1)$$

In the system of equations (A,1) only two equations are independent. We take δ_{12} and δ_{32} as independent variables. For station 2.... $E_{q2} = E_{d2}$. In terms of deviations, after linearization, we get

$$\left.\begin{aligned} \Delta P_1 &= A_1\,\Delta E_{q1} + B_1\,\Delta E_{q3} + C_1\,\Delta\delta_{12} + D_1\,\Delta\delta_{32};\\ \Delta P_3 &= A_3\,\Delta E_{q1} + B_3\,\Delta E_{q3} + C_3\,\Delta\delta_{12} + D_3\Delta\delta_{32} \end{aligned}\right\} \qquad (A,2)$$

where

$$A_1 = \frac{\partial P_1}{\partial E_{q1}} = \frac{E_{q2}}{x_{12}}\sin\delta_{12} + \frac{E_{q3}}{x_{13}}\sin\delta_{13};$$

$$B_1 = \frac{\partial P_1}{\partial E_{q3}} = \frac{E_{q1}}{x_{13}}\sin\delta_{13};$$

$$C_1 = \frac{\partial P_1}{\partial\delta_{12}} = \frac{E_{q1}E_{q2}}{x_{12}}\cos\delta_{12} + \frac{E_{q1}E_{q3}}{x_{13}}\cos\delta_{13};$$

$$D_1 = \frac{\partial P_1}{\partial \delta_{32}} = -\frac{E_{q1} E_{q3}}{x_{13}} \cos \delta_{13};$$

$$A_3 = \frac{\partial P_3}{\partial E_{q1}} = \frac{E_{q3}}{x_{31}} \sin \delta_{31};$$

$$B_3 = \frac{\partial P_3}{\partial E_{q3}} = \frac{E_{q1}}{x_{31}} \sin \delta_{31} + \frac{E_{q2}}{x_{32}} \sin \delta_{32};$$

$$C_3 = \frac{\partial P_3}{\partial \delta_{12}} = -\frac{E_{q3} E_{q1}}{x_{31}} \cos \delta_{31};$$

$$D_3 = \frac{\partial P_3}{\partial \delta_{32}} = \frac{E_{q3} E_{q1}}{x_{31}} \cos \delta_{31} + \frac{E_{q3} E_{q2}}{x_{32}} \cos \delta_{32}.$$

From equations (A,2) and (1) we get,

$$\left.\begin{aligned} A_1 \Delta E_{q1} + B_1 \Delta E_{q3} &= -(C_1 + T_{j1} p^2) \Delta \delta_{12} - D_1 \Delta \delta_{32}; \\ A_3 \Delta E_{q1} + B_3 \Delta E_{q3} &= -C_1 \Delta \delta_{12} - (D_3 + T_{j3} p^2) \Delta \delta_{32}. \end{aligned}\right\} \quad (A,3)$$

The system of equations (A,3) must be solved with respect to the variables E_{q1} and E_{q3}. To consider the magnetic asymmetric of the machine we write down the relationships between the quantities E_d and E_q, viz.

$$\left.\begin{aligned} E_{d1} &= \left(1 + \frac{x_{d1} - x_{q1}}{x_{11}}\right) E_{q1} - \frac{(x_{d1} - x_{q1})}{x_{12}} \cos \delta_{12} E_{q2} - \\ &\quad - \frac{x_{d1} - x_{q1}}{x_{13}} \cos \delta_{13} E_{q3}; \\ E_{d3} &= -\frac{x_{d3} - x_{q3}}{x_{13}} \cos \delta_{31} \cdot E_{q1} - \\ &\quad - \frac{x_{d3} - x_{q3}}{x_{23}} \cos \delta_{32} \cdot E_{q2} + \left(1 + \frac{x_{d3} - x_{q3}}{x_{33}}\right) \cdot E_{q3}; \\ E'_{d1} &= \left(1 + \frac{x'_{d1} - x_{q1}}{x_{11}}\right) E_{q1} - \\ &\quad - \frac{(x'_{d1} - x_{q1})}{x_{12}} \cos \delta_{12} \cdot E_{q2} - \frac{x'_{d1} - x_{q1}}{x_{13}} \cos \delta_{13} \cdot E_{q3}; \\ E'_{d3} &= -\frac{x'_{d3} - x_{q3}}{x_{13}} \cos \delta_{31} \cdot E_{q1} - \\ &\quad - \frac{x'_{d3} - x_{q3}}{x_{23}} \cos \delta_{32} \cdot E_{q2} + \left(1 + \frac{x'_{d3} - x_{q3}}{x_{33}}\right) E_{q3}. \end{aligned}\right\} \quad (A,4)$$

x_{11}, x_{12}, etc., are the self and mutual inductive reactances in the equivalent representation of the generators by the quadrature components of the synchronous reactances.

The system of equations (A,4) may also be written in terms of the partial differentials of the deviations, viz.

$$\left.\begin{aligned}
\Delta E_{d1} &= E_1 \Delta E_{q1} + F_1 \Delta E_{q3} + G_1 \Delta\delta_{12} + H_1 \Delta\delta_{32};\\
\Delta E_{d3} &= E_3 \Delta E_{q1} + F_3 \Delta E_{q3} + G_3 \Delta\delta_{12} + H_3 \Delta\delta_{32};\\
T_{d1} \Delta E'_{d1} &= E'_1 \Delta E_{q1} + F'_1 \Delta E_{q3} + G'_1 \Delta\delta_{12} + H'_1 \Delta\delta_{32};\\
T_{d3} \Delta E'_{d3} &= E'_3 \Delta E_{q1} + F'_3 \Delta_{q3} + G'_3 \Delta\delta_{12} + H'_3 \Delta\delta_{32}.
\end{aligned}\right\} \qquad (A,5)$$

The partial differentials E_1, F_1, E_3, F_3, E'_1, F'_1, F'_3, E'_3 remain equal to the coefficients of E_q of the corresponding columns of the system of equations (A,4), for example

$$E_1 = \frac{\partial E_{d1}}{\partial E_{q1}} = 1 + \frac{x_{d1} - x_{q1}}{x_{11}} \quad \text{etc.}$$

The partial differentials of the deviations of the angles are.

$$\left.\begin{aligned}
G_1 &= \frac{\partial E_{d1}}{\partial \delta_{12}} = + \frac{x_{d1} - x_{q1}}{x_{12}} \sin\delta_{12} E_2 + \\
&\quad + \frac{x_{d1} - x_{q1}}{x_{13}} \sin\delta_{13} E_{q3};\\
H_1 &= \frac{\partial E_{d1}}{\partial \delta_{32}} = - \frac{x_{d1} - x_{q1}}{x_{13}} \sin\delta_{13} E_{q3};\\
G_3 &= \frac{\partial E_{d3}}{\partial \delta_{12}} = \frac{x_{d3} - x_{q3}}{x_{13}} \sin\delta_{13} E_{q1};\\
H_3 &= \frac{\partial E_{d3}}{\partial \delta_{32}} = - \frac{x_{d3} - x_{q3}}{x_{13}} \sin\delta_{13} E_{q1} + \\
&+ \frac{x_{d3} - x_{q3}}{x_{23}} \sin\delta_{32} E_2;\\
G'_1 &= T_{d1} \left(\frac{x'_{d1} - x_{q1}}{x_{12}} \sin\delta_{12} E_2 + \right.\\
&\quad \left. + \frac{x'_{d1} - x_{q1}}{x_{13}} \sin\delta_{13} E_{q3} \right);\\
H'_1 &= T_{d1} \left(- \frac{x'_{d1} - x_{q1}}{x_{13}} \sin\delta_{13} E_{q3} \right);\\
G'_3 &= T_{d3} \left(\frac{x'_{d3} - x_{q3}}{x_{13}} \sin\delta_{13} E_{q1} \right);\\
H'_3 &= T_{d3} \left(- \frac{x'_{d3} - x_{q3}}{x_{13}} \sin\delta_{13} E'_{q1} + \right.\\
&+ \left. \frac{x'_{d3} - x_{q3}}{x_{23}} \sin\delta_{32} E_2 \right).
\end{aligned}\right\} \qquad (A,6)$$

Substituting into equation (2) the values of the e.m.f.'s, we get from equations (A,5):

$$\left.\begin{aligned}
\Delta E_{de1} &= (E_1 + pE'_1) \Delta E_{q1} + (F_1 + pF'_1) \Delta E_{q3} + \\
&\quad + (G_1 + pG'_1) \Delta\delta_{12} + (H_1 + pH'_1) \Delta\delta_{32};\\
\Delta E_{de3} &= (E_3 + pE'_3) \Delta E_{q1} + (F_3 + pF'_3) \Delta E_{q3} + \\
&\quad + (G_3 + pG'_3) \Delta\delta_{12} + (H_3 + pH'_3) \Delta\delta_{32}.
\end{aligned}\right\} \qquad (A,7)$$

The deviation of the voltage on the rotor rings resulting from the action of the regulator may be expressed as follows:

$$\left.\begin{aligned}\Delta E_{de1} &= \frac{M(p)_1\,\Delta\delta_{12}}{(1+pT_{e1})(1+pT_{p1})} = \frac{M(p)_1}{Z(p)_1}\,\Delta\delta_{12};\\ \Delta E_{de3} &= \frac{M(p)_3\,\Delta\delta_{32}}{(1+pT_{e3})(1+pT_{p3})} = \frac{M(p)_3}{Z(p)_3}\,\Delta\delta_{32}.\end{aligned}\right\} \qquad (A,8)$$

We have for, $$Z(p) = (1 + pT_{ex})\ \ (1 + pT_{reg});$$

where

T_{ex} is the time constant of the excitor;
T_{reg} is the time constant of the regulator. With regulation by an angle $M(p) = k_0 + k_1 p + k_2 p^2$.

Substituting the values E_{q1}, E_{q3} obtained from the solution of the system of equations (A,3), into equations (A,7) and considering the expression (A,8), we get two equations involving $\Delta\delta_{12}$ and $\Delta\delta_{32}$, viz,

$$\left.\begin{aligned}\left(Q_1 + \frac{M(p)_1}{Z(p)_1}\right)\Delta\delta_{12} + Q_2\,\Delta\delta_{32} &= 0;\\ Q_3\,\Delta\delta_{12} + \left(Q_4 + \frac{M(p)_3}{Z(p)_3}\right)\Delta\delta_{32} &= 0.\end{aligned}\right\} \qquad (A,9)$$

In equations (A,9) the coefficients of the deviations of the angles were obtained by substitution.

The determinant composed of the coefficients of the angle deviations yields the characteristic equation (4) required. In stability investigations the characteristic equations must be written in explicit form and arranged in descending powers of p.

REFERENCES

1. F.G. Baum; *Voltage Regulation and Insulation for Large Power Long Distance Transmission Systems, Trans. AIEE*, 40, p. 1017 (1921).
2. P.S. Zhdanov; *The 1000 MW Transmission System Kuibyshev–Moscow, Elektrichestvo,* No.13 (1936).
3. S.A. Lebedev; *Investigation of artificial Stability, Reports of the All–Union Electrotechnical Institute,* No.40, *Gosenergoizdat* (1940).
4. M.M. Botvinnik; *Excitation Regulation and steady-state Stability of the synchronous Machine, Gosenergoizdat* (1950).
5. V.A. Venikov and I.V. Litkens; *Effect of the Excitation Regulation on the Transmitting Capacity of long Transmission Lines, Elektrichestvo,* No.11 (1955).
6. E.L. Bronshtein and M.S. Fezi-Zhilinskaya; *Model of a long Transmission Line, Reports of Central Electrical Research Laboratory,* No.2, *Gosenergoizdat* (1954).
7. N.A. Kachanova and V.E. Krutikova; *Investigation of the Methods of Improving the Stability of long Transmission Systems (A.C.)* (1955).
8. M.A. Aizerman, *Theory of automatic Control of Motors, State Publishing House of technical and theoretical Literature* (1952).

CONTROLLING A MILL WITH SEPARATELY DRIVEN ROLLERS*

O.V. SLEZHANOVSKII

(Received 12 December 1956)

The separate drive of the rollers of large rolling mills, though possessing considerable advantages over group drives, complicates the control system and introduces some novel requirements, of which the basic one is the necessity of securing rolling without bending with a sufficiently uniform distribution of the loads between the roll-drive motors. Most existing systems do not satisfy these requirements; moreover, the systems are also unnecessarily complicated and do not ensure a satisfactory transient response. A new system proposed by the author (Fig. 1) is sufficiently simple and eliminates the above disadvantages.

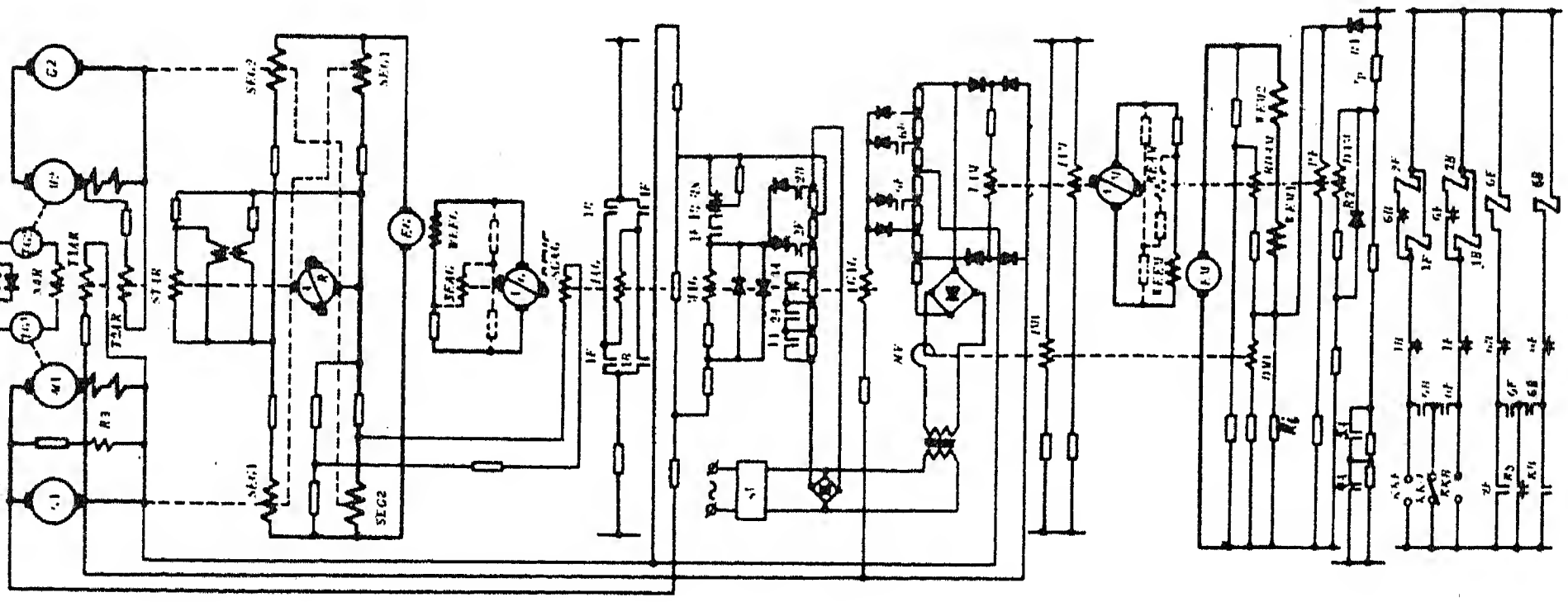

FIG. 1. Elements of the control circuit of a mill with individual roll-drives.

The field windings of the generators are connected to a bridge ciruit fed by the common exciter EG†). The regulator *AR* co-ordinating speed and current of the roll-drive motors is connected in the diagonal arm of the bridge. When the control acts, the field of one generator increases and that of the other decreases. The regulator

* *Elektrichestvo* No. 5, 12 – 20, 1957 [Reprint Order No. EL 19].

† The bridge circuit may also be formed by windings and ohmic resistances or by two windings and armatures of the exciters where two exciters are used.

windings are connected to the voltage drops in the sections of the main circuit of each of the roll-drive motors and to the voltage difference of the tachogenerators. The field windings of the motors receive their supply from the exciter *EM* whose excitation is provided by the amplidyne *AM*, so that the character of the transient processes comes near the possible optimum. This is achieved by arranging the m.m.f. of the input winding *IAM* in the positive direction, a "cut-off" of the field current by the differential winding *DAM*, and a positive feedback of the field currents *PB*. The m.m.f.'s are denoted by F_{im}, F_{dm} and F_{pf}.

The m.m.f. of the input winding determines the polarity of the exciter in the steady-state. The differential winding is connected to the difference of two voltages, viz. a voltage proportional to the field current of the motor and the voltage of the calibrating potentiometer. The rectifier *R*1 in the circuit of the differential winding prevents its action when the exciting flux of the motor increases, but towards reducing the field current. The rectifier *R*2, shunting the winding, limits its m.m.f. during periods of decreasing flux of the excitation.

The steady-state characteristics of the control system of the excitation of the generators and of the roll-drive motors are shown in Fig. 2a and b. The method of plotting them is similar to that described in [1]. The analysis of the steady-state characteristics confirms in principle the usefulness of the system adopted. The resulting m.m.f. of the amplidyne *AG* of the generators is in all cases determined within narrow limits, and the m.m.f. of the amplidyne *AM* of the motors changes in such a way that it creates favourable conditions for the forcing of processes of decreasing or increasing the fluxes of the roll-drive motors.

By altering the amplification factor of the positive feedback for the motor field current and the m.m.f. of the input winding it is possible to adjust the character of the increase of the exciting flux in the most appropriate way to suit the actual conditions of operation of the drive. If the machines of the main drive have a low voltage between segments, a small flywheel moment and a large magnetic time constant, it is expedient to increase the m.m.f. of the input winding. Increased flux forcing at the beginning of the process is so obtained and the braking conditions are also established correctly from the viewpoint of energy economy, since the speed is first reduced by the strong increase of the motor field and then by the reduction of the generator voltage. Cases are possible where during a forced increase of the field the load regulator, tending to limit the current of the main circuit, also slightly increases the generator voltage above its rating.

With machines having a large voltage between segments, which would not permit the voltages to exceed the rated values during braking periods, it is necessary to decrease the m.m.f. of the input winding and to increase the positive feedback of the field current. By this re-arrangement the initial forcing of the motor field is reduced to the correct value and the forcing increased subsequently as the motor flux increases, in accordance with the requirements set out in [1] and [2].

Rotating machines are not used as sources of reference voltages in the circuit suggested. The generator of the reference voltage of the voltage regulator is re-

placed by a voltage stabilizer and the generator of the reference voltage of the power regulator by a magnetic amplifier. Flexible feedbacks of the generator voltage and field current are provided by a Birfeld differential-bridge circuit without stabilizing transformers.

The use of this circuit introduces several novel characteristics. Fig. 3a shows that the transfer function $K(p)$ of of the (ideal) differential bridge without load can be found as follows:

$$U_0 = U_i \frac{r_2}{r_1 + r_2} \frac{r_4}{r_3 + r_4} \frac{1}{(1 + pT)}$$

In the balanced bridge

$$\frac{r_2}{r_1 + r_2} = \frac{r_4}{r_3 + r_4} = Kbb,$$

then

$$K(p) = \frac{U_0}{U_i} = K_{bb} \frac{pT}{(1 + pT)} \qquad (1)$$

where

$$T = \frac{L}{r_3 + r_4}.$$

Comparing the expression with the transfer function of the stabilizing transformer (Fig. 3b):

$$K(p) = \frac{U_0}{U_i} =$$

$$K_S \frac{p}{p^2 T_1 T_2 (1 - \sigma^2) + p(T_1 + T_2) + 1}$$

where

$$K_S = \frac{MR}{R_1(R + R_2)}; \quad \sigma^2 = \frac{M^2}{L_1 L_2}; \quad T_1 = \frac{L_1}{R_1}; \quad T_2 = \frac{L_2}{R + R_2}.$$

Neglecting leakage, i.e. assuming $\sigma = 1$, and introducing $T_1 + T_2 = \tau$; $K_{st} = \frac{K_S}{\tau}$ we obtain

$$K(p) = K_{cm} \frac{p\tau}{(1 + p\tau)}. \qquad (2)$$

It follows that on the assumptions made the transfer functions of the bridge and of the stabilizing transformers have the same form. Since, however, the time constants of the stabilizing transformers differ in most cases from the time constants in the circuits of the machine windings forming the branches of the bridge, the effects of the use of the circuits compared will also be different.

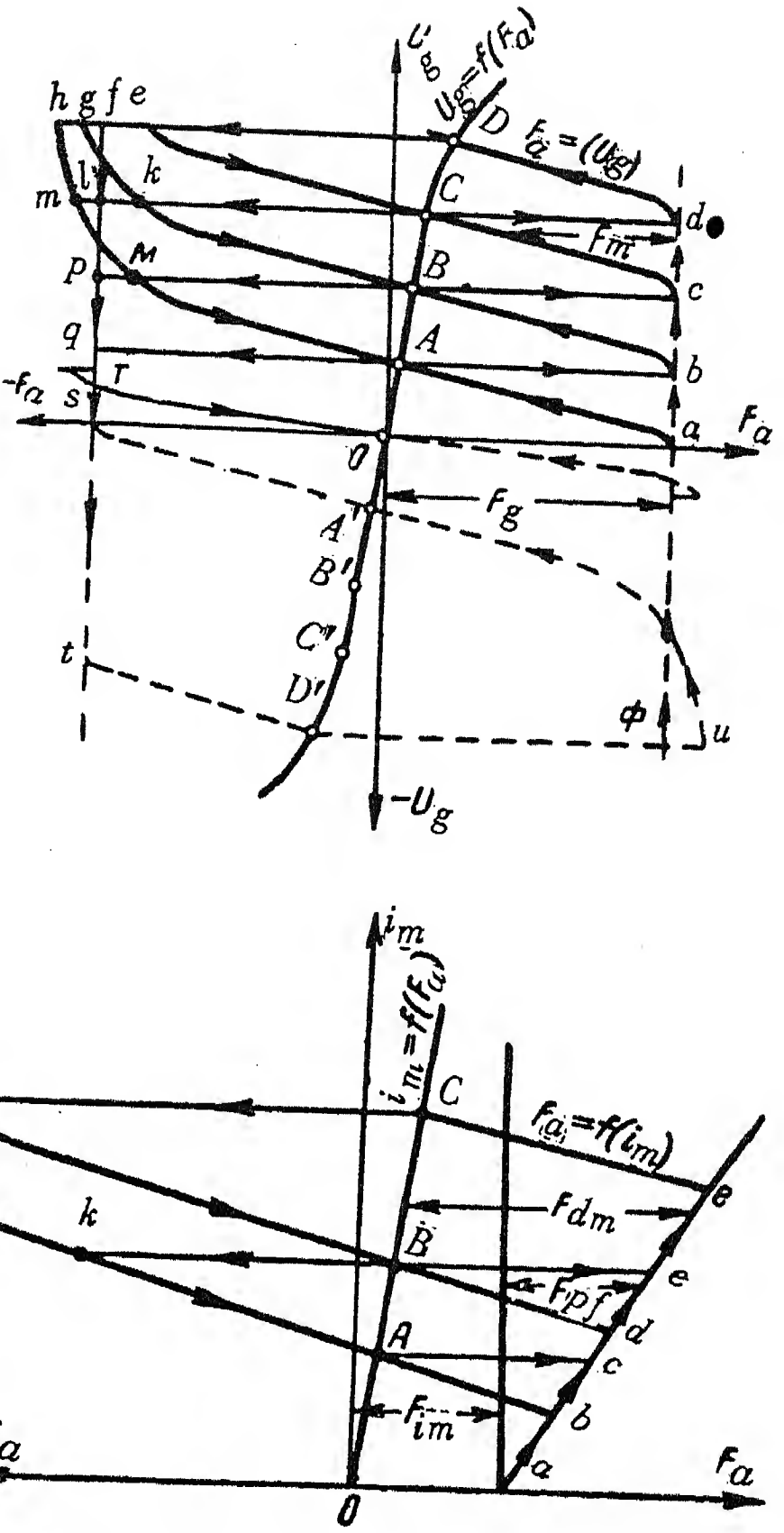

FIG. 2. Steady-state characteristics of the field control of the generators and motors.

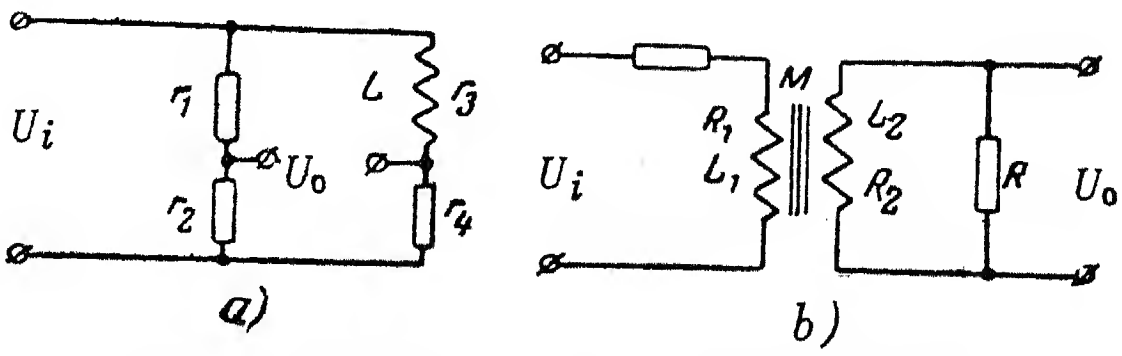

FIG. 3. Stabilizing bridge and stabilizing transformers.

It is easy to show that this difference may be intrinsic. If the input voltage U_i is the exciter voltage U_{eg} of the generators, we find from the relation $U_{eg} = E_g \frac{(1+pT_g)}{K_g}$ that when the bridge circuit is used, $U_0 = U_{eg} K_{bb} \frac{pT_g}{(1+pT_g)} = \frac{K_{bb}}{K_g} T_g p E_g$.

Denoting $\frac{K_{bb}}{K_g} T_g = \alpha$, we obtain

$$U_0 = \alpha p E_g. \tag{3}$$

The m.m.f. of the amplidyne supplied with the output voltage is approximately

$$F_{bg} \approx K_{bg} p E_g \approx K_{bg} p U_g, \tag{4}$$

where

$$K_{bg} = K_{bb} \frac{W_w}{r_w}.$$

When the stabilizing transformer is used the following expression results for the output voltage U_O:

$$U_0 = \frac{K_{st}}{K_g} \tau \frac{(1+pT_g)}{(1+p\tau)} p E_g = \beta p E_g \frac{1}{(1+p\tau)} + \gamma p^2 E_g \frac{1}{(1+p\tau)}. \tag{5}$$

Analysis of the expressions for U_O shows that the bridge circuit enables a feedback proportional to the net first derivative of the generator e.m.f. to be obtained whereas the stabilizing transformer gives with the same input voltage two components the first of which is proportional to the first derivative of the generator voltage, and the second to the second derivative. Also an additional time delay element is introduced which is determined by the denominator $(1 + p\tau)$.

To obtain an expression similar to (5) by the bridge circuit, it is necessary to have at the input of the bridge the voltage U_{ag} of the amplidyne, and not that of the exciter.

Indeed, since in this case $U_0 = U_{ag} K_{bb} \frac{pT_{eg}}{(1+pT_{eg})}$,

we get by transition from U_{ag} to E_g,

$$U_0 = \frac{K_{bb}}{K_{eg} K_g} T_{eg} (1 + pT_g) p E_g = \mu p E_g + \varepsilon p^2 E_g. \tag{6}$$

The m.m.f. of the amplidyne winding connected to U_O will be

$$F_{be} \approx K_{be} (1 + pT_g) p E_g \approx K_{be} (1 + pT_g) p U_g. \tag{7}$$

where

$$K_{bc} = \frac{K_{bb}}{K_{eg} K_g} T_{eg} \frac{W_w}{r_w}.$$

Comparison of the equations (5) and (6) shows that for small values of τ they practically coincide.

It is obvious that with relatively small values of τ and with divergences between τ and T the effects of flexible feedback obtained by means of stabilizing transformers and bridges respectively, are very much different for the same input voltage. Under these conditions the flexible bridge feedback acts like the feedback of a stabilizing transformer connected to the output of the following cascade.

The above considerations enable us to explain the advantages of the accepted

method of increasing the anti-hunting time constant τ to values equal to the time constant T_g of the generator [3].

In the generator - motor system considered [3] with amplidynes the expression for the flexible feedback assumes in the case of $\tau = T_g$ a form similar to that obtained for the bridge circuit (4), and since by means of the feedback pE_g, the derivative of the generator e.m.f., is controlled, we obtain conditions resulting in uniformly accelerated transient processes of field control of the generator. However, the great varying values of time constants T_g encountered render it difficult to maintain the condition $\tau = T_g$ by the use of stabilizing transformers. This difficulty is obviated by the use of the differential bridge circuit where the problem resolves itself since $T = T_g$.

There is a fair number of systems in which control by the first derivative of the generator e.m.f. is advisable. The control system of the excitation of the generators of the main drives belongs to these. In developing the circuit, a basic flexible link was provided by the bridge circuit connected to the field winding of the generators. The use of an intermediate feedback, shown dotted in Fig. 1, should be avoided or its effect reduced to the minimum necessary with regard to the stability conditions.

Determination of the parameters of the flexible feedback and character of the control operations

For the generator voltage (not considering the action of the regulator, neglecting the time constants of the control windings of the amplidyne, eddy current effects and assuming a linear magnetization characteristic of the machines) the following equation can be written:

$$U_g = F_{ag} K \frac{1}{(1+pT_a)(1+pT_{eg})(1+pT_g)}, \qquad (8)$$

where $K = K_a K_{eg} K_g$, the amplification factor of the system:

$$K_a = \frac{\Delta U_{ag}}{\Delta F_{ag}}; \quad K_{eg} = \frac{\Delta U_{eg}}{\Delta U_{ag}}; \quad K_g = \frac{\Delta U_g}{\Delta U_{eg}}; \qquad T_a,\ T_{eg},\ T_g -$$

T_a, T_{eg}, T_g time constants of the amplidyne, exciter and generator respectively; $F_{ag} = F_i - F_{dg} - F_{bg} - F_{be}$ the m.m.f. of the amplidyne AG; F_i, F_{bg}, F_{be} the m.m.f.'s of the input and stabilizing windings; $F_{dg} = K_{dg}(U_g - U_{co})$ the m.m.f. of the differential windings;

Hence

$$F_{ag} = F_i + K_{dg} U_{co} - U_g \{K_{dg} + p[K_{bg} + K_{be}(1+pT_g)]\}.$$

Substituting the expression for F_{ag} in equation (8), we obtain:

$$U_g = (F_i + K_{dg} U_{co}) \frac{1}{K} \frac{1}{(1+pT_a)(1+pT_{eg})(1+pT_g) + K\{K_{dg} + p[K_{bg} + K_{be}(1+pT_g)]\}} \qquad (9)$$

Up to the cut-off of the forcing, i.e. when the differential winding is not connected:

$$U_g = F_i K \frac{1}{(1+pT_a)(1+pT_{eg})(1+pT_g) + Kp[K_{bg} + K_{be}(1+pT_g)]} \qquad (10)$$

Neglecting the action of the intermediate feedback ($K_{be} = 0$) and bearing in mind that

the time constants of the links included by the flexible feedback can be neglected when the time constant of the transfer function of the feedback is many times larger than the time constant of these links, we find for an approximate calculation:

$$U_g = (F_i + K_{dg} U_{co}) \frac{K}{(1 + K_{dg} K)} \frac{1}{1 + p \dfrac{T_g + K_{bg} K}{1 + K_{dg} K}} \tag{11}$$

or

$$U_g = (U_{go} - U_{g.fin}) \exp^{-\frac{t}{T_{g.red^1}}} + U_{g.\,fin}, \tag{12}$$

and before cutting-off the forcing with zero initial conditions

$$U_g = F_i K \frac{1}{1 + p\,(T_g + K_{bg} K)} \tag{13}$$

or

$$U_g = F_i K \left(1 - \exp^{-\frac{t}{T_{g.red^2}}}\right) \tag{14}$$

In the expressions (12) and (14) $T_{g.red^1} = \dfrac{T_g + K_{bg} K}{1 + K_{dg} K}$ and $T_{g.red^2} = T_g + K_{bg} K$ are the reduced time constants of the generator after "cutting-off" forcing and before, when the circuit is open. U_{go} and $U_{g.fin}$ are the initial and final values of the voltage, determined by the change of the cut-off voltage U_{co}.

Assuming the control time $t = t_r$ we can find the coefficient of the feedback K_{bg} from the above equations. Beginning from the conditions of starting before "cutting-off" forcing (14), we obtain

$$K_{bg} = \frac{1}{K} \left[\frac{t_r}{\ln \dfrac{F_i K}{F_i K - U_{co}}} - T_g \right]. \tag{15}$$

The right choice of K_{bg} can be checked by calculating the transient process by the complete equation.

The equation and the parameters of the field control of the roll-drive motors are set up in a similar way:

$$i_m = F_{am} K_m \frac{1}{(1 + pT_a)(1 + pT_{em})(1 + pT_m)}, \tag{16}$$

where $K_m = K_{am} K_{em} K_m$, the amplification coefficient of the system; T_a, T_{em}, T_m – the time constants of the amplidyne, the exciter and the motor respectively;

$$K_{am} = \frac{\Delta U_{am}}{\Delta F_{am}}; \quad K_{em} = \frac{\Delta U_{em}}{\Delta U_{am}}; \quad K_m = \frac{\Delta i_m}{\Delta U_{em}} = \frac{1}{\Sigma R};$$

$F_{am} = F_{im} + F_{pf} - F_{dm} - F_b$ the m.m.f. of the amplidyne AM:

$$F_{am} = F_{im} + K_{dm} i_{coc} + i_m [K_{pf} - K_{dm} - p\,(K_{bem} + K_{bm} + K_{bem} pT_m)],$$

where

$$F_{pf} = K_{pf} i_\partial; \quad K_{pf} = \frac{R_i}{\Sigma r_{pf}} w_{pf};$$

$$F_{dm} = K_{dm}(i_m - i_{coc});$$

$$K_{dm}=\frac{F_{im}+\frac{i_{mn}}{K_m}(K_{pf}K_m-1)}{i_{mn}-i_{co}}\;;\; i_{co}=\frac{U_s}{R_p}\cdot\frac{r_p}{R_i}\;;$$

$$F_b=F_{bem}+F_{bm}=pi_m[K_{bem}(1+pT_m)+K_{bm}],$$

where U_s is the system voltage; R_p is the total effective resistance of the standard potentiometer, $F_b=F_{bem}+F_{bm}$ the m.m.f. set up by the two flexible feedbacks.

Substituting these expressions in (16) we obtain $i_m=(F_{im}+K_{dm}i_{co})K_m$.

$$\frac{1}{(1+pT_a)(1+pT_{em})(1+pT_m)+K_m\{K_{dm}-K_{pf}+p[K_{bm}+K_{bem}(1+pT_m)]\}} \qquad (17)$$

In the period of increasing flux up to the instant of "cutting-off" forcing the differential winding does not take part in the operation.

Therefore, assuming $K_{dm}=0$, we obtain for the given condition:

$$i_m=F_{im}\cdot K_m\frac{1}{(1+pT_a)(1+pT_{em})(1+pT_m)+K_m\{p[K_{bm}+K_{bem}(1+pT_m)]-K_{pf}\}} \qquad (18)$$

or

$$i_m=F_{im}K_m\frac{1}{T_aT_{em}T_mp^3+[T_m(T_{em}+T_a+K_mK_{bem})+T_aT_{em}]p^2+[T_a+T_{em}+T_m+K_m(K_{bm}+K_{bem})]p-(K_mK_{pf}-1)} \qquad (19)$$

Usually $K_mK_{pf}\gg 1$. In this condition one root of the characteristic equation is positive, which indicates the increasing rate of rise of the field current. When the current i_m has reached the cutting-off value, it is necessary to use (17).

In order to use the analytical formula for zero initial conditions for the calculation of the excitation flux increase, the calculation is suitably made not for the current itself but for the field current increment, i.e. the co-ordinate origin must be transferred to the point corresponding to the initial steady-state excitation current of the given state of excitation. In this case we have always to calculate first the initial theoretical effective value F_{im}.

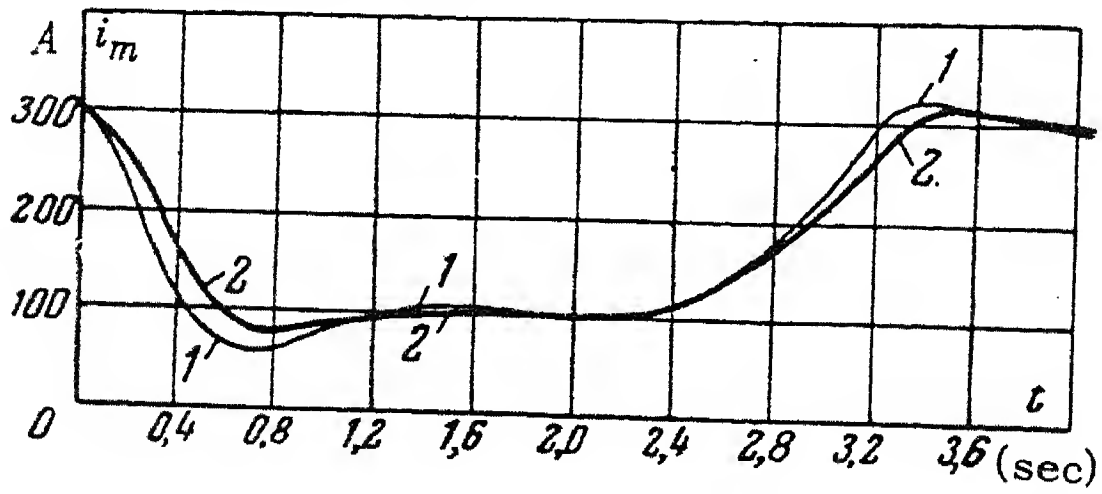

FIG. 4. Conditions of the control of the excitation flux of the roll-drive motors 300 ... 100 ... 300 A. $i_{mn}=300$ A; $i_{co}=240$ A; $i_{min}=100$ A; $F_{im}=20$ AT; $K_m=K_aK_{em}K_m=5.2, 5.2=\lambda\pi$ A/AT; $k_{pf}=0.6$ AT/A; $K_{dm}=3$ AT/A; $T_a=0.1$ sec; $T_{em}=0.3$ sec; $T_m=6$ sec. 1 - with $K_{bm}=0.18$; $K_{bem}=0$; 2 - with $K_{bm}=0.1$; $K_{bem}=0.005$.

$$F_{imr} = F_{imo} + \frac{i_{mr}}{K_m}(K_m K_{pf} - 1), \tag{20}$$

where F_{imo} is the m.m.f. of the input winding; i_{mr} is the motor field current corresponding to the initial state of excitation.

For a more precise determination of the effect of the positive feedback of the excitation current and of the flexible feedbacks on the transient control process calculations were carried out for two values of the coefficient of the positive feedback K_{pf} and for two different methods of obtaining the flexible feedback:

a) $K_{bm} \neq 0$; $K_{bem} = 0$;

b) $K_{bm} \neq 0$; $K_{bem} \neq 0$.

Diagrams of the calculated transient processes are shown in Figs. 4 and 5.

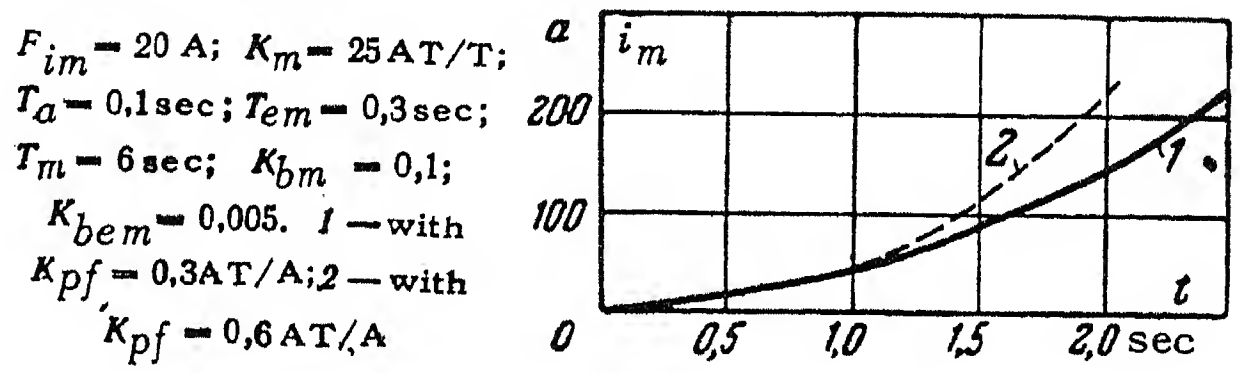

FIG. 5. Increase of the excitation flux of the roll-drive motors.
F_{im} = 20 A; K_m = 25 A/AT;
T_a = 0.1 sec; T_{em} = 0.3 sec;
Tm = 6 sec; K_{bm} = 0.1;
K_{bem} = 0.005.
1 - with K_{pf} = 0.3 AT/A;
2 - with K_{pf} = 0.6 AT/A.

When the intermediate flexible feedback is in action, the time constants T_a and T_{em} can no longer be neglected, since owing to the inclusion of a large resistance in the field circuit of the exciter, the time constant T_{em} is relatively small. The calculations must be made according on the complete third-order equation. However, in some cases it is possible to confine it to the second order. Just as in the field control of the generators, the intermediate flexible feedback is not absolutely necessary here. In this case

$$K_{bm} = \frac{1}{K_m}\left\{\frac{(K_{pf}K_m - 1)\,t}{\ln\left[\frac{i_m}{F_{im}K_m}(K_{pf}K_m - 1) + 1\right]} - T_m\right\}. \tag{21}$$

But in the field control system of the motors the intermediate flexible feedback results in an improvement of the transient performance when the flux is increased, although the performance deteriorates slightly when the flux is decreased.

Fig. 6 shows an oscillogram of the control processes of the motor field ob-

tained on a laboratory model with only one intermediate flexible feedback in operation. The character of the change of the flux Φ is entirely satisfactory. The over-regulation of the flux is small, the over-regulation of the field current i_m reaches 17%. This discrepancy between current and flux is explained by the effect of eddy currents.

It is recommended to provide the controller for balancing the loads and speeds with a non-linear resistor in the circuit of the winding connected to the difference of the tachogenerator voltages. The function of this resistor is not to prevent the regulator from balancing the motor loads. Owing to the non-linearity the winding begins to act effectively only from a certain permissible difference in speed onwards.

The m.m.f. of the regulator AR, produced by the current windings, is proportional to the difference of the load currents $F_{\Delta I} = K_I \Delta I$.

The m.m.f. of the winding connected to the difference of the tachogenerator voltages is $F_{\Delta n} = K_n \Delta n$.

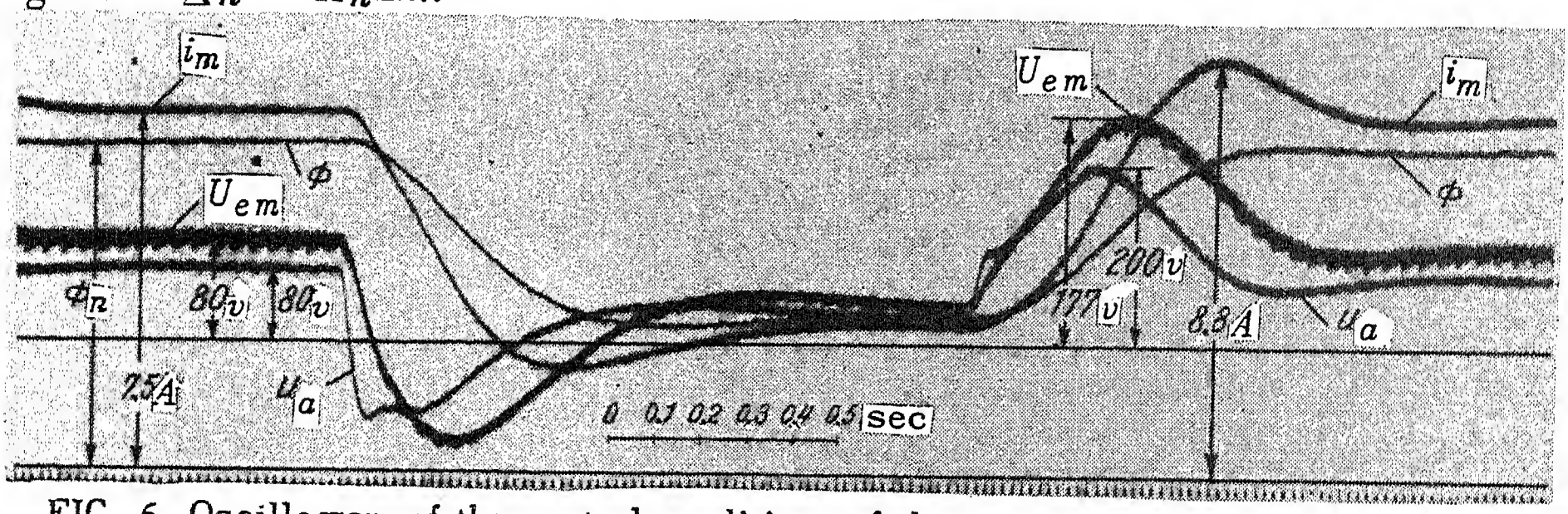

FIG. 6. Oscillogram of the control conditions of the excitation flux of the motors of the laboratory model. $i_{mn} = 7.5$ A; $i_{co} = 4.9$ A; $i_{min} = 3$ A; $K_m = 1.5$ A/AT; $K_{pf} = 8.33$ AT/A; $T_a = 0.05$ sec; $T_{em} = 0.117$ sec; $T_m = 1.06$ sec; $K_{dm} = 29.8$ AT/A;

The speed difference produced by the rolling process determines the unavoidable difference of the loads under conditions of equality of the initial value of the generator e.m.f.'s $E_{g1} = E_{g2}$. and of the e.m.f.'s of the motors $E_{m1} = E_{m2}$. In this case

$$F_{\Delta n} = K_n \frac{R_{arm}}{C\Phi} (1 + pT_{arm}) \Delta I,$$

where R_{arm} and T_{arm} are the resistance and time constant of the armature respectively, C is the motor constant.

The m.m.f. of the error signal of the controller F_e consists of two components $F_{\Delta I}$ and $F_{\Delta n}$.

$$F_e = F_{\Delta I} + F_{\Delta n} = \Delta I \left\{ K_I - K_n \frac{R_{arm}}{C\Phi} (1 + pT_{arm}) \right\}$$

or

$$F_e = \Delta I \left\{ \left(K_I - K_n \frac{R_{arm}}{C\Phi} \right) - K_n \frac{R_{arm}}{C\Phi} pT_{arm} \right\}.$$

Denoting $\frac{R_{arm}}{C\phi} = A$ with $T_{arm} = 0$, we obtain: $F_e = \Delta I (K_I - K_n A)$.

This equation shows that the presence of the winding setting up $F_{\Delta n}$ prevents the balancing of the loads. On the other hand, it is obvious that this winding can prevent the possibility of the development of a large discrepancy of speeds which is especially undesirable during the gripping of ingots by the rolls.

The load controller is designed according to well established principles. The m.m.f. of the current winding of the amplidyne *AG* decreases the acceleration of the motors during the overloading on starting and retards the reduction of the generator voltage during braking periods. The m.m.f. of the current winding of the amplidyne *AM* increases the excitation flux of the motor when the current exceeds the set value. As the speed of the motor rises, the setting is reduced by the amplidyne, one of which is connected to a voltage proportional to the field current. The amplification factor must be chosen for the extreme case viz. overloading in the beginning of the weakening of the excitation flux of the motor. The m.m.f. of the current winding must discontinue initiating a decrease of flux and effect its increase [2]. During this period the motor current may exceed the setting (error of the steady-state regulator) by a value ΔI, smaller than the difference between the setting of the first stage protection and the setting of the regulator.

In some cases, where it is desirable to have a large amplification coefficient of the regulation and to improve the characteristic of the drive, it is recommended to use an amplidyne in conjunction with a magnetic amplifier and filters similar to the arrangement shown in [4]. The large number of control windings of the magnetic amplifier enables all the feedbacks described to be connected up. When an amplidyne system without a magnetic amplifier is used, where the number of control windings (four windings) is not sufficient, the introduction of feedbacks into the motor field control system can be achieved by means of stabilizing transformers connected to the output of the amplidyne, which corresponds to the intermediate feedback and to the unbalanced bridge circuit connected to the field winding of the motor. The unbalanced system furnishes a m.m.f. consisting of two components one of which is proportional to the field current and the second, to the rate of change of the flux.

Testing the new system

The basic solutions of the new system passed a laboratory test; successful introduction of the new system into the industry has begun. On the plate mill 2800 at Voroshilovsk operating station the system shown in Fig. 7 has been used. The drive of the upper and the lower rolls was obtained from virtually independent systems, connected only through the windings of the amplidynes *AG* 1 and *AG* 2. The windings were connected to the difference of the voltage drops in the interpoles and the compensating windings of the motors, and also to the difference of the voltages of the two tachogenerators. The amplification factors of these amplidynes were very low, otherwise, there would have been a danger of loss of stability. On the other hand, a reinforcement of the stabilizing devices would lead to an inadmissible reduction of the intensity of the forcing of the basic transient processes owing to the common control channels. The balancing members operated very unsatisfactorily after the "cut-off" of the forcing when the voltage control system prevented its ac-

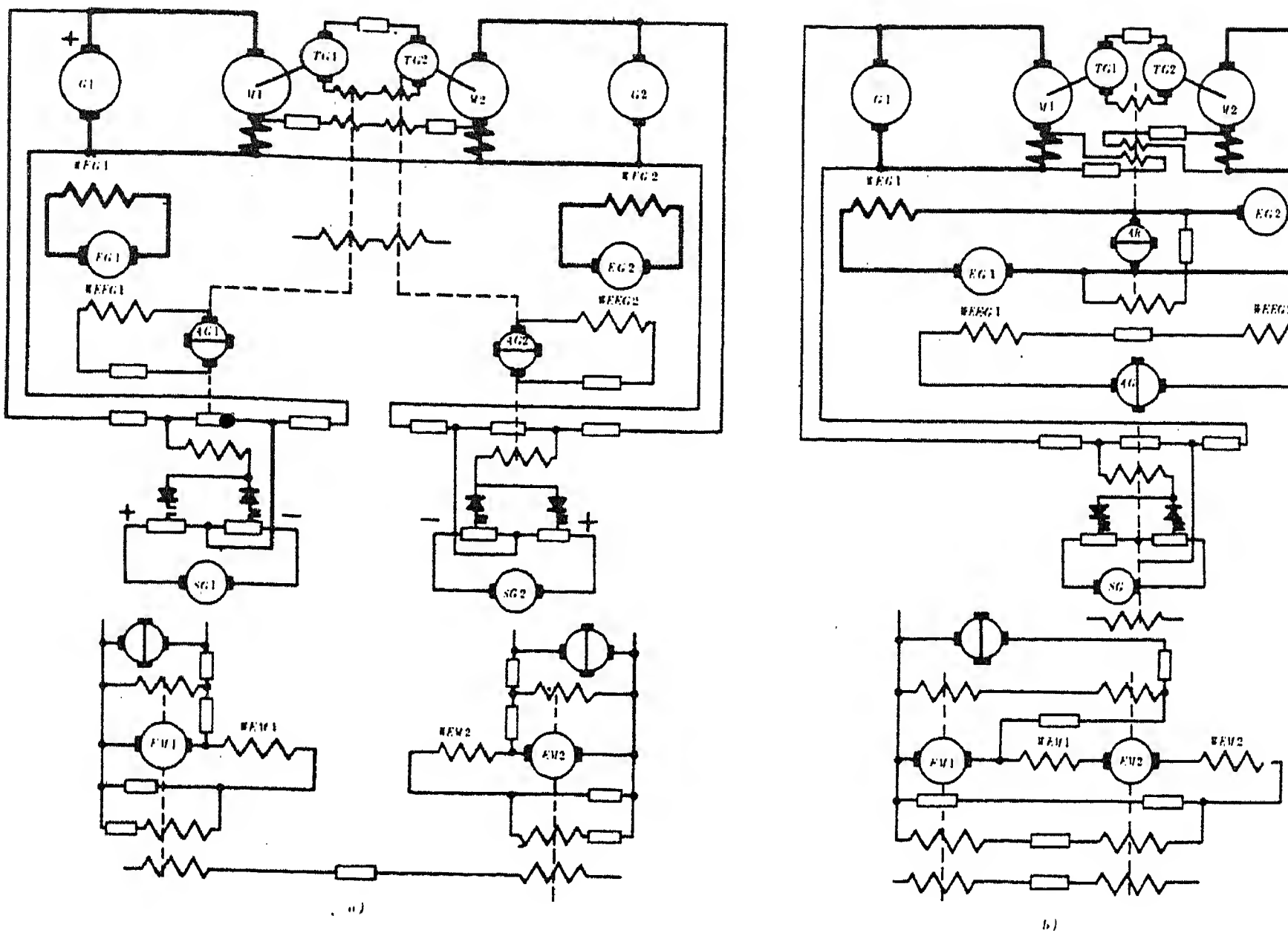

FIG. 7. Elements of the control system of the mill 2800.
a) before b) after modernization.

tion.

As a result of these shortcomings inadmissible bending of the ingots was observed during rolling and the difference in the motor loads reached 50 - 60% of the rating, and sometimes even higher values.

On our recommendations the system was altered to that shown in Fig. 7b. The exciters used in the original circuit and part of the amplidynes were retained. In the modernized ciruit the controller was connected into the diagonal arm of the bridge formed by the windings of the generators and the armatures of the exciters.

The system as a whole was considerably simplified, one amplidyne. one setting generator, scveral stabilizing transformers and other elements being eliminated as no longer required.

The positive results of the combination of the controls of the basic processes and the regulator performance are shown in the oscillograms Fig. 8.

Fig. 8a shows the rolling with disconnected regulator; the difference of the loads I_1 and I_2 was in this case smaller than that observed before modernization.

Fig. 8b shows the rolling with the regulator operating but with the winding acting on the difference in speeds disconnected. It follows from an analysis of the oscillogram that as a result of the regulator action the steady-state motor currents

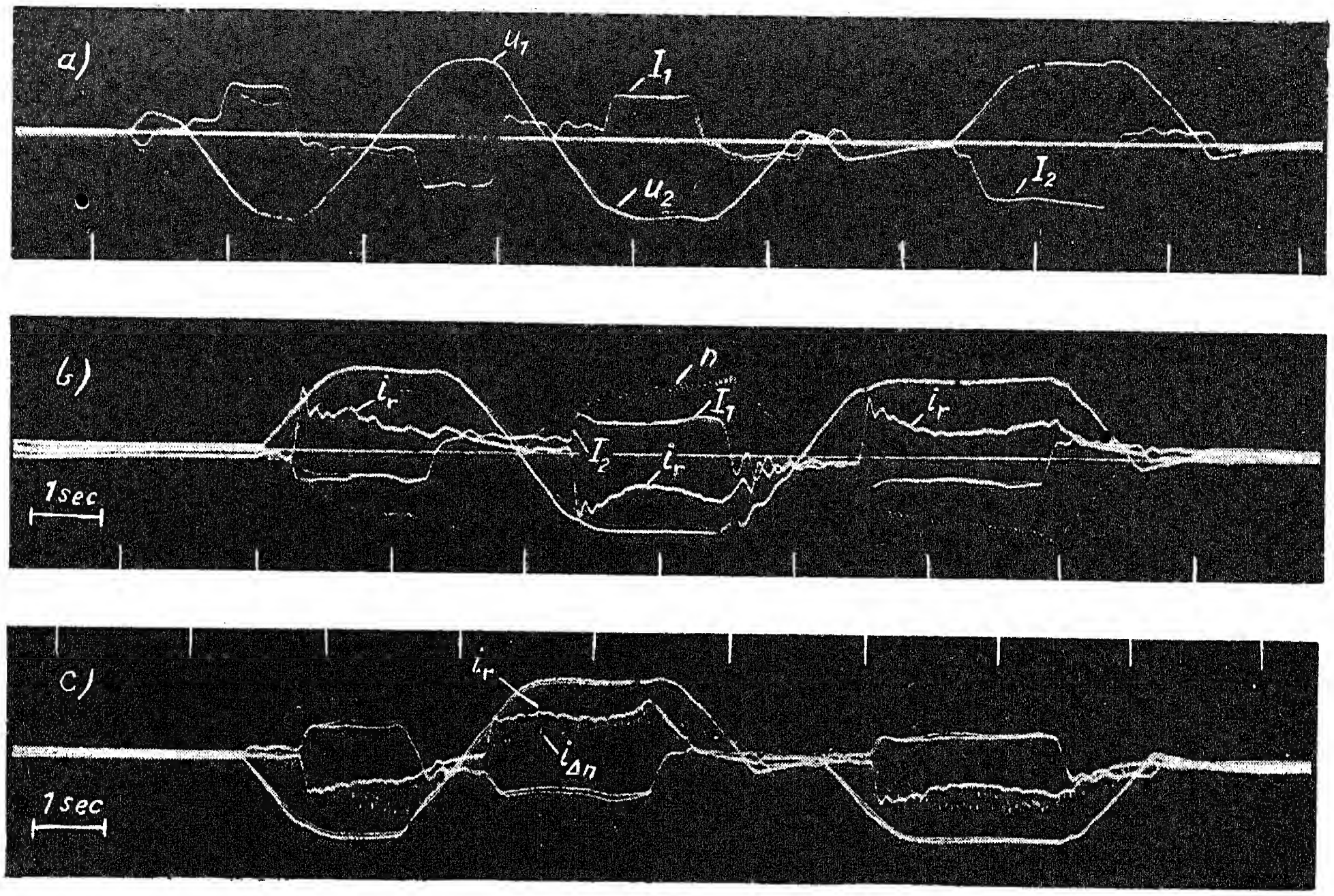

FIG. 8. Oscillogram of rolling operation on the 2800 mill after modernization. a - regulator disconnected b - regulator connected, but without the winding speed balancing c - regular connected with all its windings. U_1, U_2 - generator voltages; I_1, I_2 - motor currents; I_r - armature current of the amplidyne (regulator current) $i_{\Delta n}$ - current of the windings of the amplidyne AR connected to the difference of the tachogenerator voltages; n - motor speed.

during the rolling are sufficiently close together. The largest discrepancy between I_1 and I_2 is observed immediately after the gripping of the metal by the rolls, which is explained by the difference in speed between the upper and the lower roll during gripping. The regulator current i_r caused by the difference of the motor currents rises fairly steeply and leads to the balancing of the loads.

Fig. 8c shows the operation of the system with the regulator in action, all its windings being connected. It can be seen that as a result of the action of the windings responding to the difference of speeds (current $i_{\Delta n}$ shown) the generator voltages U_1 and U_2 differ very li ttle in no-load conditions and, consequently, the difference of speeds and the difference of the motor currents I_1 and I_2 is negligible.

The increase of the difference of the currents in steady-state conditions of rolling, caused by the effect of the speed-balancing windings is small and does not impair its positive effect under other conditions.

The results of the analysis of the control system of the rolling mill with independent drives of the rolls, the tests of the component circuits and also the experience with the modernization of the electric drive of the rolling mill 2800 at the Voroshilovsk works enable the new system to be recommended for newly planned or

reconstructions of existing rolling mills. The replacement of stabilizing transformers by differential-bridge circuits simplifies the control system and can improve the transient (dynamic) features of certain types of drives.

REFERENCES

1. O.V. Slezhanovskii; *Analysis of control systems of blooming mills by means of drooping characteristics. Elektrichestvo,* No. 3, (1953).
2. O.V. Slezhanovskii, *Analysis of the control system of a reversing rolling mill. Elektrichestvo,* No. 5, (1955).
3. V.V. Imedadze; *Investigation of systems of automatic regulation and control of the auxiliary mechanisms of blooming mills and large excavators.* Thesis (1953). *Lenin Library.*
4. A.G. Efanov,and Yu.R. Reungol'd, *Electric drives of large excavators. Elektrichestvo,* No. 4, (1956).

INVESTIGATION OF OVER-VOLTAGES DUE TO ARCING EARTH-FAULTS IN 6-10 kV SYSTEMS WITH INSULATED NEUTRAL *

N.N. BELYAKOV

(Received 4 September 1956)

The mechanism of the formation of over-voltages at arcing earth-faults in systems with insulated neutral or neutral earthed across high active or inductive resistance and the possible magnitude of these over-voltages is still not sufficiently known. It is believed that arcing fault over-voltages can reach 4-5 times the phase voltage and perhaps more.

In the power systems of the Soviet Union the over-voltages due to arcing earth faults are considered to be harmless for normal insulation i.e. insulation that withstands operational test voltages [1]. Actually, experience shows that with systematically conducted prophylactic tests and with planned routine maintenance of the system earth-faults on one phase are not followed by faults on the other phases. But deductions of the magnitude of the over-voltages from the puncture or flashover voltages of the insulation require caution. A wrong opinion of the magnitude of the over-voltages and their increased danger may be formed in poorly insulated systems, tems, especially cable systems in the absence of prophylactic tests [3].

The principle of the formation of the over-voltages during arcing was discovered by Petersen [4] who also estimated the maximum magnitude with consideration of the majority of the influencing factors including phase to phase capacitance and attenuation.

The behaviour of the arc is important, especially the moment of restrike and extinction, for a realistic estimate of over-voltages. The theories of the formation of over-voltages through arcing earth-faults put forward by different authors [4-7] are based on different assumptions of the arc properties. Petersen assumes that the arc extinguishes at the zero passage of the current of the natural oscillations ($i_{osc} = 0$) and strikes again at the next maximum of the power frequency voltage. Such idealization of the arc properties gives the severest possible conditions and therefore the upper limit of the over-voltages obtained by Petersen is doubtless correct.

* *Elektrichestvo* No.5, 31-36, 1957 [Reprint Order No. EL 20].

But none of the proposed theories has been verified by tests. One can often find in oscillograms the extinction of the arc in accordance with Petersen's theory ($i_{osc} = 0$) or with that of Peters-Slepian (at zero passage of the power frequency current i_p). For example oscillogram in Fig. 1 shows that the arc extinguishes several times at $i_p = 0$ (points 1, 3, 6), once at $i_{osc} = 0$ (point 5). Besides that extinctions after zero passage of the oscillating current are observed (point 4).

Thus the forms of behaviour of the capacitive arc are manifold. And the existing theories do not explain the phenomena actually occurring. The laws governing the extinction of the intermittent arc remain unexplained.

Ch. M. Dzhubarly did not obtain over-voltages exceeding 3 U_{ph} [8] in tests carried out at the TsNIEL, but his theoretical explanation of the limitation of the arc over-voltages is not convincing.

The purpose of the present article is to determine the properties and the behaviour of the capacitive arc in 6-10 kV systems from systematical tests and to establish the over-voltage level on the basis of these data.

Arc and over-voltage tests were made on system models with lumped capacitances. The basic 6 kV system was supplied through a 5600 kVA transformer 35/6 kV. Tests were also made in a 6 kV cable system without load.

The models permitted a variation of the test conditions over a wide range and the obtained over-voltages include a certain margin since in actual system condition the distributed capacitance and the attenuation will further reduce the over-voltages.

Greatest attention was given to systematical tests of the arc in air, drawn out by an isolator. Other tests were made with the arc across a pin-type insulator, in the slot of a machine, in a cable, under oil, in a cable joint, etc.

The extinction conditions of the capacitive arc

The character of the recovery of the voltage in capacitive circuits has a strong effect on the arc behaviour. The phenomena connected with the extinction of the capacitive arc may be considered for the case of the single-phase circuit, Fig. 2a.

The voltage at the unfaulted capacitance may be U_0 at the moment of zero passage of the current, when extinction takes place. After extinction the system neutral is displaced by the voltage value $U_{dis} = \frac{1}{2} U_0$. The voltage of the system generator is superposed to this. But the transition from the original condition ($U_f = 0$) to this new condition takes place in form of the extinction oscillations with the frequency $\omega_{osc} = 1/\sqrt{LC/2}$. In half a cycle of such oscillation ($T_{osc}/2$) after the zero passage of the current, the voltage across the arc gap reaches its first high-frequency maximum U_{om} (Fig. 3). The voltage reaches its second

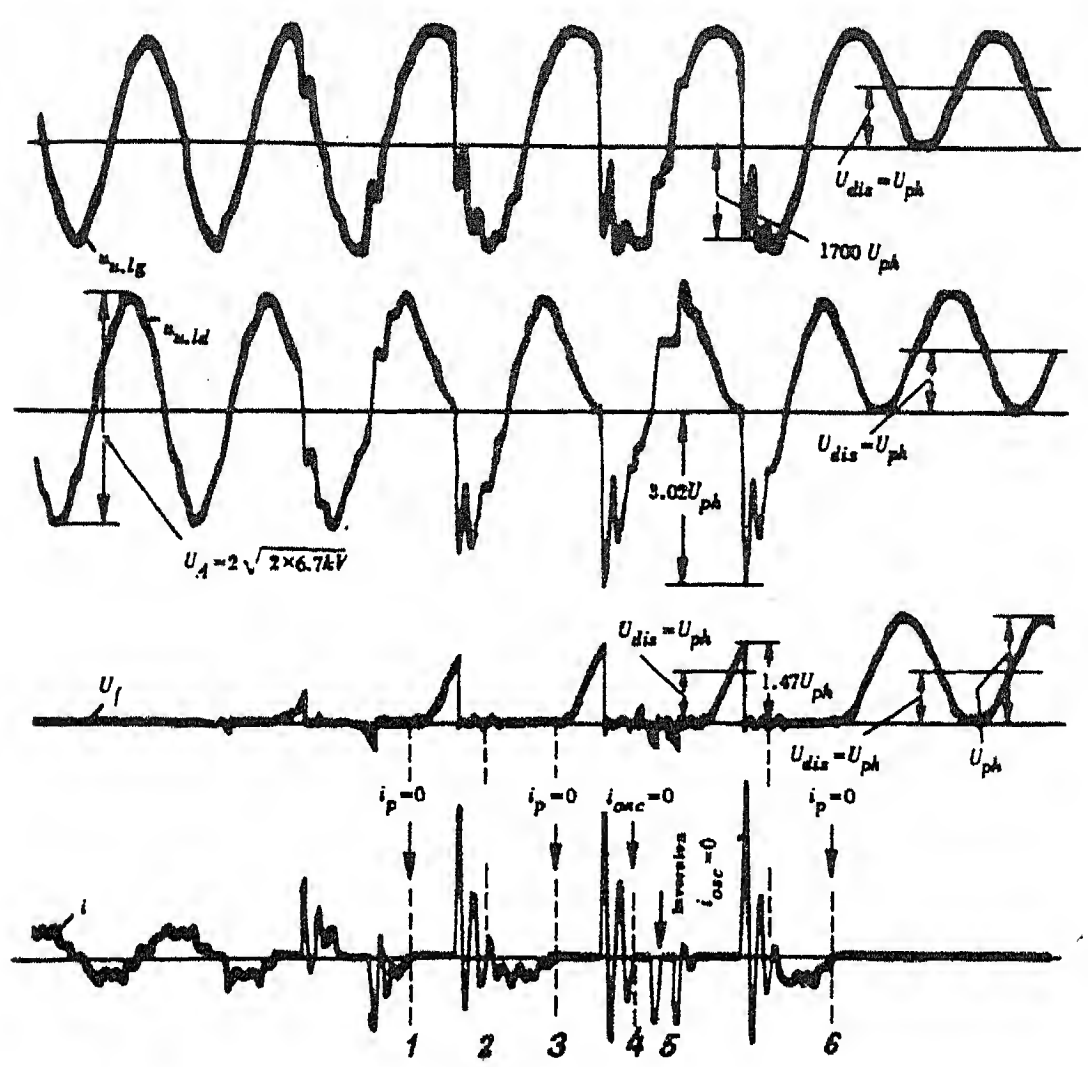

FIG. 1. Earth-fault in a three-phase system with insulated neutral.

Voltage 6 kV, Capacitive earth fault current $I_c = 105$A, phase-earth capacitance $C = 28.8\ \mu$ F, phase-phase capacitance $C_m = 0$. Transformer 5.6 MVA, 35/6 kV.

$u_{u,\,lg}$ voltage of the unfaulted phase, lagging behind

$u_{u,\,ld}$ - voltage of the unfaulted phase, leading the faulty phase.

u_f - voltage of the faulty phase.

i - arc current.

maximum as a result of the change of the generator voltage of power frequency.

The magnitude of the high-frequency maximum of the restriking voltage equals twice the difference between the displacement voltage and the phase voltage

$$U_{om} = 2\,(U_{dis} - U_{ph}) \tag{1}$$

Fig. 2a, shows that the voltage on the capacitance of the unfaulted phase at the moment of arc extinction differs from the generator voltage by the voltage drop across the inductance of the circuit, therefore

$$U_{dis} = \frac{U_0}{2} = \frac{2U_{ph} + L\left(\frac{di}{dt}\right)_{i=0}}{2}.$$

Substituting U_{dis} in (1) we obtain

$$U_{om} = L\left(\frac{di}{dt}\right)_{i=0}, \tag{2}$$

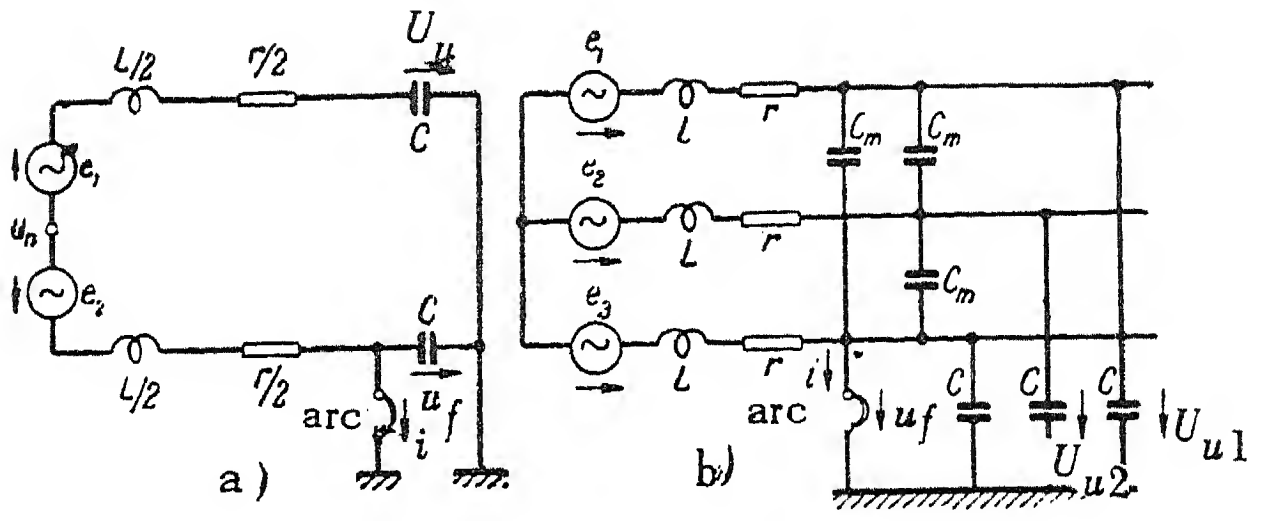

FIG. 2, Circuit diagram of the system with insulated neutral.
a - single-phase. $e_1 = U_{ph} \sin(\omega t + \psi)$ $e_2 = -U_{ph} \sin(\omega t + \psi)$
b - three-phase. $e_3 = -U_{ph} \sin(\omega t + \psi)$ - e.m.f. of faulty phase.
$e_1 = -U_{ph} \sin(\omega t + \psi - 120^0)$.
$e_2 = -U_{ph} \sin(\omega t + \psi + 120^0)$ - e.m.f. of the unfaulted phase.

i.e. the high frequency maximum of the restriking voltage equals the inductive voltage drop of the circuit at the moment of zero passage of the current. The relation (2) remains correct at any phase of the e.m.f. of the generating source at the extinction moment.

The recovery of the voltage after extinction of the earth-fault arc in a three-phase system with insulated neutral (Fig. 2b) has also the character shown in Fig. 3.

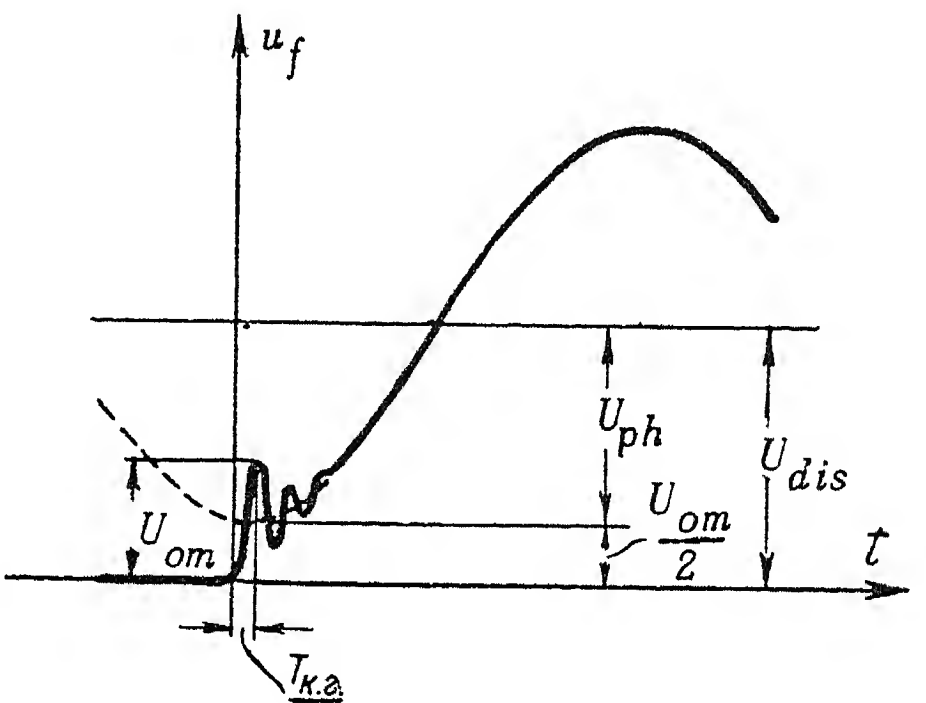

FIG. 3. Recovery of the voltage on the faulty phase after extinction of the capacitive current.

A more thorough examination of the arc extinction process by means of c.r.o. permitted to establish the following essential fact: The extinction of an open capacitive earth-fault arc takes place at each zero passage of the current but the arc strikes again within a small fraction of the natural oscillation cycle. The formation of the arc takes place following the breakdown of the gap before the first maximum (Fig. 4, points 1 - 5). With a large rate of rise of current this breakdown takes place long before the restriking voltage has reached its first maximum. This breakdown voltage may be designated as U_{bd}. The existence of the extinction and the rapidly following restrikes is also ahown by the fact that the current in the

oscillograms in every new half-cycle of the h.f. oscillations has a steep front which is explained by the surge of the discharge current of the capacitance of the faulty phase.

The conditions where the capacitive arc extinguishes after a long time interval (after a greater part of the power frequency cycle) are of major interest. Experiments show that this type of extinction is possible only when the first maximum of the restriking voltage does not exceed a certain critical value:

$$U_{om} \leq U_{cr} \tag{3}$$

This critical value U_{cr} obviously depends on the dielectric strength of the gap for the time interval of one half-cycle of the natural oscillations. If the condition (3) is not fulfilled the extinction is not achieved, i.e. the arc strikes again (Fig. 5).

In order to determine the numerical value of the critical voltage U_{cr} from the oscillograms it is necessary to determine the magnitude of U_{om} or U_{bd} for every passage of current zero. Fig. 6 shows the distribution of the frequency of occurrence of these values in general for all capacitive currents since the magnitude of the current has practically no effect on this distribution. The maximum values of U_{om} and U_{bd} differ only slightly from each other and it is possible to ascribe a common upper limit of 1800 V for both. This limit determines also U_{cr}.

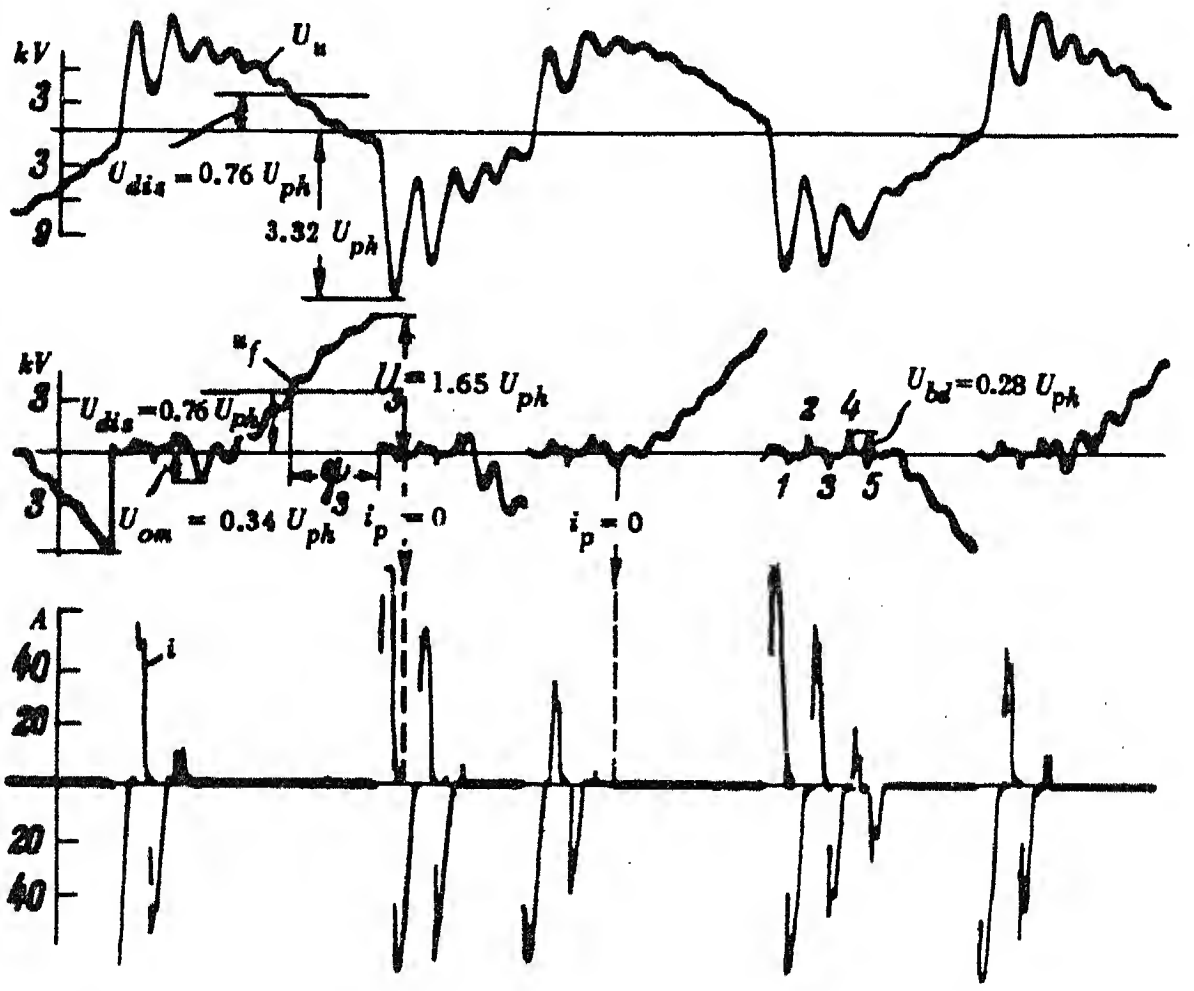

FIG. 4. Arcing earth-fault in the single-phase circuit with insulated neutral.
Arc on the isolator, $I_c = 4.4$ A, $C = 2\ \mu$ F, $C_m = 0$,
Transformer 5.6 MVA, 35/6 kV.

The experiments show that the velocity of drawing out the arc with the iso-

lator affects only the rise of the restriking voltage but not the extinction conditions. The fact that the current magnitude and the velocity of drawing out the arc have no effect on the extinction conditions of the capacitive arc is explained by the same growth in electrical strength of the gap in all cases during the short time intervals which possibly indicates the importance of the electrode effects and the thermal inertia of the arc column. All oscillograms with relatively high values of U_{om} and U_{bd} were used in the analysis of the test results. Besides that our distribution contains oscillograms of which more than 12,000 extinctions have been recorded with values of U_{om} and U_{bd} below the obtained maximum.

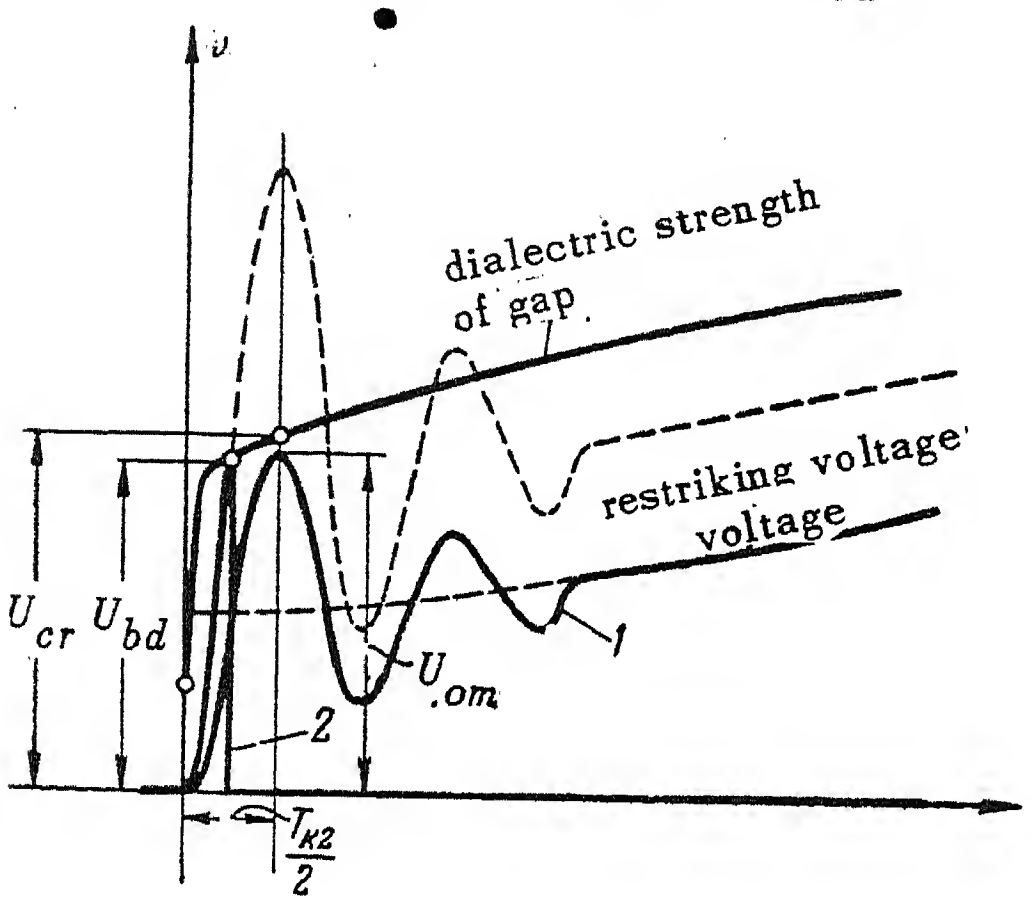

FIG. 5. Extinction and restriking of the arc.
1 - extinction achieved, 2 - extinction not achieved.

The task is to determine the upper limit U_{cr}. Therefore, one has to set out from the minimum oscillating frequency possible in practice. The above value of U_{cr} was obtained from tests in which this frequency was reduced down to $\omega_{osc} = 5\ \omega$ although in actual systems this value is ten times the power frequency or more.

The above value of U_{cr} is $0.37\ U_{cr}$ for 6 kV and $0.22\ U_{ph}$ for 10 kV systems. For simplification of the calculations and also for inclusion of some margin in the estimate of the possible over-voltages we assume for 6 and 10 kV systems $U_{cr} = 0.4\ U_{ph}$ *

We see that

$$U_{om} \leq 0.4\ U_{ph} \qquad (4)$$

The tests with the arc across a pin-type insulator, in the machine insulation, in a cable, under oil and in a cable joint give a relation between U_{om} and U_{ph} close to that obtained with the arc across the isolator. Therefore, the magnitude of the h.f. maximum of the restriking voltage U_{om} remains the limit under different conditions of striking the arc and the maximum over-voltages are the same as with the arc across the isolator.

The arc in the cable and in the machine insulation has a low striking voltage

* Our rounding off means in the case of 10 kV systems an increase in the over-voltage magnitude of 3%.

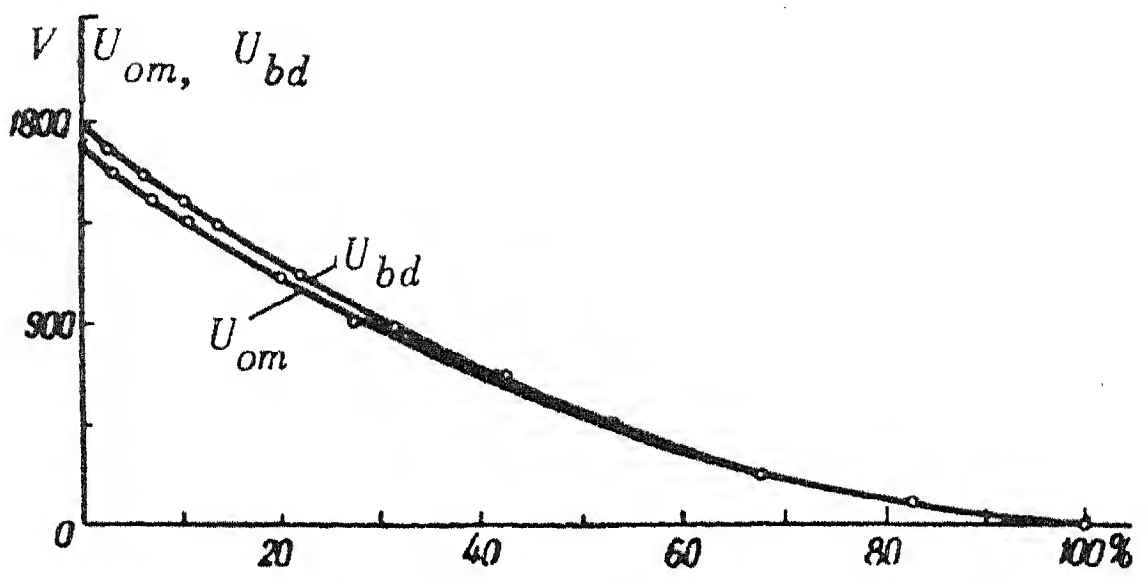

FIG. 6. Distribution curve of the values of U_{om} and U_{bd} (plotted on the basis of 2800 extinctions).

($U_s < U_{ph}$) and its magnitude hardly changes while the arc is burning. The arc can stay for a very long time.

Maximum over-voltages

The important value of the displacement voltage U_{dis} of the neutral (the general potential of the system with respect to earth after arc extinction) is limited owing to the limitation of the voltage U_{om}. Actually Fig. 3 shows that

$$U_{dis} \doteq U_{ph} + \tfrac{1}{2}\, U_{om} \tag{5}$$

and since $U_{om} \leq 0.4\, U_{ph}$, that always

$$U_{dis} \leq 1.2\, U_{ph} \tag{6}$$

Equations (5) and (6) are valid for single-phase and three-phase systems. The magnitude of the over-voltages can be determined from the formula

where $$U_{max} = U_{fin} + (U_{fin} - U_{in}) \frac{C}{C + C_m} (1 - d), \tag{7}$$

U_{fin} and U_{in} are the final and initial voltages;

C and C_m are the phase-earth and phase-phase capacitances

$\frac{C}{C + C_m}(1 - d)$ -- is the coefficient taking account of the decrease in amplitude owing to phase-phase capacitance and attenuation.

The tests show that the main cause of attenuation is not the loss in the arc, as it was considered to be by some investigators [8], but the losses in the other parts of the circuit. With metallic fault connection no decrease of the attenuation was observed as compared with the intermittent arc. With the drawn out arc the arc

voltage drop was very often considerably smaller than the source-voltage (50 - 100 V against 6000 V) even up to the moment of final extinction. Thereby the coefficient $(1-d)$ may be about 0-98 - 0.99 [7, p. 530]. During the tests on the models the highest value of $(1-d)$ was 0.9. This value should be taken for the determination of the maximum over-voltage since the attenuation in actual systems is even greater.

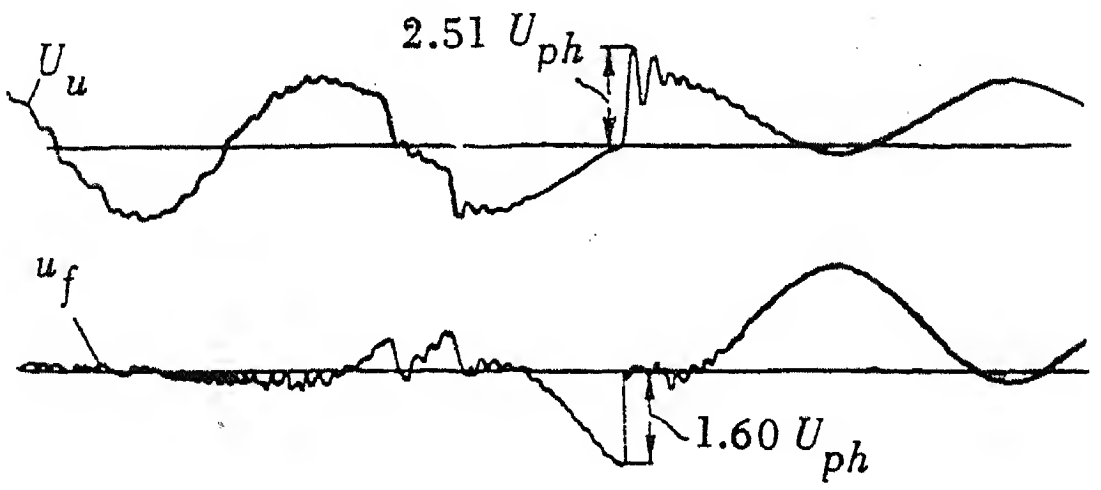

FIG. 7. Arcing fault in a single-phase system with insulated neutral (arc under oil).
$I_c = 11$ A, $C = 5\ \mu$F, $C_m = 0$. Transformer 3.2 MVA, 35/6 kV; u_u voltage of the unfaulted phase, u_f voltage of the faulty phase.

The tests show that restriking can take place at any moment including the moment for which the over-voltage becomes highest.

Thus, knowing the magnitude of the displacement voltage and the attenuation coefficient and assuming that the restriking takes place at the moment which produces the highest over-voltage, one can determine the maximum over-voltage.

Assuming that restriking takes place at the moment of maximum e.m.f. of the faulty phase with the same sign as the displacement voltage we obtain for the single-phase circuit and for $C_m = 0$

$$U_{in} = U_{ph} - 1{,}2U_{ph} = -0{,}2U_{ph}$$

and

$$U_{max} = 2U_{ph} + [2U_{ph} - (-0{,}2U_{ph})]\,0{,}9 \approx 4U_{ph}$$

Applying (7) to the three-phase circuit we consider that the e.m.f. of the faulty phase changes according to the law $e_f = -U_{ph} \sin(\Omega t + \psi_s)$ whereby the time is counted from the moment of restrike. We determine the magnitude of the positive over-voltage on the unfaulted phase ($U_{max} > 0$) which is lagging behind the faulty phase. Considering that for the formation of such over-voltage the restrike must occur with negative e.m.f. of the faulty phase and that with a negative displacement voltage ($U_{dis} < 0$) we obtain

$$U_{in} = -U_{ph} \sin(\psi_3 - 120°) + U_{dis} = U_{ph} \cos(30° - \psi_3) + U_{dis}$$

$$U_{fin} = \sqrt{3} U_{ph} \sin(\psi_3 + 30°);$$

$$U_{max} = \sqrt{3} U_{ph} \sin(\psi_3 + 30°) + (U_{ph} \sin\psi_3 - U_{dis}) \frac{C}{C + C_m}(1 - d). \qquad (8)$$

The maximum over-voltage occurs on restrike at

$$\psi_s = \tan^{-1}\left[\frac{2}{\sqrt{3}}\frac{C}{C+C_m}(1-d)+\sqrt{3}\right]$$

With $C_m = \frac{1}{3} C$, which is characteristic for 6 - 10 kV cable systems and $(1-d) = 0.9$ and more, the maximum over-voltage would occur on restrike at $\psi_s = 68°$, i.e. when restriking occurs somewhat before the maximum of the voltage. Substituting in (8) the values: $(1-d) = 0.9$, $C = 3C_m$, $\psi_s = 68°$ and $U_{dis} = -1.2\ U_{ph}$, we obtain for the maximum overvoltage:

$$U_{max} = 3.2\ U_{ph}.$$

On the faulty phase the over-voltage may reach the value:

$$U_{max,f} = U_{dis} + U_{ph} = 2.2\ U_{ph}.$$

The formation of the maximum over-voltage in a three-phase system is illustrated in Fig. 8.

For verification of the calculated maximum over-voltage mass observations were made with c.r.o. with very small time scale. An oscillogram thus obtained in a single-phase circuit is shown in Fig. 9.

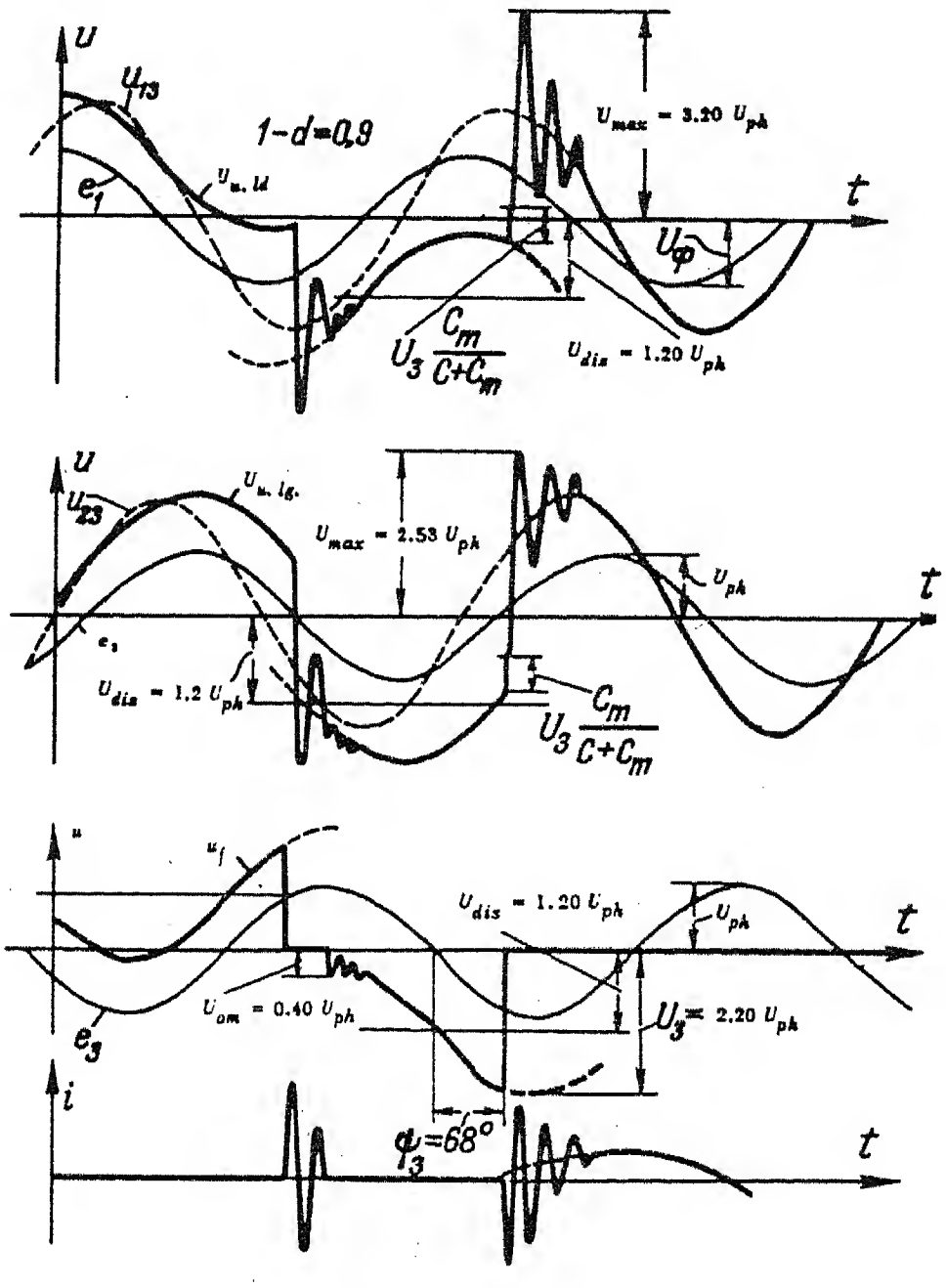

FIG. 8. Formation of the maximum possible over-voltage in a three-phase system with insulated neutral.

Symbols (u_u, $lg\ u_u$, ld, u_f, i) as in Fig. 1.

The calculated and measured over-voltage values for the three-phase circuit are given in the table, which shows that the measured values are in good agreement with the calculated ones. The maximum over-voltages are practically independent of the capacitive current and are relatively rare since several conditions must coincide for their formation.

		$I_c = 7.5$ A $C = 2\mu$F		$I_c = 23$ A $C = 6\mu$F		$I_c = 45$ A $C = 12\mu$F		$I_c = 100$ A $C = 30\mu$F		
Calculated Values	C_m μF	U_{max}	$U_{max, f}$	U_{max}	$U_{max, f}$	U_{max}	$U_{max, f}$	U_{max}	$U_{max, f}$	Number of faults
3.62	0	3.45	2.00	—	—	—	—	—	—	200
3.62	0	—	—	3.30	2.02	—	—	—	—	100
3.20	2	—	—	2.91	2.15	—	—	—	—	200
3.62	0	—	—	—	—	3.50	2.10	—	—	200
3.20	4	—	—	—	—	3.05	2.14	—	—	300
3.62	0	—	—	—	—	—	—	3.44	2.12	100

The actual mechanism of the formation of the over-voltages

Extinction takes place when the h.f. maximum of the restriking voltage is sufficiently small and therefore also the rate of change of the current is sufficiently small at the zero passage. This is the case for the first zero of the oscillating current (usually with small striking voltage) and after some attenuation of the transient process. Arc extinction is also possible after transition of the oscillating current into the power frequency current, especially when the latter goes through zero.

For the formation of the maximum over-voltage it is not necessary to have a number of restrikes. Therefore, it is sufficient for its determination to consider one cycle extinction-restrike. In that cycle the extinction must take place at the moment of maximum e.m.f. of the faulty phase and at the maximum rate of change of the current permitted for the extinction, and the following restrike must occur somewhat before the voltage peak. The cause of the often observed increase of the over-voltage towards the end of the arcing time is not the cumulative effect (i.e. the increase of the displacement voltage) but the gradual increase of the striking voltage owing to the increased arc length.

The increase of the displacement voltage of the neutral is connected with the simultaneous increase of the h.f. maximum of the restriking voltage. The actual arc gap cannot withstand a rapid increase of the restriking voltage so that the possible maximum of the oscillation is limited and consequently also the displacement voltage. Thus, the limit to the over-voltage is set by the finite and relatively low electric strength of the arc gap which by the very nature of the phenomenon

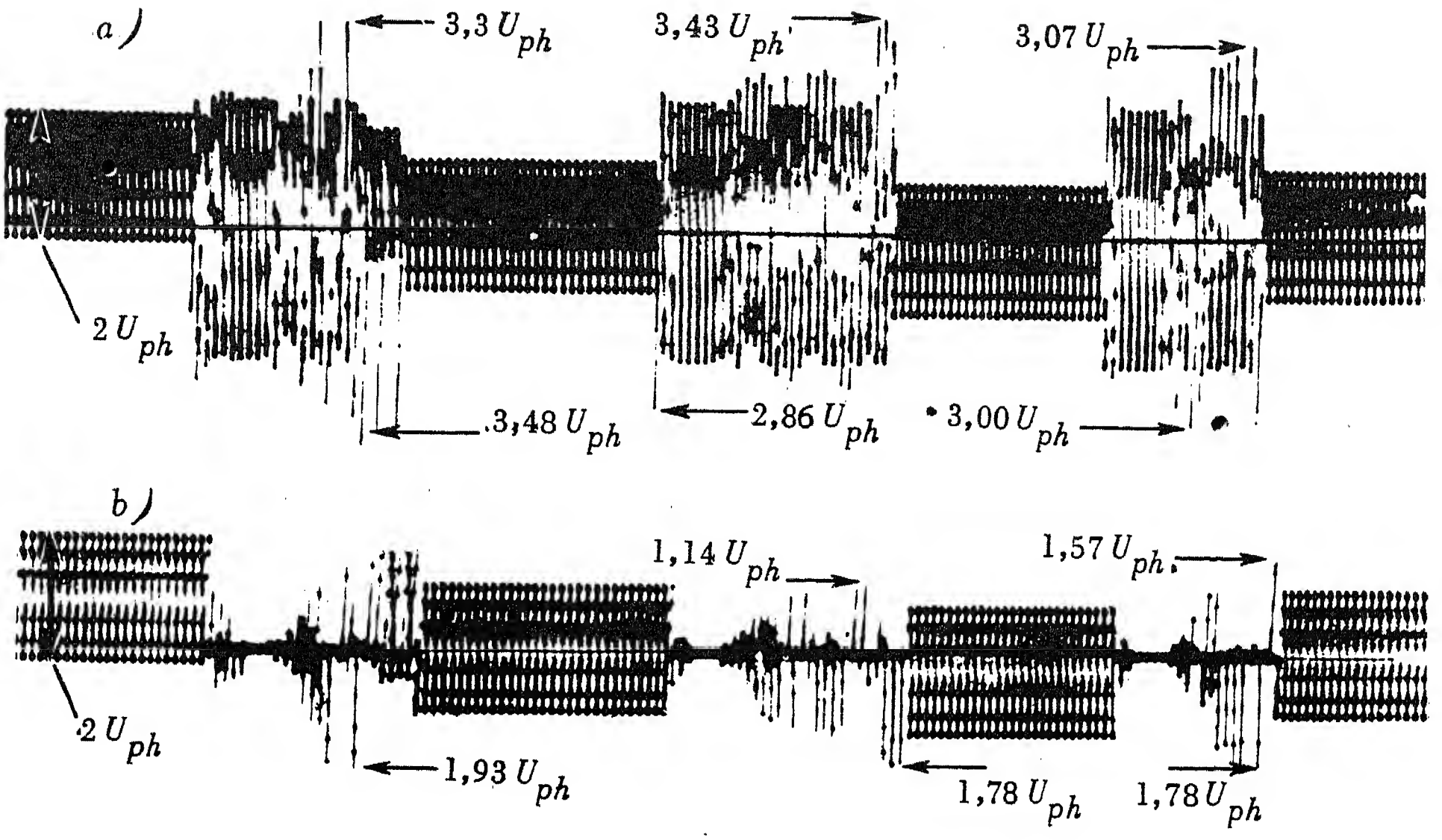

FIG. 9. Values of the over-voltages in the single-phase circuit with insulated neutral. $I_c = 55$ A, $C = 25.3\ \mu F$, $C_m = 0$. Transformer 3.2 MVA, 35/6 kV. a - voltage of the unfaulted phase, b - voltage of the faulty phase.

cannot de-ionize instantly.

The attenuation coefficient (1 - d), obtained in a cable system of 6 kV, with load, is 0.7 - 0.75. It is naturally smaller than on the model. The resistance of the current path of the natural oscillations has a strong effect on the attenuation in actual systems. The effect can be so strong that the actual system may be incapable of oscillating. This is the case when the earth-fault in a system with high capacitive current occurs at a point remote from the centre. This is illustrated by the oscillogram, Fig. 10, *) obtained in a system with a capacitive earth-fault current of 100 A. The earth-fault occurred at a point in the system remote from the supplying busbars. The transient process after striking is aperiodic. The voltage of the unfaulted phase did not exceed the phase-earth voltage, i.e. over-voltages did not occur.

Conclusion

The laws governing the extinction of the intermittent earth-fault arc and the possible magnitude of the over-voltages under different conditions of the arc (including different system voltages) are found by determination of the electric strength of the arc gap immediately after extinction and its comparison with the magnitude of the h.f. maximum of the restriking voltage.

* The oscillogram was kindly offered by F.A. Likhachev (ORGRES).

The extinction of the capacitive arc is not controlled by the frequency of the natural oscillations nor by the power frequency. Extinction takes place if the h.f. maximum is below a certain value. The extinction conditions set a limit to the displacement voltage of the neutral.

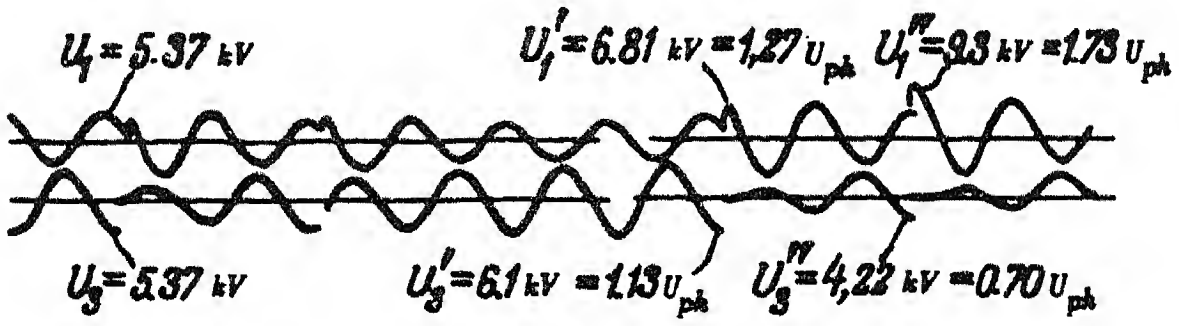

FIG. 10. Arc fault on an insulator in a compensated system, 6 kV, with load.
U_1 voltage of the unfaulted phase, U_3 voltage of the faulty phase. Degree of mistuning $v = -9$ per cent.
Earth fault current $I_e = 9.6$ A.

Since the check tests under different conditions of arc formation agree with the results of arc tests on an isolator, a general conclusion can be drawn on the magnitude of the over-voltages caused by earth-fault arcs in 6 - 10 kV systems with insulated neutral. The maximum values of these over-voltages do not exceed 3.2 U_{ph} and they are not directly dependent on the magnitude of the capacitive current. They occur relatively rarely since for their formation several conditions must be fulfilled simultaneously. With large capacitive currents the arc may remain more stable and thus reduce the over-voltages.

The author is indebted to V.V. Burgsdorf for a number of valuable suggestions in the preparation of the present article.

REFERENCES

1. *On the operating conditions of the neutral earthing and the protection against earth-faults in 6 - 35 kV systems. A solution of the Technical Department of the Ministry of Electric Power Plants*, No. 89/3 of 28.5.1949. *Elekt. Stantsii*, No. 10, (1949).
2. I.A. Syromatnikov; *Operating conditions of the system with small earth-fault currents. Elekt. Stantsii*, No. 2, (1951).
3. N.N. Belyakov; *Analysis of damage from earth-faults in cable systems. Elekt. Stantsii*, No. 6, (1952).
4. W. Petersen; *Der aussetzende Erdschluss. ETZ*, No. 47, 553, No. 48, p. 564, (1917).
5. J.F. Peters, J. Slepian; *Voltages induced by arcing grounds, Trans. AIEE*, p.478, (1923).
6. P. Steinmetz; *Frequency conversion by arcing class conductor and mechanism of the arcing ground. Trans. AIEE*, p. 470, (1923).
7. R. Rudenberg; *Transient processes in electric power systems. Izdatel'stvo inostrannoi literatury*, (1955).
8. Ch. M. Dzhuvarly; *On the theory of over-voltages from earth-fault arcs in systems with insulated neutral. Elektrichestvo*, No. 6, (1953).

ARC-QUENCHING PROCESSES IN AIR-BLAST CIRCUIT-BREAKERS*

V. GUSA and Ya. TSIGELKA

(Received 1 August 1956)

The increasing powers of modern electrical systems account for a corresponding increase of the breaking capacity of the h.v. circuit-breakers, particularly the air-blast breakers, the use of which is spreading all the time. The present communication proposes to investigate the factors influencing the quenching of the arc in air-blast circuit-breakers and the practical methods available for increasing the breaking capacity of these breakers.

The experiments were carried out on circuit-breakers of type SR, rated at 10 kV. The design of the quenching arrangement of this breaker type is shown in Fig. 1 and the main parameters given in the following Table.

Breaker type	Rated air pressure abs. atm.	Nozzle diameter (d) mm	Travel of moving contacts. (l) mm
SR205 – 10/600	12	22	185
SR405 – 10/600	12	35	210
SR605 – 10/600	21	45	225

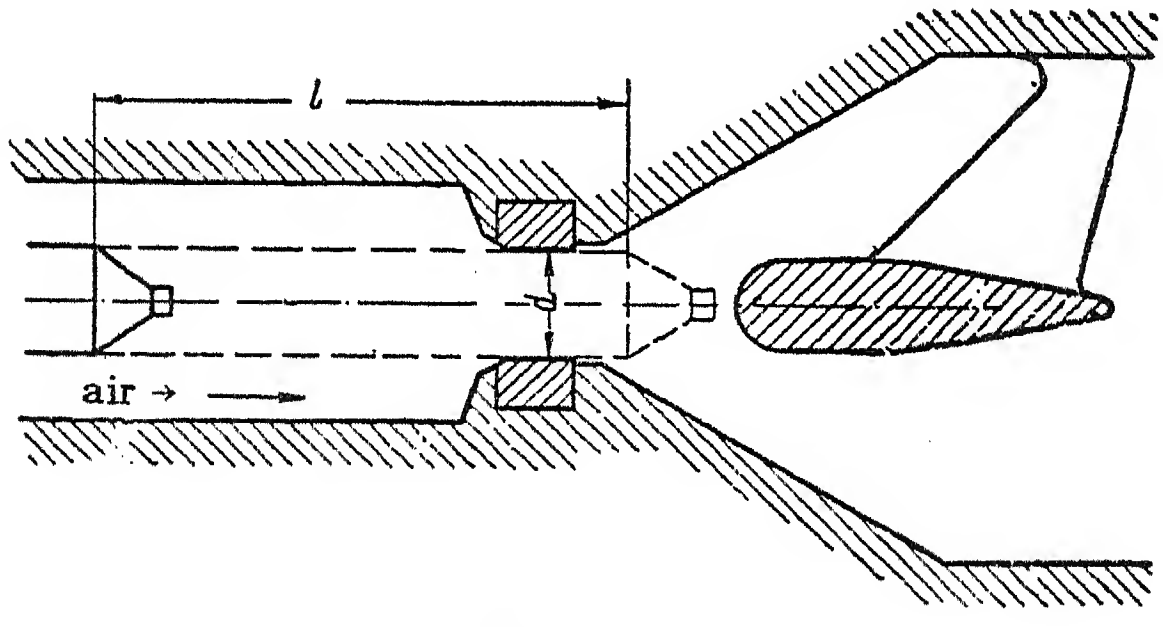

FIG. 1.

* *Elektrichestvo* No. 5, 37-39, 1957 [Reprint Order No. EL 21].

Tests on the clearance of single-phase short-circuits, carried out at 9 kV and at a frequency of the restriking voltage of 4.5 kc/s produced results which can be represented by the following empirical formula,

$$I_{sh} = 5.35\, p^{0.30} F^{0.54}, \qquad (1)$$

where, I_{sh} is the amplitude value of the limiting short-circuit current cleared, kA;
p the air pressure in the air receiver of the circuit-breaker, abs. atm.;
F cross-sectional area of the nozzle, cm².

This relationship is graphed for the pressures of 12 and 21, abs. atm. in Figs. 2 and 3.

The limiting breaking current, represented by (1) corresponds to the current at which the nozzle of the breaker is pluged by the thermal energy evolved by the

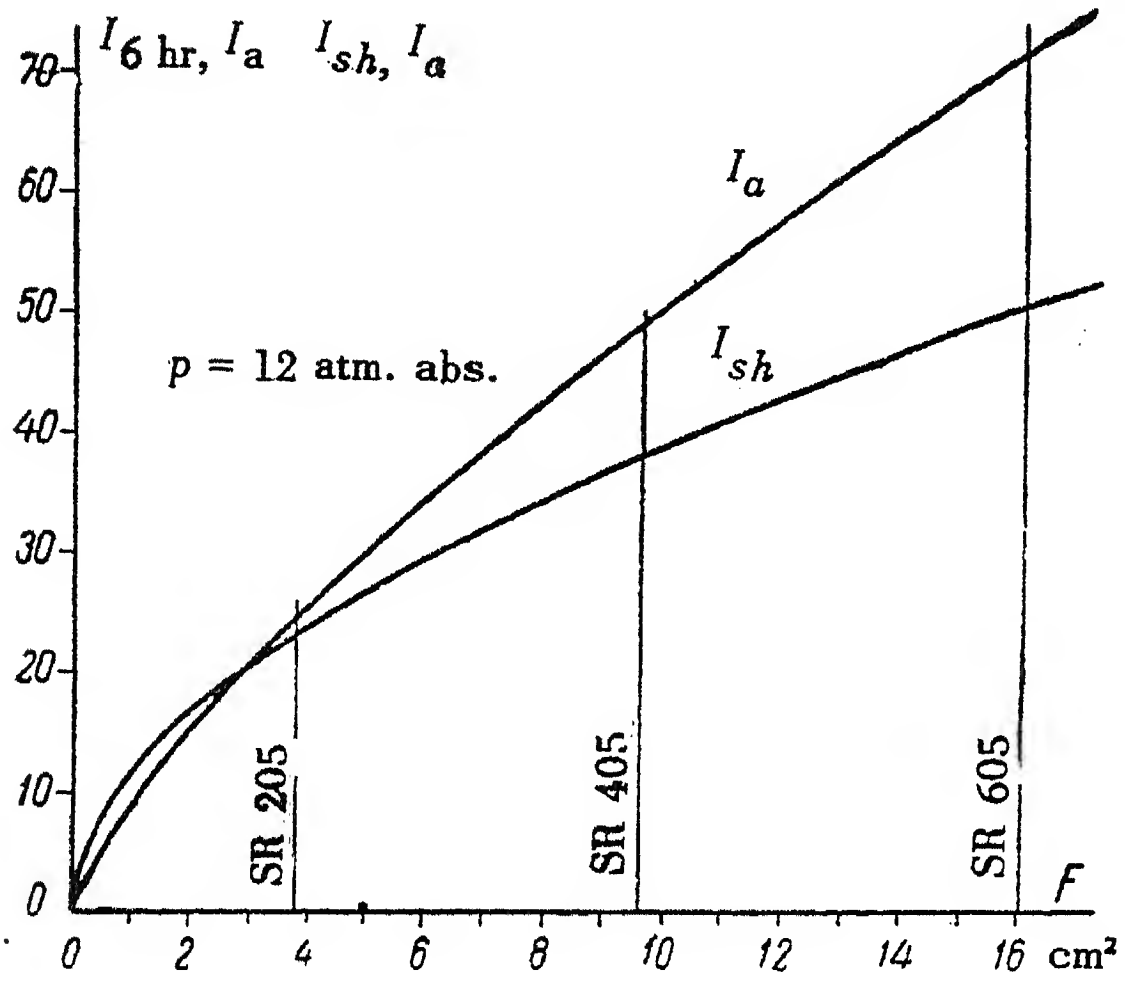

FIG. 2.

FIG. 3.

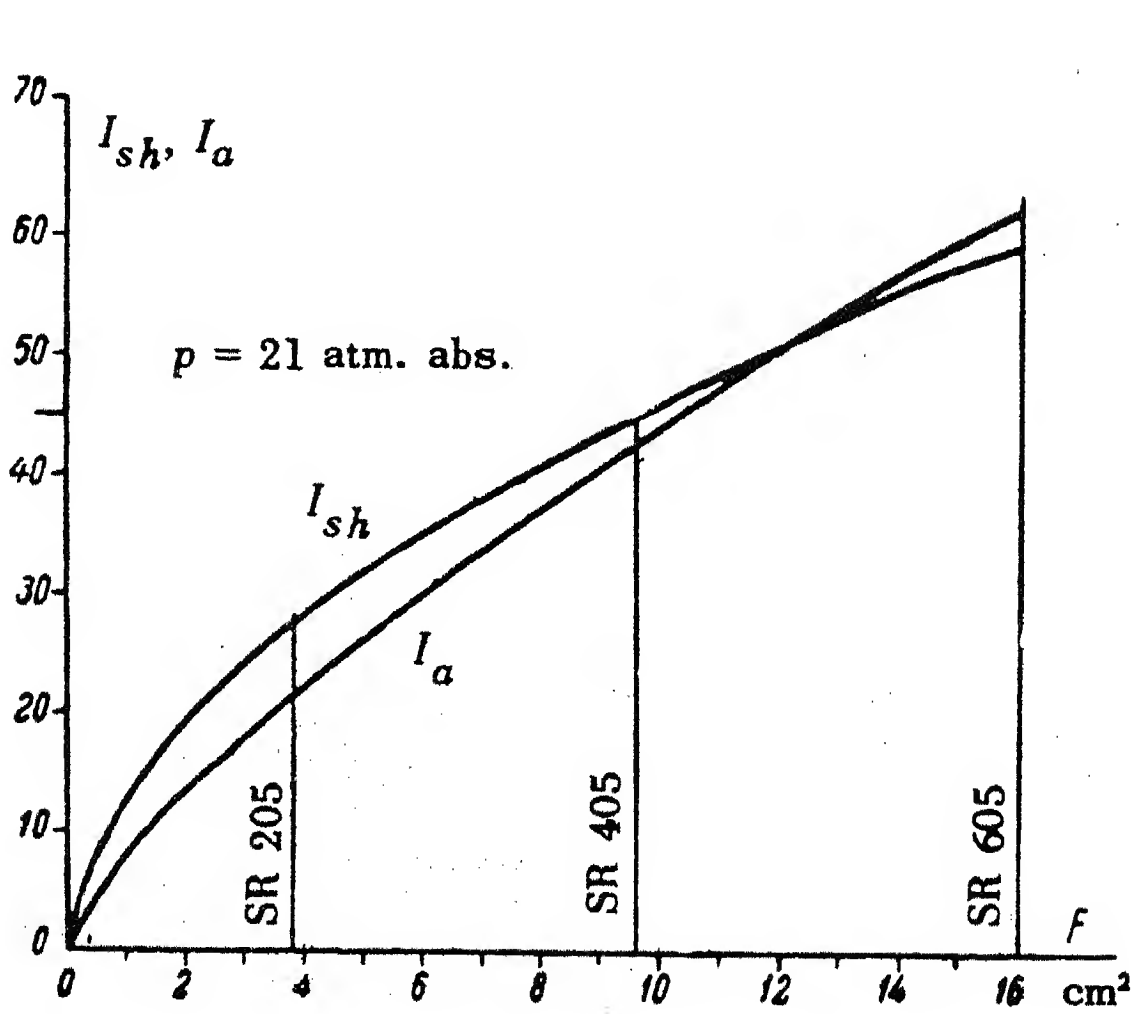

arc. This phenomenon is generally interpreted in the following way.

Evolution of heat by the arc reduces, as it were, the cross-section of the nozzle, this reduction of the effective cross-section being the greater, the higher the current passing through the circuit breaker. The reduction of the cross-section of the nozzle entails a corresponding reduction of the air supply for arc quenching, so that at a certain magnitude of the short-circuit current the circuit breaker will no longer be able to interrupt this current; in other words, the nozzle of the circuit-breaker is plugged.

It is clear that for equal values of the breaking-current the phenomenon of nozzle-plugging will be more marked at smaller nozzle diameters, i.e. smaller nozzle diameters will reduce the breaking capacity of the given circuit-breaker.

However, experiments showed that the magnitude of the limiting breaking current does not always correspond to the volume given in (1). For example, a breaker of type SR205 at pressure 21 abs. atm. of the quenching air can interrupt a current of 42 kA as against 19.5 according to (1).

To find the causes of this surprising increase of the breaking current during the circuit-breaker tests, we carried out measurements of the voltage drops in the arc. These measurements showed that for the short-circuit current of 30 kA the voltage drop in the arc after the zero-passage of the current begins to rise steeply, falling again with similar abruptness after reaching a certain value, to rise again only immediately before the end of the half-period of the current curve (Fig. 4,a). At a current of 15 kA there are no such "breaks" in the curve of the voltage in the arc (Fig. 4,b). This phenomenon may be interpreted as follows. At every instant the diameter of the arc depends on the current in the arc at that instant and so long as the arc diameter is small, the arc will burn, being drawn out to a comparatively great length (Fig. 5,a). The voltage drop in the arc will then have a certain value. When the current increases, there will be an instant at which the actual diameter becomes equal to the diameter of the nozzle, in this case the length of the arc is considerable reduced and the arc fills out completely the nozzle opening. This is the instant at which the nozzle is plugged by the arc column (Fig. 5,b). This causes a considerable decrease of the voltage drop in the arc.

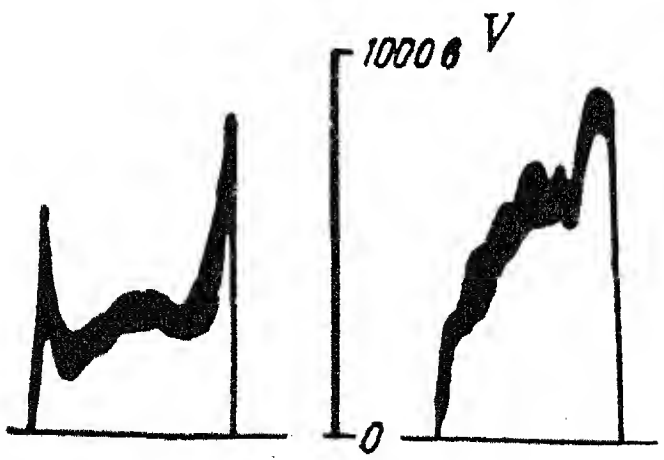

FIG. 4.

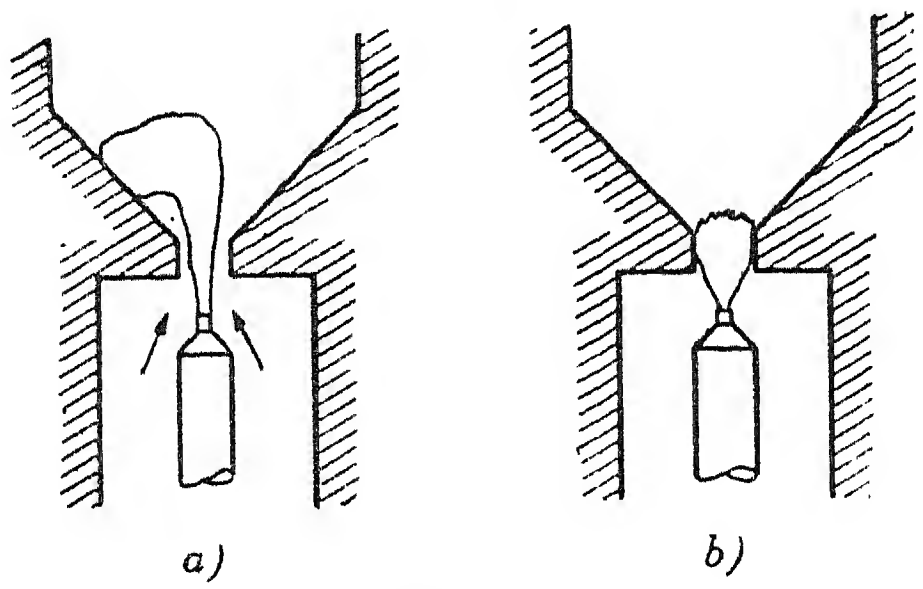

FIG. 5.

Later on the current, having passed through its peak value, falls with a simultaneous reduction of the diameter of the arc column and at a certain value of the current the arc diameter becomes again smaller than the diameter of the nozzle opening. At this instant the air pressure detaches the arc from the walls of the nozzle and draws the arc out; the voltage drop in the arc increases again.

The plugging of the nozzle interrupts the air flow, as the result of which the pressure of the air before the nozzle increases to the value of the pressure in the air receiver. The great difference of the pressures before and behind the nozzle quickly restores the maximum velocities of the air flow once the nozzle is free again, which leads to rapid arc-quenching.

We find, therefore, that the plugging of the nozzle by the arc column is a positive factor acting towards an increase of the limiting breaking-current. It is by this phenomenon that we can explain the increase of the limiting breaking current of the circuit breaker type SR205 at the pressure 21 abs. atm. as against the value obtained from (1).

On the other hand, we have to consider that at an increase of the short-circuit current the time interval between nozzle opening and zero-passage of the current is reduced which, in the last result prevents the velocity of the air flow from reaching the values required for arc-quenching, so that the circuit-breaker can no longer clear the short-circuit currents.

Let us analyse the phenomenon of the nozzle-plugging by the arc column. We assume that the arc is a cylindrical absolutely black body whose temperature, and consequently, charge density is constant over the cross-section. The stage of ionization of the gas in the column may be expressed in Saha's equation

$$\frac{x^2}{1-x^2}\cdot p = 3.2\cdot 10^{-7} T^{2.5} e^{-\frac{eE_i}{kT}}, \qquad (2)$$

where x is the stage of ionization of the gas;
p the gas pressure, abs. atm.;
E_i the ionization potential, V;
T the temperature, °K;
ϵ the electron charge, coulomb;
k Boltzmann's constant.

In (2) the quantity x^2 may be neglected against unity. The justification of this assumption will be shown below. The relation between the stage of ionization and the current density in the arc may be found from the following equations

$$x = n/N \text{ and } n = j/\epsilon E b^-$$

where n is the number of electrons in 1 cm³ of gas;
N the initial number of neutral atoms in 1 cm³;
j the current density in the arc;
E the electric gradient in the plasma;
b the electron mobility.

Remembering that,

$$b^- = \sqrt{\frac{T}{T_0}} \cdot \frac{p_0}{p} b_0^- \quad \text{и} \quad N = \frac{T_0}{T} \cdot \frac{p}{p_0} N_0,$$

where $P_0 = 1$ abs. atm.;
$T_0 = 273^0$K;
$b_0 = 5.9 \times 10^3$ cm²/V. sec;
$N_0 = 2.7 \times 10^{19}$ 1/cm³, or considering that for nitrogen $\epsilon E_i/k = 1.68 \times 10^5$ we get after rearrangement the equation of the arc current, viz

$$I_\partial = 238 \cdot EF \frac{1}{\sqrt{p}} T^{0.75} e^{-\frac{8.4 \cdot 10^4}{T}} \tag{3}$$

where F is the cross-section of the arc in cm².

The energy radiated from the surface corresponding to unit length of the arc is determined by Stephan-Boltzmann's law on the assumption that convection at high temperatures is so insignificant as against radiation, that it may be neglected, viz.

$$EI_\partial = CT^4 \cdot \pi d \cdot 10^{-7} = 2CT^4 \sqrt{\pi F} \cdot 10^{-7}, \tag{4}$$

where d is the diameter of the arc in cm;
$C = 5.73 \times 10^{-5}$.

Considering that the arc current $I = jF$ and solving simultaneously equations, (3) and (4) we get

$$I_\partial = 6.94 \cdot 10^{-5} p^{-0.25} F^{0.75} T^{2.375} e^{-\frac{4.2 \cdot 10^4}{T}}. \tag{5}$$

The results of measurements carried out on a circuit-breaker of type SR205 at a pressure of the quenching air of 21 abs. atm., showed that the plugging of the nozzle by the arc column occurs at the instant at which the instantaneous value of the short-circuit current is 21.2 kA. Assuming that up to the instant of complete plugging of the nozzle the air pressure before the nozzle rises to the value of the pressure in the air receiver of the circuit-breaker, i.e. that $p = 21$ abs. atm., and that the section of the arc is then equal to the section of the nozzle i.e. $F = 3.8$ cm² we find from (5) that the arc temperature equals 13070°K.

Since we may assume that the temperature of the free arc is independent of the value of the arc current, we find by substituting the above value of the temperature into (5) the following relationship between arc current, its cross-section F and the pressure of the quenching air, p

$$I_a = 16.65.p^{-0.25} F^{0.75}$$

This relationship is plotted in Figs. 2 and 3 for the pressures 12 and 21 abs. atm.

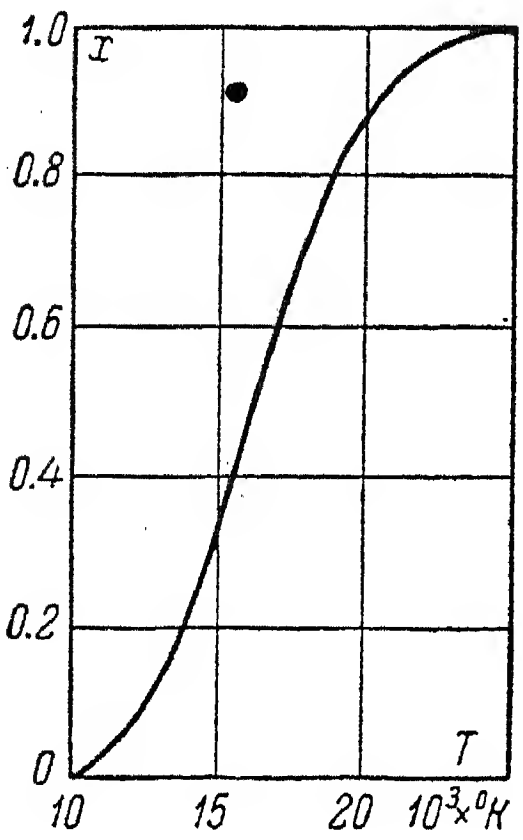

FIG. 6.

From Fig. 6 we can determine that for nitrogen at the temperature $T = 13070°K$ the degree of ionisation $x = 0.117$. It follows that our assumption of the smallness of x^2 in equation (2) by comparison with unity is justified.

Fig. 2 also shows that for sections smaller than 12 cm² curve I_a is below curve I_{sh}. This means that for these cross-sections the plugging of the nozzle of the circuit-breaker by the arc column precedes the clearance of the short-circuit current. In the range of cross-sections greater than 12 cm², curve I_a is above the curve I_{sh}. This indicates that within this range no plugging of the nozzle by the arc colum takes place.

From Fig. 2 follows furthermore, that the cross-section of the nozzle of the circuit-breaker SR205 falls into the range where the phenomenon of plugging of the nozzle by the arc column takes place. For a nozzle corresponding to that of the circuit-breaker SR405 the difference between the currents at which either plugging of the nozzle by the arc column or plugging by the effect of the heat liberated in the arc takes place, becomes insignificant and the short-circuit current is, therefore, determined by the curve I_{sh}. The cross-section of the circuit-breaker SR605 falls into the range of plugging of the nozzle as an effect of the heat evolved by the arc.

In the light of the various phenomena of plugging of the nozzle of the circuit-breaker considered here the pressure of the quenching air has an effect in the following direction. With increasing air pressure the point of intersection of the curves I_{sh} and I_a shifts towards the range of larger sections of the nozzles and the distance between these curves on the left and their point of intersection increases (Fig. 2 and 3). Consequently, in this range of sections the conditions of arc-quenching improve. This fact explains, in particular, the comparatively greater increase of the breaking capacity of the circuit-breaker type SR205 when the pressure is increased from 12 to 21 abs. atm. than is obtained for the circuit-breakers of types SR405 and SR605.

We may conclude from the above fact that the density of circuit-breakers should select its parameters with a view to obtaining plugging of the nozzle of the breaker by the arc column before the nozzle is plugged by the heat liberated in the arc. It must also be borne in mind that during the plugging of the nozzle by the arc column that the nozzle itself is scorched. For this reason an arc-quenching device in which the nozzle represents simultaneously one of the circuit-breaker contacts is unsuitable. In particular, the experimental part of the present study which was carried out on circuit-breakers with such a nozzle designed (Fig. 1). The deterioration of the contact characteristics by the clearance of a particularly high short-circuit-current may be of such an order that on the subsequent closing of the breaker no sufficiently reliable contact-making can be achieved. The design of the quenching device should be such that the nozzle serves exclusively the purpose of arc-quenching. A further indispensible condition is that the arc route should, right from the beginning, be situated in the critical cross-section of the model.

In the case that the section of the arc increases to a value equal to the cross-section of the nozzle and the current still continues to rise, the arc can no longer increase its section with increasing current. Owing to this, the current density rises as well as the degree of ionization and, as follows from equation (5), so does the arc temperature. For exactly this reason stabilized electric arcs used for a number of scientific investigations have higher temperatures than the arcs in circuit-breakers.

DETERMINATION OF THE IN-FEED CURRENTS (FROM INDUCTION MOTORS) TO SHORT-CIRCUITS IN LOW-VOLTAGE SYSTEMS *

M.O. KAMENETSKII

(Received 28 May 1956)

It is a peculiarity of the short-circuit conditions in power systems operated at voltages below 1000 V that when the voltage falls induction motors send for a certain time current to the point of the fault; this has become known as "in-feed current from induction motors".†

This peculiarity is not fully considered by the methods of short-circuit current calculations in h.v. systems. The determination of the in-feed currents from the induction motors was therefore based on various recommendations, so that they are determined in very many different ways.

An experimental determination of the short-circuit currents in an actual 380 V industrial system was carried out by the Projecting and Experimental Department of the Leningrad "Tyazhpromelektroproekt". Together with the use of the method described below the ratings of the induction motors taking part in the in-feed were determined; for the calculation of the short-circuit currents the resistances and reactances of the 380 V system were measured and compared with data in reference books.

The magnitude of the in-feed currents depends on the power rating of the motors connected to the system at the time of the fault and on their distance from the point of the fault. Other basic data for the calculation of the in-feed currents (ratio of starting current and e.m.f. of the motors) can be considered as constant for a given motor group.

No method for the determination of the power rating of induction motors which send in-feed current to the fault point has yet been suggested. The separation of this power from the total installed power of all the motors connected to the system by direct observation is very laborious and with a large number of operating motors distributed over a wide industrial area it is impracticable. The present recommendations for the calculation of the fault current in systems

* *Elektrichestvo* No.5, 40-45, 1957 [Reprint Order No. EL 22].

† The transient electromagnetic processes taking place in the motor during this period are described in [1].

up to 1000 V ignore, as a rule, this problem; this cannot be justified where a large number of motors is connected to an industrial supply system and is dealt with summarily. The method of determining the power rating of the motors connected to the system at the instant of fault by arbitrary coefficients referred to the rating of the step-down transformers has not found a wide introduction since these coefficients cannot be reliably determined. Nor does this method consider the system impedances through which the in-feed currents flow.

In the calculations carried out in parallel with the experiments it was found convenient to determine the required power rating of the motors on the basis of the load before the fault. This power was determined (at the junction points) for the groups of motors, which are replaced by equivalent motors. The procedure suggested by S.A. Rinkevich [2] for determining the total power connected (rated power at the shaft) of a group of induction motors from their reactive power demand may serve as a basis for the adoption of the above method.

Assuming that the reactive power absorbed by the induction motors at different loads (60 – 80 per cent) is constant, S.A. Rinkevich introduces the concept of the "relative VAr" of all the motors (ratio of the VAr to the power installed

$$q_{\text{rel}} = \frac{Q}{P_n},$$

which on the assumptions made, which are analysed in the appendix, can also be considered to be a constant quantity.

S.A. Rinkevich determined experimentally values of the relative kVAr. He measured the kVAr demand of a motor group at no-load and then determined from these data and the (total) kVA rating of the motors of the group their relative kVAr.

It is easy to show that the relative kVAr can also be determined analytically, for which purpose the kVAr demand and the rated power should be expressed in terms of the kW demand, viz,

$$Q = \sqrt{3} U_n I \sin \varphi_i = P_a \tan \varphi_i;$$

$$P_n = \frac{P_a}{k_c} = \frac{P_a \eta_i}{k_i};$$

$$q_{y\partial} = \frac{Q}{P_n} = \frac{P_a \tan \varphi_i k_i}{P_a \eta_i} = k_i \frac{\tan \varphi_i}{\eta_i}, \qquad (1)$$

where

η_i is the efficiency of a given motor if P_a and Q are the powers at its terminals;

k_c is the demand factor of the group of motors;

k_i is the relative load of the given motor.

As follows from (1), the relative kVAr can be determined for a value of tan ϕ and the efficiency corresponding to the given load of the (equivalent) motor. In view of the arbitrariness of the assumption of the constancy of the relative kVAr q_{rel} may be determined for greater accuracy at loads near the rated values. The values of efficiency and power factor at different loads of motors of different ratings and nominal parameters (no-load current, speed etc.) and also kVAr of motors are given in reference books [3 and 4].

Thus according to the parameters of the motors, the relative kVAr can be calculated for the "average" motor of the given group, this being characterized by several values of rated efficiency and power factor.

Once the relative kVAr and the kVAr demand are known, it is easy to determine the rating of the equivalent motor and its short-circuit current:

$$I_s = K_{st}\, I_n = K_{st}\, \frac{P_n}{\sqrt{3}\, U_l\, \eta_n \cos \phi_n},$$

where

K_{st} is the ratio of the starting current to rated current.

If the system impedance is neglected, the in-feed current from the equivalent motor is approximately equal to the short-circuit current directly at its terminals:

$$I_{sm} = \frac{E_0}{z_m} = \frac{aU}{z_m};$$

where

E_0 is the phase e.m.f. of the stator of the motor (V);
U the phase voltage of the motor (V);
a the ratio of the e.m.f. to the voltage;
z_m the motor impedance.

During a fault, not at the terminals of the equivalent motor but at some other point of the system, the in-feed current must be determined from the formula:

$$I_{sm} = \frac{E_0}{z} = \frac{aU}{z};$$

where z is the resulting impedance of the windings of the equivalent motor and of the parts of the system (per phase) to the point of the fault (ohms).

The formula for the determination of the in-feed current in the special case of a radial system takes the following form:

$$I_{sm} = \frac{aU}{\sqrt{(r_c + r_m)^2 + (x_c + x_m)^2}} ;$$

where

r_c and x_c are the resistance and reactance of the system respectively;
r_m and x_m the resistance and reactance respectively of the motor.

The resistance of an induction motor can be approximately determined from the following formula:

$$r_m = 0.5 \frac{U}{I_n} (1 - \eta)$$

or from the exact formula

$$r_m = z_m \cos \phi_{st}$$

The reactance of the motor is

$$x_m = \sqrt{z_m^2 - r_m^2} .$$

The relation of the e.m.f. to the voltage can be determined according to an investigation by V.S. Mogil'nikov ([1], who showed theoretically and experimentally that for an induction motor

$$E_0 = 0.93 - 0.95\ U.$$

For the experimental determination of the fault current one section of the distribution busbars of a step-down transformer substation was disconnected from the system. The section was supplied through a 1000 kVA, 6/0.4 kV transformer, to which one feeder of the workshops and two of the boiler house were connected (Fig. 1). The substation 6/0.4 kV was supplied from the main 35/6 kV substation of the works which was connected to the power system. The short-circuit capacity was the 35 kV system 330 MVA, that at the 6 kV busbars 85 MVA.

The main consumers of the system were the induction motors. The normal load of the industrial system was 500 – 600 A, that of the boiler house 450 – 500 A.

Faults were applied (Fig. 1) at the substation distribution panel (1), at the entrance to the workshops (2), at the power cubicle (3) and at the busbar assembly (4).

For the subdivision of the total fault current into in-feeds from the system and in-feeds from the motors, the currents were recorded by oscillograph at the

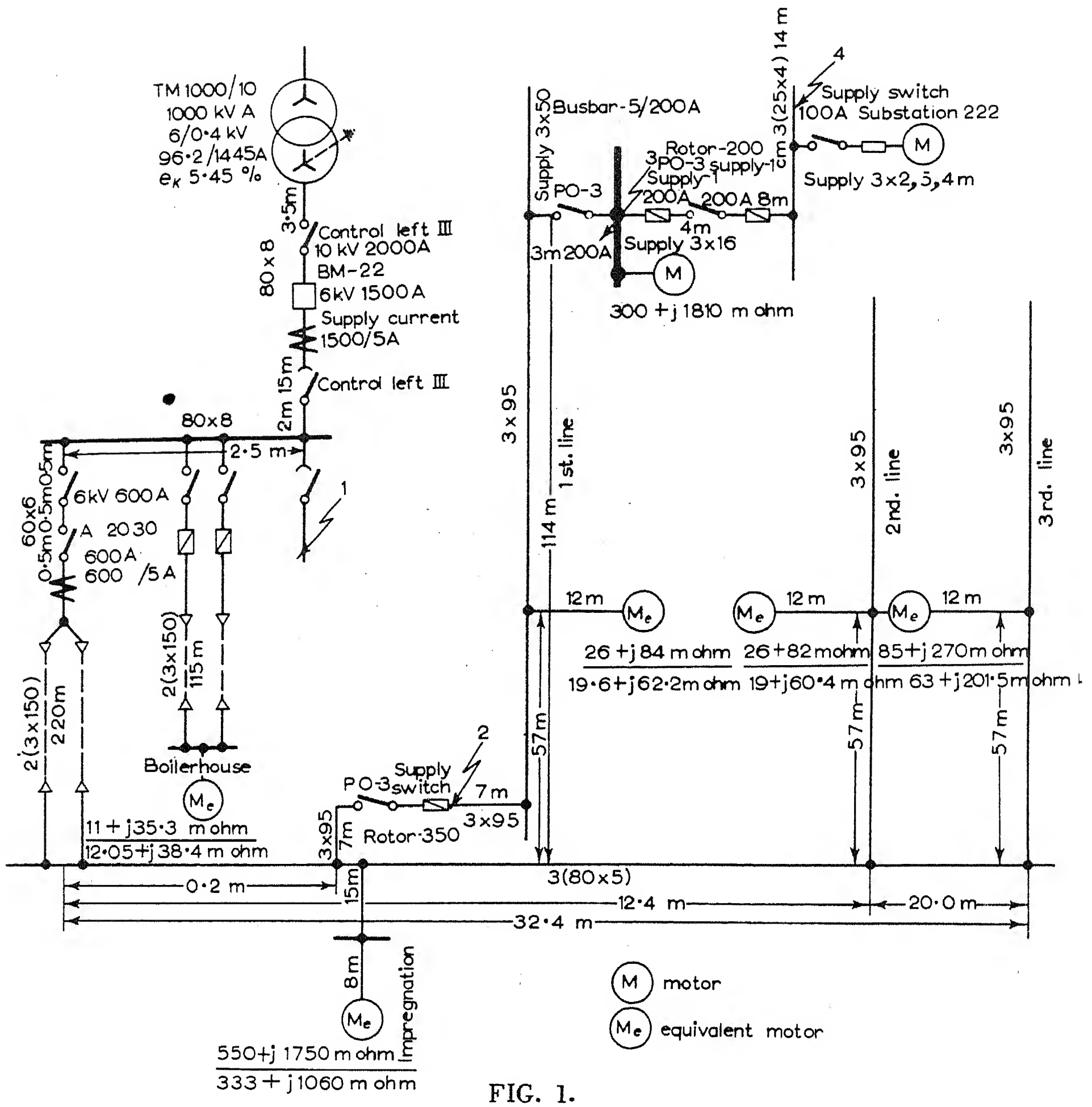
TM 1000/10
1000 kV A
6/0·4 kV
96·2/1445A
e_K 5·45 %
3·5m
Control left III
10 kV 2000A
BM-22
6kV 1500A
Supply current
1500/5A
2m 15m
Control left III
80x8
2·5 m
80x8
60x6
0·5m 0·5m 0·5m
6kV 600A
A 2030
600A
600 /5A
2(3x150)
220m
2(3x150)
115 m
Boilerhouse
Me
11 + j35·3 m ohm
12·05+j38·4 m ohm
1
2
Supply switch
PO-3
7m
3x95
7m
Rotor·350
0·2 m
15m
8m
Me
550+j 1750 m ohm
333 + j1060 m ohm
Impregnation
3(80x5)
12·4 m
20·0 m
32·4 m
Busbar-5/200A
Supply 3x50
PO-3
3m 200A
Supply 3x16
M
300 + j 1810 m ohm
Rotor-200
3 PO-3 supply-1
Supply-1
200A 200A 8m
4m
3(25x4) 14 m
4
Supply switch
100A Substation 222
M
Supply 3x2,5,4m
3x95
1st. line
114 m
12 m
Me
26 + j 84 m ohm
19·6+j62·2m ohm
3x95
2nd. line
12 m
Me
26+82mohm
19+j60·4 m ohm
57m
3x95
3rd. line
12 m
Me
85+j 270m ohm
63 + j201·5m ohm
57m
M motor
Me equivalent motor

FIG. 1.

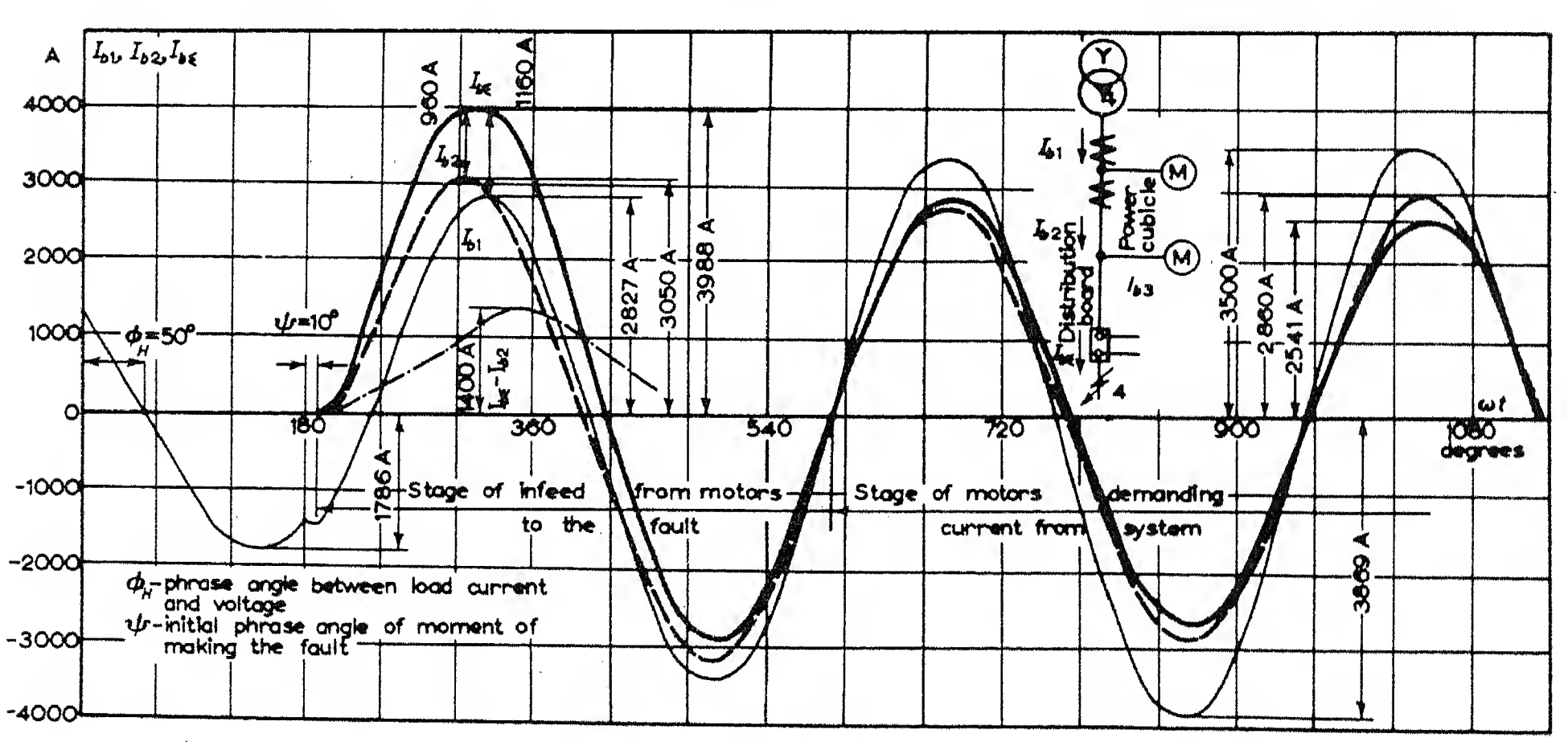
A
I_{b1}, I_{b2}, I_{bE}
4000
3000
2000
1000
0
-1000
-2000
-3000
-4000
960 A
1160 A
I_{bE}
I_{b2}
I_{b1}
2827 A
3050 A
3988 A
400 A
$I_{bE} - I_{b2}$
1786 A
ϕ_H=50°
ψ=10°
180
360
540
720
900
1080
degrees
ωt
Stage of infeed current from motors to the fault
Stage of motors demanding current from system
ϕ_H-phrase angle between load current and voltage
ψ-initial phrase angle of moment of making the fault
Y
Δ
I_{b1}
I_{b2}
I_{b3}
M
M
Power cubicle
Distribution board
4
3500 A
2860 A
2541 A
3869 A

FIG. 2.

fault points, at the substation and also at intermediate points of the system through which the in-feed currents from the motors were passing.

An electronic device was used for the control of the instant of the application of the fault (within the period)in order to obtain maximum impulse current. At the substation and at the point of the fault the short-circuit currents were recorded in all three phases.

For example, Fig. 2 shows the oscillogram and the test connexions of a three-phase fault at the point 4. The oscillogram shows that the initial phase angle at the moment of making the short-circuit was 10 electrical degrees. (The voltage curve passing through the coordinate origin is not shown in the figure.) The recorded load current (I_{bl}) at a phase angle of 180° (before inception of the fault) may have been caused by the start at that instant of a motor of a crane or a similar drive.

The short-circuit current has various phase angles according to the fraction of motor in-feed currents it contains. At the moment of the first current peak the in-feed at the point of the fault was 1160 A, but the maximum value of the in-feed current reached 1400 A (after the maximum of the total fault current).

Beginning from the second stage of the process, the fault current measured at the transformer exceeded the current at the fault point owing to the motor current (starting and working).

For the calculation of the fault currents the impedances of the system sections were determined by direct measurements and the impedances of some parts were taken catalogue data. The measurements confirmed the catalogue data for the equipment installed in the given system.

For the determination of the rated power of the motors contributing to the in-feed currents the efficiency of the "average" motor was assumed as 0.9, the rated power factor 0.84, and the relative reactive power (at 75 per cent load) 0.6 kVAr/kW.

The calculations of the power rating of the motors sending in-feed current to the fault were checked wherever possible by visual inspection. The difference between the observed and calculated values for the different fault points was 3 — 11 per cent. (Table 2).

The ratio of starting current to rated current of the equivalent motor was assumed to be 6, the e.m.f. of the motor 205 V. To determine the motor in-feed at every fault current an equivalent circuit diagram of the system sections and the equivalent motors was drawn up from which the resultant impedances were determined. The total current at the point of the fault was determined by the arithmetic superposition of the current in-feeds from the system and the in-feeds from the motors *

* Owing to the fact that in the test circuit the short-circuit making device constituted

(continued)

TABLE 1.

Designation of section	Impedance of section in milliohms					
	Resistance		Inductive Reactance		Total Impedance	
	from catalogue data	measured	from catalogue data	measured	from catalogue data	measured
From transformer to substation distribution panel (fault point 1)	2.83	4.97	11.66	13.28	11.95	14.10
From transformer to entrance of workshops (fault point 2)	19.63	20.46	20.20	20.26	28.2	28.9
From transformer to Power cubicle (fault point 3)	50.19	44.37	47.28	49.44	69.0	66.2
From transformer to busbar assembly (fault point 4)	116.45	88.97	79.88	120.43	141.5	149.9

Note. The impedance calculated from catalogue data included the reduced impedance of the h.v. system of 1.87 milliohms.

The measured impedance included also the impedance of the fault-making device equal to $0.84 + j\ 1.305$ milliohm (in phase A during faults at points 1 and 2) and $0.944 + j\ 0.975$ milliohm (in phase C during faults at points 3 and 4).

Reference data of the individual elements of the l.v. system have been obtained mainly from the work of the Rostov department of the Tyazhpromelektroproekt (1953).

TABLE 2.

Designation of the equivalent motor	Oscillogram Data				Connected capacity of equivalent motors kW	
	load current (*A*)	phase voltage (*V*)	sin ϕ	kVAr	from kVAr	from inspection
Fault at point 1						
Workshop feeder . . .	556	220	0.819	300	500	–
In particular						
1st line	–	–	–	–	220	–
2nd line	–	–	–	–	215	–
3rd line	–	–	–	–	65	–
impregnating . . .	–	–	–	–	10	–
1st boiler feeder	288	220	0.707	134	480	497
2nd boiler feeder	272	220	0.806	154		
Fault at point 2						
Workshop feeder . . .	547	236	0.982	380	630	–
In particular						
1st line	220	236	0.945	149	248	280.5
2nd line	–	–	–	–	–	289.1
3rd line	–	–	–	–	–	87.0
impregnating . . .	–	–	–	–	–	16.5
Boilers	–	–	–	–	–	455
Fault at point 3						
Power cubicle (in mine)	–	–	–	–	–	60
Fault at point 4						
Busbar assembly by . .	–	–	–	–	–	67.5
motor connected to cubicle.	–	–	–	–	–	10

Note. Resistances and reactances of the motors are shown directly in Fig. 1 in numerator for fault point 1, and in denominator for fault point 2.

TABLE 3.

Fault point	Number of fault point	≤ System phase voltage prior to fault	Symmetrical fault current: from system: calculated	Symmetrical fault current: from system: test	Symmetrical fault current: from system: ratio	Symmetrical fault current: from motors: calculated	Symmetrical fault current: at fault point, calculated	First peak of fault current: from system: calculated	First peak of fault current: from system: test	First peak of fault current: from system: ratio	First peak of fault current: from motors (in-feed): calculated	First peak of fault current: from motors (in-feed): test	First peak of fault current: from motors (in-feed): ratio	First peak of fault current: at fault point: calculated	First peak of fault current: at fault point: test	First peak of fault current: at fault point: ratio	ratio at first peak at fault current at fault point to that at transformer
0.4 kV busbars	1	220	15,600	15,300	0.97	6,610	22,210	29,350	27,160	0.925	9,310	7,400	0.795	38,660	33,240	0.865	1.225
Workshop feeder	2	236	8,160	7,560	0.93	6,710	14,860	12,200	10,200	0.845	9,470	9,050	0.96	21,670	19,250	0.885	1.80
Branch from workshop feeder to power cubicle	3	216	3,260	3,230	0.985	545	3,805	4,940	4,400	0.895	768	650 1,850	0.847 2.4	5,708	6,250	1.09	1.42
Distribution busbar assembly	4	214	1,435	1,900	1.32	745	2,180	2,260	2,830	1.25	1,055	960 1,160 (1,400)	0.91 1.1 (1.32)	3,315	3,990	1.2	1.41

Notes. 1. Test values of the first peak of the fault current in-feeds from motors (graph 13) are determined as the difference of measured current at the fault from that at the transformer. An exception is point 1, where the in-feed from the motor is measured directly. For points 3 and 4, where the in-feed takes place from motors between fault point and supply, two values are given; the first is the in-feed from motors on the other side of the fault compared with calculated values the second is the in-feed from all motors (Fig. 2). Owing to the lack of a practical method of calculating short-circuit currents at system points where the e.m.f. of the motor equals that of the system, the in-feed currents from motors between the fault and the supply point were not calculated in cases of fault points 3 and 4.

2. During faults at the end of the circuit 4 the test values of the symmetrical component of the fault current and of the first current peak (from the system and at the fault point) were larger than the calculated values, obviously because the reduction during the fault of the resistance and reactance of the steel busbars of the distribution panel against the values as measured at the rated current (due to the skin effect in ferromagnetics)were neglected.

The results of the calculation of the impedance of the system sections to the short-circuit points are given in Table 1. The determination of the equivalent ratings of the motors is detailed in Table 2; and the short-circuit currents are given in Table 3.

The difference between the experimental and the calculated values of the fault currents is about 10 – 15 per cent. This comprises the errors in measurements, estimated at about 6 – 10 per cent, the increase in the impedance of the experimental system at the time of the fault by the formation of the arc in the fault-making device and by the approximative character of the mathematical description of the short-circuit processes. But, as can be seen, the difference is within the limits of experimental and calculating errors. In individual cases Table 3 gives a short explanation of the causes of the discrepancy.

Conclusions

Experiment and calculation confirm that, when the system impedances during fault conditions and the rating of the motors sending current to the fault, are correctly estimated, the results of short-circuit current calculations are entirely satisfactory in cases in which the fault takes place near the supply point of the low-voltage system. For medium and long distances to the fault point the calculated values of the in-feed currents from the motors may be too small because the in-feed of some motors on the supply side of the fault point is neglected.

The in-feed currents attenuate rapidly and need be taken into account only for the first peak of the short-circuit current at the fault. For medium and long distances the motors located between fault and supply point rapidly cease to end current to the fault and soon will require to be supplied with current again; During faults at points 3 and 4 the value of the current therefore measured at the transformer (at the input end of the circuit) became larger than at the first fault current peak.

The in-feed currents from the induction motors have a considerable magnitude especially at medium and long distances from the fault in the system shown in Fig. 1 the first fault current peak exceeded the corresponding current of the supply transformer by 22 – 80 per cent.

The resistances and reactances of the low-voltage system have a considerable effect on the magnitude of the fault currents. In the system shown in

* *(Continued)*
a common impedance for currents from both sources, strictly speaking the calculations should have been made with different distances of the sources (consideration of self and mutual impedances). However, such a calculation is very complicated and would have rendered, according to a check, the result only about 3 – 5 per cent more accurate than the calculation made individually from each in-feed source.

Fig. 1 the current at the far end of the system was 10 times smaller than that at the busbars.

It is possible to calculate the in-feed currents from a given group of motors fairly exactly by using a value of the rating of the motors sending current to the fault determined from the load before the fault and from the value of the relative kVAr determined analytically.

Appendix

The kVAr Demand. The assumption of constant kVAr demanded from the system at different loads of induction motors is based on the following considerations:-

The total kVAr demand by a motor comprises the kVAr for magnetization Q_o and the kVAr for the leakage reactance Q_D. The magnetization kVAr are virtually independent of the motor load and are determined by the equation:

$$Q_o = \sqrt{3}\, U_l\, I_o\ ,$$

where

U_l is the line voltage of the system (V);
I_o the no-load current (A).

The total kVAr demand from the system in particular at the rated load can be determined from the expression:

$$Q_n = \sqrt{3}\, U_l\, I_n \sin \phi_n\ ,$$

where

I_n is the rated stator current (A).

It is easy to show that the magnetizing kVAr are equal to the total kVAr in the special case that the stator current is equal to no-load current and the phase displacement between the current and the voltage is 90°.

The specific value of the magnetizing kVAr, independent of the loading of the motor, is given by the ratio:

$$\frac{Q_o}{Q_n} = \frac{\sqrt{3}\, U_l\, I_o}{\sqrt{3}\, U_l\, I_n \sin \phi_n} = \frac{I_o}{I_n \sin \phi_n}\ ,$$

If the no-load current is expressed by the rated stator current [5]

$$I_o \approx I_n\ (\sin \phi_n - \frac{\cos \phi_n}{2\, b_n}$$

then the ratio

$$\frac{Q_o}{Q_n} = \frac{I_n \left(\sin \phi_n - \frac{\cos \phi_n}{2\, b_n}\right)}{I_n \sin \phi_n} =$$

$$= \frac{\sin \phi_n - \frac{\cos \phi_n}{2b_n}}{\sin \phi_n} = 1 - \frac{\cot \phi_n}{2b_n},$$

where

b_n is the ratio of the maximum torque to the rated torque of the motor.

Substituting likely values of cot ϕ_n and b_n it is easy to determine the limits of the ratio

$$\frac{Q_o}{Q_n}$$

In [4] it is shown that for induction motors the relative value of no-load kVAr become, owing to the fact that the motors are not fully loaded, practically as follows: For a rated p.f. of 0.91 – 0.93 approximately 85 per cent and for rated p.f. of 0.77 – 0.79 approximately 90 per cent.

REFERENCES

1. V.S. Mogil'nikov, *Pull-out of induction motors during short-circuits in the system. Elektrichestvo,* No. 11, (1954).
2. S.A. Rinkevich, *On the individual power demand of metal-cutting lathes in mechanical engineering works. Sbornik informatsionnykh materialov Energosbyta Lenenergo (Information Handbook of the Power Sales Department of the Leningrad Power Authority)*, 3rd Edition, (1948).
3. M.P. Kostenko, *Electric machines. Gosenergoizdat* (1944).
4. L.V. Litvak, *Problems of raising the power factors in industrial plants. Gosenergoizdat* (1950).
5. I.A. Syromatnikov, *Operating conditions of induction motors. Gosenergoizdat* (1955).

WIND PRESSURE ON OVERHEAD TRANSMISSION LINE CONDUCTORS*

V.V. BURGSDORF

(Received 9 January 1957)

The correct assessment of wind pressure on conductors is of great importance in the design of transmission lines. This applies particularly to double-circuit lines and lines equipped with release clamps and safety (swivelling or collapsible) cross-arms, since in these cases there is an upper limit imposed for the maximum permissible wind loading. In designing large installations, it is necessary to know accurately the aerodynamic characteristics of conductors and the distribution of wind pressure.

As is well known, strong winds are always of turbulent nature and consist of fast-and slow-moving air masses. In other words, the wind velocity is never uniform along the front of a gust. The total load on a long object is therefore determined not by the maximum, but by some mean value, of the wind velocity. For spans longer than 200 m this lack of uniformity may be of considerable importance.

The first experimental investigations to ascertain the extent of the non-uniformity in the distribution of the wind velocities affecting the total load on conductors date back over 25 years [1] and [2]. These tests showed that for wind speeds up to 20 m/sec. this non-uniformity can be neglected for spans up to 100 m. long, but that it becomes sufficiently noticeable on spans about 200 m. long.

Later investigations carried out in Sweden in 1939 revealed a possibility of reducing the design value of wind load because of the finding that the wind pressure becomes less uniform with velocity [3]. Similar experiments were also carried out in other countries: France in 1951 [4] and [5], Australia in 1949 [6]; Belgium in 1952 [7]. Recently investigations were made in West Germany [8] and in the U.S.S.R. where eight experimental stations were erected with span lengths from 220 to 350 m.

The reduction co-efficient considering the non-uniform distribution of the pressure along the span was introduced in the Soviet Regulations for Trans-

* *Elektrichestvo* No.5, 47-52, 1957 [Reprint Order No. EL 23].

mission Lines in 1947 [9]. These regulations recommend the following formula

$$P = \alpha C_x \frac{v^2}{16} \tag{1}$$

where P is wind pressure in kg/m² of projected area;
α is the reduction co-efficient;
C_x is the head resistance of conductor;
v is the wind speed in m/sec.

In the above formula the wind speed is taken usually as the maximum velocity registered by a meteorological station, for a period of 5 to 10 years. The head resistance of the conductor which can be referred to conductor diameter and wind speed, is normally taken as 1.2 [10]. The coefficient α is 0.85.

The coefficient α depends not only on the conditions existing in a given locality, but also on the method of measurement of the wind velocity.

It should be pointed out that the anemometers used in the U.S.S.R. were of the pressure-plate type whereas those used abroad were generally of the pressure – tube type (i.e. working on the Pitot-tube principle). The latter anemometers can register the velocity of a wind gust lasting 10 to 15 sec. whereas the pressure-plate instrument, according to the instruction book, should register a mean position of the plate for 2 min. It is obvious that the maximum velocities as recorded by low-inertia anemometers should be higher than those recorded with the pressure-plate anemometers. This, in fact, explains the various statements on low wind speed prevailing in the U.S.S.R.

The wind load on conductors is usually computed from the measurement of the angle of swing of the insulator string or the coupling link from which the conductor is suspended. This gives directly the horizontal force on the tower and the reduction of the clearance to the tower. To determine the maximum wind loading for a given period of time, continously recording instruments were used in Sweden, Germany, and U.S.S.R. and maximum-swing indicators were used in France and Belgium. The deflection angles thus obtained were checked against records of the maximum wind velocities measured in the immediate vicinity of the experimental span or at a near-by meteorological station.

A visual method of measuring the angle of deflection of the conductor at midspan was used in Australia. Readings were taken "only when the conductor was fairly steady" obviously because such a method is not particularly suitable for measuring maximum deflections. Moreover, the readings were checked against wind velocities measured by a cup-type anemometer and consequently, in this investigation, one can speak only of some average conductor deviation and wind speed. A simultaneous underestimation of conductor deflection and wind speed leads to the cancellation of the error. Thus, such results cannot be accepted as being characteristic of maximum wind loadings and will not be utilized in the following considerations.

In the U.S.S.R. the wind velocity was invariably recorded by means of

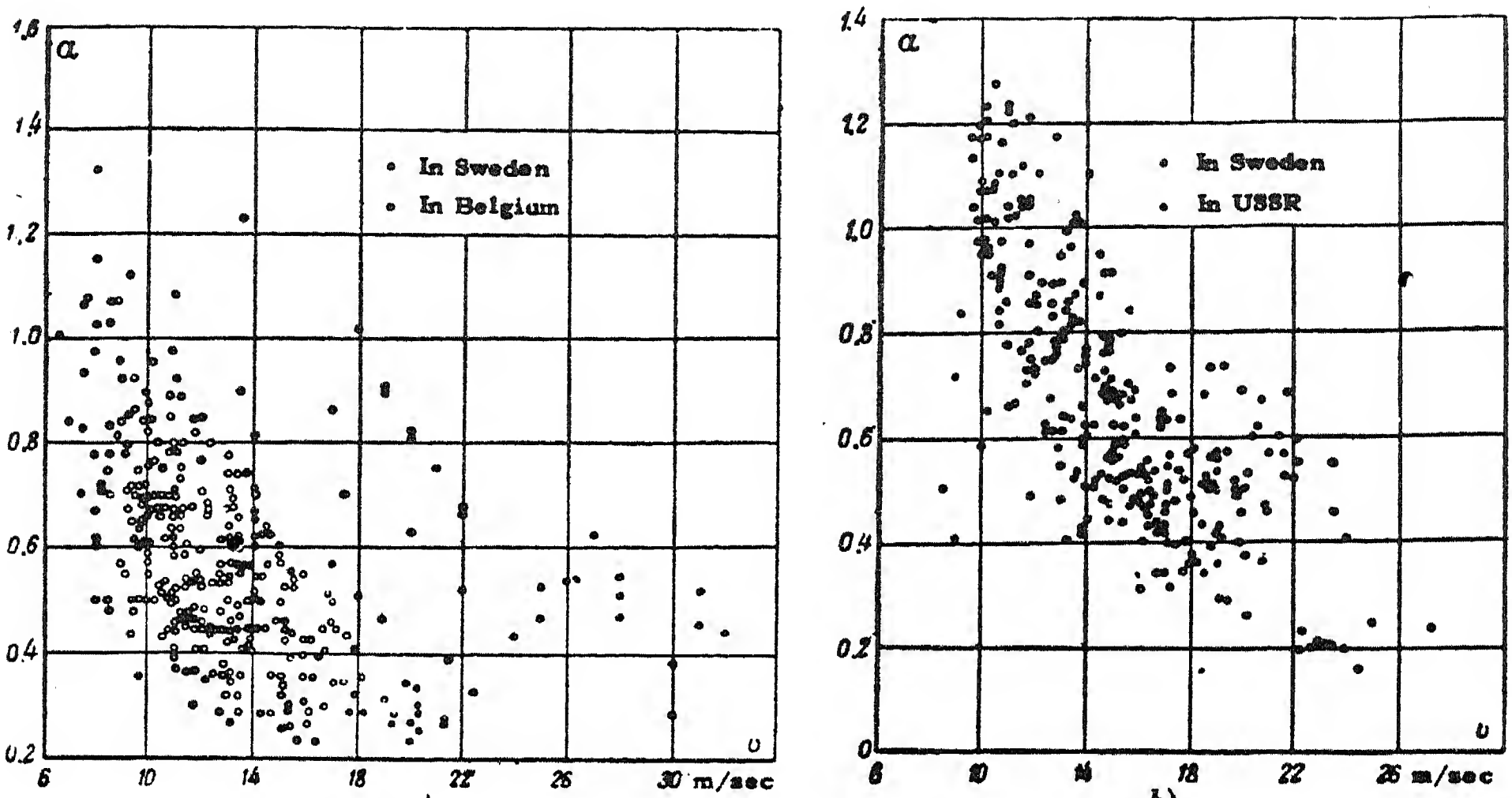

FIG. 1. Relationship between the coefficient a and wind velocity
a — measurements in Sweden (inland regions): d = 25 to 27.7 mm, l = 155 to 300 m; measurements in Belgium: d = 9.5 mm, l = 120 and 190 m;
b — measurements in Sweden: d = 15.8 mm, l = 200 m; measurements in U.S.S.R. (coastal area): d = 19.1 mm, l = 250 m.

pressure plate anemoters, except in one case in which a pressure-tube instrument was used.

The results of various investigations are presented in different ways. For example, Swedish publications give the measured wind pressure on conductors as a fraction of the wind pressure on a large plane ($C_x = 2$), i.e. the measured pressure is characterized by a quantity which is less than the coefficient a; in French investigations the results are expressed in terms of the ratio of the measured to calculated angle of conductor deflection (the calculations being performed in accordance with the method accepted in France). In order to compare the results from various countries the data were recalculated on a common basis. The quantities calculated were the coefficient a from (1) and the effective load per square metre of the projected area normal to the direction of wind*. For each particular case the head resistance was taken as depending on the type of conductor and wind speed in accordance with the results of tests in wind tunnels carried out in the U.S.S.R. [10]. In this way it was possible to arrive at more accurate values of the coefficient a.

The results of this re-calculation are shown in dotted lines on the accompanying figures. Figs. 1,2 and 3 show the values of the coefficient a for the various countries, and Fig. 4 the envelopes drawn through the points of maximum value. Two points differing from the others are shown in Fig. 4 separately.

* It is regretted that the results of German investigations could not be recalculated because of the insufficiency of published data.

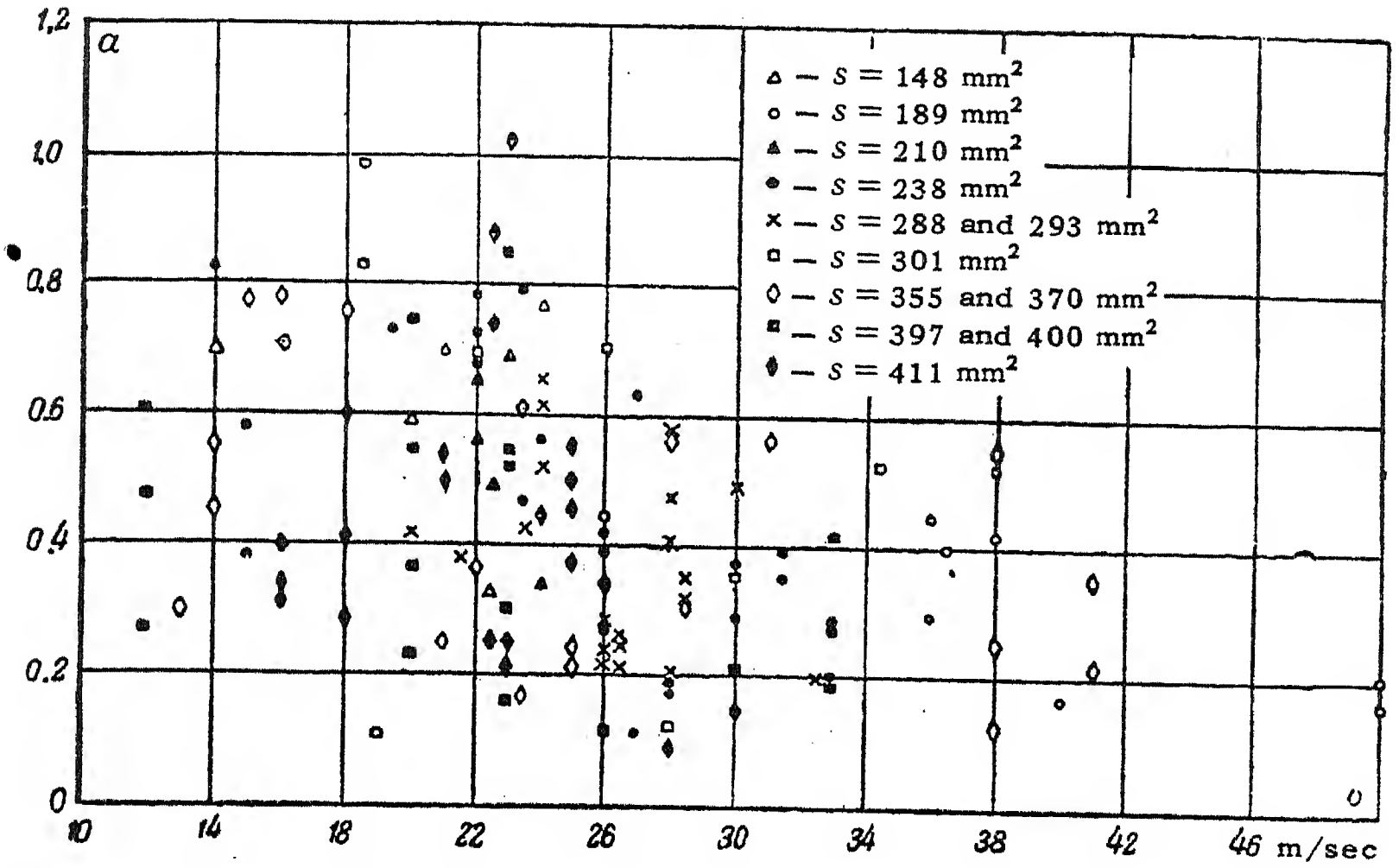

FIG. 2. Relation between the coefficient α and wind speed according to the results obtained in France.

When analysing results of measurements, apart from the non-uniform distribution of the wind speed along the span, one should also consider the case when the wind speed at the span is higher than that at the point of location of the anemometer. In this case the coefficient α becomes greater than unity. It is characteristic that for high wind speeds (20 m/sec and more) no such case has been observed in practice.

The manner in which the experimental points are distributed allows us to establish beyond any doubt the fact that the wind pressure becomes less uniform along the span as the wind becomes stronger. Also, the influence of the different physical and geographical factors pertaining to different geographical areas is clearly brought out. Moreover, this is true not only for coastal and inland regions within one country such as, for example, Sweden. The first measurements carried out in the Leningrad area with low-inertia instruments yielded values * for the coefficient α greater than those obtained for a coastal region in Sweden. Even greater values of the coefficient were obtained in Belgium and yet greater values in France.

In France values between 0.5 and 0.55 were obtained for the coefficient α for wind velocities up to 38 m/sec. It is regrettable that no information is available on the experimental span lengths but it can be taken that in France the span length for conductors of 300 mm² or more† cross-sectional area, is, as a rule, more than 400 m and only rarely 350 m.

* Here and later on the values of the coefficient α are taken for the same, and not for the maximum wind speeds, recorded in the given localities.

† It can be shown that for a wind speed of 34.5 m/sec, $\alpha = 0.52$ (Fig. 2) was recorded on a span 462 m long.

The coefficients α obtained from measurements in the U.S.S.R. by using pressure-plate anemometers with loaded plate (Fig.3) correspond mainly to wind speeds of up to 20 – 25 m/sec. However, there is enough experimental data to establish the fact that the coefficients obtained in this way are greater than those resulting from measurements with low-inertia instruments. One fact stands out, viz. the large number of points whose values are considerably greater than unity for wind speeds up to 18 m/sec and also the number of points having values of the order of 0.8 for wind speeds of about 25 m/sec for long spans.

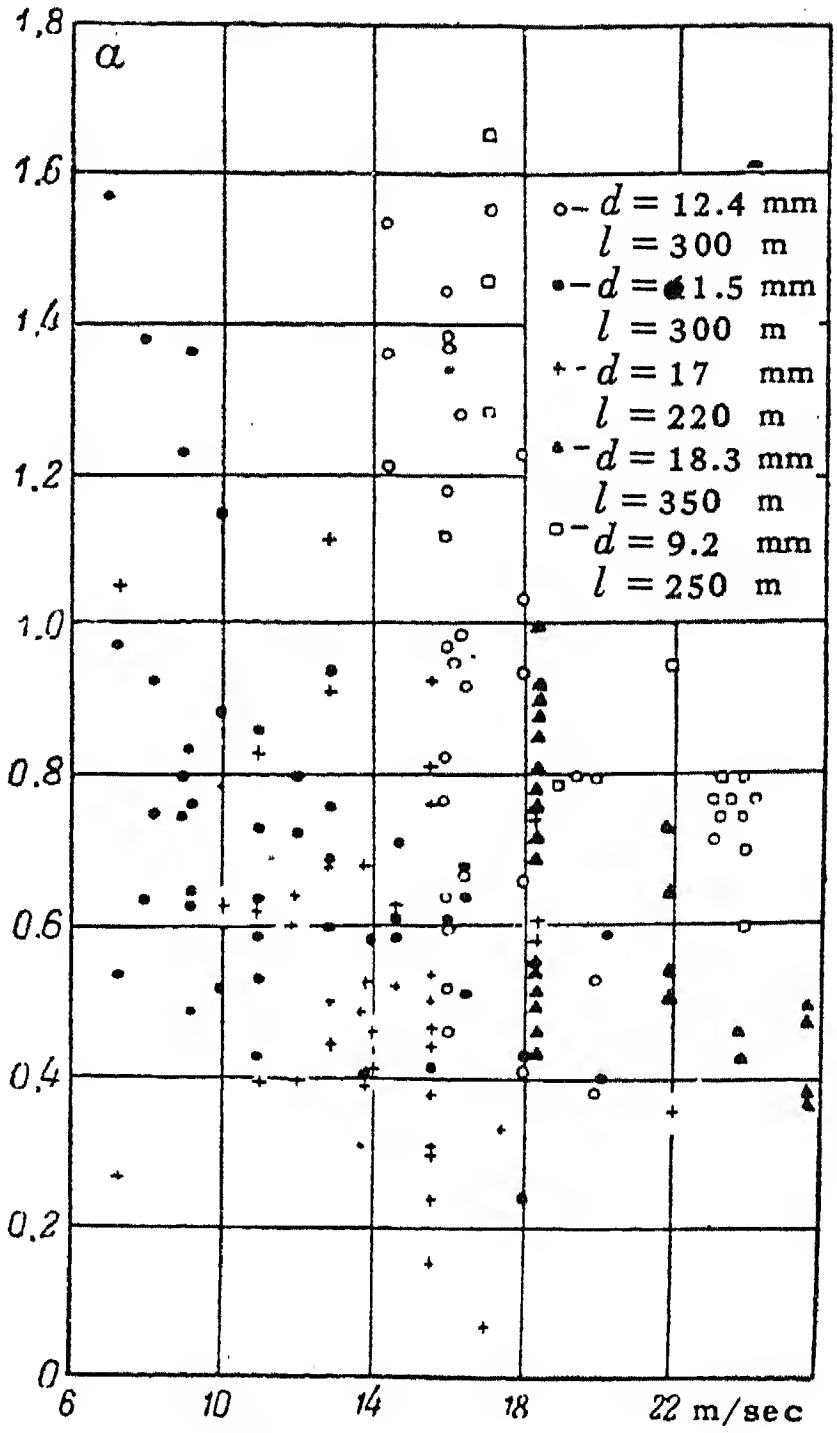

FIG. 3. Relation between coefficient α and wind speed according to results obtained in the U.S.S.R.

A comparison of the curves shown in Fig. 4 indicates that the coefficient α depends on the degree to which a given district is exposed to high winds. In this respect the comparison of the Swedish data for coastal and inland regions and of the Belgian and French data are characteristic. From Fig. 4 it is seen that the curves of the reduction coefficient obtained for different regions are shifted with respect to each other, and the coefficients α for districts subjected to stronger winds are higher than those for districts with less intense winds for a given wind speed. Therefore, if a coefficient α is obtained for a region with strong winds, it cannot be extended to maximum wind speeds of regions with moderate winds. For example, the value of α at 25 m/sec for the region with the design wind speed of 30 or 35 m/sec cannot be applied to a line erected in a region where the design wind speeds is 25 m/sec, since in this latter case the value of α is smaller.

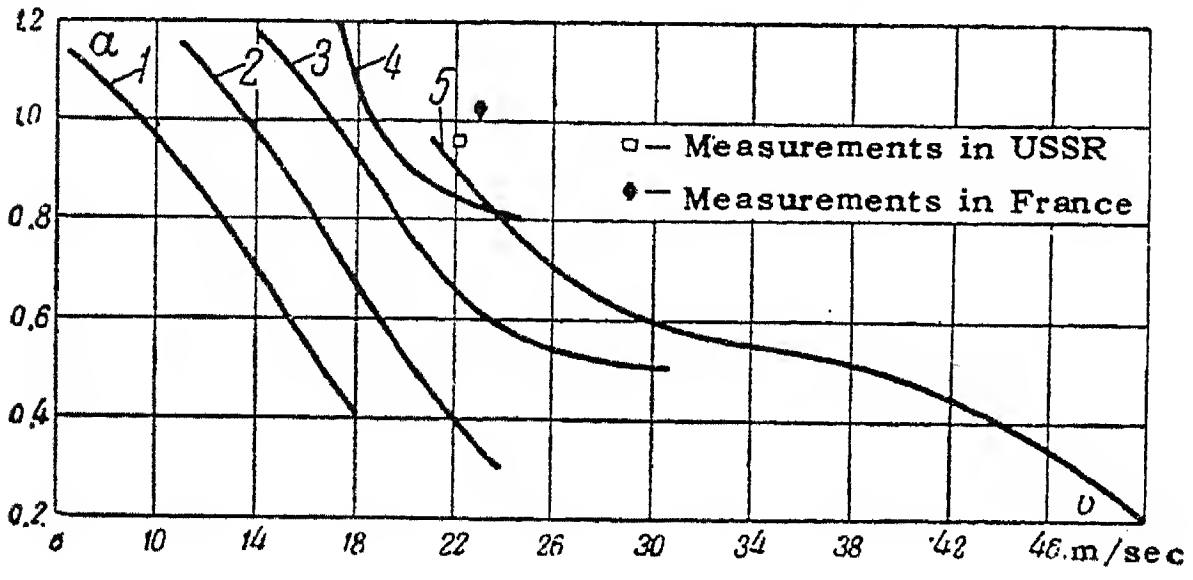

FIG. 4. Relation between greatest values of coefficient α and wind speed as measured in different countries:
1 – in Sweden (inland regions);
2 – in Sweden (coastal regions);
3 – in Belgium;
4 – in U.S.S.R; 5 – in France.

To facilitate further analysis, mean values of wind pressure on a conductor for one span recorded at various wind speeds are plotted in Figs. 5 – 7. The distribution of these points is typical. The curves shown in these figures are drawn from (1) for $C_x = 1.2$ and

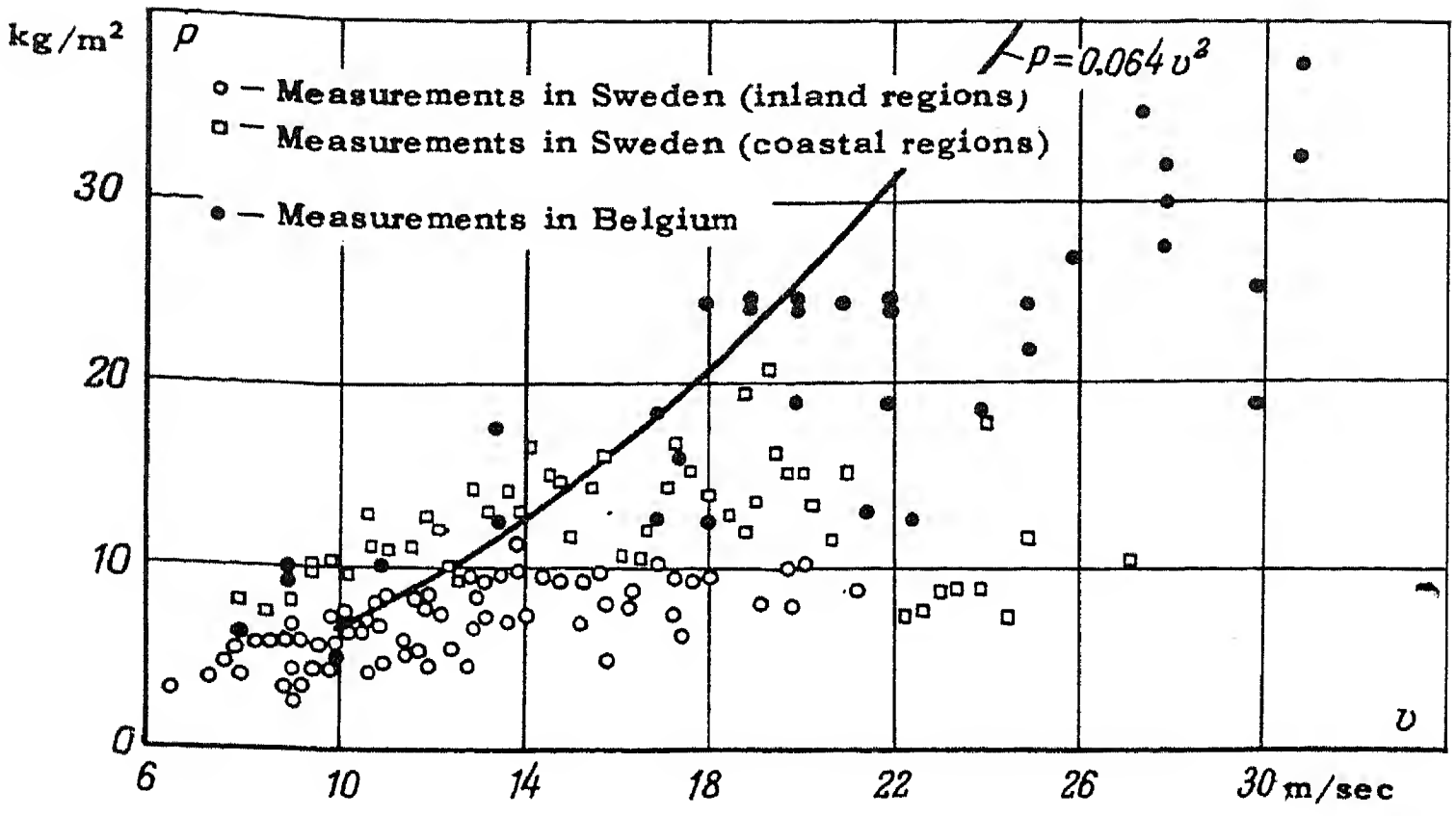

FIG. 5. Relation between wind pressure on conductor projection area normal to wind direction and wind speed according to measurements in Sweden and Belgium.

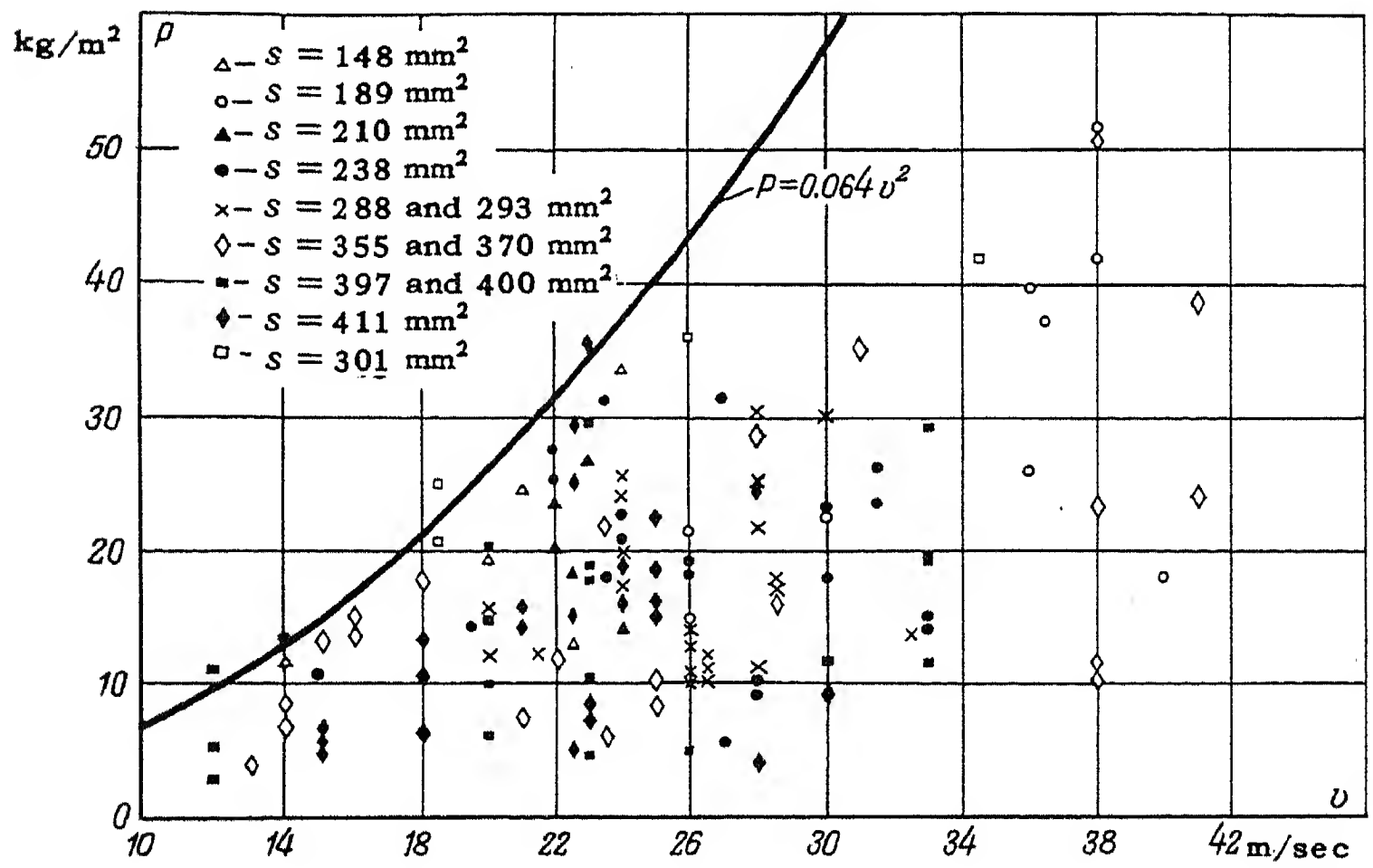

FIG. 6. Relation between wind pressure on conductor projection area normal to wind direction and wind speed according to measurements in France.

$\alpha = 0.85$ in accordance with the recommendations given in the Regulations for the Erection of Electrical Installations [9].

The practical conductor loading in Sweden (especially in inland regions) is noticeably lower than it is in Belgium and this, in turn, is lower than in France. For wind speeds up to 15 m/sec the experimental points lie not infrequently above the design curve and for velocities of 15 to 20 m/sec they are, in general,

the same as the higher values observed in Belgium and France. At still higher wind velocities the measured wind load is smaller than the calculated one which is obviously due to the lowering of the coefficient α.

Of a similar character is the distribution of experimental points obtained from short-period tests in the U.S.S.R., though the quantitative relations are here different *: wind pressures greater than those given by (1) occur often at speeds of up to 18 or 19 m/sec, and at 25 m/sec they are almost as high as the highest values recorded.

The material presented demonstrates convincingly the importance of the correction factor for wind pressure at high wind speeds. This coefficient should be different for speeds measured with the low-inertia and the pressure-plate anemometers.

The West European investigators working with low-inertia anemometers suggest a value of 0.5 for the reduction coefficient; they are also referring to a considerable local wind speed of 35 m/sec. The investigators in Sweden, where the wind speed has also been measured with low-inertia anemometers, recommend the coefficient $\alpha = 0.4$ on the basis of a wind speed of 28 m/sec. Such a lowering of the coefficient appears to be justifiable on the ground that undoubtedly the winds in Sweden are not so strong as those in Belgium and France.

The value of the coefficient α should be greater if this is worked out from the data on wind velocities obtained with the method which is accepted in the U.S.S.R. The relation between the coefficient obtained with the two types of anemometer is given by

$$\left(\frac{v_{li}}{v_{pp}}\right)^2,$$

where v_{li} is the speed measured with the low-inertia, and v_{pp} with the pressure-plate anemometers. At the present time work is being done to determine this ratio, but it can be said even now that no great reduction can be expected in the present value (0.85) of the coefficient α. Indeed, taking the West European coefficient $\alpha = 0.5$, the ratio

$$\frac{v_{li}}{v_{pp}} = \sqrt{\frac{0.85}{0.5}} = 1.3$$

which may be regarded as a sufficiently realistic figure for the ratio of short duration (10 to 20 sec) to one minute maximum wind velocity.

The above statement is verified by the damages to transmission lines occur-

* This is obviously connected with the different method of measurements (pressure-plate anemometers) used in the U.S.S.R.

ring at strong winds when the effective wind pressure on conductors is nearly 60 kg/m² and the wind speed (measured by pressure-plate anemometer) 32 to 35 m/sec.

A more substantial reduction of the coefficient a can be expected for regions where the design wind speed is 35 m/sec or more, and also where the repetition rate of the assumed design speed comes near the highest observed.

To give a fuller picture of practices in various countries the tables 1 and 2 of design wind loadings on conductors and metal supports were compiled.*

It is seen from Table 1 that the conductor loading used in the U.S.S.R. is about the same, or even sometimes lower, than in other countries.† The lowest wind loading is applied in Finland where, as in the Leningrad district and Karelian A.S.S.R., the wind speeds are not very high due to favourable geographical conditions.

Recent research on the effects of non-uniform wind pressures is now being accepted as a basis for the reduction of the design wind loadings in Belgium and France, where until recently these loadings have been excessively high.

The design wind loadings on supports are invariably higher abroad than in the U.S.S.R., sometimes by as much as 50 or even 100 per cent.

It appears from the foregoing that the design values used in the U.S.S.R. for wind loading are in every respect more modern than in most other countries where only recently the regulations were slightly eased-up, which brings the foreign design values nearer to the Soviet values. It should be made clear, however, that this does not preclude the possibility of a future reduction in the design wind loading for transmission lines.

This further reduction should be well substantiated by more extensive investigations to determine realistic loadings for various regions and to obtain more accurate aerodynamic characteristics of conductors and supports and the possible values of the coefficient a.

From experiments which have been carried out up to now it is possible to reduce the design head resistance to 1.1 for the values of the product $vd \geq$ 400 m/sec. mm. It is also possible to take the coefficient $a = 0.75$ if the supports are checked for the highest wind loads ††. This relaxation of the design conditions can be extended also to localities with the design wind velocity of

* In the U.S.S.R. the loads are taken for the average wind speed of 25 m/sec.

† The accepted thickness of ice for Sweden varies between 1.3 and 3.2 cm. Therefore the resulting wind load on tower becomes considerably greater than in the U.S.S.R.

†† The speeds considered are the maximum values for a given region, occurring once in 5 years, and not the design speeds.

TABLE 1. Design wind loadings on conductor projection area without ice used in various countries.

	Country	USSR	Great Britain	Belgium	Germany	Italy	Canada	USA	Sweden	Switzerland	Finland	France
Design load	kg/m²	40	39	72*** / 45	44-53	72	39	44	25*	50	25	72** / 48
	%	100	97.5	180*** / 112.5	110-130	180	97.5	110	—	125	62.5	180** / 120

* With and without ice load.
** Numerator — present standards; denominator — standards recommended at the present time, publications referred to
*** Numerator — present standards; denominator — proposed new standards with $C_x = 1.2$.

TABLE 2. Design wind loadings on flat tower sections used in various countries.

	Country	USSR	Great Britain	Germany	Italy	Canada	USA	Sweden	Switzerland	Finland	France
Design load	kg/m²	54.9	120	77	120	63	70.5	100	100	100	120
	%	100	220	140	220	115	128	182	182	182	220
Pressure on leeward face %		100	—	81	60-80*	100	100	80/100**	60-80	100	60-80*

* Depending on projected tower area.
** Depending on distance between tower sides.

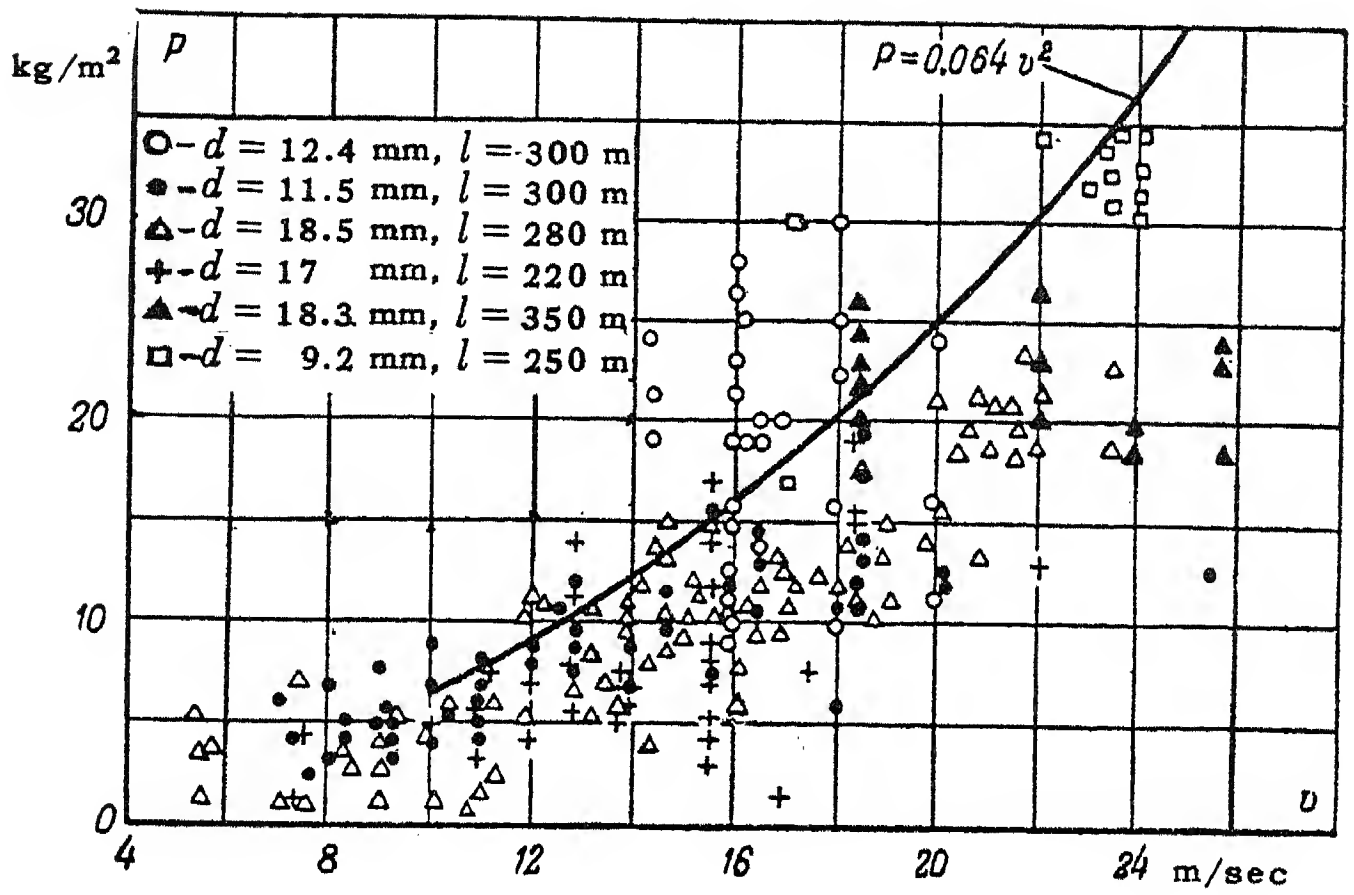

FIG. 7. Relation between wind pressure on conductor projection area normal to wind direction and wind speed according to measurements in the U.S.S.R.

35 to 40 m/sec, except for the regions adjacent to large water areas. The question of specifying more precise value for the coefficient a will be decided from the results of experiments now being carried out in the U.S.S.R.

It is also necessary to consider more closely the actual conditions under which a line is expected to operate. In particular the present practice of extending the design wind speed of 25 m/sec. to regions with light wind should be abandoned. In all cases the design wind speeds should be chosen in accordance with observations. For lines passing through woodlands the design speed should be taken at least 5 m/sec. less than the speed for the main region.

REFERENCES

1. W.D. Tuck, *Variation in Distribution of Wind Pressure on Overhead Lines. Brit. Electr. a. All. Indust. Research Assoc. Tech., rep.* X (1934).
2. R.H. Sherlock and M. Stont, *Storm Loading a. Strength of Wood Pole Lines a. Study of Wind Gusts. Edis. El. Inst.* (1936), *University of Michigan, Anu Arbor.*
3. O.P. Zetterholm and S. Sandin, *Wind Pressure on Overhead Transmission Line Conductors.* CIGRE Rep., 202 (1954).
4. R. Poyart, *Effect of High-Velocity Winds on Overhead Line Conductors. Bull. Soc. France des electriciens,* XI (1953).
5. P. Schuepp *et al, Investigation of Mechanical Overload in Insulators of Transmission Lines Under Normal Service Conditions. Rev. Gen. Electr.,* No. 2 and 3 (1955).
6. H.C. Harrison, *Factors Affecting the Mechanical Design of Transmission Lines.* Pt. 1, CIGRE. Rep. 218 (1956).
7. L.H. Marchal *et al, The Action of Wind on Overhead Line Conductors.* CIGRE. Rep. 206 (1956).
8. H. Mors *et al, Wind Pressure on Overhead Transmission Line Conductors.* CIGRE., Rep. 220 (1956).

REFERENCES (*continued*)

9. *Recommendations for Erection of Electrical Installations. Gosenergoizdat* (1947).
10. V.V. Burgsdorf, *Fundamental Problems in Erection of Overhead Transmission Lines. Trudy Central Scientific Research Electrochemical Laboratory.* 5th Edition.

Note:

(CIGRE *stands for Conference Internationale des Grands Reseaux Electriques.)*

THE PROTECTION OF A REGULATING AUTOTRANSFORMER*

A.N. KOZHIN

(Received 23 March 1956)

The voltage regulation on load in the h.v. systems of the USSR is increasingly carried out by transformers with booster groups. The use of autotransformers with regulating gear for this purpose is spreading.

Fig.1 is the diagram of a power transformer with a booster group. The latter consists of a regulating autotransformer (or transformer) and a transformer in series with it.

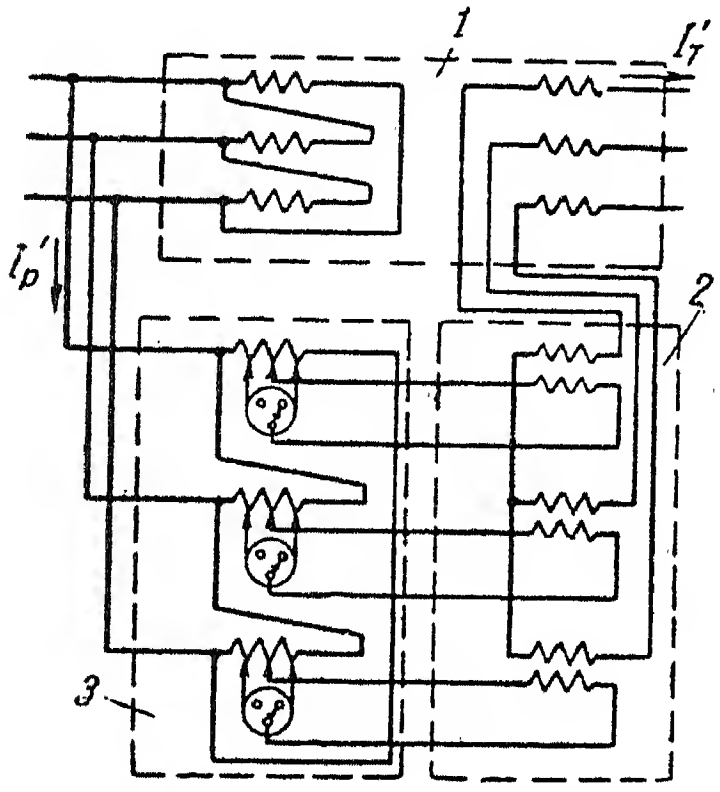

FIG.1. Schematical representation of a transformer with on-load voltage-regulating gear.
1-Main Transformer; 2-Series Transformer; 3-Regulating Autotransformer.

The present communication considers the protection of a regulating autotransformer (or transformer) against phase-phase faults and short-circuits between the lead-outs of its secondary winding. Our considerations will deal more specifically with the protection of autotransformers. However, they can be extended to include the case of a regulating transformer, and also other circuits comprising a power transformer or autotransformer with a booster group.

For a regulating autotransformer high-speed protection is desirable. Yet the use of the simplest types of high-speed protection entails certain difficulties.

The difficulty in using a tripping coil ("current cutout") consists in the fact that the currents set up at faults inside the autotransformer and at external faults may be of the same order. This makes it impossible to design a protection system of satisfactory sensitivity and operate from the short-circuit currents at external faults.

The difficulty in using a differential protection resides in the fact that the

* *Elektrichestvo* No. 5, 52 – 56, 1957 [Reprint Order No. EL24].

transformation ratio of the autotransformer varies between wide limits. The operating current of the protection, selected with allowance for the unbalance current set up by a variation of the transformation ratio of the autotransformer, may become so high that it may be impossible to assure the required sensitivity to short-circuits in the protected zone.

An inclusion of the autotransformer in the zone protected by the differential protection of the main transformer requires the sensitivity of this protection to be reduced. Also, the fault current in the autotransformer will, as a rule, be negligible in comparison with the operating current of the relay and the protection will then not operate in the case of such a fault.

A.A. Gevorkov suggested, in 1935, for the protection of autotransformers a special type of overcurrent relay connected to current transformers inserted into the primary circuit of the regulating autotransformer. At external short-circuits the protection is locked out by current relays connected into the circuit of the main transformer [1]. However, this protection system suffers from substantial disadvantages which will be considered below. For some types of autotransformers it is altogether unsuitable.

To protect a regulating autotransformer against phase-phase short-circuits and short-circuits between the lead-outs of an individual phase of its secondary winding the author of the present paper developed a new overcurrent protection with restraining characteristic (Fig.2). The current relays of this protection are connec-

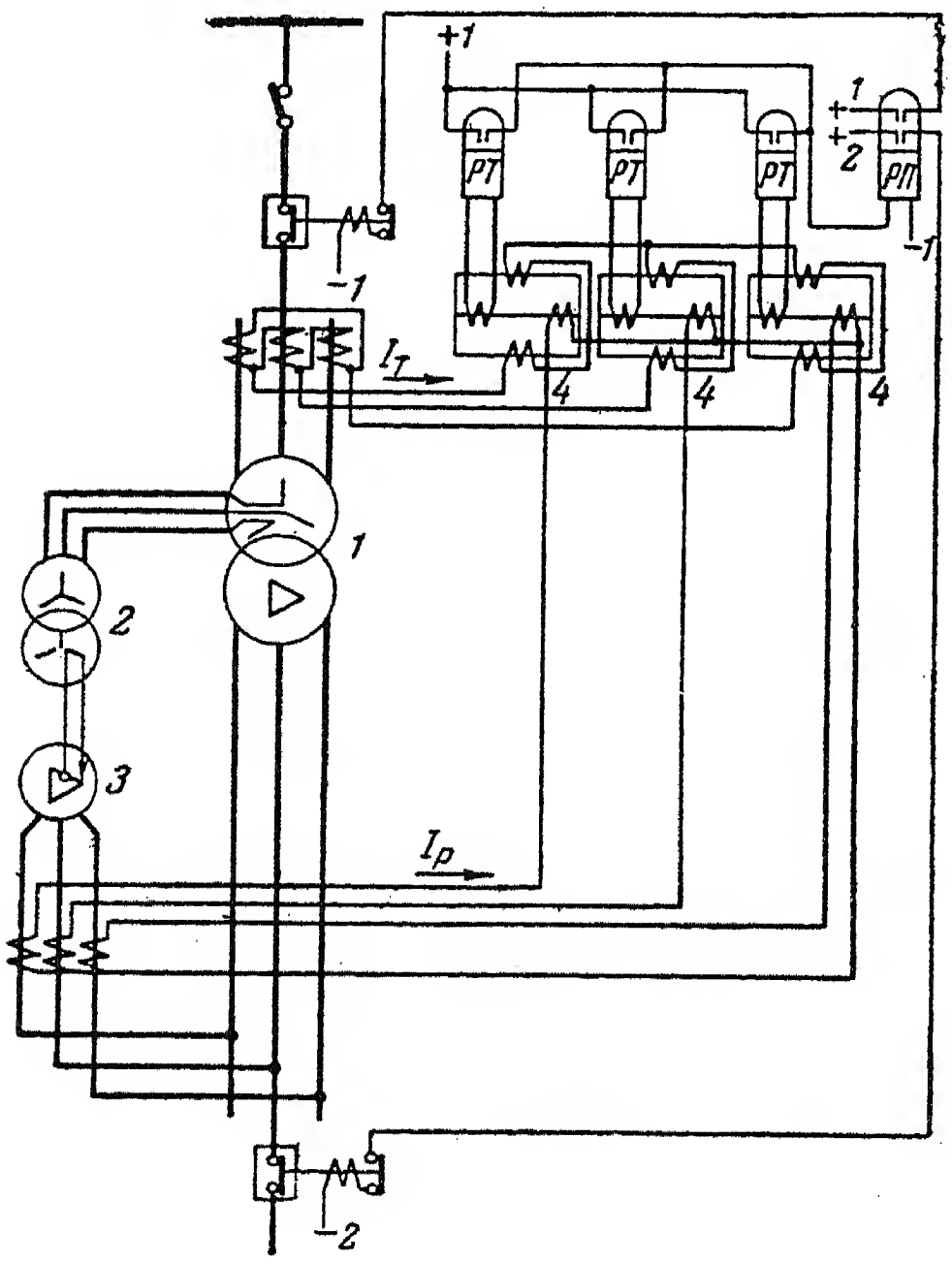

FIG.2. Protection of regulating autotransformer. 1-Main Transformer; 2-Series Transformer; 3-Regulating Autotransformer; 4-Interposing Saturable Transformers.

ted into the primary circuit of the regulating autotransformer.

To obtain magnetic restraint, the interposing transformer has in addition to its operating and secondary windings a restraining winding (Fig.3) connected to the current transformers inserted into the circuit of the winding of that side of the main transformer on which voltage regulation is carried out.

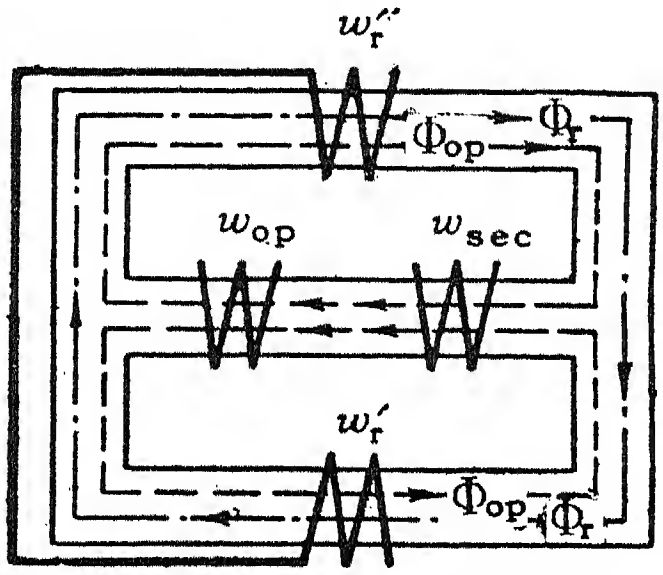

FIG.3. Interposing Saturable Transformer. w_r' and w_r'' restraining windings; w_{sec} secondary winding; w_{op} operating winding; Φ_r - flux set up by restraining windings; Φ_{op} - flux set up by operating winding.

When no current flows through the restraining windings the interposing transformer operates as an ordinary saturable transformer. The magnetic flux produced by the restraining windings when current passes through them is closed through the outer limbs, it does not enter the middle limb nor does it set up an e.m.f. in the secondary winding, but it saturates the magnetic circuit and deteriorates the conditions of transformation of the operating current. The higher the restraining current, the greater must be the current in the operating winding in order to obtain in the secondary winding a current equal to the operating current of the relay.

To show the advantages of the new system over the protection with a lock-out, we will consider the sequence of the selection of the parameters of both systems.

The operating current of the lock-out relay in the protection working with lock-out must be greater than the maximum operating current and the maximum short-circuit current in the zone protected by the relay. The latter is assumed equal to the maximum current at the point of erection of the locking relays for short-circuits on the secondary lead-outs of the autotransformer.

There are therefore two conditions for the selection of the operating current of the blocking relays, viz.

$$1)\ I_{op.bl.r} \geq K_r I_{t.op.max},$$

$$2)\ I_{op.bl.r} \geq K_r I_{sh.max},$$

where K_r is the coefficient of reliability, $I_{t.op.max}$ the maximum operating current in the winding of that side of the power transformer where the voltage is regulated, $I_{sh.max}$ the maximum current in the same winding of the power transformer at an internal short-circuit in the regulating autotransformer.

As a rule, the second condition is the decisive one. For this reason the operating current of the blocking relays becomes greater than the rated current of the autotransformer

$$I_{op.bl.r.} > I_{r.rat.} \qquad (1)$$

At through short-circuits and under normal conditions the primary current of the regulating autotransformer is

$$I_r = KI_t \tag{2}$$

where K is a proportionality factor and I_t the current in the winding of the power transformer on the side at which the regulation is carried out.

The proportionality factor K may be determined with satisfactory accuracy as the product of the transformation ratios of the regulating autotransformer and series transformer, respectively, viz.,

$$K = k_r k_s \tag{3}$$

The theoretical value of this factor K will be greater than its actual value.

Fig.4 represents the relationship $I_r = f(I_t)$ and the characteristic of the protection according to Fig.2.

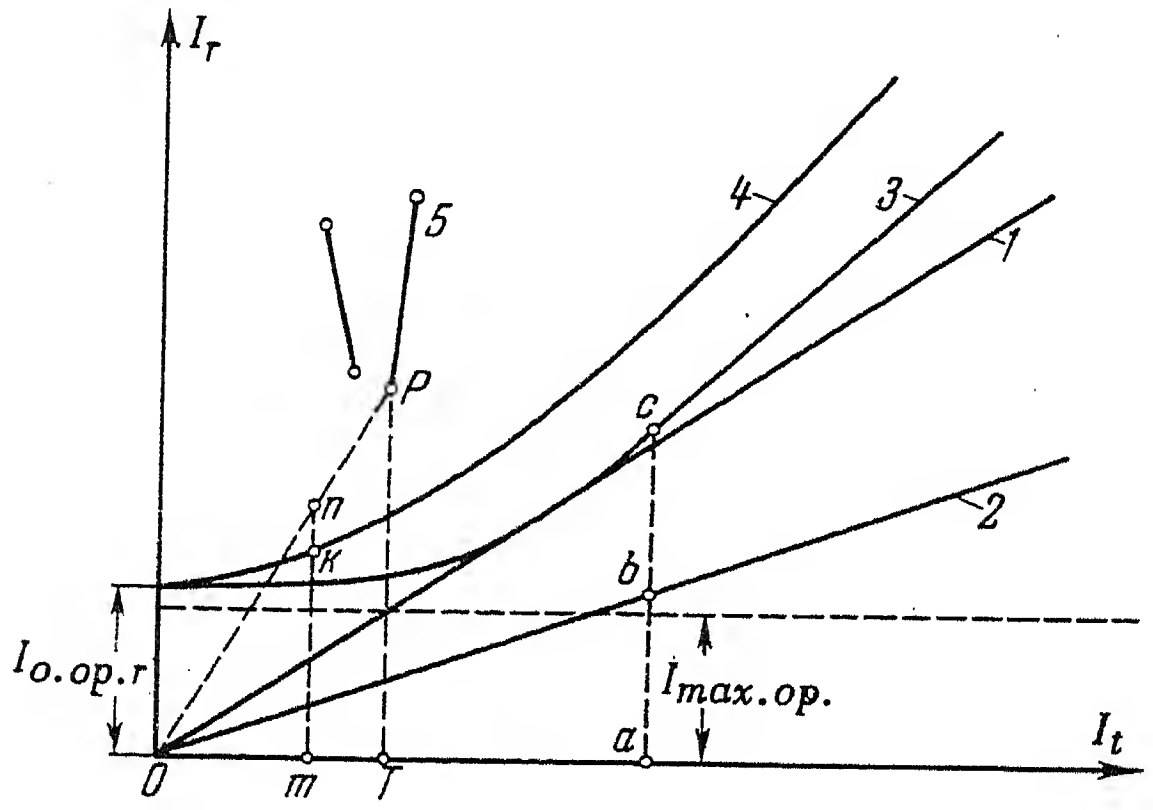

FIG.4. Relationship between Current in primary Winding of Autotransformer and Current in Winding of Main Transformer.
1 – ideal Characteristic of Protection; 2 – $I_r = KI_t$;
3 – $I_{op.r}(\mathrm{I}) = f(I_t)$; 4 – $I_{op.r}(\mathrm{II}) = f(I_t)$; 5 – $I_{r.sh.} = f(I_t)$.

For a selective action of the protection at external short-circuits the following relation must hold between the operating currents of the blocking and protective relays

$$I_{op.pr.r.} = K_r' I_{op.pr.r.} \tag{4}$$

where K_r' is the coefficient of reliability ($K_r' > 1$). Consequently,

$$I_{op.pr.r.} > I_{rat.r.} \tag{5}$$

Practical calculations showed that $I_{op.pr.r.} \gg (1.5\text{–}2)\, I_{rat.r.}$ i.e. the protection is of low sensitivity.

A protection with locking-out device may fail to operate at short-circuits in

the autotransformer where the current in the blocking relay exceeds the maximum of the theoretical short-circuit current. Also, it does not operate at phase-phase short-circuits on the lead-outs of the primary winding of the autotransformer because in this case the short-circuit current on the side where the blocking relays are placed is greater than the operating current of the latter. It may be equal to the current set up in the case of short-circuits on the low-voltage side.

Failure to respond of the protection in the cases mentioned will require the installation of a stand-by protection or the inclusion of the autotransformer into the zone protected by the differential protection of the main transformer. The latter method meets with certain design difficulties in some cases.

When the autotransformer (without its tap-changing gear) is included in the zone protected by the differential protection of the main transformer, the operating current of the blocking relays may be reduced by matching to the operating current of the differential relays; this increases the sensitivity of the protection to short-circuits in the autotransformer.

The ideal characteristic of a current protection with restraint may be represented by a straight line, whereas its actual characteristic is curved (Fig.4). Also, according to the angle α between the vectors of the currents in the operating and restraining coils of the relay, the restraining characteristic may be above or below the characteristic for $\alpha=0^{\circ}$, i.e. at the same value of I_t the operating current may have different values.

To calculate the selectivity of the protection the characteristic $I_{op.r}(\mathrm{I}) = f(I_t)$ corresponding to the angle at the minimum restraint is selected.

To prevent non-selective operation of the protection when its secondary circuits are interrupted, the operating current of the relay without restraint $I_{0.op.r.}$ is assumed greater than the operating current of the autotransformer.

The quotient of the ordinate ac (Fig.4) of the characteristic of the relay $I_{op.r}(\mathrm{I}) = f(I_t)$ adopted for calculating the selectivity by the ordinate ab of the straight line $I_r = KI_t$ for the same current I_t determines the margin of selectivity or the coefficient of reliability K_r.

The minimum value of this coefficient should not be less than 1.2.

In the case of short-circuits in the autotransformer the curve relating the current of the autotransformer $I_{r.sh.}$ with the current in that winding of the main transformer on whose side the regulation takes place is higher up than the curve $I_r = KI_t$. On a three-phase short-circuit on theconnections between regulating and series transformers fed only from the h.v. side, the above relation takes the following form

$$I_{r.sh.} = k_t I_t \qquad (6)$$

where k_t is the transformation ratio of the main transformer.

As a rule, the coefficient k_t is considerably greater than the coefficient K. Consequently, for the same value current I_t is greater than current I_r.

To calculate the sensitivity we assume the characteristic for an angle between the vectors of the operating and restraining currents corresponding to maximum restraint. The minimum coefficient of sensitivity K_{sen} is determined by the quotient of the ordinate mn of the curve $I_{r.sh.} = f(I_t)$ corresponding to the current $I_{r.sh.}$ calculated under consideration of the fault resistances, by the ordinate mk of the curve $I_{op.r}(\text{II}) = f(I_t)$ for a restraining current also calculated under consideration of the fault resistances.

The consideration of the fault resistances in the calculation of the fault currents may be carried out by reducing the currents of a dead short-circuit by factors of 1.5–2. The coefficient of sensitivity of the protection at the minimum fault current must not be below 1.2–1.3.

The minimum coefficient of restraint of the protection K_{rest} is determined as the tangent of the angle of slope of the tangent to the characteristic of restraint $I_{op.r}(\text{I}) = f(I_t)$, drawn from the origin of the coordinates. It is found from the following expression

$$K_{rest} = K_r I_{op}/I_{rest} = K_r K n_t/K_{cc} n_{t.r} \qquad (7)$$

where K_r – is the coefficient of reliability, $I_{op.}$ –the current in the operating winding of the interposing transformer, I_{rest} – the current in the restraining coil of the interposing transformer, K – the theoretical value of the coefficient of proportionality between the currents $I_{op.}$ and I_{rest}, n_t – the transformation ratio of the current transformers in the circuit of the main transformer, $n_{t.r.}$ – the transformation ratio of the current transformers in the circuit of the primary winding of the regulating autotransformer, K_{cc} – the coefficient of the circuit connections of the current transformers in the circuit of the main transformer.

By contrast to a protection with blocking relay the protection with a relay with restraint is intrinsically a high-speed protection, i.e. its reliable operation in the case of external short-circuits can be assured without introducing an additional time-lag.

Saturable interposing current transformers are also used for offsetting against magnetizing current rushes occurring when the transformer is connected under no-load conditions.

Fig.5a shows a single-line diagram of a variant of an autotransformer whose stationary lead-out is fixed at the mid-point of the winding. In this case the short-circuit currents are limited by the resistance of the winding at any position of the moving lead-out.

Fig.5b shows another variant of the autotransformer; the stationary lead-out of this is fixed at one end of the winding. When the moving lead-out is at the

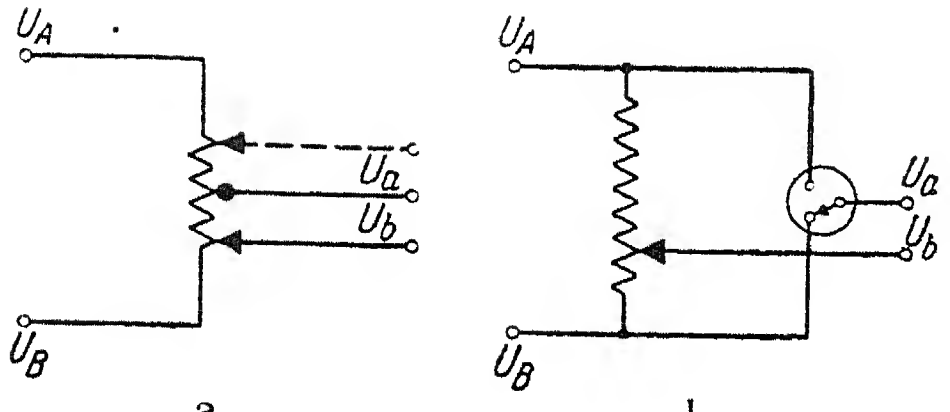

FIG.5. Variants of the Location of the stationary Lead-out of Autotransformers. a - stationary lead-out fixed at midpoint of winding; b - stationary lead-out fixed at ends of winding.

opposite end of the winding, the short-circuit currents are not limited by the resistance of the autotransformer and are of the same magnitude as on external short-circuits on the side to which the regulating element is connected. To such an autotransformer a protection with blocking relays cannot be applied since at the maximum regulation the values of the currents at the location of the blocking relays are of the same order in the cases of external short-circuits and of short-circuits at the lead-outs of the secondary winding of the autotransformer. Also, the protection with lockout may fail to respond at overload currents of the main transformer exceeding the operating current of the blocking relays.

A protection with restraining characteristic has none of the disadvantages mentioned; also, it may be made more sensitive and has a larger protected zone.

Fig.6 shows a comparison of the characteristics of the protection systems. To simplify the analysis, the effect on the characteristic of the protection of the angle between operating and restraining currents is not considered. In the shaded areas A and B the protection with lockout does not operate, but the protection with restraint does. Area A corresponds to faults with small, area B to faults with large short-circuit currents.

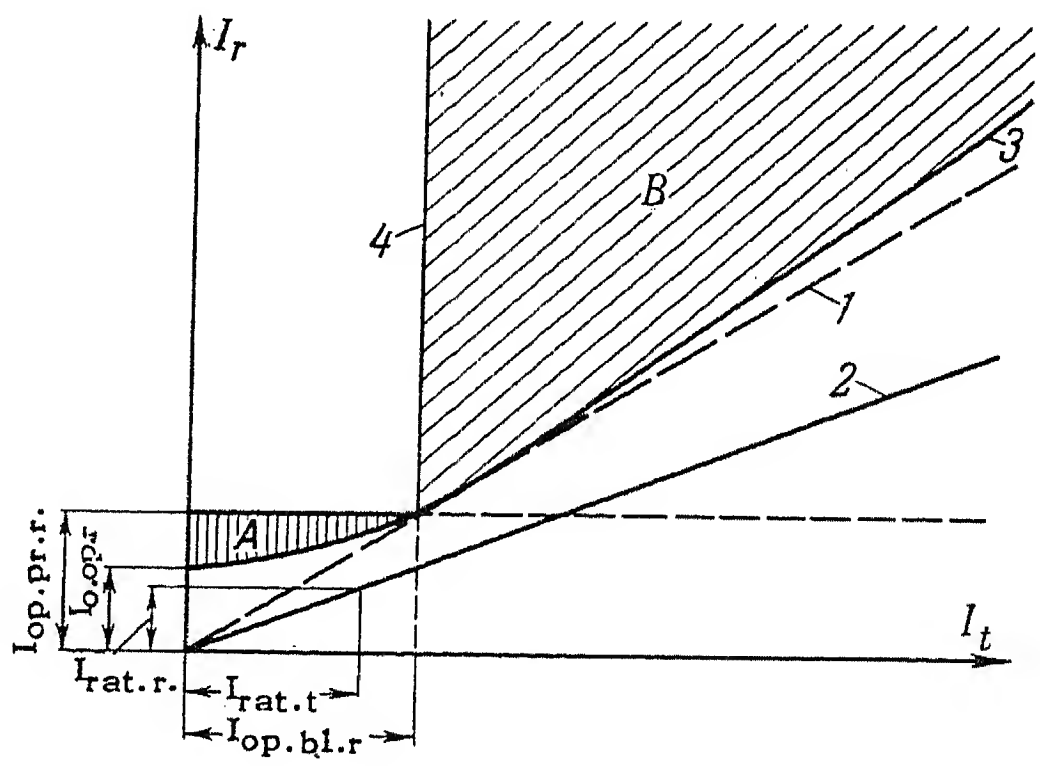

FIG.6. Comparison of Characteristics of Protection Systems for a Regulating Autotransformer.

1 - Ideal Characteristic; 2 - $I_r = KI_t$; 3 - characteristic of protection with restraint; 4 - characteristic of protection with lockout. $I_{op.op.r.}$ — operating current of operating relay; $I_{op.bl.r.}$ — operating current of blocking relay; $I_{rat.r.}$ — rated current of regulating autotransformer; $I_{rat.t.}$ — rated current of main transformer.

The zone protected by the protection with restraint includes the regulating autotransformer, the connexions between autotransformer and series transformer, and parts of the series transformer. As current relay a relay of type ET-520 may be used.

It should be noted that the protection may be designed not only

for the type of relays with restraint described above, but also with relays with independent restraining coils.

The difficulty of using commercially available relays with restraint consists in the fact that for the protection of a regulating autotransformer a relay with a high restraining factor is required. Orientating calculations show that the minimum restraining factor should be of the order of 1.5 – 2, whereas the commercial relays have only restraining factors of the order of 0.2 – 1.

Conclusions

The protection of a regulating autotransformer or transformer, using relays with a restraining characteristic has a number of advantages over a protection using blocking current relays. The protection with restraint is sufficiently sensitive for faults in a regulating autotransformer or transformer. For some types of regulating autotransformer only a protection with restraint may be used. The use of relays with restraining characteristic renders it possible to offset the relays against fault currents of external short-circuits and load currents. The protection with restraint is intrinsically a high-speed protection. It also requires fewer pieces of relay apparatus than the system with blocking relays.

REFERENCES

1. B. Ya. Smelyanskaya and A.B. Chernin; *Relay Protection of auxiliary transformers for longitudinal voltage regulation under load. Elektrichestvo* No.5 (1954).

CURRENT IN THE CHARGE MATERIALS OF A FERROSILICON FURNACE*

I.T. ZHERDEV

(Received 24 November 1957)

The type of iron-alloying furnace most frequently used nowadays is the circular-shaft three-phase type of furnace with continuous electrodes arranged in a triangle symmetrically to the axis of the furnace (Fig. 1). In normal operation the lower part of the electrodes plunges into the charge materials with which the working space of the furnace is filled. The power is supplied to the electrodes by a special furnace transformer enabling the value of the lower voltage to be altered. For any selected voltage of the transformer the load regulation is carried out by a vertical displacement of the electrodes or by altering the resistance of the charge continuously introduced through the top of the furnace.

Despite the apparent simplicity of the plant and the considerable successes achieved where equipment and operation of alloying furnaces is concerned, there is as yet very little in the way of a theory of the processes taking place in these furnaces. For this reason the main parameters of new furnace designs are usually selected by analogy with furnaces already successfully operating. For the same reason, the choice of rational operating conditions and the rapid correction of deviations from the normal course of the process requires highly skilled and experienced personnel.

That knowledge of the processes in alloying furnaces is still insufficient is also confirmed by the fact that up to the present there is no generally accepted view on the distribution and main paths of the current in the working space of the furnace and, consequently, no generally accepted views on the most suitable equivalent circuit for such a furnace.

That current passes through the charge materials of alloying furnaces was pointed out a fairly long time ago by M.S. Maksimenko [1] and Vochke [2]. In a discussion organised by the *All-Union Central Scientific Research Institute* in 1954, the view that a charge current virtually does not exist was expressed.

This considerable divergence of opinions on one of the fundamental questions associated with the problem of the correct representation of the phenomena in the

* *Elektrichestvo* No. 5, 65 – 67, 1957 [Reprint Order No. EL 25].

sondes being open;

I_1' – the current in the charge between the blades when the external circuit of the sondes is closed;

I_1'' – the current in the external circuit of the sondes when it is closed;

r_0 – the resistance of the part of the charge through which the current passes between the electrode and through the nearest blade;

r_1 – the resistance of the part of the charge through which the current passes from one blade to the other;

s – area of the blade of the sonde.

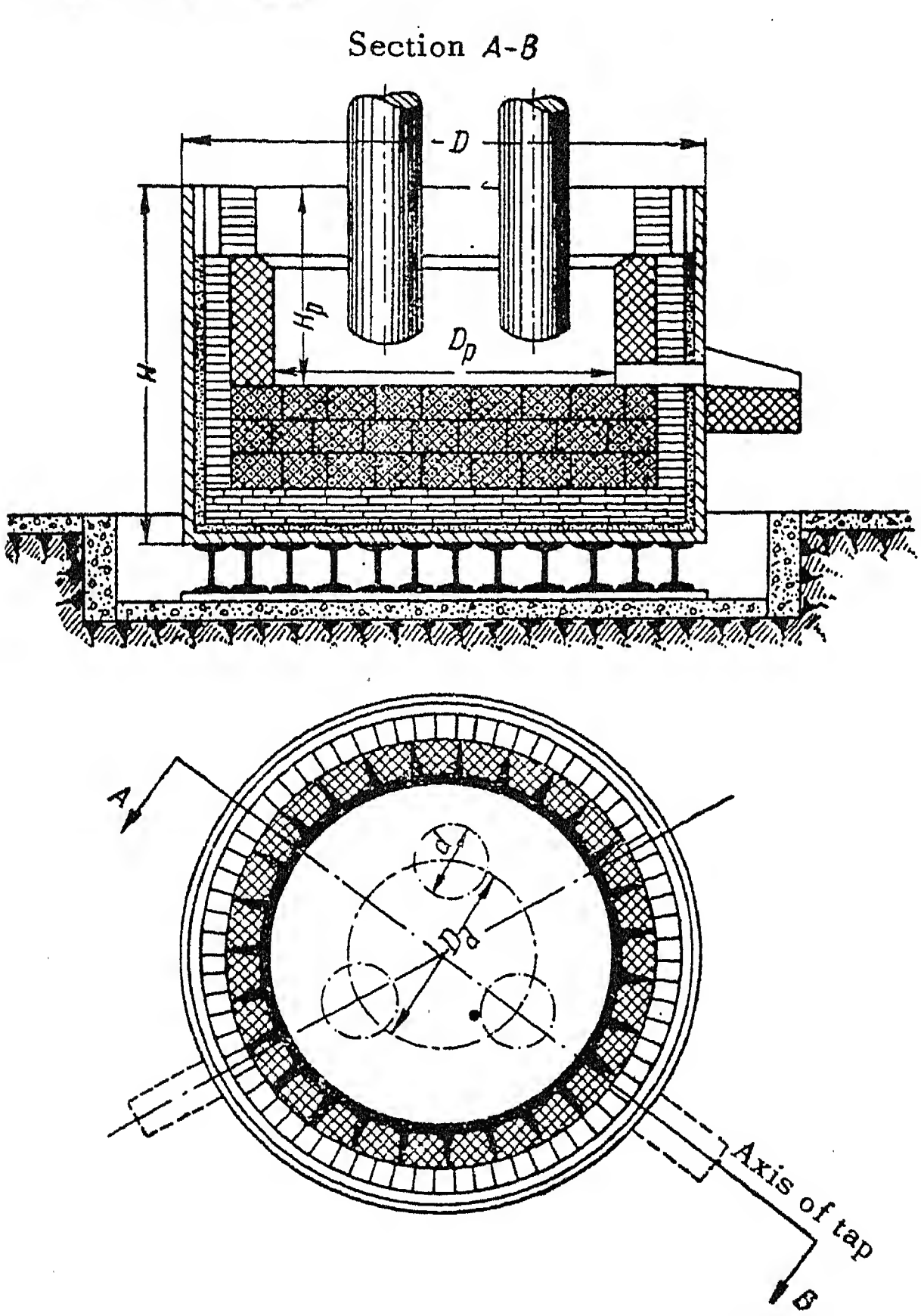

FIG. 1. Schematic plan and cross-section of a modern 3-phase alloying furnace.

Having calculated the p.d. between the blades of the sondes for open and closed external circuit of these sondes, we can express the current I_1' by the current I_1, viz:

$$I_1' = I_1 \frac{U_1 - U_2}{U_{10} - U_{20}}. \qquad (1)$$

Having determined the p.d. between the electrode and the blade of the sonde

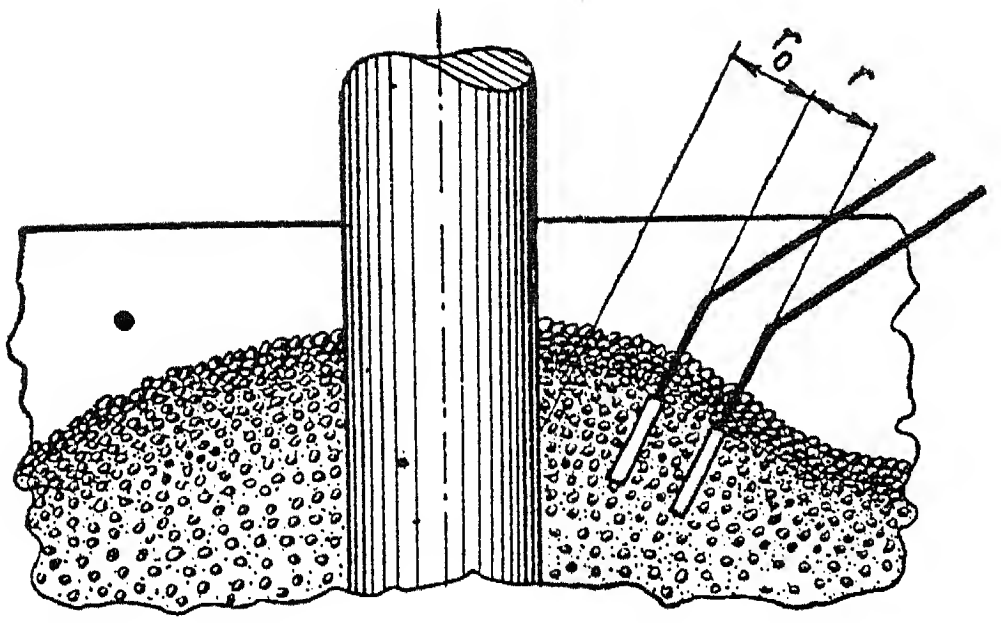

FIG. 2. Diagram of the location of the blades of the sondes for determining the current density in the charge materials.

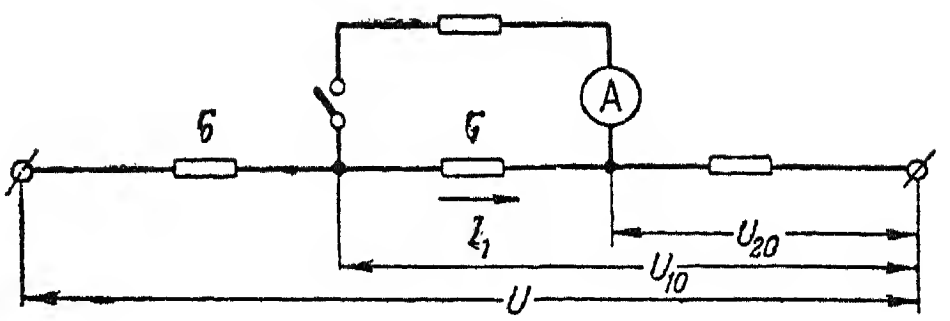

FIG. 3. Equivalent circuit for the current in the charge materials passing through the blades of the sondes.

nearest to it for open and closed external sonde circuit, we calculate the sum of the currents $I_1' + I_1''$, viz:

$$I_1' + I_1'' = I_1 \frac{U - U_1}{U - U_{10}}. \tag{2}$$

Substituting the value of current I_1 from (1) into (2), we get

$$I_1 = \frac{I_1''}{\frac{U - U_1}{U - U_{10}} - \frac{U_1 - U_2}{U_{20} - U_{20}}} \tag{3}$$

Equation 3 enables us to calculate the value of the current in the part of the charge between blades of the sondes under normal operating conditions of the furnace.

The mean current density in the charge materials in the volume enclosed by the surfaces of the blades of the sondes will be

$$j = \frac{I_1}{S}$$

From the current density and the p.d. it is easy to calculate the mean resistance of the charge between the blades of the sondes. The table brings together the results of measurements carried out by means of sondes in an actual furnace, and also the calculated current densities and resistances of the charge materials.

The above method of determining the current densities in the charge materials cannot claim to yield very accurate measuring results. In addition to the errors introduced by the basic assumptions, additional errors arise in the measurements on an actual furnace by incorrect arrangement of the blades of the sondes (deviation of the surface of the sonde from the equipotential surface), imperfect contact between the charge materials and the blades of the sondes, reduction of the area of the blades by their partial melting, etc.

It is, therefore, difficult to determine the magnitude and the character of the experimental error and the measured values of the current density shown in the table have, therefore, to be considered as purely orientating.

electric circuit of an alloying furnace is due to the absence of direct experimental demonstrations in favour of one or the other point of view.

The difficulties of carrying out experiments on an actual alloying furnace owing to the high temperature of the open top are well-known. However, it is possible to demonstrate the existence of a charge current and approximately to determine the current density in the charge materials in different parts of the working space of the furnace under conditions of industrial operation of such furnaces.

We give below a description of the method and the results of the experimental determination of current density in the charge of a ferrosilicon furnace. The measurements were carried out on a furnace (Fig. 1) producing 45 per cent ferrosilicon.

To measure the current densities in the charge we used sondes of a special form, produced from steel rods of 18 - 20 mm diameter and about 6 m length. One of the ends of each steel rod, about 300 m long, was bent to an angle of 60° and a blade of sheet steel about 10 mm thick and of an area of 200 - 300 cm² was welded to it.

The ends of the steel rods were inter-connected through a current transformer by means of clamps and flexible cables. When the cables were connected, the current of the external circuit of the sondes could be measured. The blades were plunged into the viscous charge materials in the working space of the furnace near the electrodes. The equivalent circuit of the blades is shown in Fig. 2.

To determine the current densities in the charge, the potentials of each blade relative to the neutral point of the furnace (its hearth) were measured on the sonde circuit which was opened and closed on the current transformer. In addition, the phase voltage of the electrode near which sondes were placed, and also the current in the external circuit of the sondes when it was closed, were measured.

All the following calculations to determine the densities of the charge current are based on assumptions that the resistances of the parts of the charge along the paths of the current passing through the sondes blades retain their value whether the external circuit of the sondes is open or closed; moreover, it was assumed that all the resistances in the paths of the charge mentioned and in the sonde circuit are purely active. In this case the equivalent circuit of the actual circuit of the charge current through the blades of the sondes may take the form represented in Fig. 3.

It is not difficult to calculate the current in the charge flowing in the region of the blades of the sondes when the external circuit of these sondes is open. We introduce the following symbols:

U – is the potential of the electrode relative to the neutral point of the furnace;

U_{10} and U_{20} are the potentials of the first and second blades of the sondes relative to the neutral point of the furnace when the external circuit of the sondes is open;

U_1 and U_2 are the potentials of the same blades relative to the neutral point of the furnace when the external circuit of the sondes is closed;

I_1 – is the current in the charge between the blades, the external circuit of the

Area of the blade of the sonde (cm^2)	Distance between sonde blades (cm)	Distance from electrode to nearest sonde blade (cm)	Measured with the external sonde circuit open (V)			Measured with external circuit of the sondes closed				Calcu-current density, j (A/cm^2)	Calcu-resis-tivity (ohm. cm)
			U	U_{10}	U_{20}	$U(V)$	$U_1(V)$	$U_2(V)$	$I_i(A)$		
310	20	41	64	38	10	64	20	10	180	0.43	3.3
310	20	28	72	49	32	72	48	36	90	0.87	1.0
310	20	28	72	50	25	72	47	26	100	1.1	1.2
200	10	37	58	27.5	18.5	58	26	20	40	0.52	1.7
200	15	31	78	35	24	78	22	18	150	0.80	0.9

Nevertheless, the data in the table make it possible to trace a certain regularity in the variation of the current density in the charge materials. The current density in the charge decreases with increasing distance from the electrodes; a similar relationship should also be observed for the working space of the furnace since the area of the current-carrying cross-section of the charge materials increases with increasing distance from the electrodes.

The method of measurement by means of sondes buried in the charge materials we put forward enabled us to determine the order of magnitude of the densities and resistivities of the charge of a working ferro-silicon furnace. These experimental results confirmed the necessity of considering the conductivity current of the charge in the study of the electric circuit of a ferrosilicon furnace.

REFERENCES

1. M.S. Maksimenko; *Vliiganic raspredeleniya sil toka na induktionoe soprotivlenie pechnoga kontura pechi Mige (Effect of Current Distribution on the Inductive Reactance of the Circuit of a Mige furnace)*, *Metallurg*, No. 9 (1938).
2. I. Vochke; *The Electric Smelting Furnace*, *United and Technical Publishing Houses*, 346 and 361 (1936).

LARGE SYNCHRONOUS MOTORS WITH SOLID POLES ON THE ROTOR*

Z.B. NEYMAN

(Received 4 February 1957)

For the drive of some high-speed mechanisms, e.g. blowers, pumps etc., large electric motors are required for a speed of 1500 rev/min. The use of induction motors with squirrel cage rotor is uneconomic because of the reduced p.f. It also must be considered that with increasing power of the drive and therefore, of the motor, the energy dissipated in the short-circuited rotor winding during starting increases more than the heat capacity of the rotor. With large motors it is therefore difficult to keep the temperature conditions of the rotor within the permitted limits. A further problem is how to provide sufficient mechanical strength for the rotor. These factors limit the maximum rating of induction motors with squirrel cage rotors to about 2000 kW.

Better economic characteristics are obtained by the use of synchronous salient-pole motors with a short-circuited winding for starting, located in the pole shoes. But long experience with the operation of such motors shows that they often fail because of damage to the joints and breakage of the rods of the starter winding. The fundamental difficulty of a reliable design of the rotor of the synchronous motor with starter winding on the poles is the great amount of heat developed during starting which leads to excessive heating of the winding, especially with drives having a large flywheel moment.

For driving high speed mechanisms a series of synchronous motors of 1300, 2000 and 3000 kW has been developed by the "Ural-Elektroapparat" Works with solid rotor and solid pole shoes. These motors have no special short-circuit windings which makes them very reliable in service.

The starting of the motor as induction motor is done in the same way as with synchronous machines with short-circuited winding on the pole shoes, i.e. by across-the-line starting or through a reactor with a reduced voltage of 70 per cent of the rated value.

At the beginning of the starting process the current is distributed over the surface of the solid pole shoes, since at a frequency of, or about, 50 c/s the depth of

* *Elektrichestvo* No. 6, 32 – 35, 1957 [Reprint Order No. EL 26].

penetration of the current is small. The current runs parallel to the rotor axis and is terminated in a tangential direction at the edges of the pole shoes. The pole shoes are interconnected on both sides of the rotor by copper rings so that a part of the current circuit may be closed through these rings. With increasing rotor speed the frequency of the pole shoe current decreases and the current penetrates more deeply into the steel.

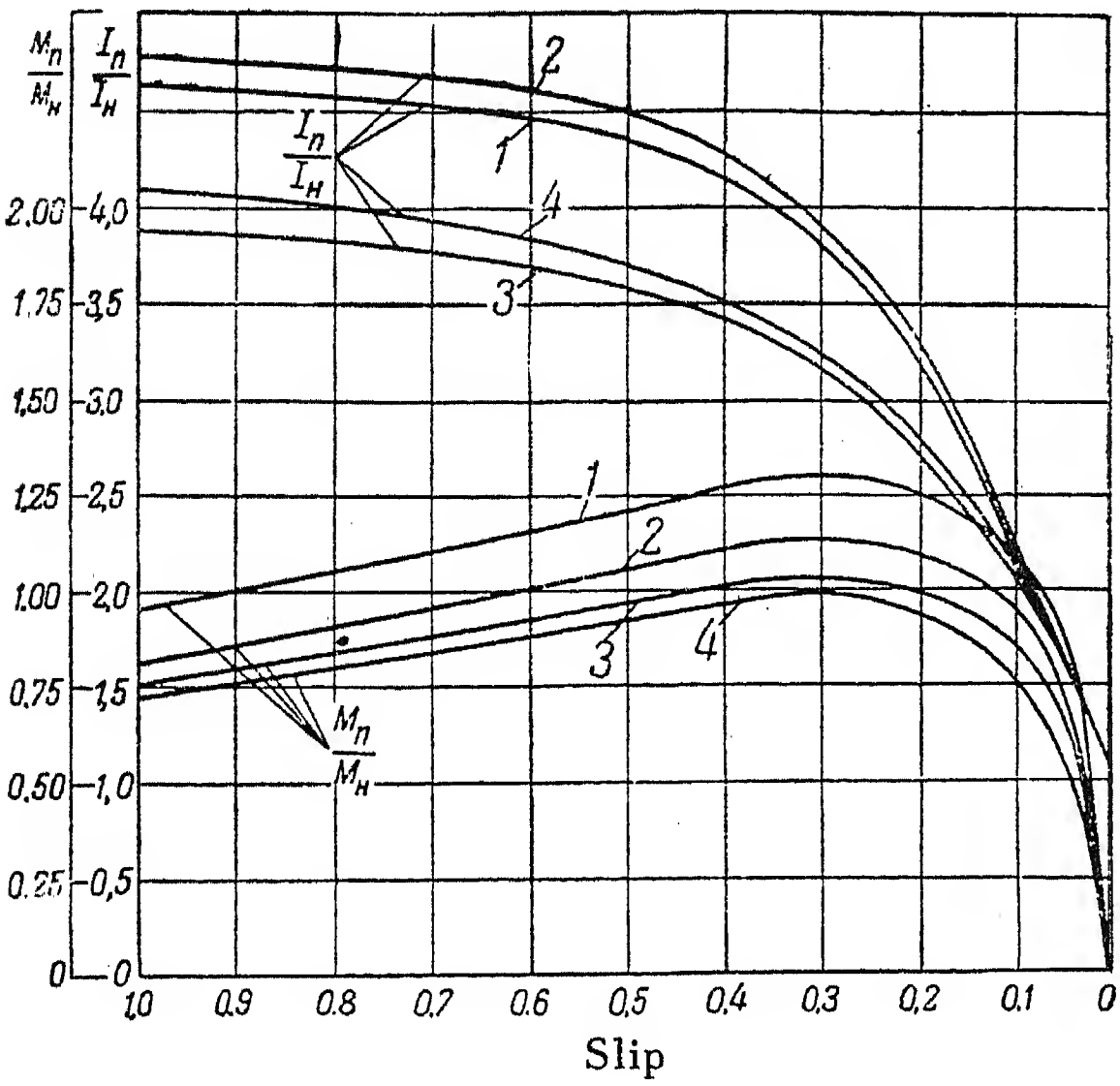

FIG. 1. Starting characteristics of the motor type DSP 116/49-4 (1300 kW, 6000 V, 1500 rev/min)
1 - rotor closed across discharge resistor, pole shoe faces connected through copper rings.
2 - rotor short-circuited, pole shoe faces connected through copper rings.
3 - rotor closed across discharge resistor, pole shoe faces open (copper rings removed).
4 - rotor short-circuited, pole shoe faces open (copper rings removed).

Fig. 1 shows the starting characteristics of the motor type DSP 116/49-4 (1300 kW, 6000 V, 1500 rev/min). These chacteristics correspond to starting at full voltage with the field winding of the motor short-circuited or closed across a discharge resistor. In order to check the effects of the rings connecting the faces of the pole shoes the starting characteristics were taken with and without these rings.

Fig. 1 shows that the asynchronous torque is considerably higher with the rings. The tests also showed that under asynchronous conditions the motor worked with better stability and pulled into synchronism more safely. As could be expected, the presence of the discharge resistor in the field circuit has a marked effect on the increase of the asynchronous torque.

The starting characteristics in Fig. 2 of a motor connected to a fan drive of the type D 3500-11 again show the favourable effect of the copper rings connecting the faces of the pole shoes.

The starting characteristics of the motor type DSP 140/74-4 (3000 kW, 6000 V, 1500 rev/min), also with solid pole shoes on the rotor, are reproduced in Fig. 3.

It should be noted that there are as yet no practical methods for determining the starting chacteristics of motors with solid poles on the rotor with the accuracy required. The method of calculating the starting process suggested by Kh. R. Bal'yan [1] yields somewhat low values of the starting characteristics.

It is known that with laminated poles the pole face losses are insignificant. But with solid poles, especially when the ratio of stator slot width to air gap is larger

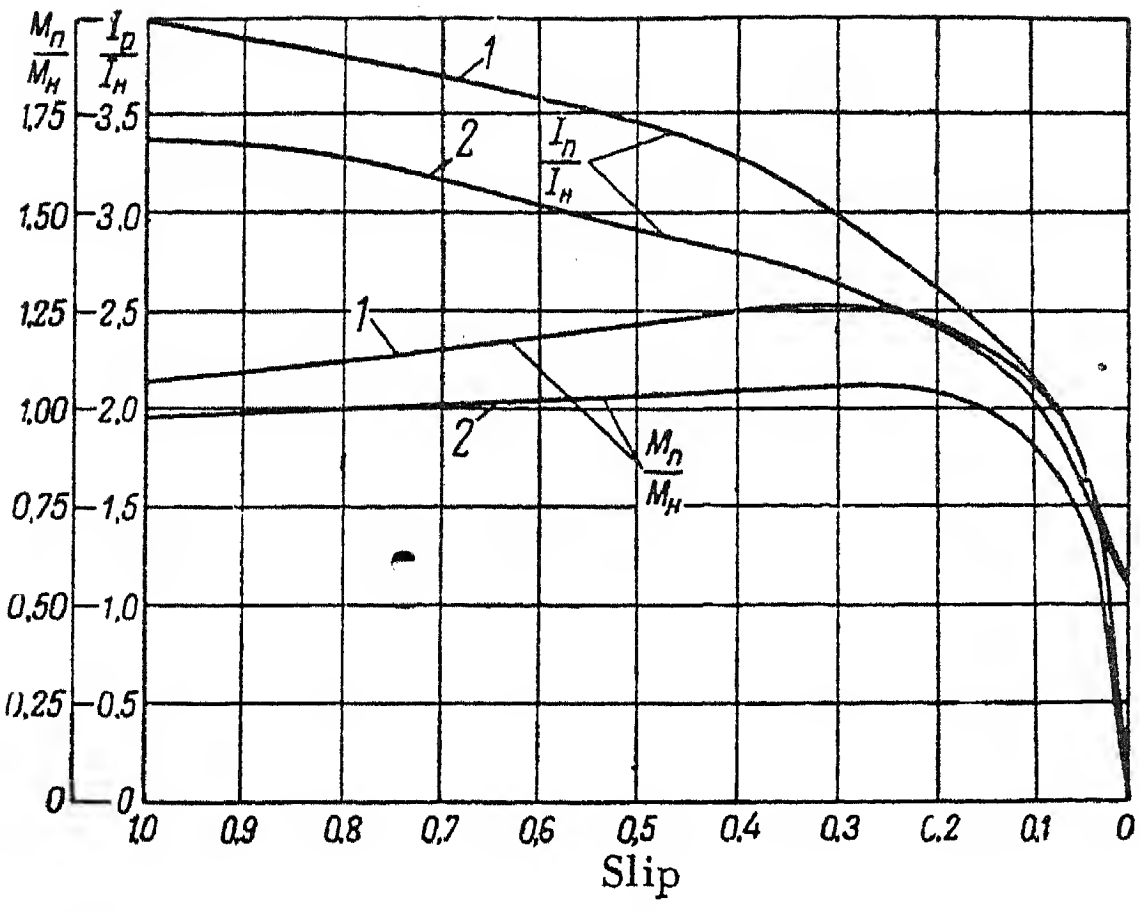

FIG. 2. Starting characteristics of the motor type DSP 116/49-4 connected with an exhauster type D 3500-11 (start on across the line with exhauster valve closed).
1 - rotor closed across discharge resistor, pole shoe faces connected through copper rings,
2 - rotor closed across discharge resistor, pole shoe faces open (copper rings removed).

than unity these losses increase considerably. On the motors of the series DSP this ratio is slightly larger than unity and therefore the effect of the surface losses on the total steel losses is insignificant. On an average, the pole face losses of these motors do not exceed about 8 per cent of the total losses in the machine.

The temperature rise of the pole shoes of the rotor during starting was determined by tests on a 1300 kW motor driving a fan type D 3500-11. During the start of the motor with resistors in the field circuit the temperature rise in the pole shoes was 100 - 130°C and in the connecting rings 140 - 180°C for an initial temperature of 50 - 60°C. Starting took about 16 sec. With direct connection of the field winding to the exciter, the temperature rise of the pole shoes was about 30 per cent higher than the above values.

These experimental data agree satisfactorily with values of the pole shoe temperature calculated from the duration of the start and the magnitude of the relative losses in the pole shoes at the instant of connecting the motor to the system. (Data of the Central Electrical Research Laboratory given in [2 and 3]).

The motors of the DSP series are of the fully-enclosed type and have two-way radial and axial ventilation. The air circulation in the machines is maintained by the rotation of the salient poles of the rotor and by two fans of the propeller-blade type mounted on the shaft at both ends of the rotor. (Fig. 4). The intake of the cool air is below the machine and so also the outlet of

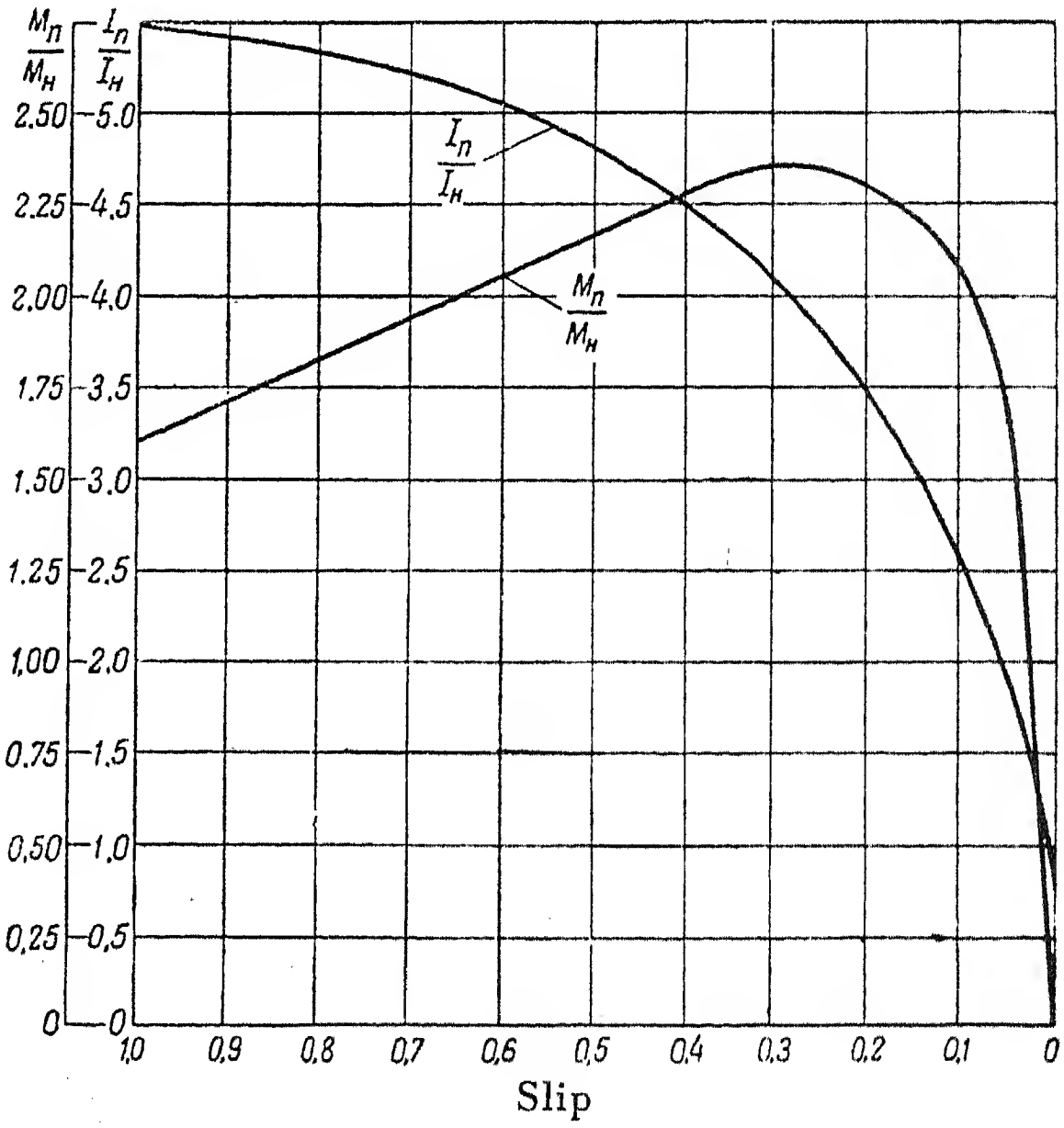

FIG. 3. Starting characteristics of the motor type DSP 140/74-4 (3000 kW, 6000 V, 1500 rev/min).

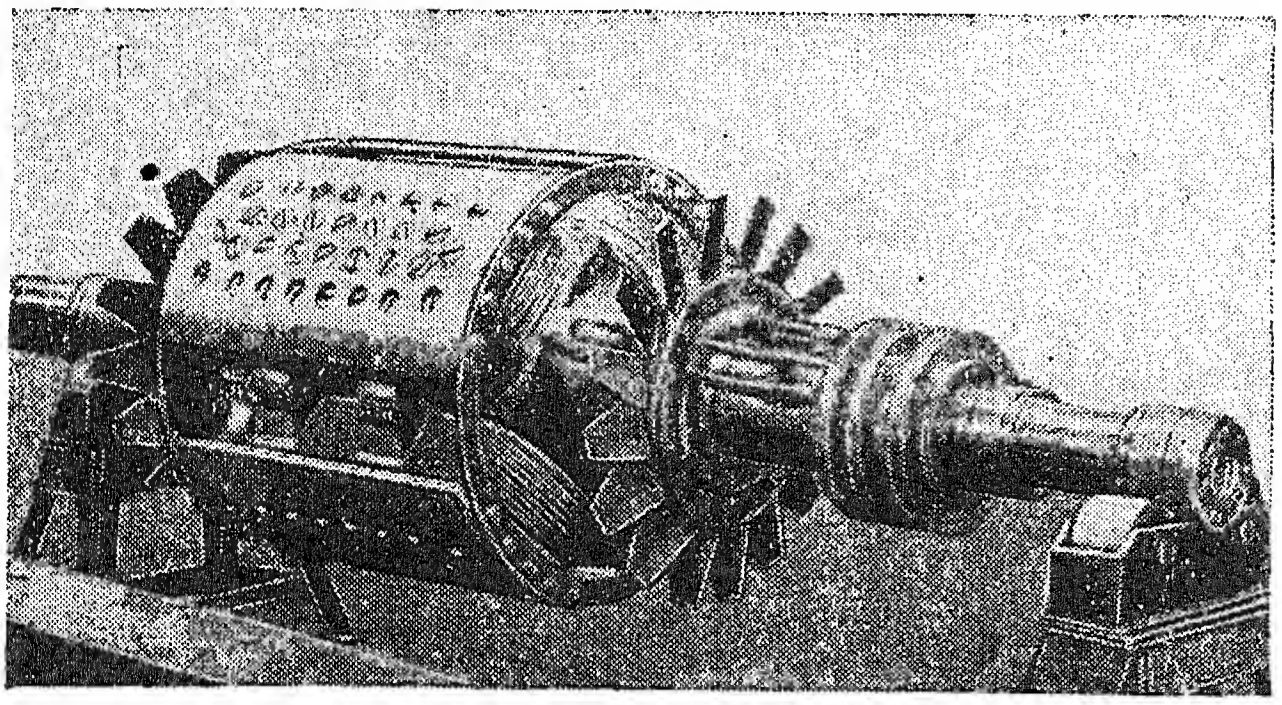

FIG. 4. Rotor of the motor type DSP 140/74-4 of 3000 kW.

the warm air through ducts of of the stator.

A special feature of the rotor design of the 1300 kW motor is its cross-shaped frame made of strong steel plates to which the four pole shoes are bolted. The copper rings are also bolted to the ends of the pole shoes.

For reasons of mechanical strength the rotors of the 2000 and 3000 kW motors are steel forgings. The rotor windings consist of bare copper strips. The turn insulation consists of varnished asbestos.

The stator bodies are of welded construction. The core is made of highly-alloyed dynamo sheets. The stator windings have reinforced mechanical clamping to ensure reliable service of the machine in transient conditions and during starting. The coil insulation is compounded mica.

The motors have bracket-type bearings with self-adjusting bushings; the working surfaces of the bearings are babbitted. The bearings of the motor have ring lubrication. The 3000 kW motors are also designed for forced-oil-lubrication. The bearings are provided with reliable oil-seals.

The excitation of the motors is obtained from directly-coupled exciters of type PN. The value of the field current for the motors of 1300 and 3000 kW is 370 and 490 A respectively. (Exciters type PN-205 and PN-400 are used.)

The motors with solid poles on the rotor have more favourable weight figures than synchronous and induction motors for 1500 - 300 rev/min (Fig. 5). Bearing in mind the weight of the exciter, which in the range considered amounts to about 5-6 per cent of the total weight of the motor, we find that the weights of the synchronous motors with solid poles are more favourable than those of four-pole induction motors. The efficiency of the synchronous motors of the series DSP is also higher than that of four-pole induction motors (Fig. 6).

The experience gained on design and operation of the four-pole synchronous machines of the type DSP of the "Ural-Elektroapparat" Works enables us to to state that the range of applications of high-speed synchronous machines of the series DSP could still be usefully extended.

Solid-pole synchronous condensers equipped with high-speed field regulation must be considered as a very promising application of the new design. Good starting characteristics of the motor with solid poles would render it possible to start the condensers at a very much reduced voltage and the presence of the large air gap between

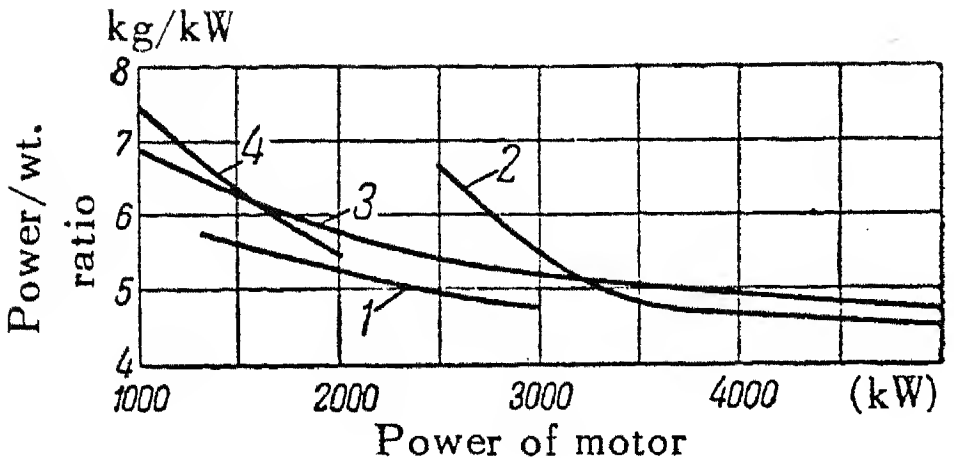

FIG. 5. Relative weights of the electric motors
1 - synchronous motors of the DSP-series, 1500 rev/min.
2 - synchronous motors of the CM-series, 3000 rev/min.
3 - induction motors 1500 rev/min.
4 - induction motors of the ATM-series, 3000 rev/min.

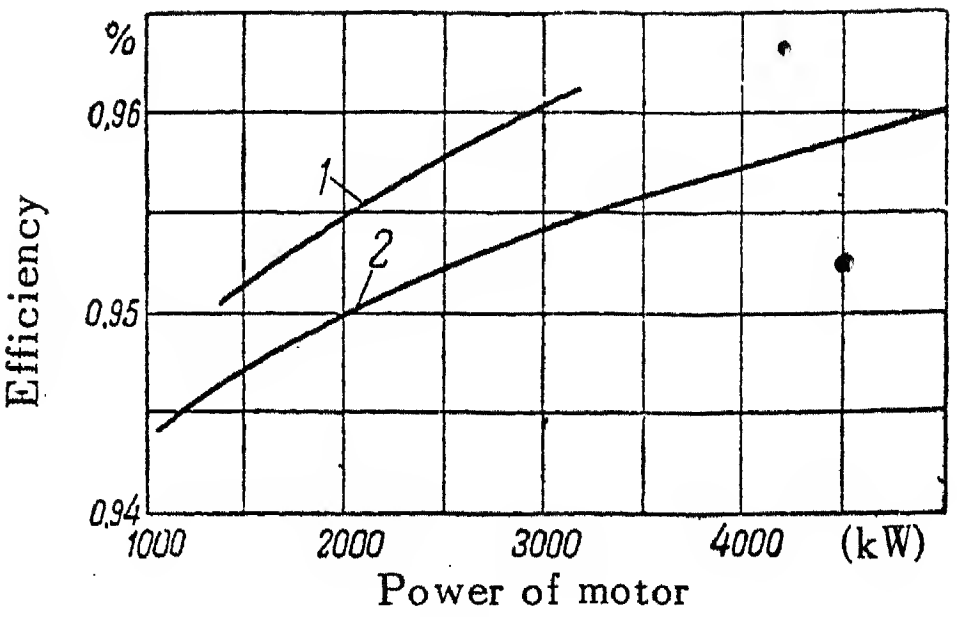

FIG. 6. Efficiencies of electric motors
1 - synchronous motors 1500 rev/min.
2 - induction motors, 1500 rev/min.

stator and rotor virtually suppresses the effect of the pole shoe face losses at the starting of the motor.

It is also suggested to develop a series of small condensers of the 2000-5000 kVA range at 1500 rev/min based on the design of the four-pole machines of the DSP series.

The experience gained in recent years with the operation of high-speed synchronous motors with solid poles on the rotor has confirmed the possibility of their wider use in place of smaller machines with laminated poles and with squirrel-cage windings in the pole shoes.

REFERENCES

1. R.Kh. Bal'yan, *On the design of the solid rotor. Elektrichestvo*, No. 6, (1955).
2. I.A. Syromatnikov; *Operating conditions of synchronous generator. Gosenergoizdat* (1952).
3. *Report No.* 1-113 *Central Electrical Research Laboratory* (1954).

TURBOGENERATOR ROTOR WITH DIRECT COOLING OF THE WINDING CONDUCTORS*

V.V. TITOV and Z.B. KOGAN

(Received 18 January 1957)

In the instructions of the Sixth Five-Year Plan for the development of the national economy of the U.S.S.R. for 1956 - 1960 by the 20th Congress of the Communist Party of the U.S.S.R. suggestions on the design and construction of large generators of ratings up to 300 MW were included.

In the course of the development of new types of large turbogenerators the "Elektrosila" Works designed and produced an experimental rotor with direct hydrogen-cooled conductors. This rotor was installed in an actual set of 30 MW rating in one of the Leningrad power stations in 1956 and was tested in service on load.

Design of the Rotor Winding

In the project the design of the rotor was based on the principle of self-ventilation with inlets and outlets for the cooling gas distributed over the whole length of the rotor. This leads to the most uniform distribution of the copper temperature along the machine.

The principle of introducing the cooling gas into the rotor directly from the air gap of the machine is well known; it is used by the American General Electric Co. In the generators of this firm the gas circulates in the longitudinal or the axial direction of the rotor through ducts formed by the hollow rotor conductors. The length of the sections of these ducts is about 500 - 600 mm. The gas enters and leaves each conductor through a system of openings in the rotor teeth and slot wedges. The gas flow in a rotor of this design is shown schematically in Fig. 1.

The "Elektrosila" Works used an original construction and layout of the ducts in the rotor conductors. The coils in the slotted part of the rotor consist of conductors of the usual rectangular cross section. On the lateral faces of the coils oblique channels 18 mm wide are milled all along the slotted part of the rotor. At either side of each coil the channels are inclined at the same angle to the axis of the conductors, but slope in different directions. The gas enters a channel

* *Elektrichestvo* No. 6, 35 - 38, 1957 [Reprint Order No. EL 27].

through an opening in the wedge, flows along and down the coil to the bottom of the slot, passes under the bottom turn, up through a channel on the other side of the coil, and into the air gap through an outlet opening also in the wedge. Inlet and outlet gas zones alternate on each side of the coil. The width of a zone equals the spacing between the inlet and outlet openings of the connected ducts. The distribution of the channels is shown in Fig. 2.

The bottom of the rotor slot is semi-circular in shape and is filled with an insulating packing which i s grooved to allow the gas to flow from one side of the coil to the other. The end connectors or parts of the coils outside the rotor body are of hollow section. Each conductor consists of two U-shaped bars forming an internal duct in the conductor which is linked to a sloping channel in the slotted part of the rotor. The gas, having passed through the duct in the end connector, is discharged through the lateral sloping channel into the air gap. Provided a sufficiently high velocity of gas flow through the ducts and channels is assured, this design will result in a good heat dissipation and in practically uniform copper temperature all along the winding.

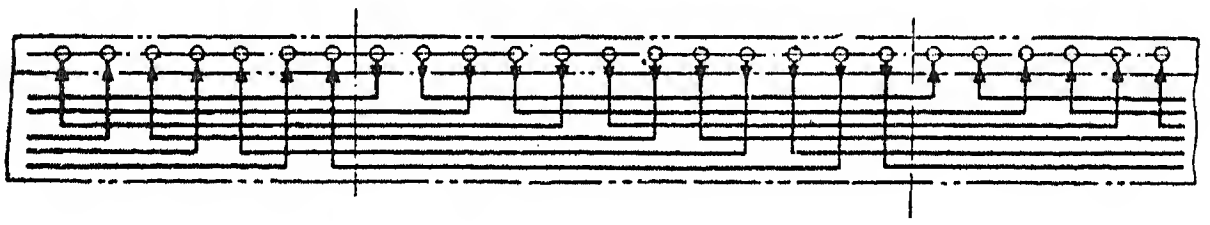

FIG. 1. Schematical diagram of gas flow along rotor winding conductors. General Electric Company.

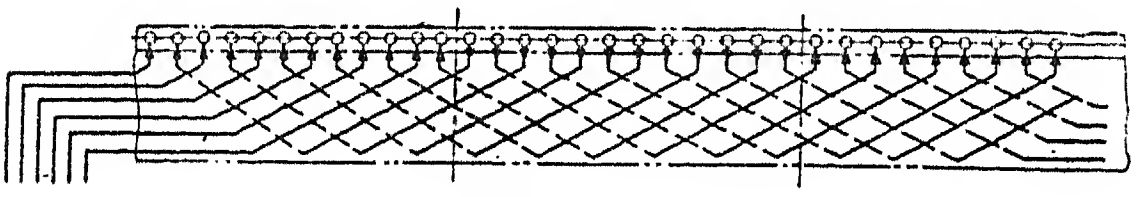

FIG. 2. Schematical representation of gas flow along winding conductors of rotor of "Elektrosila" Works.

The gas velocity in the ducts and channels is greatly affected by the shape and dimensions of the inlet and outlet openings for the cooling gas. On the experimental rotor the openings in the wedge were designed in the simplest manner which would still enable smooth inlet and outlet passage between the gap and the slot to be obtained (Fig. 3.). In the gas inlet zone the slot wedge was provided with a lip projecting slightly above the surface of the rotor. The channels in the slot wedges through which the gas enters the slots are arranged alternately in the leading and trailing edge, thus assuring a uniform distribution of the gas on both sides of the coil in every slot. The rotor teeth opposite the inlet openings in the wedges are chamfered in a radial direction. In the gas outlet zone the openings in the wedges are arranged on a slightly smaller diameter and the wedges do not project above the surface; the outlet openings also face annular grooves turned with a uniform pitch at the rotor surface. During the tests it was found that the gas velocity in a channel was on an average 20-25 per cent of the peripheral speed of the rotor.

The manufacture of the experimental rotor made it possible for the new design to be thoroughly tested. In contrast to the production processes required for a rotor of normal design the production of the coils and their insertion into the slots required the development of many specialized techniques. The U-shaped copper end connections were wound as coils and cut into four parts. The individual parts and the rectangular strips for the slots were fitted in a template and welded together. The finished half-turns were checked on the template, where they were formed to their final shape. When the inter-turn insulation had been applied, they were inserted into the rotor slots and welded together.

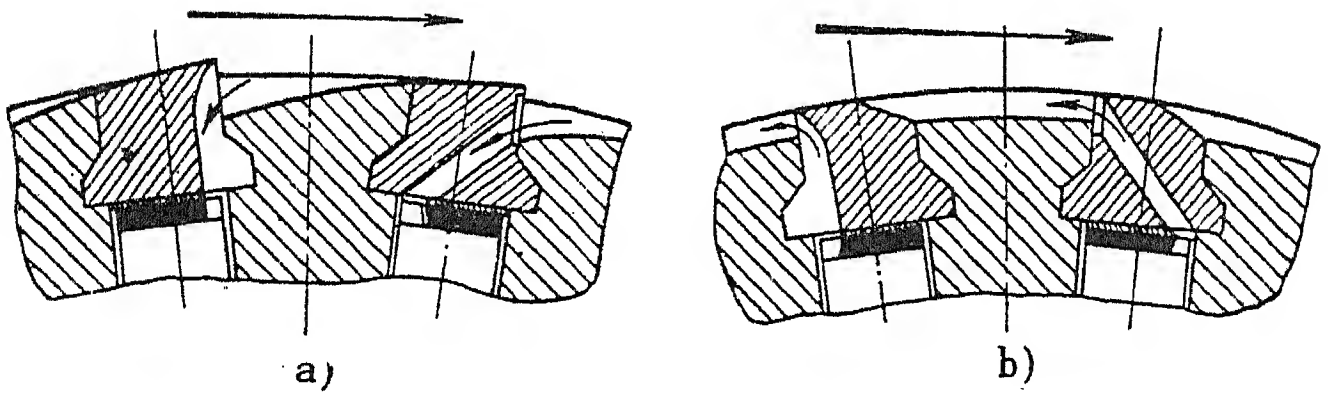

FIG. 3. Section through teeth and slot wedges a-gas inlet zone; b-gas outlet zone

The slot insulation was made of glass-textolite. The forming and stoving process of the coils did not take long, although the insertion and matching of the turns was very difficult. The machining of the rotor surface was not very difficult, since the gas inlet and outlet openings were not in the teeth, but in the slot wedges. In future it is proposed to use pressure cast wedges of a light and strong alloy. This will enable suitable shaped openings to be obtained with a satisfactory surface finish without further processing.

Owing to the fact that the rotor end connector is a hollow bar and is deeper than in a normal design, the total number of turns per pole is smaller, and the exciting current is correspondingly increased. If the exciting current on load in an ordinary turbogenerator rotor of 30 MW rating is 470-490 A, the corresponding current in the experimental rotor with direct-cooled conductors is about 1500 A. This required the rotor brush gear and slip rings to be correspondingly larger. The width of the brush contact surface of the slip rings was doubled in comparison with the normal design (cuts of worm wheel shape being also made in their middle parts), with a view to improving the cooling of the rings. The contact area between the current carrying studs and the slip rings, and the slip ring lead in the rotor bore were also enlarged.

The generator in which the experimental rotor was tested was provided with a new excitation system. A direct driven synchronous high-frequency generator supplied to a system of semi-conductor rectifiers, the rectified current being supplied to the rotor slip rings. The new excitation system is now being subjected to tuning-up and service tests.

The new design of rotor is mechanically stiffer than a normal rotor for the same turbogenerator. This is due to the reduction in weight of the rotor winding owing to the internal cooling of the conductors, and to the reduced over-hang of the end connectors resulting from reduced inter-coil spacing and solid packing of the end turns. In the new design it was possible to increase slightly the diameter of the rotor shaft under the end connectors and as a result, the deflection of the rotor shaft is reduced, thus relieving the stresses in the bearings.

Assembly and Operation

In recent years, sufficient data on the operation of turbogenerators with a hydrogen pressure of 0.05 - 0.1 atm gauge have become available. There are, furthermore, some operational results available at still higher pressures. For example, as early as 1953 tests were carried out on a set of 30 MW rating with special radial seals for operation at a gas pressure of 0.5 atm. Continued operating experience enables us to conclude that this type of seal is the most convenient and would make it possible to raise the gas pressure to 2 - 3 atm.

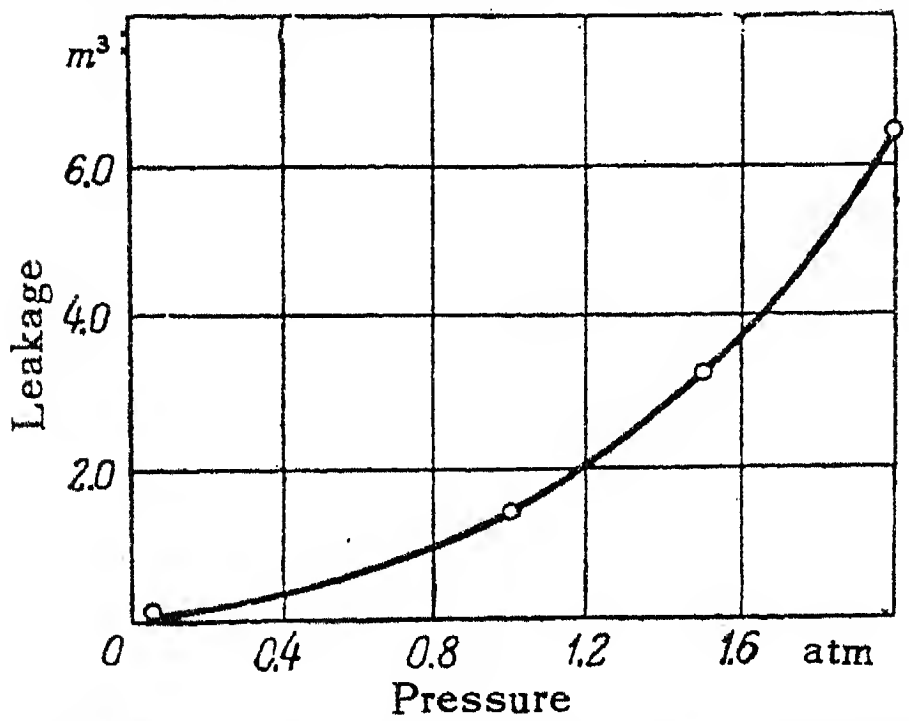

FIG. 4. Relationship between hydrogen leakage per day and pressure.

During a long period of operation it was also found that the oil pressure on the seals must exceed the gas pressure in the machine by not less than 0.3 atm. At a gas pressure of 0.05 atm the impellar-type oil pump of the turbine, producing an oil pressure of 0.3 - 0.35 atm at the seals, assures normal operation of the unit. When the gas pressure is raised, it is necessary to adjust the oil pumps, which must run continuously.

On the generator considered, two oil pumps were provided, viz. the working pump and a stand by pump, with a head of 3.5 atm gauge. The stand-by pump is automatically started when the oil supply to the sealing bearings fails or if the oil pressure falls below a pre-set value.

To improve the performance of the oil seals the rotor shaft has a conical part immediately behind the seal to prevent the oil from creeping along the shaft. After a period of operation of the generator in air, an inspection was carried out in which complete absence of oil on the surface of the shaft behind the seals was established. It should be noted that if the temperature of the sealing bearings was previously found to be of the order of 50 - 57° C., this was reduced by the new design to 45 - 46°.

Before the installation of the experimental rotor designed to work at a hydro-

gen pressure of 2 atm gauge, the stator of the machine was tested by compressed air at a pressure of 3 atm gauge. Points of gas leakage were carefully observed and removed by scaling the individual micro-cracks by welding. This considerably reduced the gas leakage from the generator during operation. It is recommended that in future compressed air tests on stators should be carried out in the works, as this results in a considerable improvement in the quality of the machines delivered and also facilitates and accelerates the change-over of newly erected generators to hydrogen cooling.

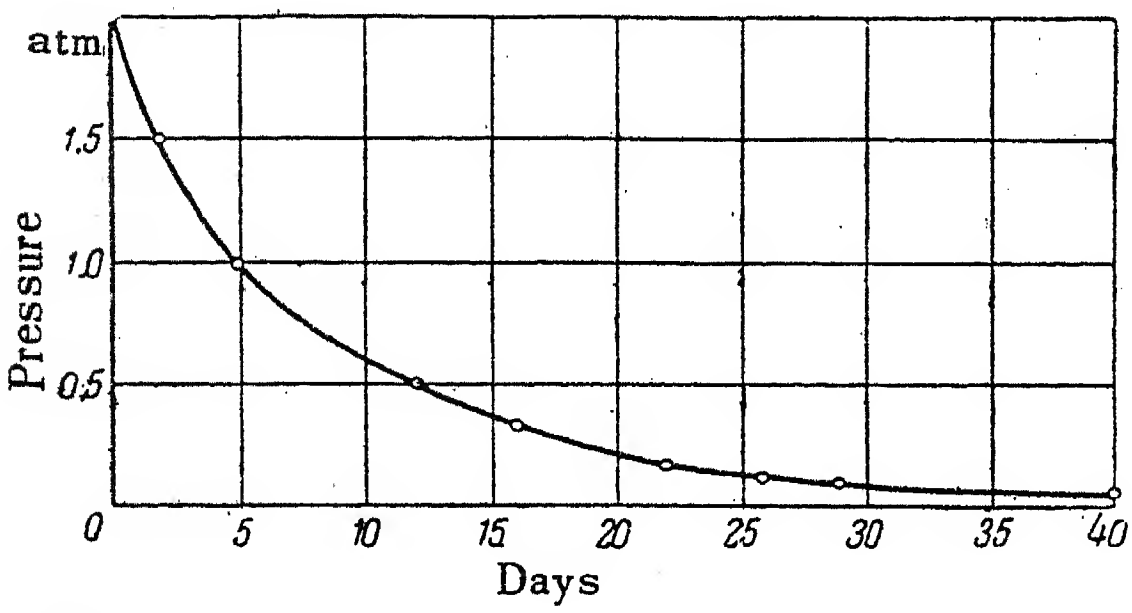

FIG. 5. Reduction of gas pressure in a turbogenerator.

The operation of the generator at higher hydrogen pressures required a number of alternations in the gas circuit to be carried out. In particular, the design becomes more convenient, if the liquid relay is removed from the hydrogen panel and erected separately. A new system of sutomatic hydrogen supply was also installed.

Sustained operation of the set on full load at a hydrogen pressure of 0.05 atm gauge showed that the hydrogen leakage was of the order of 0.10-0.12 m^3 per day. When the gas pressure is raised, the gas leakage increases considerably (Fig. 4). Since an analysis of the gas sampled from the oil detraining pipe does not reveal any changes of its composition at various gas pressures, we must assume that the leakage is not confined to the seals, but also finds its way through leaks in the casing of the machine.

At pressures of 0.5-2 atm gauge the purity of the hydrogen hardly varies at all and keeps within limits of 95.7-95.3 per cent.

The quality of the hermetic sealing of the machine is indicated by Fig. 5, which shows that in a period of 40 days the gas pressure fell from 2 to 0.5 atm gauge in the running machine in the complete absence of a further supply (topping up). During these tests the relationship between the oil consumption of the seals and pressure was established (Fig. 6).

Results of the Thermal Tests

Fig. 7a shows that when the temperature rise of the rotor copper is 105°C., i.e. the maximum permissible temperature rise of insulation of class VS, a rotor with surface cooling by air may be loaded to 420A (curve 1). If, however,

the load of the generator is 30 MW and the power factor 0.8, the exciting current will be 490A and the temperature rise of the copper will be about 140°C.

The direct cooled rotor running in air and with an exciting current of 1450A, corresponding to the same load of 30 MW, has a temperature rise of 62.5°C. (curve 1. Fig. 7b) i.e. only 45 per cent of the figure applying to surface cooling. We see, therefore, that even with air cooling the new rotor assures reliably the full output of the generator. The test results obtained on the rotor showed that if the hydrogen pressure is not increased, the temperature rise of the copper under the rated conditions of operation will also be 45 per cent of the value obtaining for surface cooling by hydrogen (curves 2 and 4 of Fig. 7).

If, however, the hydrogen pressure is 2 atm gauge, the temperature rise of the copper under the rated operating conditions is only 16 per cent of the temperature rise for surface cooling by hydrogen at a pressure of 0.05 atm gauge.

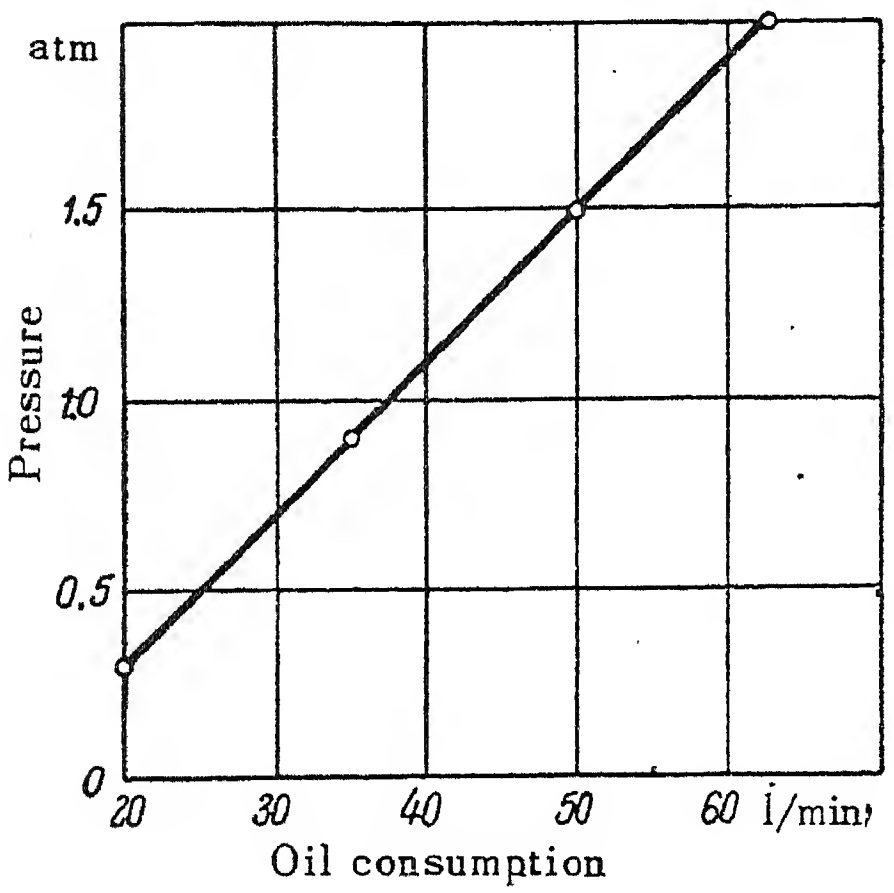

FIG. 6. Relation between hydrogen pressure and oil flow through seals.

If we keep the temperature of the copper at the previous level, the maximum rotor current could be increased by a factor of 2.5. However, since the insulation of the rotor winding and, particularly, the inter-turn insulation of direct cooled conductors works under more severe conditions, it is preferable to maintain the average temperature of the winding at a slightly lower level with a view to reducing the thermal deformation of the turns. This is particularly important from the viewpoint of the reliable operation of a generator under conditions of repeated shorttime overloads and forced excitation on short-circuits. The increased current density in the rotor winding (approximately double the usual value) causes considerable short-time temperature rises which must not impair the dielectric strength of the inter turn insulation.

Assuming the average temperature rise of the copper, measured by the resistance method, as equal to 65-70°C., we can obtain with the same dimensions of the active part of the rotor a total rotor current 2.0-2.2 times higher than with

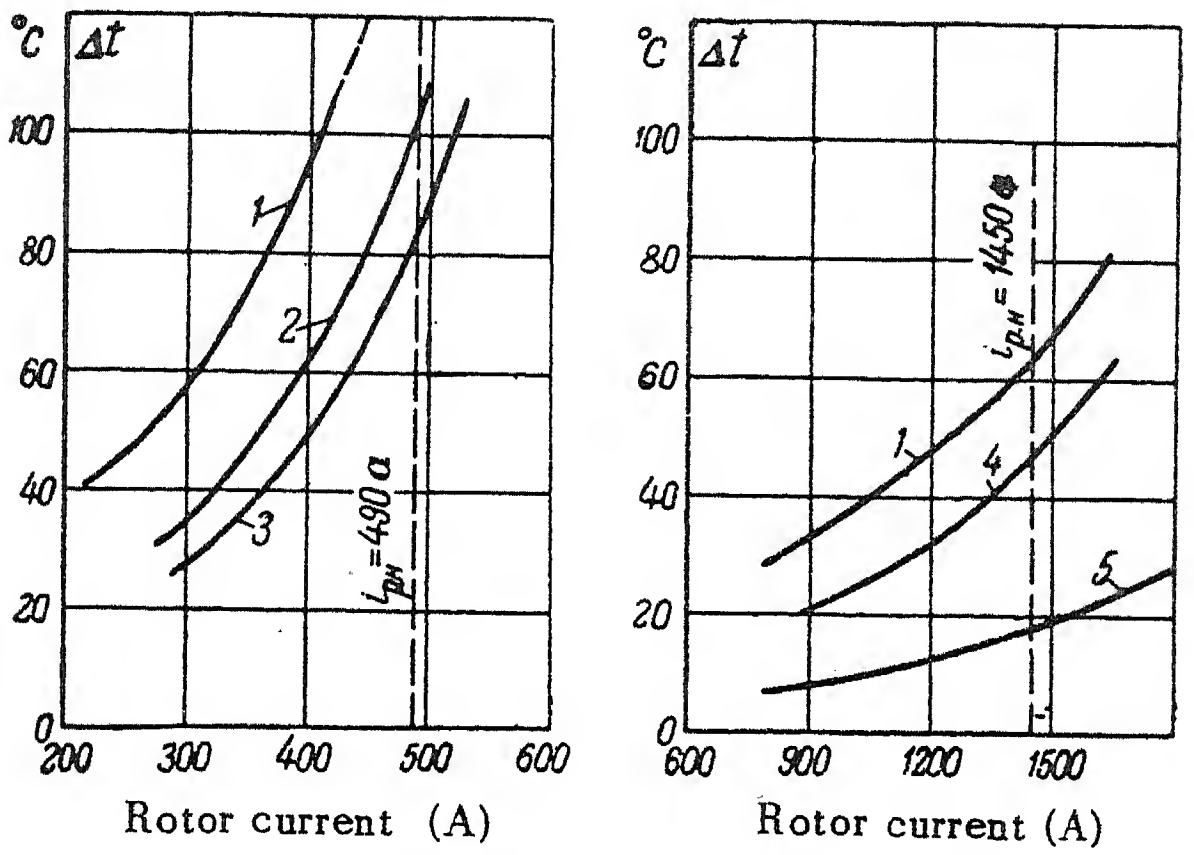

FIG. 7. Temperature rise of rotor winding above ambient temperature
a) rotor with surface cooling; b) rotor with direct cooled winding.
1) air cooling; 2) hydrogen cooling, p = 0.35 atm gauge;
2) id., p = 0.5 atm gauge; 4) id., p = 0.05 atm gauge;
5) id., p = 2 atm gauge.

surface cooling of the winding. The possible increase of the exciting current vs. hydrogen pressure is plotted in Fig. 8.

CONCLUSIONS

1. The experience gained in manufacture and the results of thermal tests on the experimental rotor designed by the "Elektrosila" Works permit us to expect that this method of direct cooling of the rotor conductors may be used in the design of turbogenerators rated at 200 to 300 MW.

2. The calculations show that the utilization of the materials in a turbogenerator with a rotor of the new design and a conventional stator is improved on an average by 60 per cent as against the most fully utilised machines of normal design. Also, the operating temperature of the rotor winding is then not more than 80 per cent of the permissible temperature for the rotor insulation with the usual cooling system.

3. The new design of rotor winding may be used successfully for hydrogen cooled turbogenerators of 30-150 MW rating; this means that though the main operational parameters of the machine are unchanged, its weight and dimensions can be reduced by 30-35 per cent against those of existing machines. This is a considerable advantage from the point of view of reducing the production costs of generators. and also to facilitate transport and installation.

4. The manufacturing processes for the new design of rotor winding are undoubtedly more difficult than those of the conventional machine. However, if the technique is appropriately developed and carried out with the use of special, but not referred to unit output of the machine, may not on the whole be greater than with the present design.

5. For generators working at higher hydrogen pressure the use of shaft seals of a special type is recommended.

6. The stators of hydrogen cooled turbogenerators should be tested in the works with compressed air.

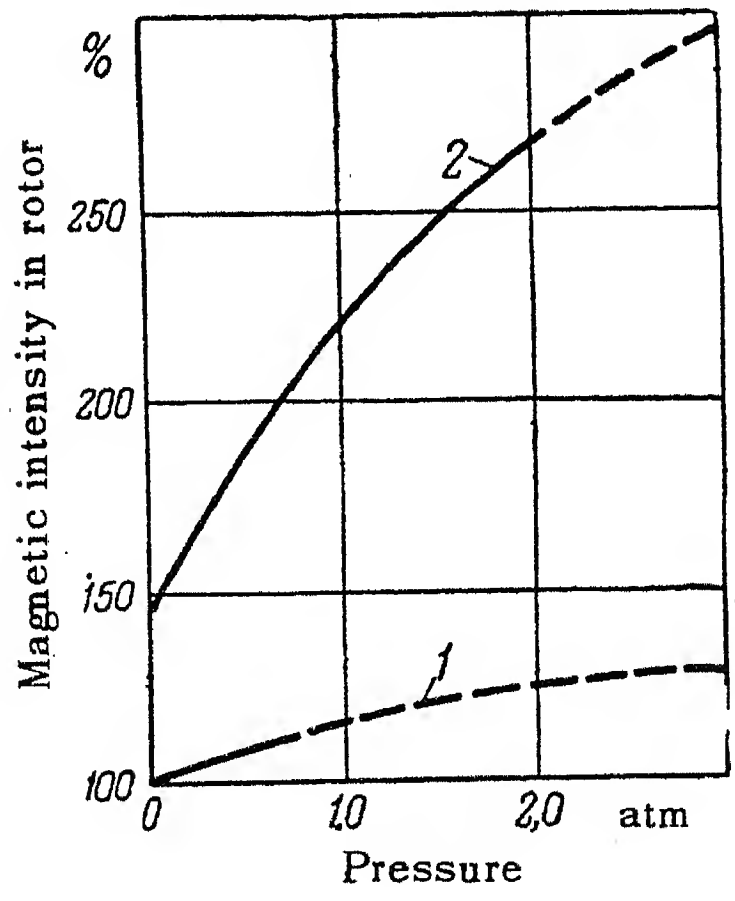

FIG. 8. Rotor ampere-turns vs. hydrogen pressure for various methods of cooling rotor winding.

HIGH-VOLTAGE AUTO-TRANSFORMERS*

A.G. KRAIZ

(Received 17 January 1957)

The present communication considers some characteristic features of the operation and design of H.V. auto-transformers. The basic circuit diagram of an auto-transformer is shown in Fig. 1. The H.V. winding and the M.V. winding are taken conventionally as the series and the common windings, respectively.

Conditions of operation of auto-transformers

The most important conditions of operation are the following:

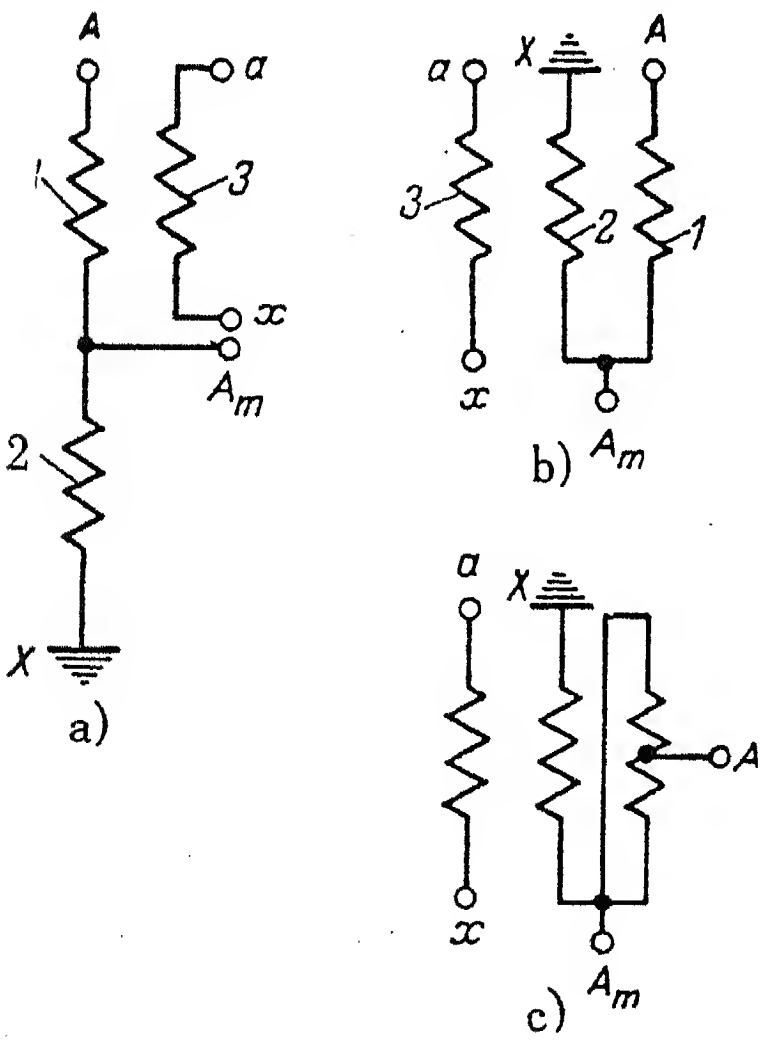

FIG. 1. Basic diagram of an auto-transformer. a) schematic arrangement of windings; b) actual arrangement of windings, H.V. bushing at end of winding; c) actual arrangement of windings, M.V. bushing at midpoint of winding. 1-H.V. winding; 2-M.V. winding- 3-L.V. winding.

a) *Operating conditions H.V.-M.V. and M.V.-H.V.* This case refers to pure auto-transformer operation. A step-down auto-transformer with H.V. and M.V. windings arranged in series will, as a rule, deliver to the load its full rated kVA. With a step-up auto-transformer having the L.V. winding placed between the H.V. and M.V. windings it is sometimes necessary to limit output below the auto-transformer rating, to avoid an excessibely additional iron loss due to magnetic flux leakage. The short-circuit loss will under these conditions be 60-70 per cent of the maximum loss.

b) *Operating conditions H.V.-L.V. and L.V.-H.V.* Under these conditions the machine operates as a pure transformer and the output kVA is equal to the kVA rating of the L.V. winding. The short-circuit loss is about 55 per cent of the maximum loss.

c) *Operating conditions M.V.-L.V. and L.V.-M.V.* Operation as a pure transformer with output kVA equal to the rated kVA of the L.V. winding. The short-circuit loss is 45-55 per cent of the maximum loss (for a step-down auto-

* *Elektrichestvo* No. 6, 39 – 44, 1957 [Reprint Order No. EL 28].

transformer).

d) *Combined transformer-auto-transformer operation H.V.-M.V.* simultaneously with L.V.-H.V. Under these conditions there is the greatest short-circuit loss. The maximum permissible load is limited by the current in the H.V. winding which should not exceed the rated current I_{1n}. If the load on the L.V. side is $S_3 = 0$, the machine operates as a pure auto-transformer (conditions H.V.-M.V. and M.V.-H.V.). If S_3 increases, there should be a corresponding decrease of S_2 on the M.V. side to avoid overloading the H.V. winding.*

To determine the permissible loads S_2 and S_3 for different values of the power factor, let us consider the current vector diagram of an auto-transformer operating under combined conditions and supplied on the H.V. side (Fig. 2a). Also, let us assume that the rated current I_{1n} flows in the H.V. winding, i.e. that the auto-transformer is being supplied with (or supplies) on the H.V. side its rated kVA. On this vector diagram $I_2' = I_2/k_{12}$ and $I_3' = I_3/k_{13}$ represent currents referred to the H.V. side; $k_{12} = U_{1n}/U_{2n}$ is the transformation ratio between the H.V. and M.V. sides and $k_{13} = U_{1n}/U_{3n}$ is the ratio between the H.V. and L.V. sides.

From the vector diagram it follows that

$$I_2'^2 + I_3'^2 + 2I_2' I_3' \cos(\varphi_2 - \varphi_3) = I_{1n}^2. \tag{1}$$

Multiplying (1) by $(U_{1n})^2$, we get an expression for kVA loads.

$$S_2^2 + S_3^2 + 2S_2S_3 \cos(\phi_2 - \phi_3) = S_{1n}^2 \tag{2}$$

Dividing both sides of (2) by S_{1n}^2, we get an equation relating the relative loads (i.e. loads expressed as fractions of rated output of the auto-transformer) $S_2 = S_2/S_n$ and $S_3 = S_3/S_n$.

$$s_2^2 + s_3^2 + 2s_2s_3 \cos(\varphi_2 - \varphi_3) = 1. \tag{3}$$

By the use of this equation it is possible to determine the permissible loads on the M.V. and L.V. sides for different values of the power factors $\cos\phi_2$ and $\cos\phi_3$. Fig. 3 gives curves plotted from (3) for $\cos\phi_2 = 1$ and $\cos\phi_3$ varying between 0 to 1.

As stated above (3) and the curves of Fig. 3 were obtained for the condition of full-load on the H.V. winding i.e. for $I_1 = I_{1n}$. It is of interest also to determine for this case the current I_{MV} passing through the common part of the auto-transformer winding (the M.V. winding). Let $I_{*MV} = I_{MV}/I_{MVn}$ denote the relative magnitude of this current referred to the rated current of the M.V. winding, $I_{MVn} = I_{1n}(k_{12} - 1)$. It is not difficult to obtain an expression for the current I_{*MV} from the vector diagram.

$$I_{*MV} = \sqrt{s_2^2 + \left(\frac{s_3}{k_{12}-1}\right)^2 - \frac{2s_2s_3}{k_{12}-1}\cos(\varphi_2 - \varphi_3)}. \tag{4}$$

If $k_{12} = 2$, (4) assumes the following form:

$$I_{*MV} = \sqrt{s_2^2 + s_3^2 - 2s_2s_3 \cos(\varphi_2 - \varphi_3)}. \tag{5}$$

Fig. 4 shows curves plotted from (5). These curves represent the current in the M.V.

* All quantities referring to the H.V., M.V., and L.V. sides will be denoted by subscripts 1,2 and 3, respectively.

winding at cos $\phi_2 = 1$ for different values of cos ϕ_3 and for different loads on the L.V. winding. In the particular case when the loads on the M.V. and L.V. sides are non-reactive, and with the L.V. winding fully loaded ($s_3 = 0.5$), $I_{*MV} = 0$, i.e. although the M.V. winding supplies in this case a load equal to one-half of the rated output of the auto-transformer, it does not carry any current.

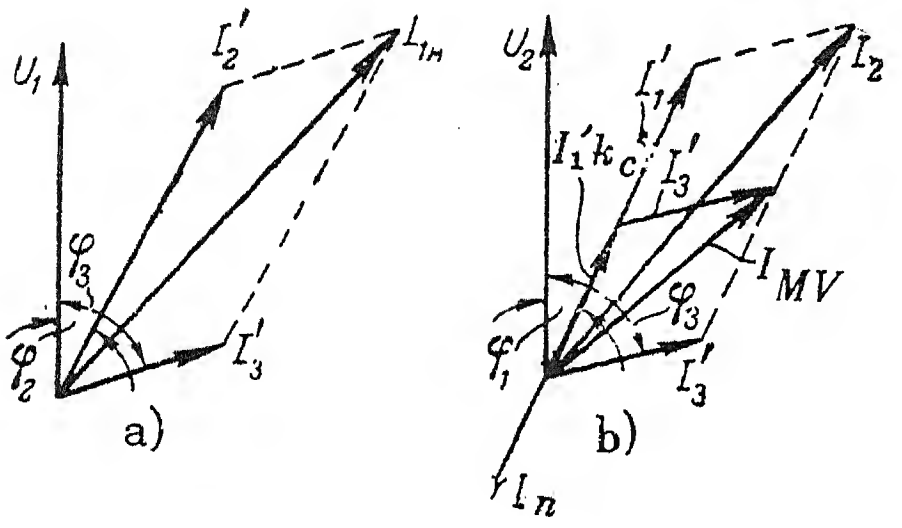

FIG. 2. Vector diagrams of the auto-transformer. a) Conditions H.V. - M.V. simultaneously with H.V.-L.V. b) Conditions M.V.-H.V. simultaneously with M.V.-L.V.

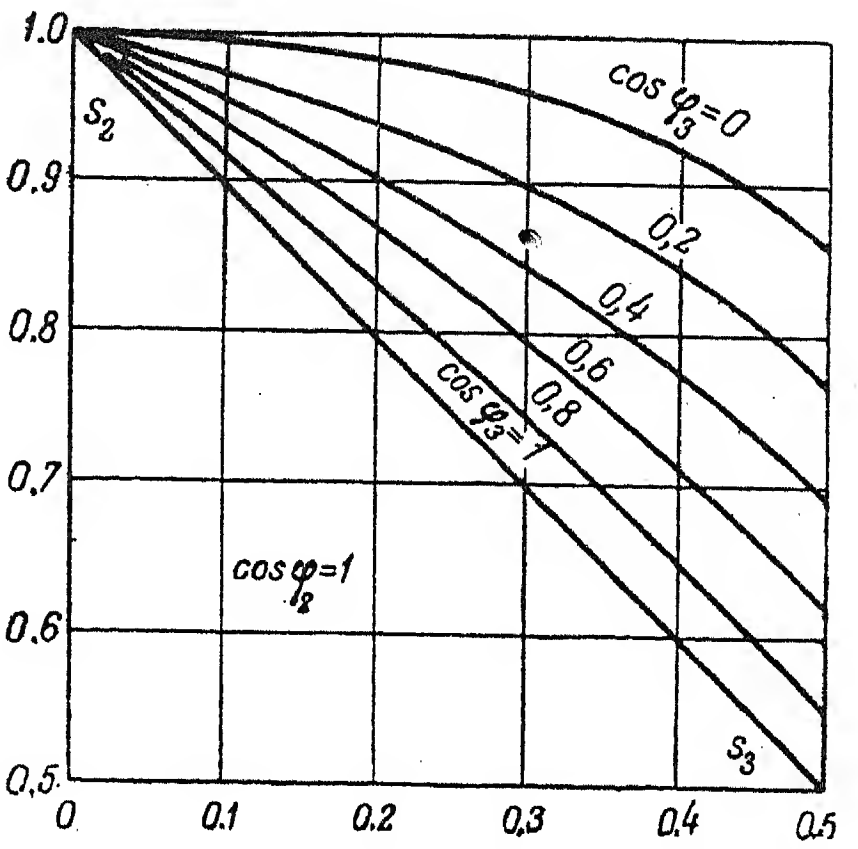

FIG. 3. Curves of permissible loads s_2 and s_3 for an auto-transformer operating under conditions H.V.-M.V. simultaneously with H.V.-L.V.

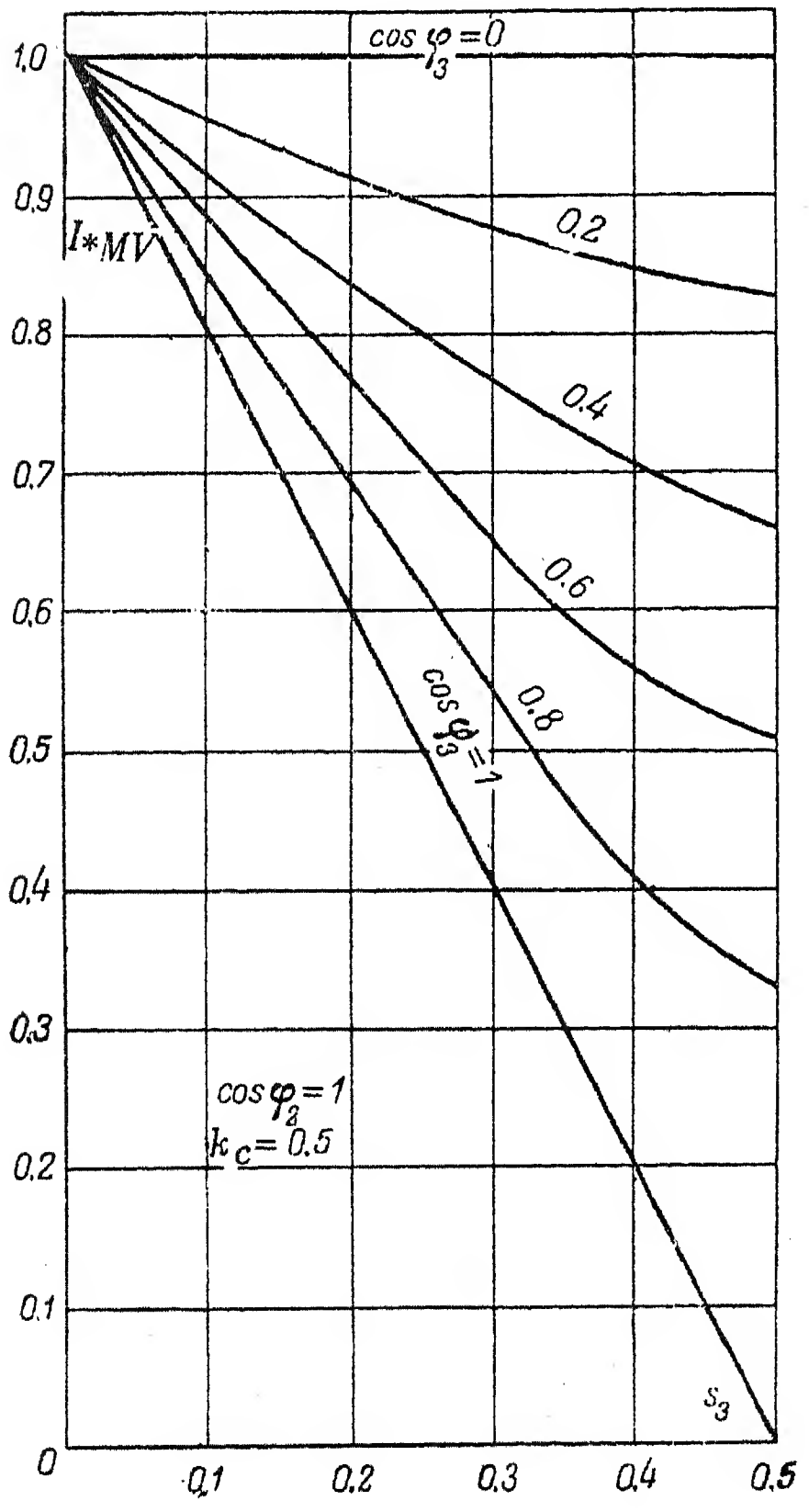

e) *Combined transformer-auto-transformer operation* H.V.-M.V. simultaneously with L.V.-M.V., or M.V.-H.V. simultaneously with M.V.-L.V. Under these conditions the greatest input or output kVA on the M.V. side are limited by the current I_{MV}. Let us assume that the M.V. winding is fully loaded, i.e. the current carried by it is

$$I_{MV} = I_{MVn} = k_c I_{2n} = I_{1n}(k_{12} - 1), \quad (6)$$

where

$k = 1 - \frac{1}{k_{12}}$ is the auto-transformer transformation co-ratio, or the capacity coefficient.

The case when the M.V. winding is the primary is represented by the vector diagram of Fig. 2b.

FIG. 4. Relative current in M.V. winding against L.V. winding load. Conditions of operation H.V.-M.V. simultaneously with H.V.-L.V.

According to this diagram the rated current of the M.V. winding is

$$I_{MVn} = \sqrt{(I_1' k_c)^2 + I_3'^2 + 2I_1' I_3' \cos(\varphi_1 - \varphi_3)}, \qquad (7)$$

where

$$I_1' = I_1 k_{12} \text{ and } I_3' = \frac{I_3}{k_{23}}.$$

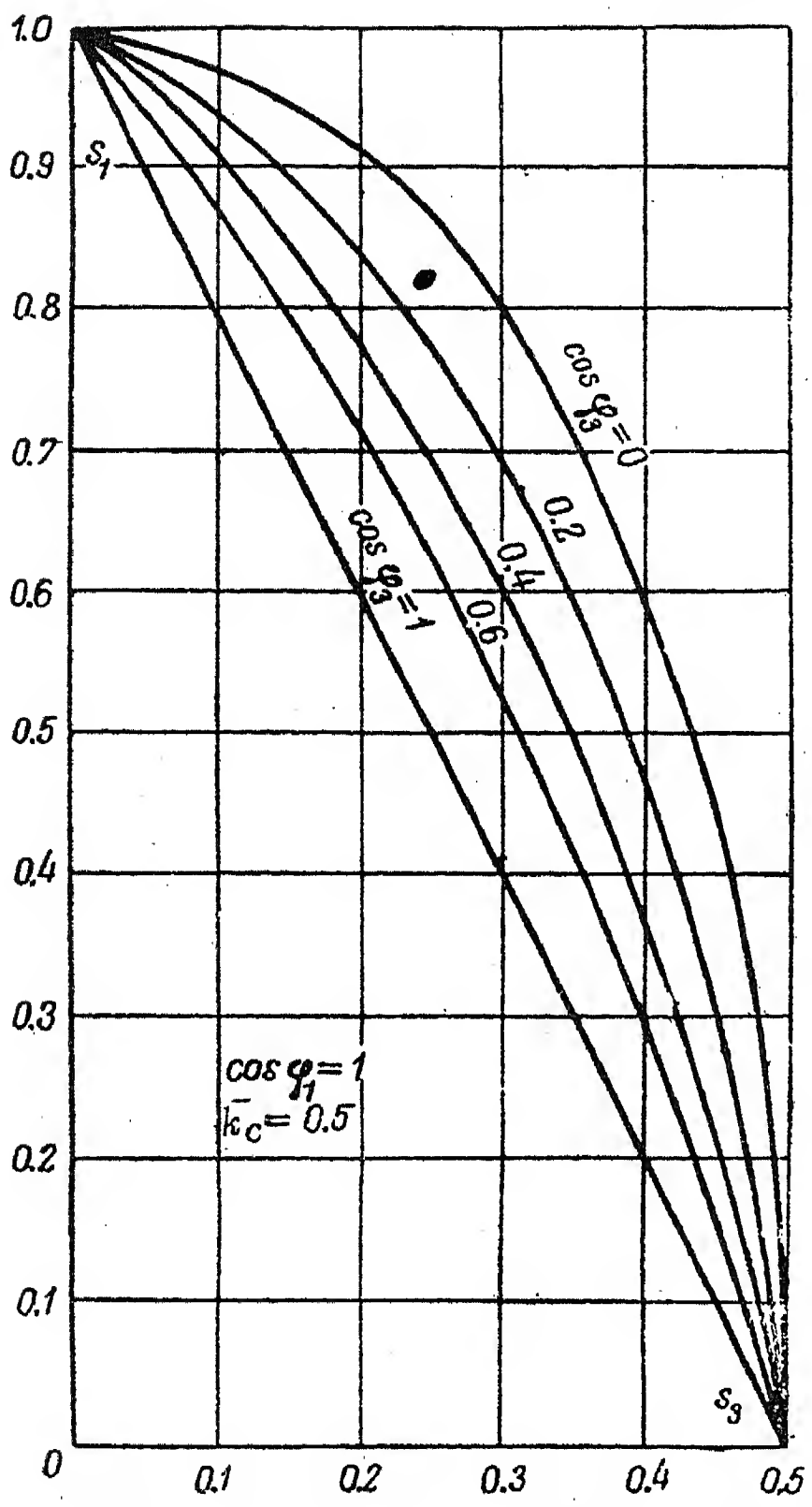

FIG. 5. Curves of permissible loads s_1 and s_3 for auto-transformer operating under conditions M.V. - H.V. simultaneously with M.V. - L.V.

From (7) we get after simple transformations and using the expressions for the relative loads,

$$s_1 = \frac{S_1}{S_n} \text{ and } s_3 = \frac{S_3}{S_n},$$

$$s_1^2 + \left(\frac{s_3}{k_c}\right)^2 + \frac{2 s_1 s_3}{k_c} \cos(\varphi_1 - \varphi_3) = 1. \qquad (8)$$

This equation enables for the operating conditions considered the permissible loads s_1 and s_3 of the primary and tertiary windings to be determined, if the corresponding power factors are known.

Equation (8) takes the following form if $k_c = 0.5$. (for 220/110 kV auto-transformers).

$$s_1^2 + 4 s_3^2 + 4 s_1 s_3 \cos(\varphi_1 - \varphi_3) = 1. \qquad (9)$$

Using (9) the graphs of Fig. 5 were constructed for cos ϕ_1 = 1 and for different values of cos ϕ_3.

Voltage regulation

On-load voltage regulation by means of a boosting unit connected between the common neutral point of the H.V. and M.V. windings and earth is provided nowadays for auto-transformers of home production (Fig. 6). This type of construction results in "tied" voltage regulation in these windings since the e.m.f. of the series transformer adds to the e.m.f.'s of both the H.V. and M.V. windings at the same time.

Using the diagram of Fig. 6, let us find the relation between the additional e.m.f. and the primary and secondary voltages for a step-down auto-transformer.

$$E_{add} = \frac{U_2}{k_c} - \frac{U_1}{k_{12} - 1} \qquad (10)$$

Expressing the voltages and the additional e.m.f. as percentages, viz.,

$$e_{add}\% = \frac{E_{add}}{U_{1n}} 100\%; \quad u_1\% = \frac{U_1}{U_{1n}} 100\%; \quad u_2\% = \frac{U_2}{U_{2n}} 100\%,$$

we get

$$e_{add}\% = \frac{u_2\% - u_1\%}{k_{12} - 1}. \qquad (11)$$

Equation (11) allows us to determine the additional e.m.f. (in per cent of the rated H.V. winding voltage) for given values of u_1 and u_2. Substituting into (11) for $u_2\% = 100\% = \text{const}$, we get the additional e.m.f. necessary to maintain rated voltage on the secondary of the auto-transformer when the voltage on the primary changes (under no-load conditions).

Substituting $u_1\% = 100\% = \text{const}$, we get the additional e.m.f. necessary to obtain a given secondary voltage while the primary voltage is kept at its rated value.

Fig. 7. shows curves for both the above cases. It is seen that the additional e.m.f. becomes greater as the transformation of the auto-transformer, k_{12}, decreases.

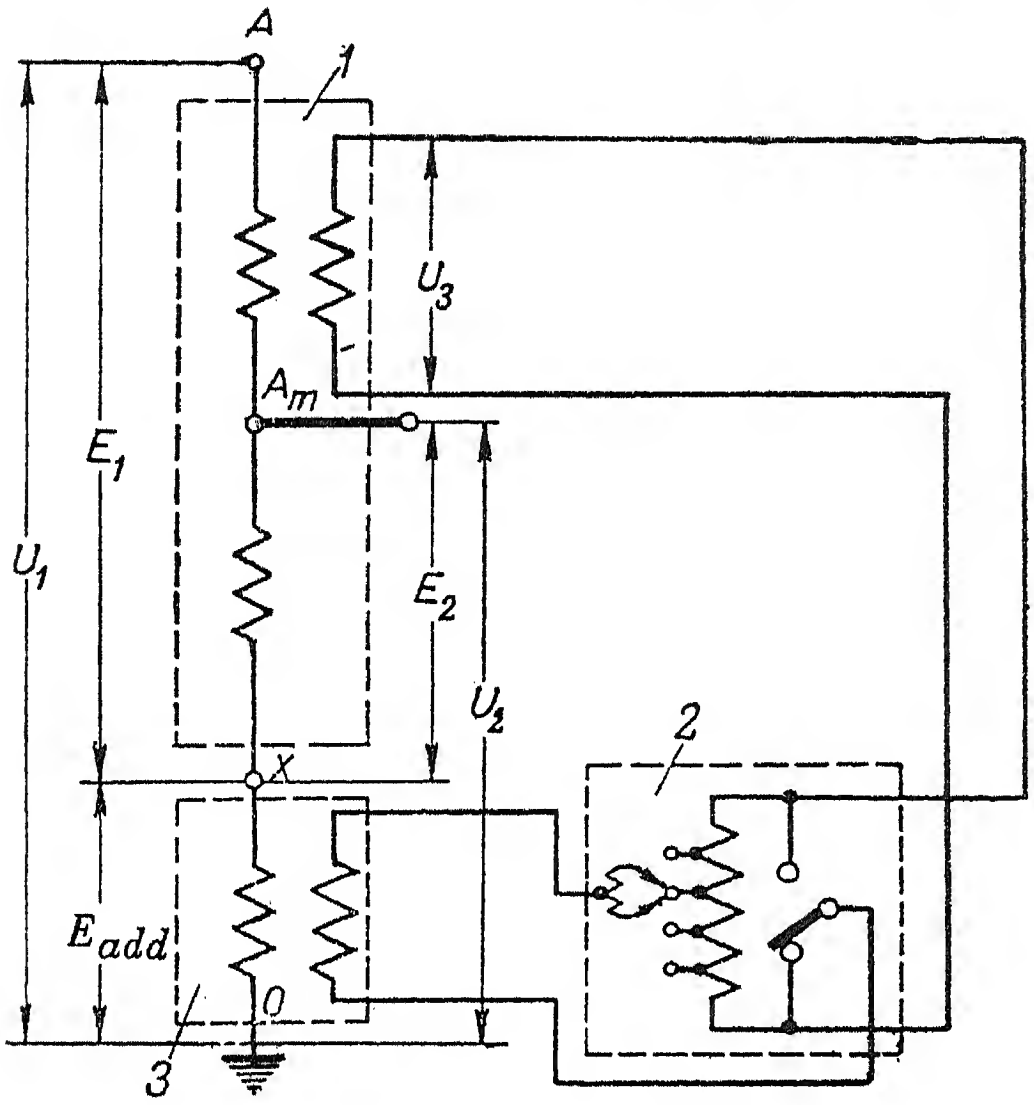

FIG. 6. Circuit diagram of auto-transformer with boosting unit connected to the common neutral point of the H.V. and M.V. windings. 1 - main auto-transformer; 2 - regulating auto-transformer; 3 - series auto-transformer.

The coefficients k_{12} and k_c used above are collected in Table 1, for various auto-transformer standard voltage ratings.

TABLE 1.

U_{1n}/U_{2n}	k_{12}	k_c
150/110	1,365	0,267
220/150	1,47	0,32
400/220	1,82	0,45
220 110	2,00	0,50
400/150	2,67	0,63
110,35	3,14	0,68
400/110	3,64	0,73

The system of voltage regulation by means of a boosting unit connected to the neutral point of the auto-transformer leads in some cases to over-excitation of the latter, in others to under-excitation. Auto-transformer over-excitation expressed in absolute values is given by $\Delta E_1 = E_1 - E_{1n}$

or in percentage values $\Delta e_1\% = \dfrac{E_1}{U_{1n}}\ 100\%$.

The percentage excitation can be calculated using the following formula

$$\Delta e_1\% = \frac{1}{k_c}\left(u_1\%_0 - \frac{u_2\%_0}{k_{12}}\right) - 100. \qquad (12)$$

Fig. 8 gives curves constructed from (12). The curves show auto-transformer excitation for various values of k_{12} and for various differences between the applied primary voltage on the H.V. side and the rated voltage.

For example, if a voltage of 242 kV ($u_1\% = 110\%$) is applied to the H.V. winding of the 220/110 kV auto-transformer ($k_{12} = \dfrac{220}{110} = 2$; $k_C = 0.5$), the overexcitation is

$$\Delta e_1\%_0 = \frac{1}{0.5}\left(110 - \frac{100}{2}\right) - 100 = 20\%$$

which would lead to an excessive increase in the no-load loss and current.

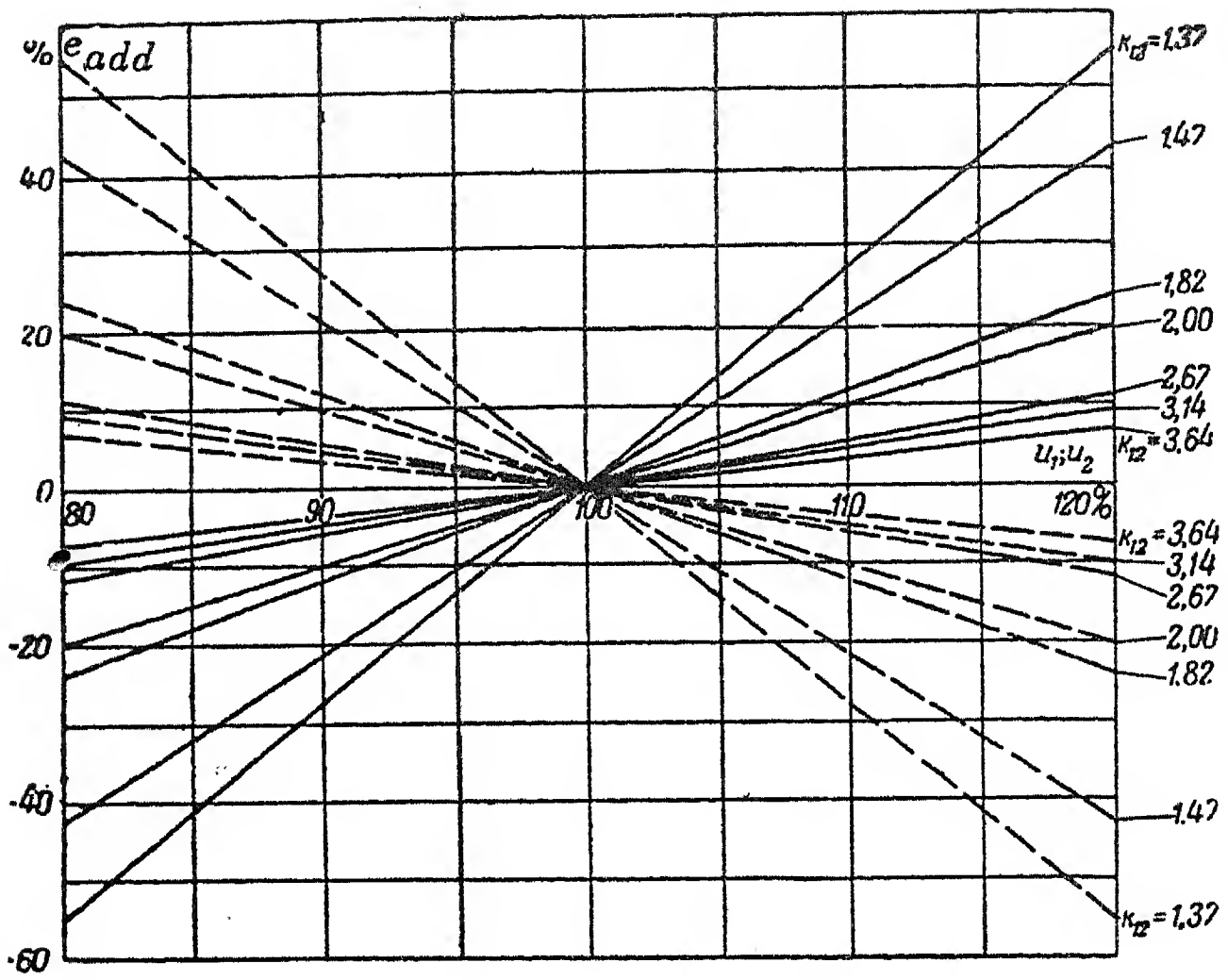

FIG. 7. Additional e.m.f. against voltage on the H.V. and M.V. sides. Continuous lines - $e_{add}\% = f(u_2\%)$ at $u_1\% = 100\% = \text{const}$. Broken lines - $e_{add}\% = f(u_1\%)$ at $u_2\% = 100\% = \text{const}$.

When tappings are provided on the H.V. winding, overexcitation can be reduced by setting the tap-changing switch to the maximum voltage position. In this case (12) becomes:

$$\Delta e_1{}^0/_0 = \frac{1}{\xi k_c'}\left(u_1{}^0/_0 - \frac{u_2\%}{k_{12}}\right) - 100, \qquad (13)$$

where ξ is the ratio of the maximum to normal transformation ratio;

Thus, with regulation stages $\pm 2 \times 2.5$ per cent on the H.V. winding and with the tap-changing switch in the + 5 per cent position, the overexcitation in the last example becomes:

$$\Delta e_1{}^0/_0 = \frac{1}{1.05 \cdot 0.525}\left(110 - \frac{100}{2}\right) - 100 = 9^0/_0,$$

which can be regarded as permissible for auto-transformers.

Fig. 8 gives auto-transformer no-load excitation for various values of $u_2\%$ when the rated voltage is applied to the H.V. side.

Abnormal excitation of auto-transformers leads to a corresponding deviation of the e.m.f. E_3 and the voltage U_3 of the tertiary winding from their rated values. This deviation, expressed as a percentage, is

$$\Delta u_3{}^0/_0 = \frac{E_3 - U_{3n}}{U_{3n}} 100^0/_0$$

and is numerically equal to the auto-transformer over-excitation: $\Delta u_3\% = \Delta e_1{}^0/_0$.

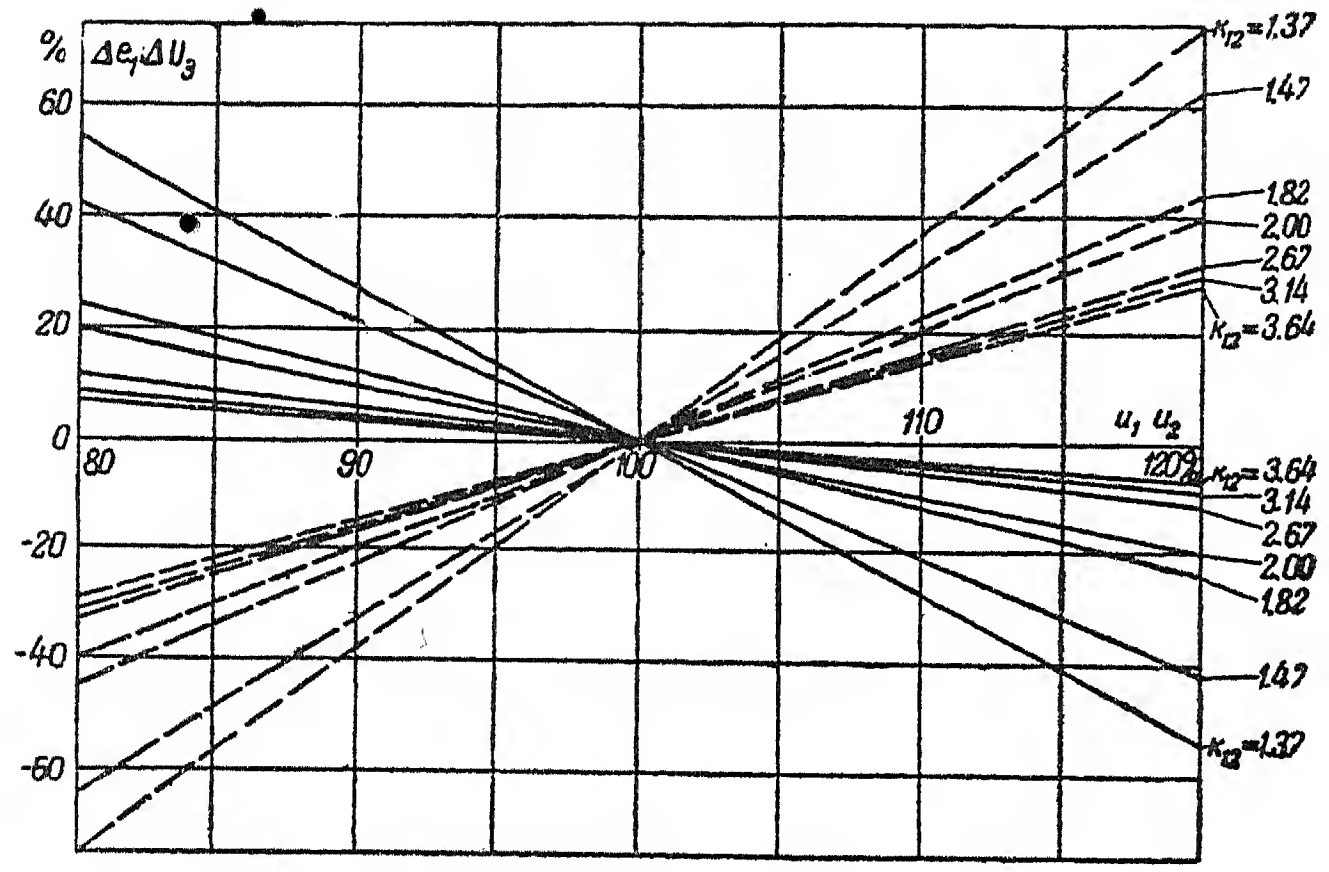

FIG. 8. Auto-transformer overexcitation $\Delta e_1\%$ and the deviation of the tertiary voltage from the rated voltage, $\Delta u_3\%$ against the voltage on the H.V. or M.V. side (for "tied" regulation).

Continuous lines - $\Delta e_1\% = \Delta u_3\% = f(u_2\%)$ for $u_1\% = 100\% = \text{const.}$

Broken lines - $\Delta e_1\% = \Delta u_3\% = f(u_1\%)$ for $u_2\% = 100\% = \text{const.}$

Thus, from (12) and (13) and the graphs of Fig. 8 we can also determine the deviation of the tertiary voltage from its rated value.

An examination of Fig. 8 reveals yet another shortcoming of the "tied" regulation. If the voltage $u_2\%$ on the M.V. side is increased while keeping $u_1\% = \text{const} = 100\%$, the voltage on the L.V. side drops ($\Delta u_3\%$ is negative).

If, however, $u_2\% = 100\%$ is kept constant, the voltage on the L.V. side varies as the applied voltage u_1 changes.

The drawbacks of the "tied" regulation can be avoided by connecting the boosting unit in the H.V. or M.V. line, or between the common and the series windings of the auto-transformer. Such systems are not entirely free from disadvantages either. These, however, cannot be discussed here because of lack of space.

It may be stated that the best solution to the problem of voltage regulation is to insert the regulating equipment always in the main auto-transformer provided that this is possible from considerations of transport requirements.

Surge phenomena in auto-transformers

The differences in the surge behaviour of transformers and auto-transformers are due to the fact that there is a direct electrical connexion between the H.V. and M.V. windings.

A surge can impinge on the H.V. winding either from the side of its line end (end A, Fig. 1) or from the opposite side - the M.V. line (end A_m, Fig. 1). In both cases the initial (capacitive) voltage distribution along the H.V. winding (the steepness of which determines the amplitude of the following oscillations) is different since it depends on the ratio of the series (coil-to-coil) to shunt (coil-to-earth) capacitances. The least steepness of the curve of the initial voltage distribution occurs when the wave enters the winding at the line end A. Thus, the effect of surges on auto-transformers should be considered for the above two cases.

In Table 2 a comparison is made between the voltages on line terminals of windings for 220/110/11 kV step-down and step-up transformers and auto-transformers impulsed with the 1.5/40 μsec full wave. The data shows that with the impulse applied to the terminal A (220 kV) the voltage on the terminal Am (110 kV) is $0.25 \times 945 = 236$ kV_{max} for step-down transformers and $0.68 \times 945 = 644$ kV_{max} for step-down auto-transformers, the full-wave impulse voltage test level being only 480 kV_{max} for the 110 kV insulation class (945 kV_{max} for the 220 kV class).

TABLE 2.

	Impulse voltage applied to terminal A			Impulse voltage applied to terminal A_m		
	A—O, (%)	A_m—O (%)	A_m—O (kV_{max})	A_m—O (%)	A—O (%)	A—O (kV_{max})
Transformer:						
a) step-down	100	25	236	100	117	561
b) step-up	—	—	—	100	220	1 030
Auto-transformer:						
a) step-down	100	68	644	100	219	1 050
b) step-up	100	100	945	100	300	1 440

With the impulse applied to A_m (110 kV) we get, correspondingly, $1.17 \times 480 = 561$ kV_{max} for transformers and $2.19 \times 480 = 1050$ kV_{max} for auto-transformers which also exceeds the full-wave impulse test level for 220 kV insulation class (945 kV_{max}).

To prevent breakdown of auto-transformer insulation under surges, the H.V. and M.V. line terminals should be protected by valve-type surge diverters of appropriate ratings regardless of whether the auto-transformer is connected to the line or not.

Table 3 shows the effects of surges on the series insulation of transformers and auto-transformers. It is seen that the maximum gradients in the oil ducts between coils are approximately the same for transformers and auto-transformers when tested with either full or chopped waves. The exception is only the region of the tap changer where the gradient between the adjacent tappings is considerably greater for auto-transformers than for transformers. This is due to the fact that with the same percentage regulation the fraction of the number of disconnected turns to the number of turns in the H.V. winding (the series part) is twice as high for auto-transformers (with $k_{12} = 2$) than for transformers.

TABLE 3.

	Full wave, 1.5/40 μsec		Chopped wave $\tau = 2$-3 μsec
	Maximum gradient in one oil duct	Maximum gradient in the tap changer region	
Transformer . . .	20	19.5	18
Auto-transformer	16	34	14

The overvoltages which appear on the tertiary winding due to impulse stressing of the H.V. and M.V. windings, are induced in it electrostatically and electromagnetically, i.e. in the same manner as in transformers.

Condition of the neutral point

High-voltage auto-transformers of home produce cannot be operated with the

neutral point disconnected from earth. This will be made clear from the following consideration. In a system with effectively earthed neutral point the voltage on the unearthed neutral of a transformer or an auto-transformer rises during one-phase-to-earth fault to a value given by

$$U_{n0} = \frac{x_0}{x_1 + x_2 + x_0} U_{ph\ 1}, \tag{14}$$

where x_1, x_2, and x_3 are positive-, negative-, and zero-sequence reactances.

Assuming $x_1 = x_2$ and substituting $\alpha = \frac{x_0}{x_1}$ and $\beta = \frac{\alpha}{2 + \alpha}$ we get

$$U_{n0} = \beta U_{ph1} = \frac{\beta}{\sqrt{3}} U_1, \tag{15}$$

where U_1 and U_{ph_1} are the line and phase voltages of the H.V. winding respectively.

At the same time the voltage of the sound phases is

$$U_{10} = \frac{U_1}{\sqrt{3}} \sqrt{1 + \beta + \beta^2}, \tag{16}$$

while the voltage at the line terminals of the M.V. winding of the auto-transformer is

$$U_{20} = \frac{U_1}{\sqrt{3}} \sqrt{\frac{1}{k_{12}^2} + \frac{\beta}{k_{12}} + \beta^2} \tag{17}$$

Taking, for example, the 220 kV voltage class and assuming $\alpha = 4$ and $\beta = \frac{4}{2 + 4} = 0.67$ we see that during one-phase-to-earth fault the voltage on the neutral and the voltage on the H.V. line terminal will not exceed the permissible levels of the respective surge diverters RVS-110_{earth} and RVS-220_{earth}, while the voltage on the 110 kV M.V. line terminal will rise to U_{20} = 141.5 kV and will therefore exceed the permissible voltage for the RVS-110_{earth} surge diverter by 47 per cent.

This explains the necessity of earthing the neutral points of 220/110 kV auto-transformers, since the insulation of their M.V. windings is coordinated with the protective characteristics of the RVS-110_{earth} surge diverter.

Construction

The constructional design of high-voltage auto-transformers is basically the same as that of transformers for the same voltage class. The characteristic differences are formed in the design of the connexions to the winding ends (the external connexions between windings and between windings and bushings). Also, there are some differences regarding connexions to the ends of the internal windings and regarding some main clearances. Fig. 9 shows a possible method of arranging the windings for the 220/110/6-10 kV step-down auto-transformer with the H.V. bushing connected to mid-point of the H.V. winding. This figure shows that the upper end of the M.V. winding (neutral X) is brought out and so has to be insulated against earth, L.V. winding, and one end of the H.V. winding. On the other hand, construction of the lower part of the auto-transformer is considerably simplified on account of the electrical connexion between the H.V. and M.V. windings since their common point A_m can be brought out directly from the H.V. winding. In the case of a transformer with separate windings, the construction of the connexion to the lower end of the M.V. windings would be the same as that to the upper end.

Also, the existence of the electrical connexion between windings in an auto-transformer makes it possible to reduce the end clearances since, in this case, the

electric field configuration is more favourable.

For a step-up auto-transformer having its M.V. winding placed next to the core instead of between the H.V. and L.V. windings, the construction of the connexions to the ends of the M.V. winding is the same as that for a transformer. The number of high-voltage bushings in a single-phase auto-transformer is one less than that in a transformer.

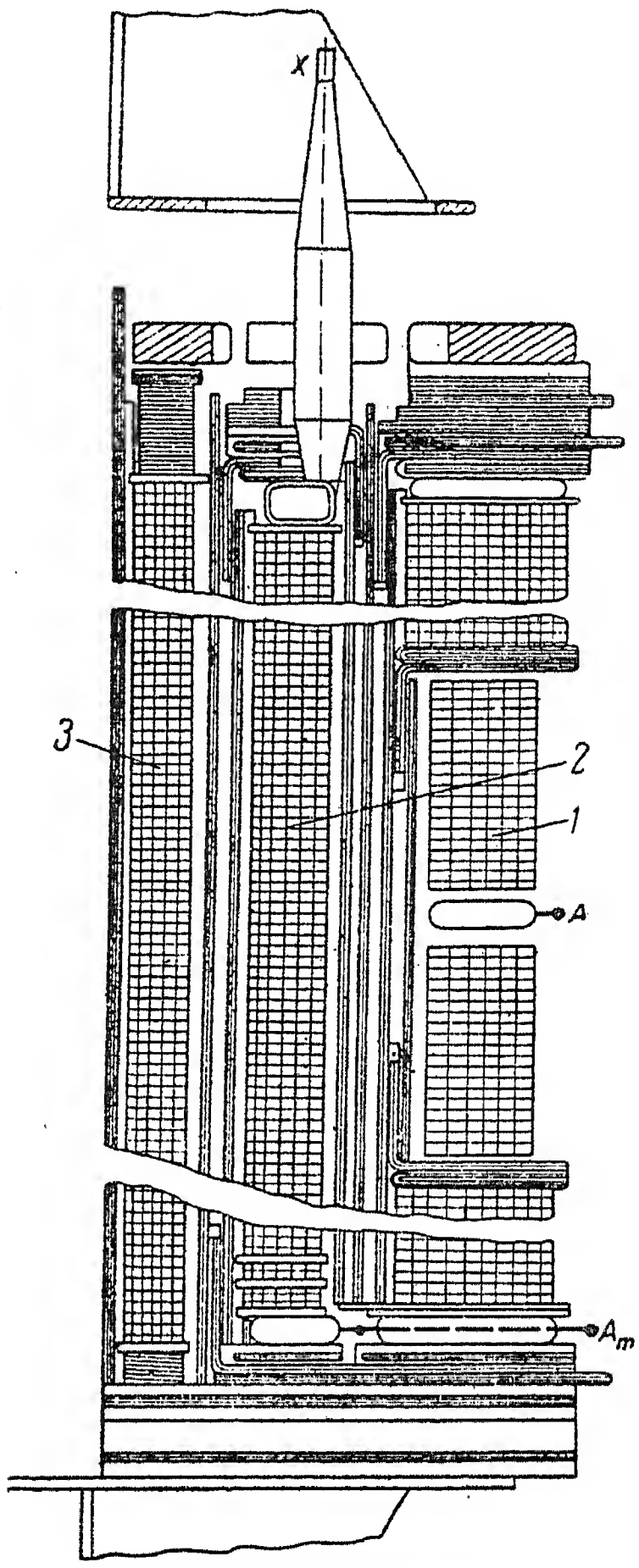

FIG. 9. Construction of 220/110/6 - 10 kV auto-transformer. 1 - H.V. winding; 2 - M.V. winding; 3 - L.V. winding.

A NEW AIR-BLAST CIRCUIT BREAKER FOR 220 kV, 7000 MVA*

T.I. SMIRNOVA

(Received 24 December 1956)

The All-Union Electrotechnical Institute "Lenin" has developed an experimental air-blast circuit breaker rated 220 kV/7000 MVA (Fig. 1), which is an improvement on the 5000 MVA circuit breaker as manufactured at present by the electrical industry.

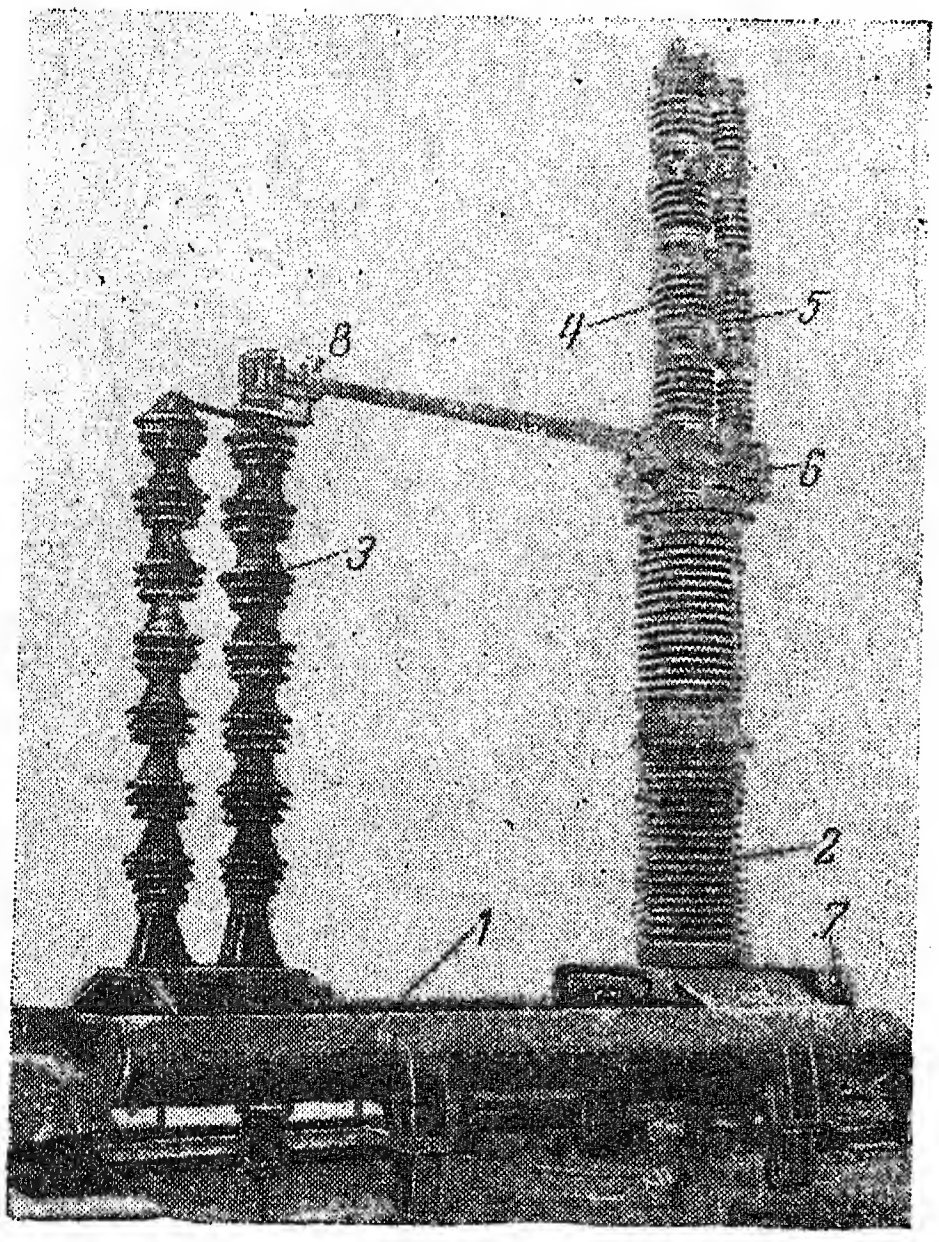

FIG. 1. One phase of the 220 kV, 7000 MVA air-blast circuit breaker.
1 — compressed air tank;
2 — column of support-insulators;
3 — column of pin-insulators;
4 — arc chamber;
5 — voltage divider;
6 — pneumatic drive of the isolator;
7 — control cubicle.

Design of the circuit breaker

Three porcelain tubes are arranged inside the supporting insulate of the breaker; one of 120 mm diameter, leads the compressed air to the arc chamber

* *Elektrichestvo* No. 6, 48-50, 1957 [Reprint Order No. EL 29].

and the two others, of 25 mm diameter, supply the compressed air to the drive of the isolator. The arc chamber is mounted on the drive of the isolator and consists of four identical elements, each of which contains a hollow porcelain insulator, a fixed and a moving contact with the pneumatic mechanism. Both fixed and moving contacts are hollow and communicate with the exhaust ducts of the flanges.

A voltage divider consisting of four metal resistors connected in parallel to the elements of the chamber is arranged beside the arc chamber. The total resistance of the voltage divider is 720,000 ohms.

The isolator drive is connected with a mechanism of switching block contacts with porcelain rods. Two insulator columns support the contact of the isolator, each of the columns consisting of insulators type IShD-35.

For remote and automatic operation each of the phases of the circuit breaker is equipped with two electromagnets. Three-phase operation can be achieved by either series or parallel connexion of the three magnets for which two different sets of coils are used. For manual operation a special pneumatic device is provided whose control buttons are arranged in a control cubicle. In this case the phase cannot be operated individually.

To prevent freezing of the air ducts in the insulators continuous air circulation is provided by means of special reduction valves in the control cubicle. Each phase of the circuit breaker is provided with an indicator, showing the state of the ventilation. The control cubicle also contains contact pressure gauges which interrupt the operating circuits at inadmissible losses of pressure in the air tanks.

The operating columns of the circuit breaker does not differ from that of the air-blast circuit breaker for 220 kV, 5000 MVA*.

Principal characteristics of the circuit breaker:

Rated voltage	220 kV
Rated current	1000 A
Rated breaking current	18.4 kA
Rated breaking capacity, allowing for rapid reclosing	7000 MVA
Max. "through" short-circuit current,	
amplitude	65 kA †
r.m.s. value	38 kA
Thermal short-circuit rating (10 seconds)	15 kA
Voltage rating of the operating magnets	220 V d.c.

* O.V.V. Afanas'ev and N.A. Makarova; Air-blast circuit breaker 220 kV, 1000 A, 5000 MVA. *All-Union Electrotechnical Institute* No. 6 (1954).

† These values have been obtained experimentally at the All Union El. Institute. The "Elektroapparat" Works recommend 55 and 32 kA, respectively.

Permissible limits of voltage variations on the operating magnets	65 – 120 per cent
Opening time (from instant of giving the tripping signal to inception of contact separation) not more than	0.06 sec.
Max. arc-duration	0.02 sec.
Total-break-time (from instant of giving the tripping signal to final arc extinction) not more than	0.08 sec.
Making time (from "On" signal to the moment of making contact with the fixed contact of the isolator) not more than	0.45 sec.
Duration of the contactless interval of the arc chamber (from opening to closing of the contact)	0.25 – 0.35 sec.
Time from signal to separation of the isolator from the fixed contact	0.14 sec.
Max. velocity of the movement of the contact knife of the isolator during making and breaking	18 – 22 m/sec
Rated air pressure	20 atm
Max. permissible air pressure in the tanks	21 atm
Min. air pressure at which the capacity of the circuit breaker is not reduced	18 atm
Capacity of the basic storage tank of one phase	1214 litres
Capacity of the additional storage tank of one phase	1214 litres
Pressure drop in the tanks during breaking	2.25 – 2.5 atm*
Air consumption for one breaking operation	5500 – 6100 ltr.†
Air consumption for one making operation about	400 litres
Pressure drop with automatic reclosing followed by breaking	4 – 4.5 atm
Air consumption for automatic reclosing	9700 – 10,900 ltr.
Air consumption for ventilation	900 ltr/hr
Weight of one phase appr.	6000 kg.
Weight of control cubicle appr.	350 kg.

Results of circuit breaker duty tests

Mechanical tests consisting of 1000 making and breaking operations were arried out with a pressure of 20 atm. In addition, 25 duty cycles were carried ut at a pressure of 21 atm and 25 cycles at 15 atm. Inspection of the individual art and of the assembly of the circuit-breaker after the mechanical tests showed hat its main elements were in good condition and that the circuit-breaker remain-d in full working order. The mechanical characteristics are shown in Fig. 2.

The tests showed that the voltage distribution on the arc chambers is as

The magnitude of the pressure drop shown takes account of the installation of the additional storage tanks.
The figures for air consumption are given for one phase and refer to atmospheric pressure.

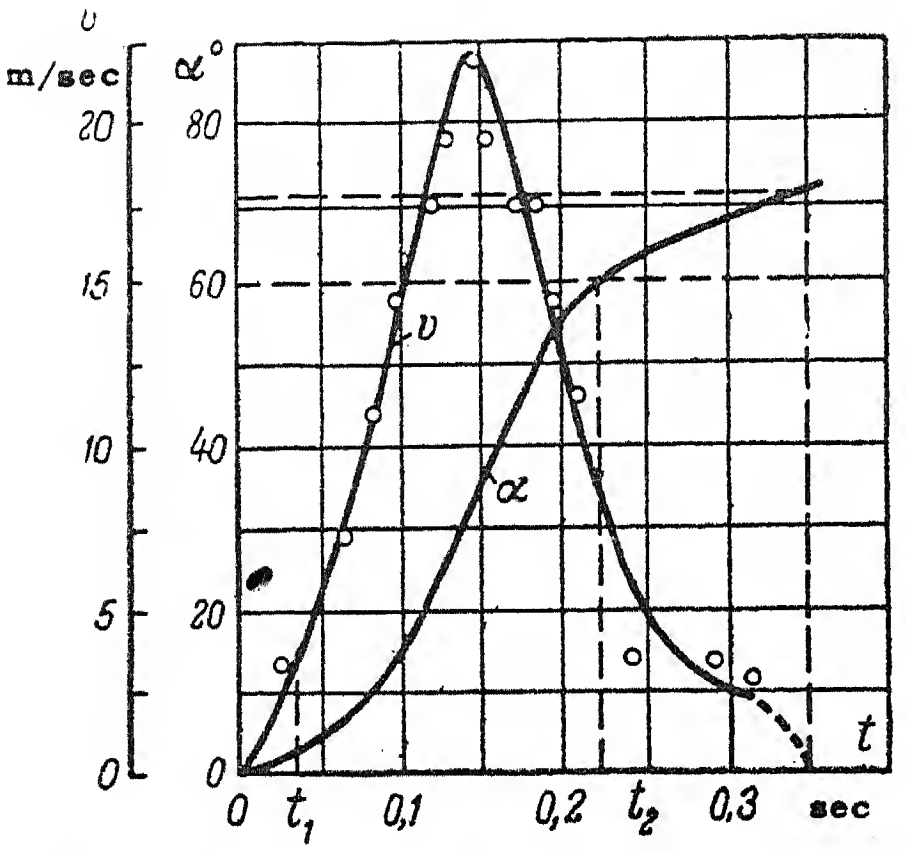

FIG. 2. Mechanical characteristics of the breaking operation.
Pressure in the tank 20 atm.
v – linear velocity of the knife end;
t_1 – moment of separation of the knife from the isolator contact
t_2 – moment of making contact in the arc chamber.

follows: The first (bottom) element takes 24 per cent of the total voltage, the second 23.6 per cent, the third 22.9 per cent and the fourth 29. 5 per cent. This sufficiently uniform distribution of the voltage enables tests of the breaking capacity to be carried out on individual elements.

The rated voltage for each circuit-breaker element is 45 kV_{max}. The magnitude of the test voltage is determined by the conditions of a three-phase short-circuit and equals 1.5 x rated voltage, i.e. 67.5 kV_{max}.

For the test of the circuit-breaker with interruption of 50 per cent of its interruption capacity (Fig. 3) the amplitude factor of the restriking voltage was assumed to be 1.6, i.e. the magnitude of the restriking voltage at one breaker element must be 108 kV_{max}. The frequency of the natural oscillations of the restriking voltage was assumed to be 2000 c/s.

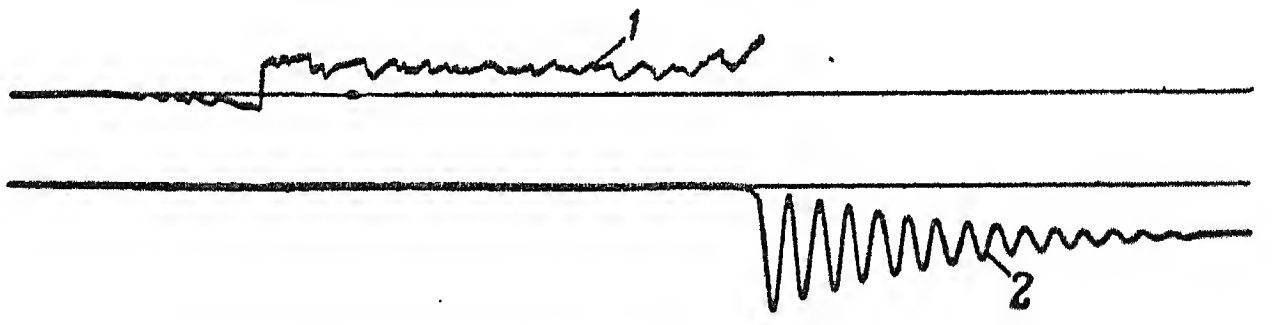

FIG. 3. Oscillogram obtained during breaking of 50 per cent of the breaking capacity of the breaker; p = 18 atm.
1 – arc voltage drop (duration of the arc 0.0138 sec)
2 – restriking voltage (frequency 2000 c/s.

The tests consisted of the check of the interruption capacity of each individual breaker element. An oscillatory circuit was used as the current source, but the restriking voltage was obtained from a surge voltage generator. These tests showed that with a pressure in the tank of 17 – 18 atm each element easily

performed its duty of the interruption of 50 per cent of the breaker capacity with a value of the restriking voltage of 110 – 130 kV_{max}. The average rate of rise of the restriking voltage was 1.65 – 1.81 kV/μ sec.

During the tests it was found that with a tank pressure of 16 atm sometimes restriking occurred at a voltage of the order of 90 – 100 kV_{max}. In order to achieve the necessary electric strength, i.e. 108 kV_{max}, it proved to be essential to raise the pressure in the storage tanks to 17 – 18 atm. Hence follows that auxiliary storage tanks of the same size as the main tanks are required if reclosing is to be provided.

For interruption of 100 per cent of the rated interruption capacity (Fig. 4) the amplitude factor of the restriking voltage was assumed to be 1.2, i.e. the restriking voltage on each breaker element must be 80.5 kV_{max}. The frequency of the natural oscillations of the restriking voltage was assumed to be 400 c/s.

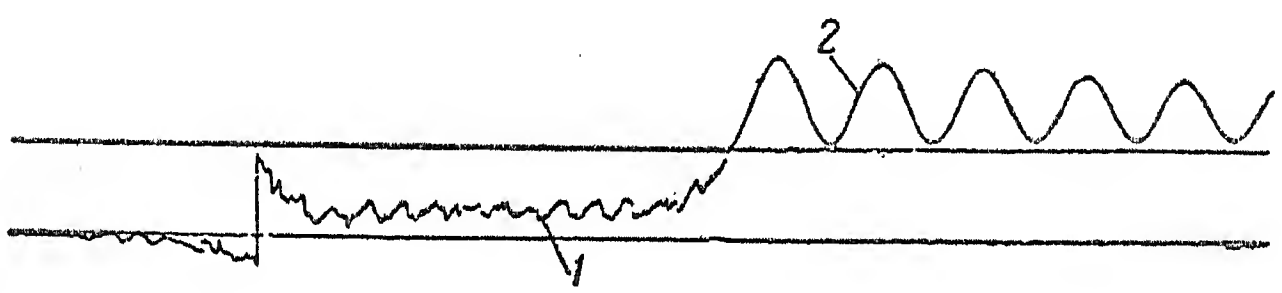

FIG. 4. Oscillogram taken during breaking of 100 per cent of the interruption capacity of the breaker; p = 16 atm.
1 – arc voltage drop (duration of the arc 0.0135 sec)
2 – restriking voltage (frequency 400 c/s).

The tests showed that with a tank pressure of 16 atm the breaker interrupts 100 per cent of its capacity with an amplitude of the restriking voltage of 83 – 90 kV and an average rate of rise of the restriking voltage of 0.3 – 0.35 kV/μ sec.

Tests were also made with respect to the interruption of capacitive current. The breaker interrupts a distributed capacitance of 3.2μF (corresponding to a line of 100 km length) with a voltage across one element of 2 x 1.3 x 45 = 117 kV_{max} (the coefficient 1.3 takes into account the increase of the voltage on the two unfaulted phases during line-earth fault with restriking arc and also the increase of the voltage at the end of a line).

The trials proved that the three lower breaker elements successfully interrupted this capacitive current with a pressure of the storage tanks of 16 atm. For the fourth element (the top one) it has been necessary to raise the pressure to 18 atm.

A METHOD FOR THERMAL CALCULATIONS OF MINING COMBINE MOTORS*

G. I. PERTSOV

(Received 10 December 1956)

Mining combines are driven by enclosed induction motors with squirrel-cage rotors. The main design features of the frames of these motors are shown in Figs. 1 and 2.

The motor represented in Fig.1 has a frame with cooling fins with internal air circulation; Fig. 2 shows a motor with a frame with cooling fins with internal air circulation and external blower-cooling.

Heat is generated in the motors in the stator winding, in the steel of stator and rotor, bars and short-circuiting rings of the rotor, in the internal fan and the sealed bearings. These parts of the machine are connected by thermal conductivities.

The heat energy of the individual parts of the motor is dissipated into the surroundings not through one homogeneous surface, but through several surfaces presenting different conditions for the air-cooling. For this reason it is not permissible to consider an electric machine for thermal calculation as a homogeneous body of infinite thermal conductivity because calculations on this basis lead to considerable discrepancies between theoretical and experimental results.

The results of calculations will be unsatisfactory also in the case that not the temperature rise of the whole machine, but only that of its winding is considered and influences of other parts are only considered by some empirical coefficients. These coefficients, found by experiment, apply only to a given motor and, strictly speaking, only to well-defined operating conditions of the machine.

In thermal calculations based on the theory of the temperature rise of two homogeneous bodies, the heating processes of stator and rotor are considered indepenently of each other.

According to the thermal energy balance for steady operating conditions and for constant heat losses we may write down the following equations.

* *Elektrichestvo* No. 6, 58-64, 1957 [Reprint Order No. EL 30].

$$\left.\begin{aligned} P_1 &= \tau_1\lambda_1 + (\tau_1 - \tau_2)\,\lambda_{12}; \\ P_2 &= \tau_2\lambda_2 + (\tau_2 - \tau_1)\,\lambda_{21}, \end{aligned}\right\} \qquad (1)$$

where r_1 and r_2 are the temperature rises of the copper (body 1) and steel (body 2), above the temperature of the ambient medium;
λ_1 and λ_2 are the thermal conductivities of bodies 1 and 2, respectively;
λ_{12} and λ_{21} are the mutual thermal conductivities of the bodies 1 and 2, respectively.

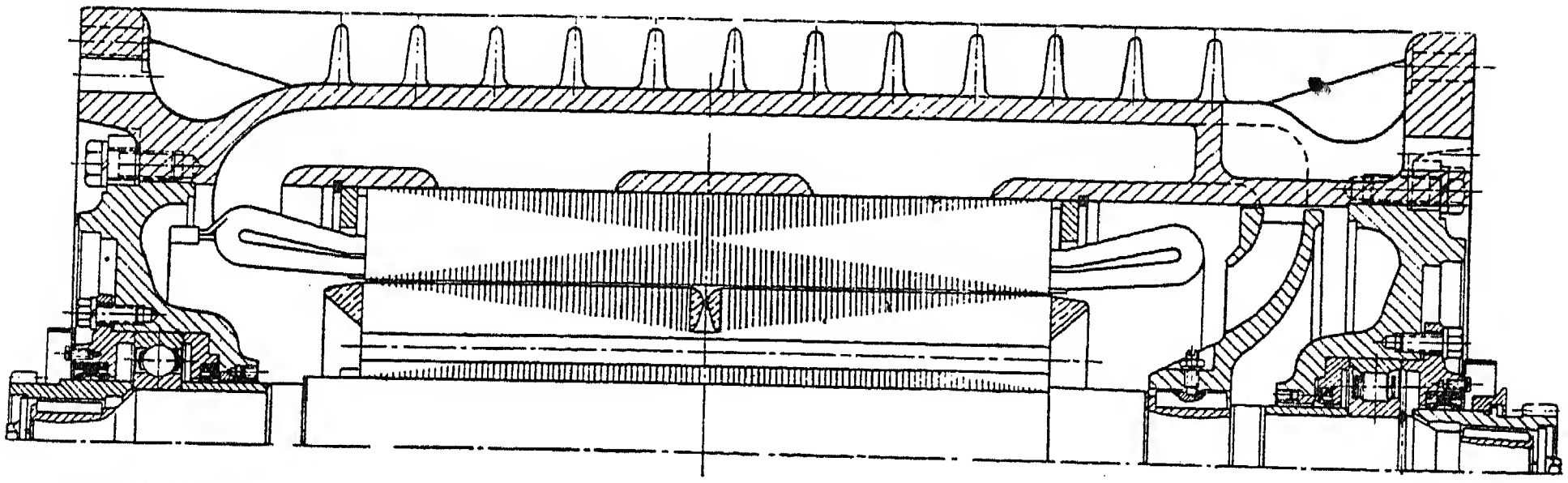

FIG. 1. Enclosed induction motor with ribbed frame and internal ventilation.

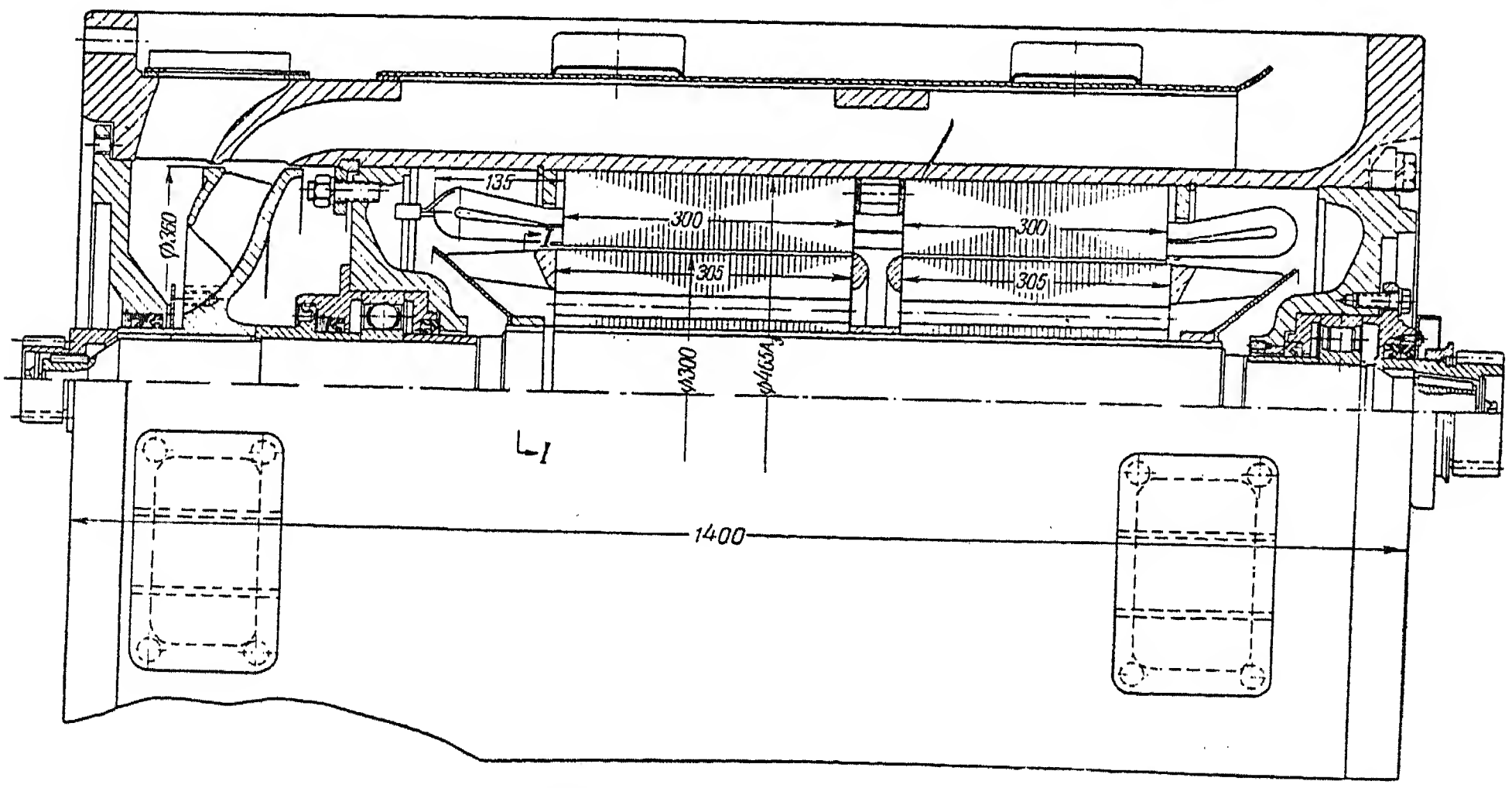

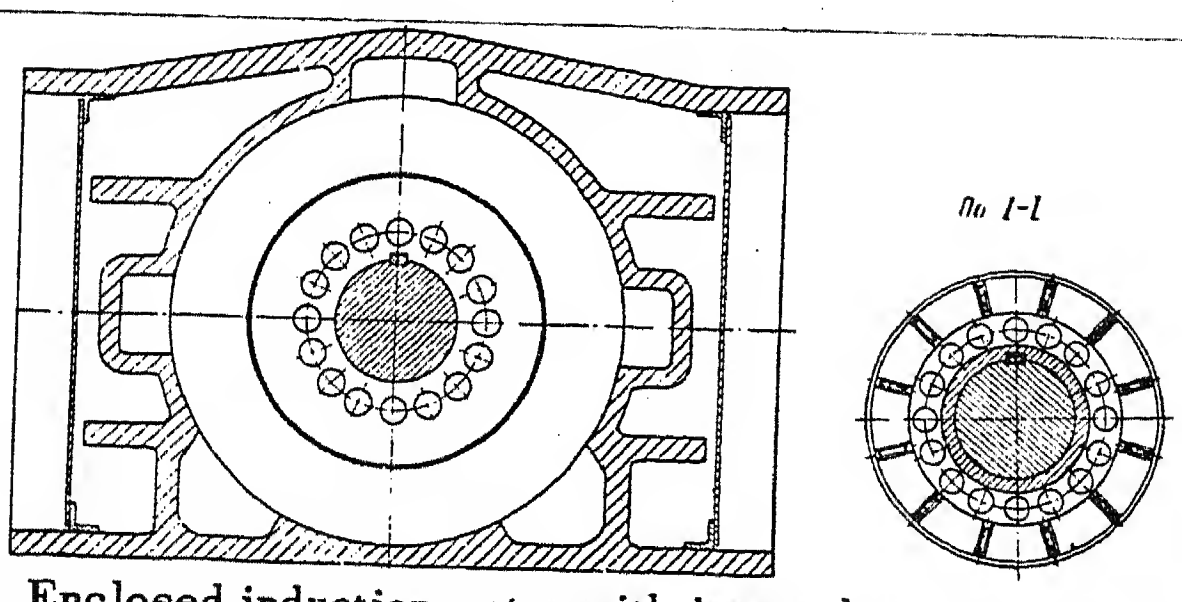

FIG. 2. Enclosed induction motor with internal air circulation and external forced ventilation.

An amount of thermal energy P_1 or P_2 of the given bodies is expended (a) by transfer to the ambient medium; (b) by transfer to the other body.

We get, therefore, a system of two linear equations. This explains the efforts of a number of authors to consider the heating-process of an electrical machine simplified as the temperature rise of two bodies. Experience has shown that the theory of the heating of two bodies yields satisfactory results in the case of a machine with a large air gap. However, in machines with a small air gap the thermal interaction of stator and rotor becomes considerable.

For this reason the theory of the heating of two bodies cannot be applied to induction motors. To take into account the influence of the rotor on the temperature rise of the stator windings B.P. Aparov suggested, on the basis of special investigations, to add to the losses in the stator copper 30 – 50 per cent of the losses in the rotor. The arbitrary addition to the copper losses of 30–50 per cent of the rotor losses leads to an incorrect rating of the installed power of the motor, and for this reason B.P. Aparov's method of thermal calculation is not acceptable.

Thermal calculations based on the theory of the heating-up of three homogeneous bodies considered the temperature rise of the copper and steel of stator and rotor (the rotor being regarded as a homogeneous body).

According to the thermal energy balance for steady operating conditions and constant heat losses we may write down the following equations:

$$\left.\begin{aligned} P_1 &= \tau_1\lambda_1 + (\tau_1 - \tau_2)\lambda_{12} + (\tau_1 - \tau_3)\lambda_{13};\\ P_2 &= \tau_2\lambda_2 + (\tau_2 - \tau_1)\lambda_{21} + (\tau_2 - \tau_3)\lambda_{23};\\ P_3 &= \tau_3\lambda_3 + (\tau_3 - \tau_1)\lambda_{31} + (\tau_3 - \tau_2)\lambda_{32}, \end{aligned}\right\} \qquad (2)$$

where τ_1, τ_2 and τ_3 are the temperature rises of the copper (body 1), stator steel (body 2) and rotor steel (body 3) above the ambient temperature;

λ_1 λ_2 and λ_3 are the thermal conductivities of the bodies, 1, 2 and 3;
λ_{12}, λ_{21} and λ_{31} are the mutual thermal conductivities of the bodies 1, 2 and 3.

Amounts of thermal energy P_1, P_2 and P_3 of the three homogeneous bodies are expended

(a) in transfer to the two other bodies;

(b) in transfer to the ambient medium.

To the system of equations (2) corresponds a definite thermal equivalent circuit, represented in Fig. 3.

Our analysis showed that in thermal calculations the temperature rise of the stator winding practically does not change, if the heat flow from the rotor to the stator copper is ignored. This heat flow is considerably less than the heat flow from the rotor to the stator steel owing to the negligible thermal conductivity of the air and the wedge in comparison with that of the steel. The effect of

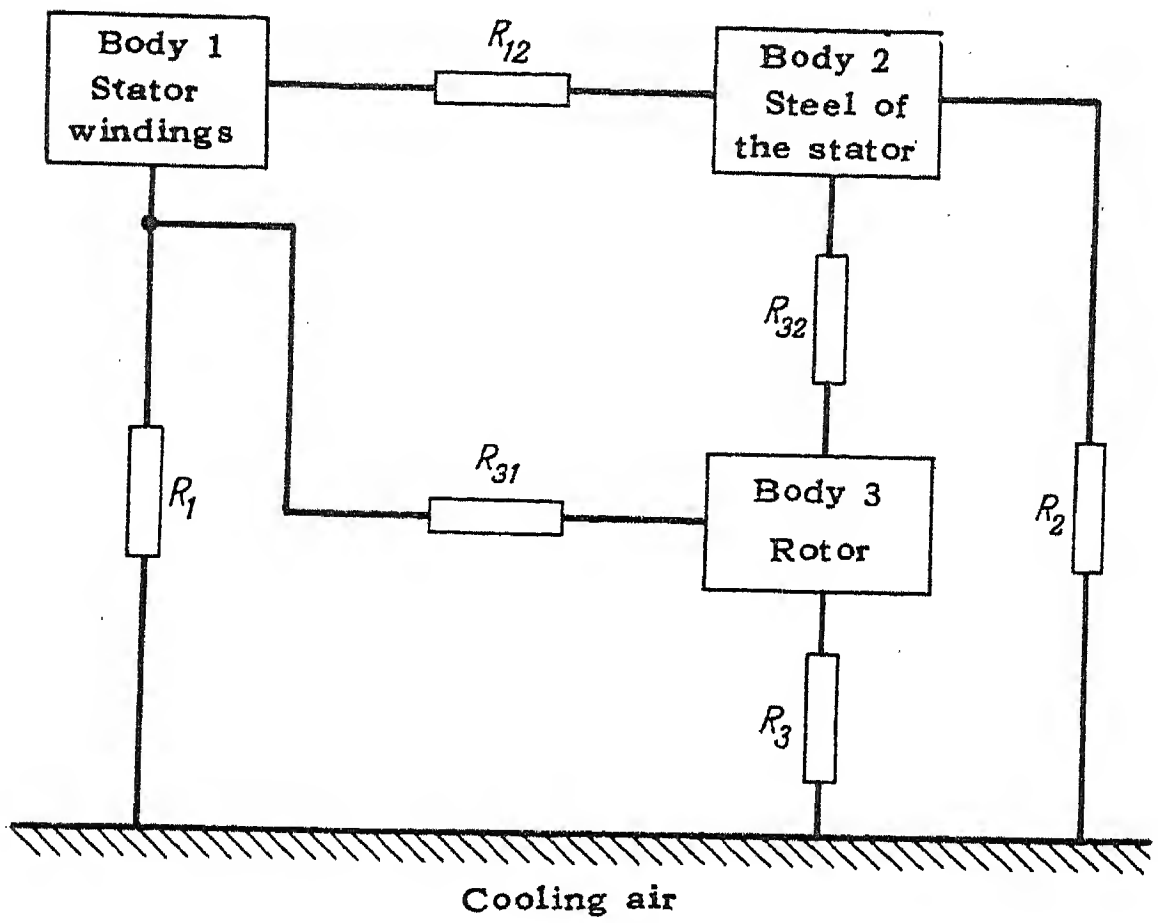

FIG. 3.

the rotor on the temperature rise of the stator winding does not manifest itself directly, but through the thermal flux from the rotor to the stator steel.

The stator steel is additionally heated by the losses in the rotor, owing to which the heat exchange from the stator copper to the steel deteriorates and, consequently, the copper temperature rises. These conditions are represented by the correct thermal equivalent circuit shown in Fig. 4.

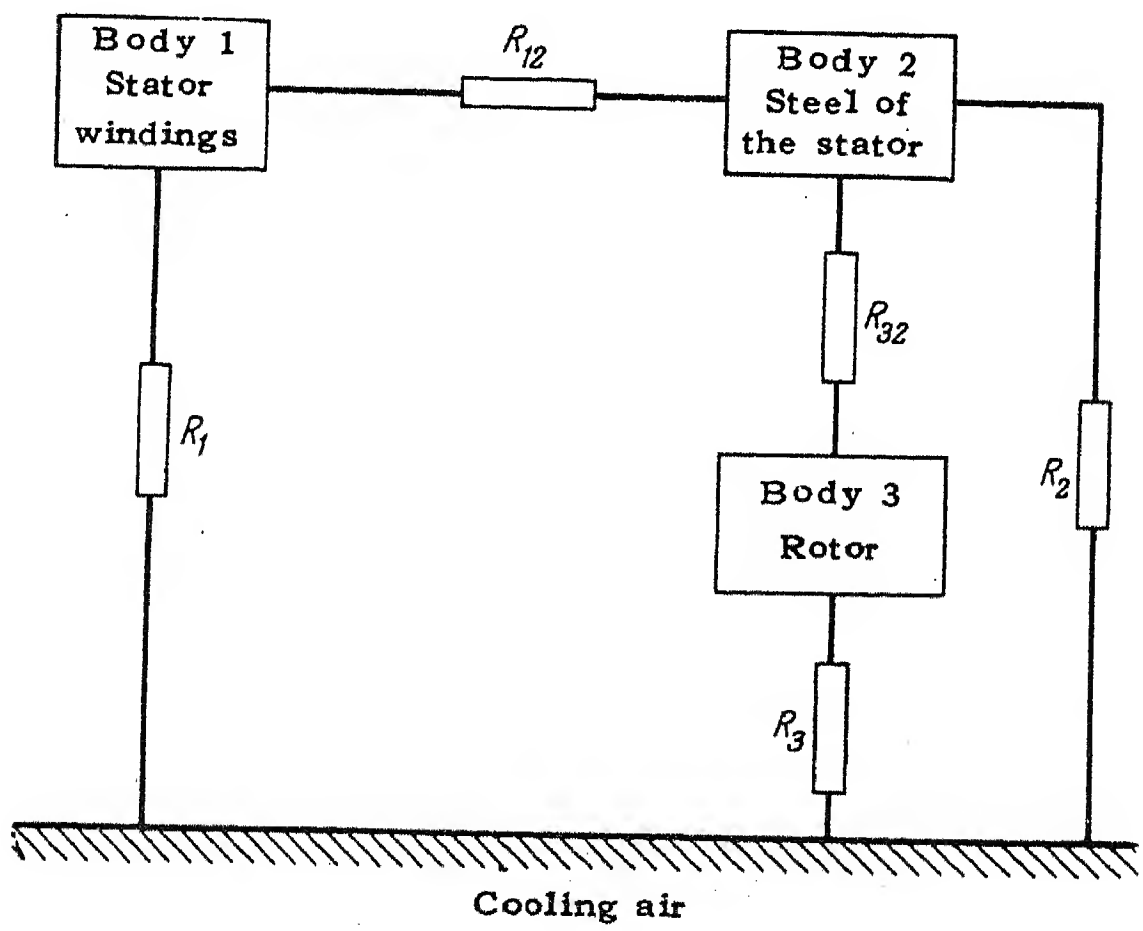

FIG. 4.

For the altered circuit we may write down the following equations in accordance with the thermal energy balance:

$$\left.\begin{aligned} P_1 &= \tau_1\lambda_1 + (\tau_1 - \tau_2)\,\lambda_{12};\\ P_2 &= \tau_2\lambda_2 + (\tau_2 - \tau_1)\,\lambda_{21} + (\tau_2 - \tau_3)\,\lambda_{23};\\ P_3 &= \tau_3\lambda_3 + (\tau_3 - \tau_2)\,\lambda_{32}. \end{aligned}\right\} \qquad (3)$$

The temperature excuss of the stator winding may be determined from the following expression:

$$\tau_1 = \frac{P_1}{aB} + \frac{P_2\lambda_{12}}{aAB} + \frac{P_3\lambda_{23}\lambda_{12}}{aABc},$$

where

$$a = \lambda_1 + \lambda_2; \quad b = \lambda_2 + \lambda_{21} + \lambda_{23};$$

$$c = \lambda_3 + \lambda_{32}; \quad A = \frac{bc - \lambda_{32}\lambda_{23}}{c};$$

$$B = \frac{Aa - \lambda_{12}\lambda_{21}}{Aa}.$$

The thermal calculation based on the concept of three homogeneous bodies for some types of squirrel-cage induction motors results in satisfactory agreement with experimental data. As regards motors of the type used for mining combines, numerous tests and calculations have established that the temperature excess of the stator windings due to the losses in the steel represents:

(a) About 75 per cent of the total temperature rise of the winding at the rated power for closed types of the motor without external forced cooling (Fig. 1);

(b) About 50 per cent of the total temperature rise of the winding at the rated power for closed types of the motor with external fan-cooling (Fig. 2).

Consequently, the temperature rise of the stator only due to the losses in the stator and rotor copper is of the order of 25 per cent for closed types without external forced cooling, and 50 per cent of the total temperature excess of the winding at the rated power for closed types with external forced cooling. When the temperature of the winding rises above the permissible value, for example, by 10 per cent, it is necessary for reducing this temperature to reduce the copper losses by 40 per cent for motor types without external cooling and by 20 per cent for motor types with external forced cooling. The useful output of closed motors of the type designed for mining combine motors varies, therefore, for a type without external forced cooling proportionately to the square of the variation of the overall temperature, and for the types with external forced cooling, approximately in a linear manner.

The thermal calculation based on the theory of three homogeneous bodies constitutes a considerable improvement in comparison with the theory of the temperature rise of two homogeneous bodies, and yet it cannot be recommended for motors for mining combines in which a considerable temperature rise of the stator winding occurs under no-load conditions owing to the constant losses. It is, in this case, necessary also to consider the following circumstances:

1. The losses in the stator winding consist of the losses in the copper of the zone of the slots and of the copper losses in the end connexions of the winding. Depending on the system of cooling of the motor and on its operating conditions, the end-connexions of the winding may dissipate the heat liberated in them in the ambient medium. In addition to this, they may absorb part of the heat liberated in the winding in the zone of the slots or inversely, pass on to the winding in the slot zone part of the heat liberated in themselves. The theory of the temperature rise of three homogeneous bodies considers the stator winding as a homogeneous body having the same temperature with all its parts.

2. The specific thermal fluxes in the steel at the back and the teeth of the stator are inhomogeneous and, consequently, the temperatures of the teeth and the back of the stator will also be unequal. The theory of the temperature rise of three homogeneous bodies regards the steel of the stator as a homogeneous body having all its parts at the same temperature.

3. Sources of heat in the rotor are: the rotor steel, the aluminium of the slotted part of the rotor and the short-circuiting rings. All these parts of the rotor are not at the same temperature, wherefore, it cannot be regarded as a homogeneous body.

4. In closed induction motors a fan is generally used for the internal circulation of the air. This internal fan is, on the one hand, a generator of heat, and on the other hand, responsible for the transfer of heat from the rotor to the frame and to the ambient medium. This fact is not considered by the equations of the temperature rise of three homogeneous bodies.

The above considerations show that for determining the rating of motors of mining combines it is necessary to introduce into the thermal calculation based on the theory of the temperature rise of three homogeneous bodies the additions enumerated above sub 1 – 4.

We suggest *a branched thermal equivalent circuit, based on eight generators of heat,* interconnected by finite thermal conductivities (Fig. 5).

Heat is liberated:

(a) in the copper of the winding in the slots;
(b) in the copper and connexions of the winding;
(c) the steel at the back of the stator;
(d) the steel at the stator teeth;

(e) the rotor steel;
(f) the aluminium of the slot part of the winding;
(g) the short-circuiting rings of the rotor;
(h) the internal fan (internal ventilation losses).

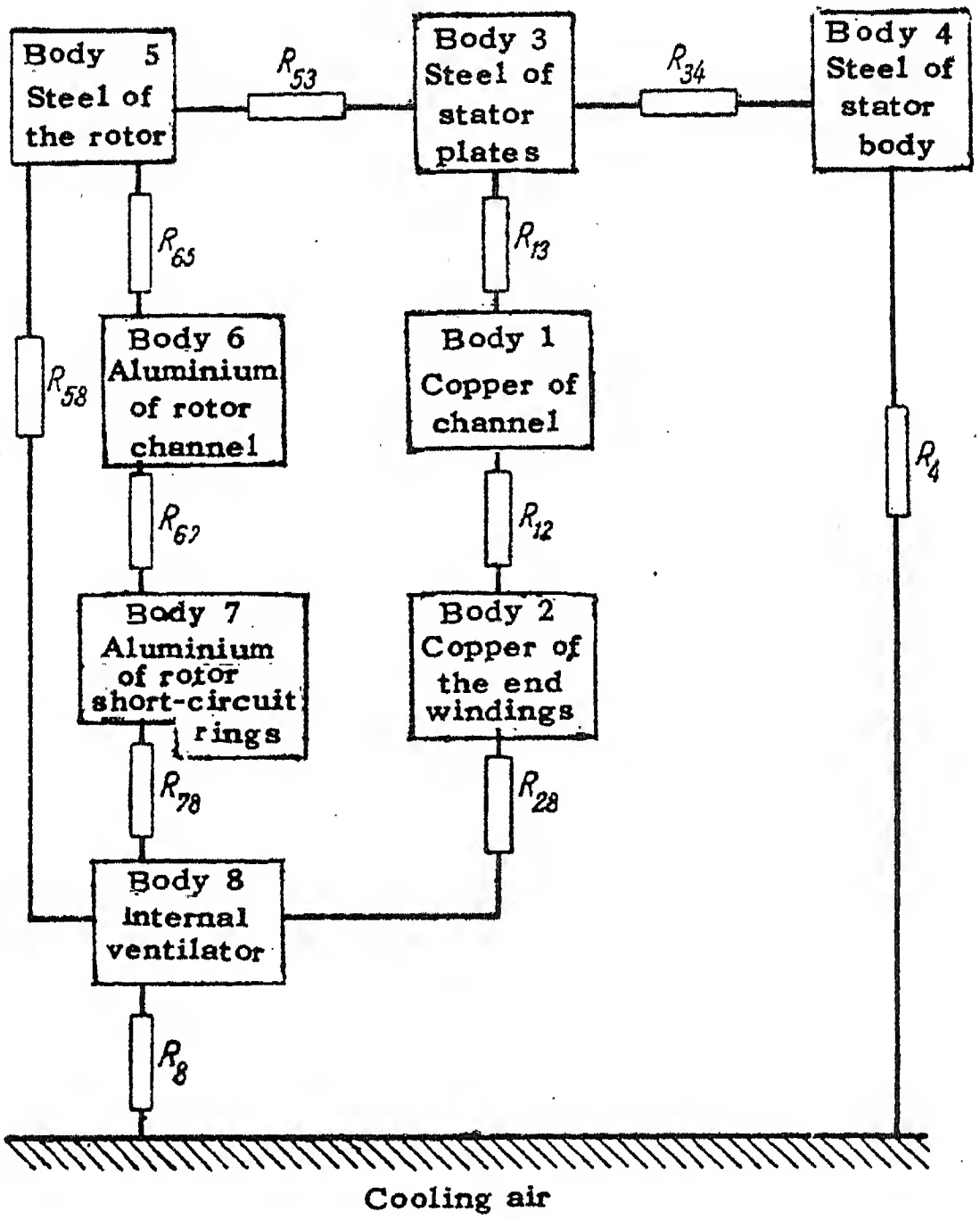

FIG. 5.

To the branched thermal equivalent network represented in Fig. 5 corresponds the following system of equations:

$$\left.\begin{aligned}
P_1 &= (\tau_1 - \tau_3)\lambda_{13} + (\tau_1 - \tau_2)\lambda_{12};\\
P_2 &= (\tau_2 - \tau_1)\lambda_{21} + (\tau_2 - \tau_8)\lambda_{28};\\
P_3 &= (\tau_3 - \tau_4)\lambda_{34} + (\tau_3 - \tau_5)\lambda_{35} +\\
&\quad + (\tau_3 - \tau_1)\lambda_{31};\\
P_4 &= \tau_4\lambda_4 + (\tau_4 - \tau_3)\lambda_{43};\\
P_5 &= (\tau_5 - \tau_8)\lambda_{58} + (\tau_5 - \tau_3)\lambda_{53} +\\
&\quad + (\tau_5 - \tau_6)\lambda_{56};\\
P_6 &= (\tau_6 - \tau_5)\lambda_{65} + (\tau_6 - \tau_7)\lambda_{67};\\
P_7 &= (\tau_7 - \tau_6)\lambda_{76} + (\tau_7 - \tau_8)\lambda_{78};\\
P_8 &= (\tau_8 - \tau_5)\lambda_{85} + (\tau_8 - \tau_7)\lambda_{87} +\\
&\quad + (\tau_8 - \tau_2)\lambda_{82} + \tau_8\lambda_8,
\end{aligned}\right\} \qquad (4)$$

where P_1 and τ_1 are the losses and temperature excess of the stator winding in the slots;

P_2 and τ_2 – the losses and temperature excess of the end-connexions of the stator winding;

P_3 and τ_3 – the losses and temperature excess of the steel at the stator teeth.

P_4 and τ_4 – losses and temperature excess of the steel at the back of the stator;

P_5 and τ_5 – losses and temperature excess of the rotor steel;

P_6 and τ_6 – losses and temperature excess of the aluminium of the slotted part of the rotor;

P_7 and τ_7 – losses and temperature excess of the short-circuiting rings of the rotor;

P_8 and τ_8 – the friction losses of the internal fan and the temperature excess of the air inside;

$\lambda_2, \ldots, \lambda_8$ – the thermal conductivities of bodies 2 . . . 8;

$\lambda_{12}, \ldots, \lambda_{87}$ – the mutual thermal conductivities of bodies 1 and 2, . . . , 8 and 7.

In practice it is required to simplify the methods of thermal calculations.

We must determine the temperature excess of the winding according to the actual physical processes taking place in the machine, even if we introduce the well-known simplifying assumptions. In setting-up the branched thermal equivalent circuit represented in Fig. 5, we make the following assumptions:

1. The thermal fluxes in the stator and rotor steel have only radial direction.

2. The thermal flux from the rotor to the stator copper is very small compared with the thermal flux directed from the rotor to the stator steel; for this reason we neglect it.

3. The outer surface of the motor frame is regarded as an equipotential surface.

In the branched thermal equivalent circuit shown we considered all the thermal flows capable of influencing the temperature rise of the stator winding. The simplifications introduced do not refer to the initial conditions, but consist in neglecting second-order quantities. The precision of the thermal calculations based on the thermal circuit shown, and assuming 8 sources of heat, is quite sufficient for determining the ratings of the fully-enclosed motors of mining combines.

A solution of the systems of equations presented above, though not intrinsically difficult, is yet very laborious and inconvenient for practical purposes.

We recall that the object of the present communication was to evolve a practical method of thermal calculations of fully-enclosed induction motors with a view to determining the rating of such motors. The rating of squirrel-cage induction motors is determined by the temperature rise of the stator winding. As re-

gards the other parts of the motor such as the stator and rotor steel, rotor aluminium, etc., their temperature rise is not limited. Consequently, it is only necessary to determine the temperature rise of the stator winding in order to establish the rating of the motor. Considering the thermal equivalent circuit with eight sources of heat which we evolve, it is only necessary to simplify the determination of the over-temperature of the stator winding; this renders it necessary to reduce the number of equations forming the system.

We explain below the suggested method of thermal calculation for enclosed motors of mining combines. It comprises the following stages:

1. Setting-up a branched thermal equivalent circuit based on the assumption of 8 sources of heat.

2. Determination of the directions of the thermal fluxes from the rotor from the stator windings.

Thermal fluxes from the rotor

There are four directions of thermal fluxes in the rotor, viz:

(a) The losses in the rotor, transmitted through the air gap to the stator steel;
(b) Losses in the rotor carried off through the axial ducts in the rotor and by the air passing through them;
(c) Losses in the slotted part of the rotor aluminium, transmitted to the rotor steel;
(d) Losses in the slotted part of the rotor aluminium, carried off to the short-circuiting rings of the rotor.

Thermal fluxes from the stator winding

In the stator winding there are two directions of the thermal fluxes from the stator winding, viz:

(a) Losses transmitted from the winding in the slots of the stator to the steel of the stator;
(b) Losses transmitted from the stator winding in the slot to the end connexions. If these values happen to be negative, the losses will be directed from the end-connexions to the part of the winding in the slots.

3. Determination of the required numerical values of the six thermal fluxes from the rotor and stator winding. To determine these we put down a system of six equations. We obtain these equations on the basis of the following conditions:

(a) The algebraic sum of all the thermal fluxes towards and from any point equals zero;
(b) The magnitude of the temperature drop between two points does not depend on any particular path through the thermal circuits comprising these points.

4. Determination of the actual thermal fluxes in all the sections from the stator winding to the ambient air. The thermal flux through the stator steel to its external surface consists of: a heat flow of constant magnitude, directed from the rotor to the stator steel; a heat flow of constant magnitude directed from the stator winding to the stator steel; the heat flow proper, set up by the losses in the steel at the teeth and the back of the stator.

5. From the actual heat flows in the various parts of the motor and from design data, it is possible to determine the temperature drops and the temperature excess of the stator winding.

It is, therefore, necessary, in order to determine the temperature excess of the stator winding according to the method suggested, to solve a system of six equations. The number of equations must be equal to the number of possible directions of heat flows from the rotor and from the stator winding. The use of external forced cooling of the frame of the motor does not alter the number of directions of the heat flows from the rotor and from the stator winding; only the coefficient of heat dissipation is altered. To determine the numerical values of the heat flows enumerated, we will carry out the calculation in the individual sections below.

Example of a system of equations

Corresponding to the branched thermal equivalent circuit of Fig. 5 ;

$$\left.\begin{aligned}
P_{x1}+P_{x2}&=P_n;\\
P_{y3}+P_{sr}&=P_{y1}+P_{y2};\\
P_{y3}+P_{y4}&=P_{a.sl.}\\
(P_{x1}+P_{y1}+P_{3})R_{34}+&\\
+(P_{x1}+P_{y1}+P_{3_t}^{t}+P_{sb})R_4&=\\
=P_{x2}R_{12}+(P_{x2}+P_e)R_{28}+&\\
+(P_{x2}+P_e+P_{fr})R_8;&\\
P_{y3}R_{65}+P_{y2}R_{58}=P_{y4}R_{67}+(P_{y4}+P_{shr})R_{78};&\\
P_{y3}R_{65}+P_{y1}R_{53}+(P_{y1}+P_{3_t}+P_{x1})R_{34}+&\\
+(P_{y1}+P_{3_t}+P_{x1}+P_{sb})R_4=P_{y4}R_{67}+&\\
+(P_{y4}+P_{shr})R_{78}+(P_{y4}+P_{shr}+P_{\theta})R_8,&
\end{aligned}\right\} \qquad (5)$$

where P_{x1} – are the losses transmitted from the winding in the stator slots to the steel of the stator;

P_{x2} – losses transmitted from the stator winding in the slots to the end-connexions; when P_{x2} has a negative value, the losses will be directed from the end-connexions to the winding in the slots;

$P_s l$ – losses in the stator winding in the slots;
P_{y1} – losses in the rotor transmitted through the air gap to the stator steel;
P_{y2} – losses in the rotor transmitted through the axial ducts of the rotor and by the air passing through them;
P_{y3} – losses transmitted to the rotor steel from the aluminium parts in the rotor slots;
P_{y4} losses transmitted to the short-circuiting rings of the rotor from the aluminium in the rotor slots; when P_{y4} is negative, the losses will be directed from the short-circuiting rings of the rotor to the winding in the rotor slots;
$P_{s.r.}$ – losses in the steel of the rotor;
$P_{a.sl.}$ – losses in the aluminium in the rotor slots;
P_t – losses in the stator teeth;
P_e – losses in the end connexions of the stator winding.
$P_{fr.}$ – friction losses between internal fan and air;
P_{shr} – losses in the short-circuiting rings of the rotor;
P_{slo} – losses in the back of the stator;
R_4 and R_8 thermal resistances between the bodies 4 and 8 and the ambient medium;
R_{12}, R_{13} etc. – mutual thermal resistance of the bodies 1 and 2, 1 and 3, etc.

Analysis of experimental data and their comparison with theoretical results

We will analyse the experimental data of a motor EDK-120, designed for the drive of a mining combine, and compare them with results obtained by thermal calculations on the method described above.

The main parameters of the motor EDK-120 are: Continuous output 55 kW; voltage W_l = 660 V; I = 64 A; speed on load n = 1485 rev/min; enclosed with ribbed frame and internal air circulation (Fig. 1); overall dimensions : length 1250 mm, with 780 mm, height 500 mm.

In the thermal tests the motor was placed on rails fixed to the bed and connected to the shaft of the loading generator. Owing to this the lower part of the surface of the frame of the motor could not freely radiate into the surroundings. The thermal tests of the motor were not carried out in a special insulating chamber, but in the test bay of the works. Despite the fact that the tested motor was during its thermal-duty tests separated from the loading generator by a special wooden screen, and at some distance from the other machines working simultaneously in the test bay, the ambient air around the fram of the motor was still slightly agitated.

The thermal-duty tests of motors for mining combines and coal cutters produced by the industry are carried out in the testing stations generally in a

similar way. It is for this reason that even though the frame of the motor may correspond to the type without external forced cooling, there will always be a certain slight cooling effect owing to the agitation of the air in the test bays. To measure the intensity of this external air flow by any instrument was impossible owing to the extremely low air velocity. However, the presence of an even very slight air circulation increases considerably the coefficient of heat transfer and, consequently, reduces the temperature excess of the frame of the motor. The temperature excess of the stator winding, Δt_w, on the other hand, is determined by the temperature drop Δt_f, between the stator winding and the frame and the temperature drop Δt_a between the frame and the ambient air, i.e.

$$\Delta t_w = \Delta t_f + \Delta t_a.$$

Our analysis of the experimental results obtained with enclosed motors of mining combines and coal cutters enabled us to establish the following approximate relations:

$$\Delta t_f / \Delta t_w = 0.25 \ldots 0.3 \text{ and } \Delta t_a / \Delta t_f = 0.75 \ldots 0.7$$

Consequently, for temperature excess of the stator winding $\Delta t_w = 95^{\circ}C$, the temperature excess of the frame of the motor (assuming the frame to be a thermal equipotential surface) will be $\Delta t_{fr} \approx 67 \ldots 71^{\circ}C$.

According to the tests the maximum temperature excess of the motor frame is $\Delta t_{fr} = 85^{\circ}C$.

The existence of a slight air current around the frame during the thermal-duty tests of the motor is also confirmed by the fact that a thread held near the frame is deflected from the vertical direction.

Tables 1 and 2 collect experimental and theoretical data on the thermal-duty of a motor EDK – 120.

TABLE 1.

	Rating (kW)	Voltage (V)	Current (A)	Slip (%)	Velocity of external air current (m/sec.)
Test results	56.5	660	66	1.2	Owing to the low air speed, the intensity of the external ventilation could not be measured.
Results of calculation	55	660	64	0.89	1 m/sec

TABLE 2.

	Losses						Temperature excesses		
	In steel (W)	Copper (W)	Aluminium (W)	Additional (W)	Windage (W)	Sum of heat losses (W)	Of winding, from resistance (°C)	Of winding, by thermo-couple (°C)	Of frame, by thermo-couple (°C)
Test results	1800	865	700	368	250	3923	98	107	85 (maximum)
Theor-etrical values	2120	810	500	300	230	3960	93	—	70 (mean)

Conclusions

1. The existing methods of thermal calculations are briefly reviewed and a new method of thermal calculations of enclosed induction motors to be used for the drives of coal cutters and mining combines is presented.

2. The method of thermal calculations suggested may form a basis for a practical method of designing enclosed induction motors to be generally accepted.

3. More research work is required on the coefficients of heat exchange of induction motors.

REFERENCES

1. B.P. Aparov; *Investigation of Temperature Rise of Induction Motors under unsteady conditions. All-Union Electrotechnical Institute* 10-11 (1939).
2. A. Dembo and B. Kuznetsov; *Thermal Testing of Induction Motors. Tr. Leningrad Industrial Inst.* No. 2 (1937).
3. A.P. Ioffe; *Temperature Rise of Squirrel-cage Motors Under Repeated Starts and Stops. All-Union Electrotechnical Institute* No. 3 (1951).
4. I.M. Postnikov; *Projecting Electrical Machines. Gostekhizdat* SSSR (1952).

VELOCITY - TIME RELATIONS FOR ELECTRIC DRIVES FOR INTERMITTENT OPERATION*

L.V. KARNIUSHIN

(Received 17 December 1956)

The theory of motor drive presented below is of practical importance for designing and operating a reversible unit consisting of an electric motor and a driven mechanism which operates intermittently with frequent starting and braking.

Depending on the design, and types of operation performed, the choice of velocity-time relations (or the corresponding load diagrams of the motor and driven mechanism) can be based on various criteria [1-3]. The criteria adopted in the present work are based on the fact that the relation between the output of the machine and the rating of the motor (the latter being fully utilized according to thermal loading) is dependent mainly on the choice of the velocity-time relation of the motor [2,3].

Thus, in the case of machines having a given duty cycle whose operating member moves through a given fixed distance (e.g. a colliery winder), the first condition for the choice of the best velocity-time curve of the driving motor is that *a given output must be secured with the smallest horse-power rating.* (First criterion). It will be shown later that this condition is equivalent to securing the maximum output with a given installed horse-power.

In a number of cases a second criterion is of importance, which is *securing the maximum output with a given rated motor torque.* This is equivalent to securing a given output at the minimum motor temperature rise.

The functional relation between the motor horse-power (or torque), the velocity-time law, and the output power can be found by solving the simultaneous equations for the velocity law of the motor, the heating of the motor, and the angular displacement of the machine shaft. If this relation is found, the question of finding the best velocity-time relation (in accordance with the first or second criterion) amounts to finding mathematically either the extremum of a certain function (for a given form of tachogram) or of the functional.

The solution of this kind of problem (when both criteria are satisfied) is

* *Elektrichestvo* No. 6, 64-71, 1957 [Reprint Order No. EL 31].

given in the literature only for one particular type of motor velocity-time curve, namely when this curve is trapezoidal [2, 4]. A more general solution, when not only the parameters, but also the shape of the velocity-time curve have to be found, is given in [3, 5, 6]. This applies to cases in which only the second criterion is satisfied. The problem of the existence of a velocity-time curve satisfying the first criterion has never been fully investigated [7].

It should be pointed out that there is still at the present time no definite opinion on the practical significance of the best velocity-time curve of the motor drive. This is because sufficiently detailed investigations covering the whole subject have not been carried out.

In preparing this paper the following assumptions have been made:

(a) the temperature rise of the motor is assumed to vary with the r.m.s. torque;

(b) the following quantities, referred to the motor shaft, are constant:- the resistance torque, T_r, the total moment of inertia, J, and the transmission efficiency, η;

(c) the following factors which impose limitations on the voltage-time laws of motor drive are neglected:- type of process, robustness of construction of the machine, conditions for supporting moveable parts, permissible mechanical overloading of motors, and electrical overloading of the supplying converter (the influence of these factors will be considered when comparing the tachograms).

The best trapezoidal velocity-time curves of the driving motor

Only symmetrical trapezoidal curves will be considered, since these are more advantageous with regard to motor heating than the asymmetrical curves [2].

For a given angular displacement, β, the time during which the motor is rotating, t_m, and time of rest, t_o, there is a certain steady (established) angular velocity of the motor, ω_{e2} (or the corresponding acceleration ϵ_2), at which the r.m.s. value of the motor torque for the interval $t_m + t_o$), T_{eq2}, (the equivalent torque) is a minimum [4]. Also there is a steady velocity ω_{e1} (or ϵ_1) at which the motor output permitted by temperature rise is a minimum. This output is given by:

$$P_{eq1} = \frac{\omega_{e1}\, T_{eq1}}{102}. \qquad (1)$$

It is shown in [4] that irrespective of the magnitude of the resistance torque of the machine (T_r = const) and the efficiency of the mechanical transmission (η = const), the minimum T_{eq2} always occurs at $\omega_{e2} = 0.75\,\omega_\Delta$ (or at $\epsilon_2 = 1.125\,\epsilon_\Delta$) where ϵ_Δ and ω_Δ are acceleration and maximum velocity in the case of

a triangular velocity curve at the same β, t_m, and t_o.

The velocity ω_{e1} which corresponds to the minimum P_{eq1} depends on the magnitude of the coefficient of dynamic loading.

$$d = \frac{1}{\mu} = \frac{J\epsilon_\Delta}{T_r}, \tag{2}$$

and lies within the limits

$$0.5 < \frac{\omega_{e1}}{\omega_\Delta} \leq 0.625 \quad [4].$$

The ratios of r.m.s. values of torques and outputs with trapezoidal and triangular velocity-time curves for the same values of β, t_m, and t_o are given by

$$\frac{T_{eq}}{T_{eq\Delta}} = \sqrt{\frac{\frac{z^3}{2z-1} + \mu^2}{1+\mu^2}}; \tag{3}$$

$$\frac{P_{eq}}{P_{eq\Delta}} = z\frac{T_{eq}}{T_{eq\Delta}}, \tag{4}$$

where $z = \frac{\omega_e}{\omega_\Delta}$

The function $P_{eq}/P_{eq\Delta}$ is a minimum at a certain value of $z = z_o$ which depends on the numerical value of μ and is given by one of the real roots of the following equation:

$$8z^4 - 5z^3 + 8\mu^2 z^2 - 8\mu^2 z + 2\mu^2 = 0 \tag{5}$$

in the region $0.5 \leq z \leq 0.625$.

By assigning different values to μ (in the majority of cases they lie within the limits $0 < \mu < 3$), it is not difficult to find from (5) the corresponding values of $z_p = \omega_{e1}/\omega_\Delta$. This also gives the optimum velocity at which the minimum required output is attained,

$$\omega_{e1} = z_o\omega_\Delta = 2z_o\frac{\beta}{t_a}, \tag{6}$$

where t_a is the duration of the accelerating period.

Having established the values for $\omega_{e\,1}$ and $\omega_{e\,2}$, we can now determine the parameters of the optimum (according to the first and second criteria) rectangular curves of the motor torque for the periods of accelerating and braking.

$$T_{a,b} = J \frac{\omega_{e\,1.2}}{t_{a\,1.2}} \pm T_r \; ; \tag{7}$$

$$t_{a\,1.2} = t_{b\,1.2} = t_m - \frac{\beta}{\omega_{e\,1.2}} \; , \tag{8}$$

where t_b is the duration of the braking period.

The optimum velocity-time relations for the drive

The time function $\omega\,(t)$, representing the required velocity-time relations, should increase steadily during the accelerating period, decrease steadily during the braking period, and pass through the points

$$\omega\,(0) = \omega\,(t_m) = 0 \tag{9}$$

With given values for the displacement β and the duration of the cycle t_c $(t_m + t_o)$, the required rated torque, T_n and the rated horse-power, P_n of the motor working under intermittent load conditions, are given by

$$P_n = \frac{\omega_n T_n}{102} \; ,$$

$$T_n = \sqrt{\frac{\int_0^{t_a} T_a^2\, dt + T_r^2\, t_e + \int_{t_a+t_e}^{t_m} T_b^2\, dt}{\alpha_1 t_u + \alpha_2 t_0}} \tag{10}$$

where t_e – period of constant velocity, α_1 and α_2 – coefficients to allow for poorer motor cooling at $\omega < \omega_n$, ω_n – rated angular velocity of the motor rotor.

The motor torques during the accelerating and braking periods are

$$T_a = J\epsilon + T_r \text{ and } T_b = J\epsilon - T_r \; . \tag{11}$$

Substituting (11) into (10) and considering the condition given by (9)

$$\int_0^{t_a} \epsilon\, dt = \int_{t_a+t_e}^{t_m} \epsilon\, dt$$

and

$$J^2 \int_0^{t_a} \epsilon^2\, dt + J^2 \int_{t_a+t_e}^{t_m} \epsilon^2\, dt = J^2 \int_0^{t_m} \epsilon^2\, dt\ ,$$

we can find the relation between P_n, T_n, the output $\Pi \equiv 1/t_c$, and the velocity-time law:

$$102^2 P_n^2 (\alpha_1 t_m + \alpha_2 t_0) = I_1; \tag{12}$$

$$T_n^2 (\alpha_1 t_m + \alpha_2 t_0) = I_2\ , \tag{13}$$

where

$$I_2 = T_r^2 t_m + J^2 \int_0^{t_m} \epsilon^2\, dt\ ; \tag{14}$$

$$I_1 = \omega_n^2 I_2 = \left(\int_0^{t_a} \epsilon\, dt\right)^2 I_2\ . \tag{15}$$

As is seen from (12) and (13), for a given output (i.e. for given values of t_m, t_0, and β), the minimum value of the required motor torque, $T_{n.\min}$, is given by a velocity-time law that minimizes the functional I_2. The minimum value of the rated output, P_n, will be obtained with a different velocity law which minimizes the functional I_1. If T_n (or P_n), β, and t_m (or t_0) are given, the highest output will be obtained with these laws (i.e. the shortest period t_0 (or t_m) and therefore, $t_{c.\min}$).

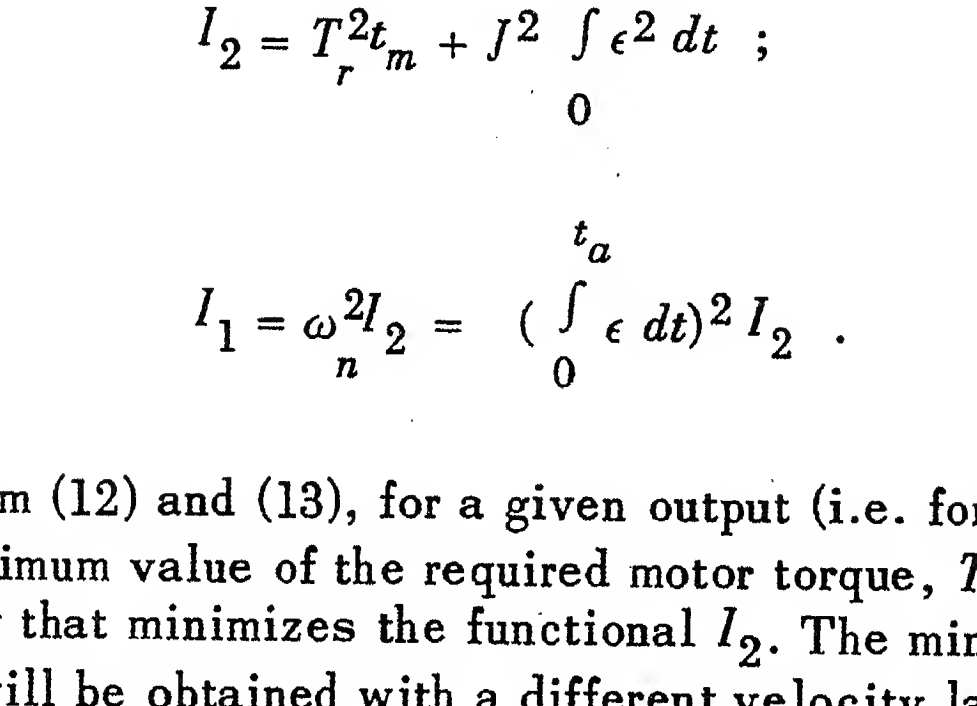

FIG. 1. a) Parabolic velocity curve with sudden change of acceleration;
b) with periods of uniform change of acceleration.

Thus the mathematical determination of the velocity-time relationships for a driving motor can be reduced to two similar isoperimetric variational problems, that is, determination of the function $\omega\,(t)$ which minimizes the functional I_1 (or I_2) and satisfies the boundary conditions given by (9), as well as satisfying an additional condition

$$\int_0^{t_m} \omega\, dt = \beta\ . \tag{16}$$

To determine the function $\omega\,(t)$ which minimizes the functional I_2 is easily done by setting up and solving Euler's equations [5,6]. The required velocity-time law for the drive motor satisfying the second criterion is a symmetrical parabola, Fig. 1a.

$$\epsilon = \epsilon_{mp}\,(1 - 2\,\frac{t}{t_m})\ ; \tag{17}$$

$$\omega = \omega_{mp}\,t\,(1 - \frac{t}{t_m})\ , \tag{18}$$

where

$$\epsilon_{mp} = 6\,\frac{\beta}{t_m^2} = 1.5\epsilon_{\Delta}\ ;\ \omega_{mp} = 1.5\,\frac{\beta}{t_m} = 0.75\omega_{\Delta} \tag{19}$$

For the same β, t_m, and t_o, the ratio of the r.m.s. value of torque for the parabolic velocity curve to the torque for the trapezoidal velocity curve is given by

$$\frac{T_{eq\ q}}{T_{eq}} = \sqrt{\frac{(0.75 + \mu^2)\,(2\,z - 1)}{z^3 + \mu^2\,(2z - 1)}}\ . \tag{20}$$

Also, the ratio of corresponding outputs is

$$\frac{P_{eq\ p}}{P_{eq}} = \frac{0.75\ T_{eq\ p}}{z\ \ T_{eq}}\ ; \tag{21}$$

The ratio of accelerations is

$$\frac{\epsilon_{mp}}{\epsilon} = \frac{1.5\,(2z - 1)}{z^2} \tag{22}$$

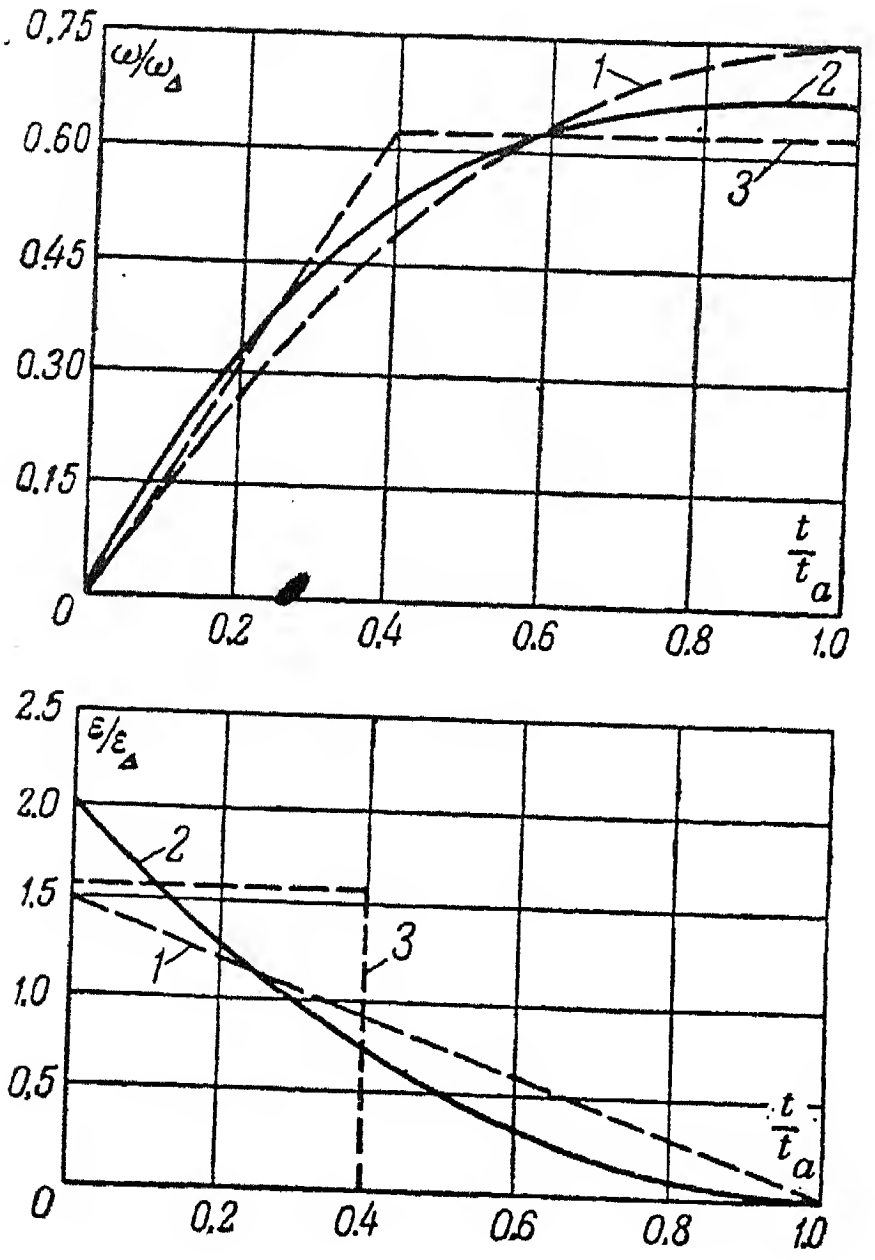

FIG. 2. Diagrams of velocity and acceleration for one-half period of displacement,
1—with "parabolic acceleration";
2—with the optimum velocity law (with respect to output);
3—with the optimum trapezoidal velocity-time curve (with respect to output) ($\mu = 0$).

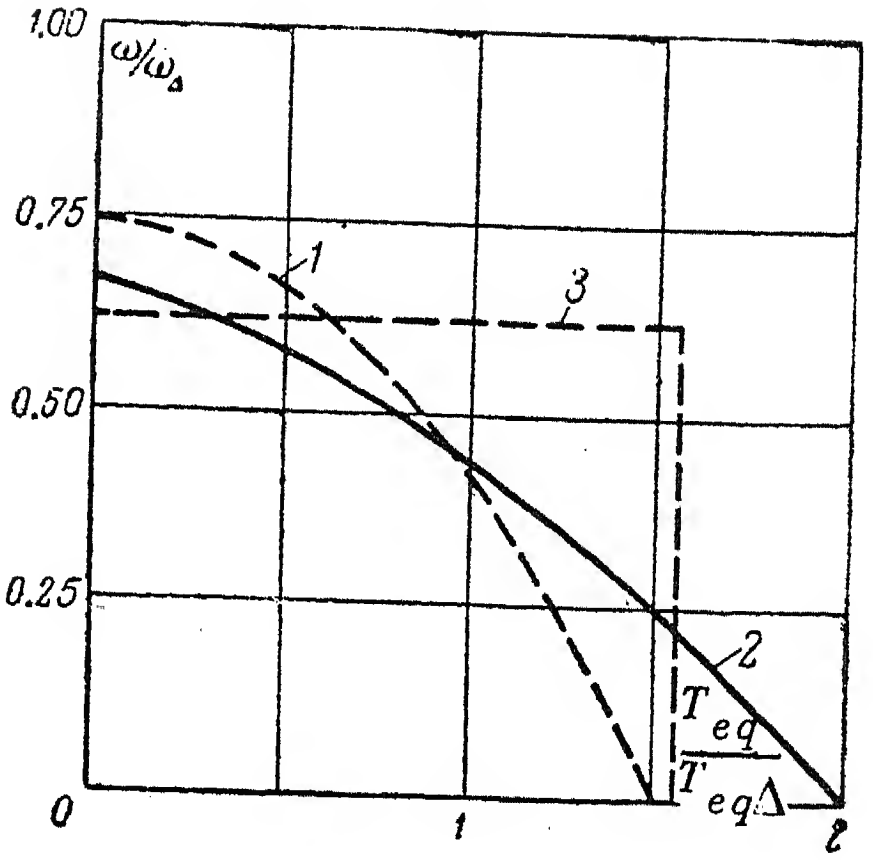

FIG. 3. Characteristics of motor necessary to obtain velocity-time curves of Fig. 2.
1—with "parabolic acceleration";
2—with the optimum velocity law (with respect to output);
3—with the best trapezoidal velocity-time curve (with respect to output).

The load diagram for the parabolic velocity curve and for $T_r = \text{const.}$ is of triangular shape,

$$T = T_r + J\epsilon = T_r + J\epsilon_m \left(1 - 2\frac{t}{t_m}\right) \tag{23}$$

(the ratio of mean height of curve to maximum height is 0.5).

The usual variational method of setting up Euler's equations is not applicable to finding the function $\omega\ (t)$ which minimizes the second functional, I_2. Therefore, it is necessary to use a direct variational method.

We shall assume a symmetrical velocity curve of the motor. To solve the problem, it is then sufficient to consider only the first half-period of the displacement from $t = 0$ to $t = 0.5\ t_m$, since it is obvious that if the conditions (9) are

satisfied, the required law will also be valid for the second half-period.

Thus, this law of motion can be found for any predetermined relation between T_r and J. We shall, however, confine ourselves to considering only the case when the frictional resistance can be neglected ($T_r \to 0$). The solution to this case will enable us to evaluate the greatest effect which can be achieved by using the law which conforms to the first criterion.

With the assumption made the problem is reduced to finding a function $\omega(t)$ minimizing a functional which is simpler than the functional I_1 and is given by

$$I_3 = \left(\int_0^{0.5t_m} \epsilon\, dt\right)^2 \cdot \int_0^{0.5t_m} \epsilon^2\, dt \tag{24}$$

for the following conditions: a) $\omega(0) = 0$; b) $\omega'(0.5t_m) = 0$;

c) $\int_0^{0.5t_m} \omega\, dt = \frac{\beta}{2}$; d) $\omega'(t) \geq 0$ for $0 \leq t \leq 0.5\, t_m$.

Condition d) represents the requirement that $\omega(t)$ is to increase steadily, while condition b) follows from the natural limiting condition for the end of the curve $\omega(t)$ which has a locus $t = t_a$, parallel to the ω axis.

The solution to this problem [7] gives as a first approximation the following optimum (with respect to the equivalent output) laws for the first half of the displacement when $\mu = 0$.

$$\omega = \epsilon_{mo} t \left(1 - 2\frac{t}{t_m} + \frac{4t^2}{3t_m^2}\right); \tag{25}$$

$$\epsilon = \epsilon_{mo} \left(1 - 4\frac{t}{t_m} + 4\frac{t^2}{t_m^2}\right), \tag{26}$$

where $\epsilon_{mo} = 8\frac{\beta}{t_m^2} = 2\,\epsilon_\Delta$ and $\omega_{mo} = \frac{4}{3}\frac{\beta}{t_m} = \frac{2}{3}\omega_\Delta$. (27)

The curves of velocity and acceleration drawn from (25) and (26) are shown in Fig. 2. The same figure also shows for comparison (with the same β, t_m, and $\mu = 0$) the parabolic curve and the optimum trapezoidal curve with respect to output. Fig. 3 shows the torque characteristics of the motor which are necessary to obtain the velocity-time curves shown in Fig. 2.

The r.m.s. value of the torque for the period of $0.5\, t_m$ when the motor acceleration follows the optimum law in accordance with the first criterion, is given by

$$T_{eq0} = \sqrt{2\frac{J^2}{t_m}\int_0^{0.5t} \epsilon^2\, dt} = 3.576\, J\, \frac{\beta}{t_m^2} = 0.894\, T_{eq\Delta} \qquad (28)$$

The equivalent output is found from (27) and (28)

$$P_{eq0} = \frac{2}{3}\, 0.894\, P_{eq\Delta} = 0.596\, P_{eq\Delta}\,. \qquad (29)$$

The ratio between mean and maximum height of the load torque curve when the optimum law (25) is obeyed is given by

$$k_z = \frac{\int_0^{0.5t_m} J\epsilon\, dt}{J\epsilon_{mo}\, 0.5t_m} = \frac{1}{3}\,.$$

The use of optimum tachograms with variable path of displacement

Because of the geometrical relationship between the displacement, β, of the operating member of the driven mechanism and the remaining parameters of the tachogram, ω, ϵ and t_m, these parameters vary with β. Also the tachogram should be corrected for permissible velocities and accelerations.

Since in the case of a varying cycle of operation the choice of the best motor tachograms is influenced by a great number of different conditions, this problem must be considered separately for each particular case of the motor drive.

In the case when a uniform regular cycle of operation and a number of fixed paths of displacement are given, the problem consists of either finding optimum tachograms corrected for ω and ϵ, for each displacement, using the condition for the maximum P_{eq} (or T_{eq}) or the maximum output π for the whole cycle.

For mechanisms with an arbitrary path of displacement (e.g. the main mechanisms of an excavator) either the first or the second criterion must be satisfied for the most typical cycle of operation; for other paths of displacement, the highest output permitted by the motor heating must be secured. For this purpose it is expedient to devise a scheme of automatic re-adjustment of the control system of the motor drive which will ensure that the optimum velocity and acceleration are achieved for each displacement.

With a constant standstill period, t_o, the effect which can be achieved with such a scheme cannot be very great. This is clearly seen in the example of the driving motor for the turning mechanism of the walking excavator type ESh — 14/75 for which the duration of the turning operation is up to 85 per cent of the duration of the whole cycle.

If the parabolic tachogram is used, the angle of turn, β, at which the motor

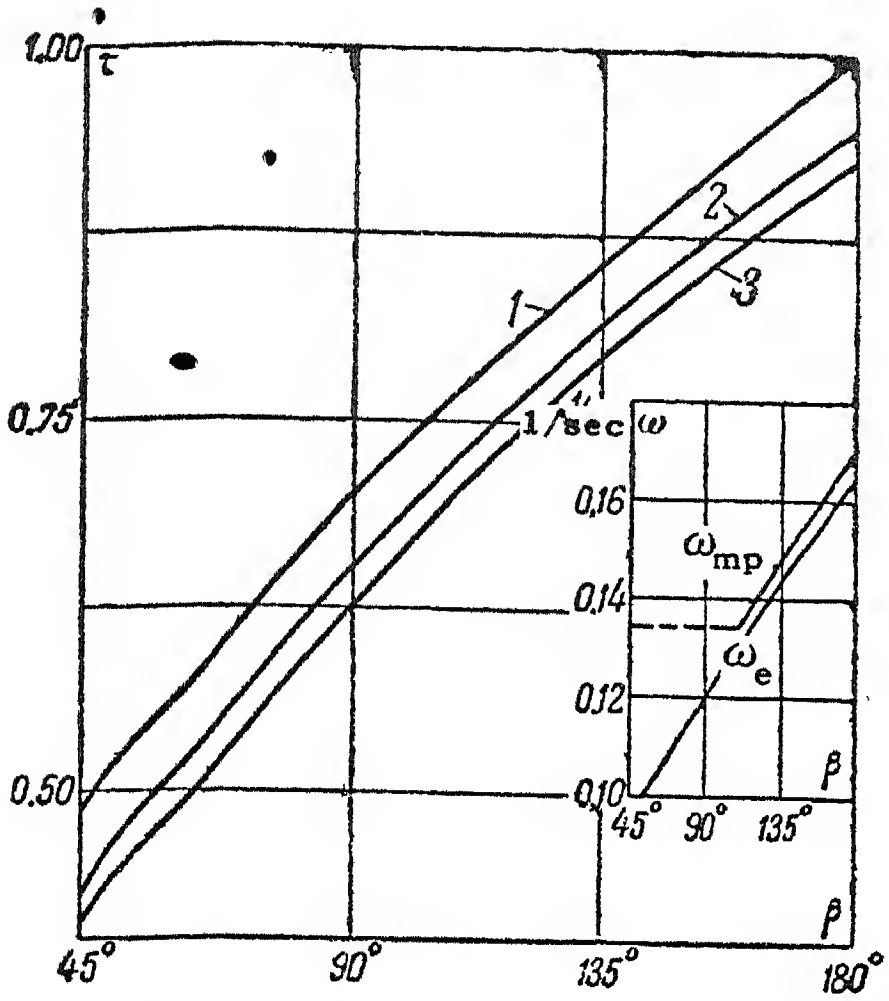

FIG. 4. Relative time of turning against angular path for the excavator type ESh – 14/75.

1 – with trapezoidal velocity-time curve, $\beta > 125^0$, and fixed acceleration and velocity (the motor is fully utilized only at $\beta = 125^0$);

2 – with the best (in accordance with the 2nd criterion) trapezoidal velocity-time curves for each angle of turning;

3 – with parabolic velocity-time curves and full utilization of the motor with regard to heating at $\beta \geq 110^0$.

and the mechanism are fully utilized (the first with respect to heating and the second with respect to permissible acceleration; $\epsilon_{perm.} = 0.025$ 1/sec²) is 110°. If $\beta > 110^0$, while keeping $T_{eqp} = \text{const}$, the acceleration ϵ_{mp} decreases. If $\beta < 110^0$, the duration of the excavator cycle is limited by the action of the lifting mechanism [1].

We shall denote $r = \dfrac{t_m}{t_{m.m}}$, where t_m is the time of turning through the angle β and $t_{m.m}$ is the time of turning through 180° when the velocity-time curve used is of trapezoidal form and ϵ and ω_e are fixed and such that the motor can be fully utilized from the point of view of heating only at $\beta = 125^0$.

Fig. 4 shows calculated curves $r = f(\beta)$ for different kinematic condition of operation of the motor drive when the period of digging is constant, $t_d = 10$ sec. It is seen from this figure that if the rotation of the driving motor follows the optimum tachogram for each angle of turn, the output of the excavator is increased by 4 to 5 per cent. The advantages of the parabolic over the best trapezoidal curve judged by the second criterion are, in this case, negligible.

Comparison of optimum tachograms for electric drive

In this comparison we shall assume that the cycle of operation consists of one period of displacement and one period of standstill; the path of displacement, β, being constant.

To assess the usefulness of the optimum velocity-time laws both in design and in practice, the following two principles should be applied:

1) *The principle of equal output.* This means that the operating member of the mechanism should move through a given path β in the same time t_m, with the same duration of time during which the motor is switched on, θ. The basic quantities which are compared using this principle are the required motor parameters.

2) *The principle of equal rated motor torque.* This means that the rated torque is maintained constant while either the time of the period of standstill, t_o, or the time of displacement, t_m, (and so π and θ) is changed. The basic quantities which are compared are the durations of the cycles for various velocity-time relations.

Apart from comparing the basic quantities, we shall also compare the mechanical overloading of the motor and the maximum velocity and acceleration of the tachograms. Moreover, we shall take into account the effects of the static resistance torque, T_r, and the total moment of inertia J referred to the motor shaft, using reasonably probable values for the dynamic index μ.

Under actual starting conditions the motor torque (and acceleration) cannot attain maximum instantaneously. (Fig. 1a). If, for example, a parabolic tachogram is used, the end parts of the curve will be slightly distorted (Fig. 1b) due to an initial smooth variation of acceleration. The existence of this initial variation of acceleration is desirable from the points of view of stability and wear of the mechanism. Since similar distortions will occur with any selected velocity-time law, their effect can be neglected for the purpose of the present comparison.

To determine numerical values of the ratios of the equivalent torques, outputs and accelerations for different values of μ and z, we shall use the expressions previously obtained.

In the case of equal outputs the ratio of the required maximum percentage overloads can be found from the velocity-time equation for the period of starting and from relation (20). Thus, we get

$$\lambda_\Delta T_{eq\Delta} = J\epsilon_\Delta + T_r \quad \text{and} \quad \lambda_p T_{eqp} = J\epsilon_{mp} + T_r ,$$

whence

$$\frac{\lambda p}{\lambda_\Delta} = \frac{(1.5+\mu)}{(1+\mu)} \frac{T_{eq\Delta}}{T_{eqp}} = \frac{(1.5+\mu)}{(1+\mu)} \sqrt{\frac{1+\mu^2}{0.75+\mu^2}} . \tag{30}$$

In a similar way

$$\frac{\lambda_p}{\lambda_{1.2}} = \frac{(1.5+\mu)}{\left(\frac{\epsilon_{1,2}}{\epsilon_\Delta}+\mu\right)} \frac{T_{eq1.2}}{T_{eqp}} . \tag{31}$$

In the case when the duration of cycle is decreased by reducing the standstill period, t_o, while keeping the same duration of the period of displacement, t_m, we have $T_{eq\Delta} = T_{eqp}$ Therefore, equations (30) and (31) become

$$\frac{\lambda_p}{\lambda_\Delta} = \frac{1.5+\mu}{1+\mu}, \tag{32}$$

and

$$\frac{\lambda_p}{\lambda_{1.2}} = \frac{1.5 + \mu}{\frac{\epsilon_{1.2}}{\epsilon_\Delta} + \mu} . \tag{33}$$

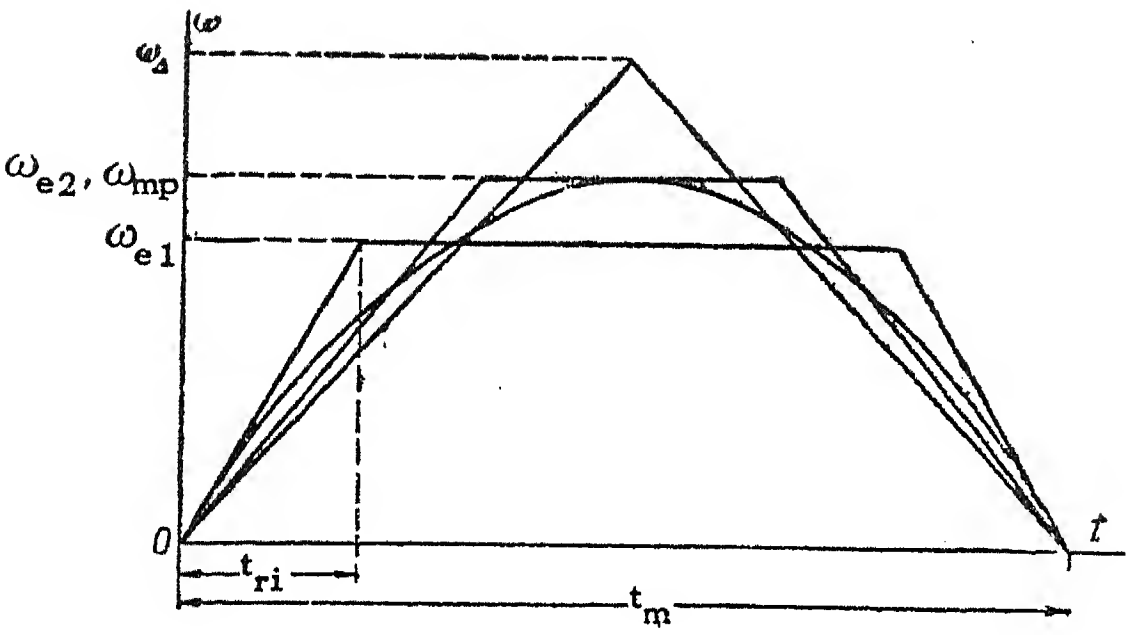

FIG. 5. Triangular, parabolic, and optimum trapezoidal velocity diagrams for the same paths and times of displacement and with $\mu = 0$.

The relative increase, $\Delta\pi$, of the output due to the reduction of the standstill period, t_o,* can again be easily found from the condition that the rated motor torque should be the same. For example, when changing from triangular to parabolic velocity-time diagram, remembering that the ratios previously found for equivalent torques over time t_c will be numerically the same as the ratios over the time t_m with the same t_m and t_o, we find that

$$\left(\frac{T_{eqp}}{T_{eq\Delta}}\right)^2 = \frac{\pi\Delta}{\theta_p} = \frac{t_{cp}}{t_c\Delta} ,$$

and thence

$$\Delta\pi = \left(\frac{\pi_p}{\pi\Delta} - 1\right) 100 = \left(\frac{t_{c\Delta}}{t_{cp}} - 1\right) 100 = \left(\frac{T^2_{eq\Delta}}{T^2_{eqp}} - 1\right) 100 . \tag{34}$$

The calculations of the increase of the output and the maximum relative percentage motor overload when t_m is reduced and t_o is constant, are not given. In this case, the time during which the motor is switched on, θ, is given by the velocity-time curve considered [6]. The calculations involve graphical solutions of complex equations. Also, since the r.m.s. torque and the required output of the motor increase much more quickly than the output (e.g., if $T_r = 0$ and $\theta = 100$ per cent, reducing t_m k times increases P_n and T_n k^3 and k^2 times respectively) these means of increasing the output by changing from one type of velocity-time curve to another become so ineffective for $\theta < 60$ per cent that they cannot be applied in practice [6].

TABLE 1. Comparison between the parabolic and optimum (as judged on torque basis) trapezoidal tachograms

$$\left(\frac{\omega_{mp}}{\omega_{e2}} = 1; \frac{\epsilon_{mp}}{\epsilon_2} = 1.33 \text{ for the same } \beta \text{ and } t_m\right)$$

Basis of comparison	Equal output			Equal T_{eq}, β, and t_m)		
μ	P_{eqp}/P_{eq2}	T_{eqp}/T_{eq2}	λ_p/λ_2	$\Delta\Pi$ (%)	$P'_{eqp}/P'_{eq2} = \omega_{mp}/\omega_{e2}$	λ_p/λ_2
0	0.942	0.942	1.41	12.7	1	1.33
0.5	0.956	0.956	1.28	9.4	1	1.23
1	0.975	0.975	1.20	5.6	1	1.18
2	0.990	0.990	1.14	2.0	1	1.12
3	0.995	0.995	1.10	1.0	1	1.09

TABLE 3. Comparison between the 1st criterion optimum, parabolic, and the optimum judged on power basis, trapezoidal velocity-time diagrams, $\mu = 0$

Basis of comparison	The same β and t_m		Equal output			Equal T_n, β, and t_m		
Index, %	$\Delta\omega_{mo}$	$\Delta\epsilon_{mo}$	ΔP_{eq0}	ΔT_{eq0}	$\Delta\lambda_0$	$\Delta\Pi_0$	ΔP_{eq0}	$\Delta\lambda_0$
Compared with best trapezoidal curve	6.7	28.0	-3.6	-9.5	42	22.0	-6.7	28.0
Compared with parabolic curve	-11.1	33.3	-8.3	3.2	29	-6.2	-11.1	33.3

TABLE 2. Comparison between the parabolic and optimum (as judged on power basis) trapezoidal tachograms

Basis of comparison	The same β and t_m			Equal output			Equal T_n, β, and t_m		
μ	z_0	$\omega_{el}/\omega_{mp} = z_o/0.75$	ϵ_1/ϵ_{mp}	P_{eqp}/P_{eq1}	T_{eqp}/T_{eq1}	λ_p/λ_1	$\Delta\Pi$ (%)	$P_{eqp}/P_{eq1} = \omega_{mp}/\omega_{e1}$	λ_p/λ_1
0	0.625	0.833	1.042	1.05	0.877	1.10	30.0	1.20	0.96
0.5	0.611	0.815	1.119	1.09	0.885	1.04	27.7	1.23	0.92
1	0.587	0.783	1.318	1.15	0.901	0.93	23.1	1.28	0.84
2	0.555	0.740	1.867	1.25	0.926	0.79	16.5	1.35	0.73
3	0.538	0.717	2.516	1.32	0.943	0.71	12.5	1.40	0.67

The results of calculations to compare the velocity-time diagrams of Fig. 5 are given in Tables 1 and 2. Table 3 collects data showing comparisons between the optimum, according to the first criterion, velocity-time curve and the best trapezoidal and parabolic tachograms judged on the power basis (Fig. 2).

Conclusions

1. There are two kinds of extremum velocity-time law of the motor drive operating under intermittent conditions of load with full utilization of the motor with respect to heating:

a) the velocity-time law (25) which gives the minimum rated motor output of the mechanism.

b) the velocity-time law (18) which gives the minimum rated motor torque which is necessary for a given output of the mechanism.

By using these laws we can achieve for a given motor the highest possible output permitted by the heating of the motor.

The parameters of the first kind of the velocity-time law are dependent on the coefficient of dynamic loading (2), whereas those of the second kind of the law are independent of it.

2. As can be seen from Table 2, the efficiency which can be obtained by using the optimum velocity-time curves depends on the relation between the static and dynamic components of the load (i.e. on the coefficient μ) and becomes a maximum for the purely dynamic load. In the case when the static load is predominant, these curves (and also the corresponding armature-current diagrams) have no substantial advantage over the best trapezoidal curves.

3. In the case when the dynamic load is predominant, the following effects can be achieved over to the optimum velocity laws:

a) If the output of an electro-mechanical device for cyclic operation is specified, considerable lowering of the installed horse-power (and consequently lowering of the cycle energy loss) can be obtained by using the velocity-time law (25).

b) If the motor is specified (or has already been installed) a substantial increase of the mechanical output can be achieved without overheating of the motor by shortening the period of rest.

However, in this case the dynamic loading of the mechanism and the percentage overload of the motor are increased.

When the output is specified or needs to be increased by reducing the duration of the period of running without altering the temperature rise of the motor, the advantages of the parabolic velocity-time diagram (18) over the best trapezoidal diagram judged on torque basis are small (Table 1).

The advantages of the optimum in accordance with the first and second

criteria velocity laws are as follows:

a) a much more uniform energy consumption during the starting period;

b) the mechanical characteristics of the driving motor (Fig. 3) which are necessary when these laws are consistent with the kind of relation between the permissible percentage overload and the speed which is peculiar to the d.c. motor;

c) it is not necessary to have a high ratio between the mean height and the maximum height of the load-current (or load-torque) curve of the motor.

4. In order to make use of the advantages presented by the best velocity-time curves in the case when the path of displacement of the operating member of the mechanism is variable, it is expedient to provide an automatic re-adjustment of the control system of the motor drive that will ensure the optimum velocity and acceleration for each displacement. The question of the establishment and application of the optimum velocity-time laws when the path of displacement is variable necessitates additional elaboration depending on the type of the motor drive.

5. The ratio between the mean height and the maximum height of the armature current curve should not be used as a criterion for assessing the usefulness of the drive control system in cases when the motor is fully utilized with respect to heating. The degree of usefulness of a control system is determined by the extent to which a most simplified and reliable system approximates the optimum velocity laws. The ratio of mean to maximum height of the current curve characterizes the usefulness of the control system only in cases in which it is necessary to use the highest acceleration permitted by the mechanism in order to achieve the shortest period of starting or the highest output, irrespective of the required motor output. Therefore, the optimum velocity law is that which gives a constant acceleration [1].

6. The various aspects of the use of the optimum velocity-time laws for motor drives should be considered not only when designing the driving motor and its automatic control system, but also when designing the driven mechanism. In particular, when establishing the permissible accelerations of the mechanisms, an allowance should be made for a possibility of using the optimum velocity-time relations for the motor drive.

The stability of the characteristics of motor drives is of great importance when using the optimum velocity-time laws.

When the motor is fully utilized with respect to heating and specified output, its required rated output and torque depend not only on the type of velocity law but also on the reduction gear ratio [1]. In connexion with this the following additional conclusions drawn from the present investigation are of interrest:

a) The smallest rated motor torque is required by using the velocity law (18) minimizing the equivalent motor torque, and a rated motor speed cor-

responding to the optimum reduction gear ratio.

b) The smallest rated motor output is required when using the velocity law (25) minimizing the motor horse power, and a rated motor speed which should preferably be less than the speed corresponding to the optimum reduction gear ratio.

REFERENCES

1. F.A. Goraĭko and L.V. Karnyushin; *The choice of reducing gear ratio for motor drives for lift-conveyer mechanisms and excavators. Transactions of Scientific and Technical Session on Motor Drive for Lifting-and-Conveying Mechanisms. Gosenergoizdat* (1955).
2. M.M. Fedorov; *The best dynamic conditions of operation for some types of ore-lifting equipment. Coal and Steel,* 11 ,12 and 14 (1956).
3. S.A. Press; *Electrical equipment for excavators.* State United Publishing House of Science and Technology (1938).
4. F.A. Goraiko; *The best suitable parameters of the motor-drive velocity-time diagram with three periods. Scientific Reports of Lvov Polytechnical Institute,* Electrotechnical Series, Vol. 40 No. 9 (1956).
5. L.V. Karnyushin; *The best velocity-time laws for a motor drive operating under starting and braking conditions. Scientific Reports of Lvov Polytechnical Institute,* Electrotechnical Series, Vo. 40. No. 9 (1956).
6. K.I. Kozhevnikov; *The current diagram for the motor for the auxiliaries of rolling mills. Elektrichestvo,* No. 6 (1956).
7. L.V. Karnyushin; *Motor drive transient velocity law minimizing the required motor output. Reports of Lvov Polytechnical Institute* Vol. II, 2nd edition (1957).

A METHOD OF DERIVING EQUATIONS FOR THE ELECTROMECHANICAL TRANSIENT IN ELECTRIC CIRCUITS*

S.V. STRAKHOV

(Received 5 October 1956)

There are basically two methods of investigating the transient electromechanical processes in electric circuits, viz:

1. Physical modelling.

2. Mathematical modelling, this comprising two sections, viz:

   (a) the section using physical analogs;

   (b) the section using digital computers (integrators) with continuous and discrete action.

The method of physical modelling, comprehensively treated in papers of V.A. Venikov [1-3], M.P. Kostenko [4-6] and of other authors, consists in the replacement of large rotating electric machines and hydraulic turbines by similar units of small ratings with due consideration to the laws of similitude. Transmission lines, tranformers, saturable reactors and static loads are replaced by assemblies of capacitances and inductances, networks with repeated members being used for transmission lines. In other words, in this case the physical character of the model and of the original are the same.

Among the advantages of the method of physical modelling, where rotating machines are concerned, we should mention the possibility of considering eddy currents, saturation, hysteresis, the actual distribution of stator and rotor windings in space, and of other factors. A drawback of this method is the difficulty of varying the parameters of individual machines, usually necessitating the availability of a number of inter-changeable rotors for them. It is, therefore, more convenient to use the method of mathematical modelling in cases where the parameters of the machines must be variable; because this method can deal in a much more simple way with such variations. However, physical modelling will still be preferable in all cases in which the system of differential equations describing the process is very complicated.

* *Elektrichestvo* No. 7, 5-10, 1957 [Reprint Order No. EL 32].

Referring to the first section of the method of mathematical modelling [1, 7 and 8], we note that rotating machines are replaced by equivalent devices (electronic circuits, electrodynamical apparatus), i.e. physical analogs according to the similar structure of their differential equations. In this case the model has a different physical character from the original. If the system contains static elements, for example, transmission lines, they are represented in the same way as in the preceding method, i.e. to these physical modelling is applied. An advantage of this method is the greater convenience of varying the individual parameters of the rotating machines, because it amounts only to a variation of comparatively easily adjustable parameters of the electronic circuits or the physical analogs. On the other hand, since the static elements of circuits consist of assemblies of coils and capacitors, no differential equations have to be set up for them. This is a great advantage of the first section of the method of mathematical modelling over the second section.

The second section of the method of mathematical modelling, consisting of the use of computing mechanisms (integrators) for the investigation of the transient electromechanical processes in the electric circuits, is nowadays widely used. Its importance is still increasing with the growing production of relatively inexpensive computor types suitable for the integration of systems of non-linear differential equations of an over-all order up to 20 – 30.

This method makes it particularly easy to vary the system of parameters within a wide range by an easy regulation of the blocks collecting the coefficients of the individual equations.

This method is suitable not only for the solution of electrical engineering problems, but also for the solution of systems of non-linear differential equations met in physics, mechanics, hydrodynamics, heat engineering, etc. In this sense it is a universal method.

A disadvantage of this method is the necessity of using a whole number of blocks of the integrator for considering the differential equations of the static circuit elements and, in particular, of long lines, since often the greater half of the overall order of the system of differential equations of the circuit is accounted for by the static circuit elements.

However, the integrators may be designed in such a way as to enable the differential equations of only one part of the whole circuit to be represented, whereas the remaining part is actually present in life-size or represented by physical models. The latter condition considerably extends the range of possible users of integrators of this type for investigations of the transient processes in interconnected systems.

Method of setting-up system of differential equations

In order to use the integrator, the system of differential equations of the circuit has to be set up, first of all, in the simplest and the most rational form.

We will then consider the differential equations of the synchronised generator, referred to all coordinate systems rigidly connected with its rotor, the equations of an induction motor and of all the static circuit elements (loads, transformers, transverse capacitances, compensating coils and lines with longitudinal compensating capacitances) referred to coordinated system rotating at an arbitrary speed, as given.

All the equations given below refer to the positive directions of the currents shown in figures.

When setting up the differential equations for any actual system it is, above all, important to choose the most rational system of rotating coordinates to which then the equations of all static circuit elements have to be referred. For symmetrical circuits the equations of the static elements may be referred to axes rigidly connected to the rotor of any of the generators [9], which follows from the symmetry of the circuit.

We will illustrate the method of setting up the system of equations on the example of the circuit of Fig. 1, being practically symmetrical.

We will refer to equations of all elements of the circuit of Fig. 1 (except *SG*2) and the equations resulting from Kirchhoff's first law, to coordinate axes rigidly connected to the rotor of the synchronous generator *SG*1.

The equations for *SG*1 are [10 and 11]:

$$\left.\begin{aligned}
u_{1d} &= -r_{C1} i_{1d} + \frac{d}{dt}(-L_{d1} i_{1d} + M_{f1} i_{1f} + M_{g1} i_{1g}) - \\
&\quad -(-L_{q1} i_{1q} + M_{h1} i_{1h}) \frac{d\theta_1}{dt}; \\
u_{1q} &= -r_{C1} i_{1q} + \frac{d}{dt}(-L_{q1} i_{1q} + M_{h1} i_{1h}) + \\
&\quad +(-L_{d1} i_{1d} + M_{f1} i_{1f} + M_{g1} i_{1g}) \frac{d\theta_1}{dt}; \\
u_{10} &= -r_{C1} i_{10} - L_{01} \frac{di_{10}}{dt}; \\
u_{1f} &= r_{f1} i_{1f} + \\
&\quad + \frac{d}{dt}\left(-\frac{3}{2} M_{f1} i_{1d} + L_{f1} i_{1f} + M_{fg1} i_{1g}\right); \\
0 &= r_{g1} i_{1g} + \\
&\quad + \frac{d}{dt}\left(-\frac{3}{2} M_{f1} i_{1d} + L_{g1} i_{1g} + M_{fg1} i_{1f}\right); \\
0 &= r_{h1} i_{1h} + \frac{d}{dt}\left(-\frac{3}{2} M_{h1} i_{1q} + L_{h1} i_{1h}\right);
\end{aligned}\right\} \quad (1)$$

$$T_{\partial 1} - \frac{3}{2}\left[(L_{d1} - L_{q1})\, i_{1d}\, i_{1q} - M_{f1}\, i_{1f}\, i_{1g} - \right.$$

$$\left. - M_{g1}\, i_{1g}\, i_{1q} + M_{h1}\, i_{1h}\, i_{1d}\right] = J_1 \frac{d^2\theta_1}{dt^2}\,.$$

In an analogous way, by altering subscript 1 to subscript 2, we write the equations for *SG2*, since we refer to its equations to axes rigidly connected to its rotor.

The equations for *IM1* [10 and 12] are:

$$U_{1d} = r_{\partial 1}\, i_{\partial 1d} + L_{C11}\frac{di_{\partial 1d}}{dt} + L_{ad1}\frac{di_{1pd}}{dt} -$$

$$-(L_{C11}\, i_{\partial 1q} + L_{ad1}\, i_{1pq})\frac{d\theta_1}{dt}\,;$$

$$U_{1q} = r_{\partial 1}\, i_{\partial 1q} + L_{C11}\frac{di_{\partial 1q}}{dt} + L_{ad1}\frac{di_{1pq}}{dt} +$$

$$+ (L_{C11}\, i_{\partial 1d} + L_{ad1}\, i_{1pd})\frac{d\theta_1}{dt}\,;$$

$$U_{10} = r_{\partial 1}\, i_{\partial 10} + L_{C01}\frac{di_{\partial 10}}{dt}\,; \qquad (2)$$

$$0 = r_{p1}\, i_{1pd} + L_{p11}\frac{di_{1pd}}{dt} + L_{ad1}\frac{di_{\partial 1d}}{dt} -$$

$$-(L_{ad1}\, i_{\partial 1q} + L_{p11}\, i_{1pq})\left(\frac{d\theta_1}{dt} - \omega_{\partial 1}\right);$$

$$0 = r_{q1}\, i_{1pq} + L_{p11}\frac{di_{1pq}}{dt} + L_{ad1}\frac{di_{\partial 1q}}{dt} +$$

$$+ (L_{ad1}\, i_{\partial 1d} + L_{p11}\, i_{1pd})\left(\frac{d\theta_1}{dt} - \omega_{\partial 1}\right);$$

$$0 = r_{p1}\, i_{1p0} + L_{p01}\frac{di_{1p0}}{dt}\,;$$

$$\frac{3}{2}L_{ad1}\,(i_{1pd}\, i_{\partial 1q} - i_{1pq}\, i_{\partial 1d}) - T_{C1} = J_{\partial 1}\frac{d\omega_{\partial 1}}{dt}\,.$$

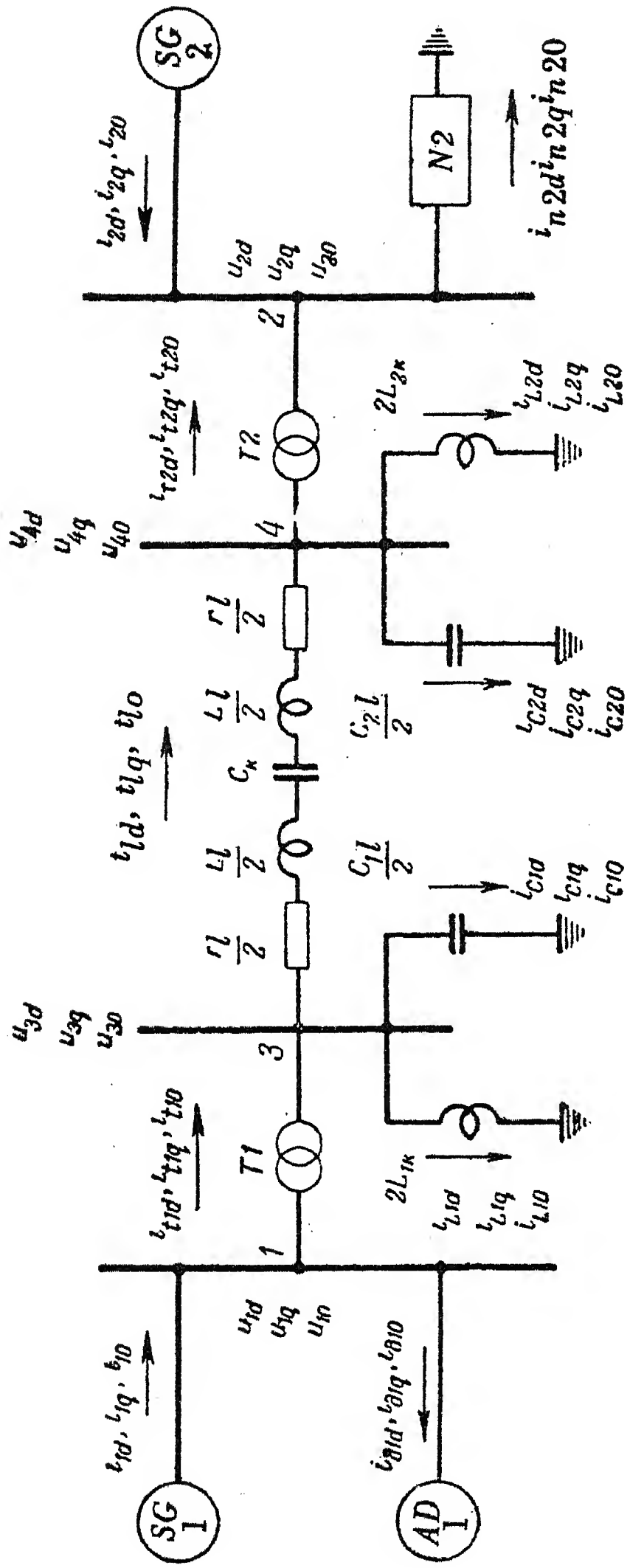

FIG. 1.

The equations following from Kirchhoff's first law [*cf.* (1)] are as follows:

$$\begin{aligned} i_{1d} - i_{\partial 1d} - i_{t1d} &= 0\,; \\ i_{1q} - i_{\partial 1q} - i_{t1q} &= 0\,; \\ i_{10} - i_{\partial 10} - i_{t10} &= 0\,. \end{aligned} \tag{3}$$

The equations for static load [9 and 10] are:

$$\begin{aligned} &U_{2d}\cos(\theta_2 - \theta_1) - U_{2q}\sin(\theta_2 - \theta_1) - \\ &- r_{n2}\, i_{n2d} - L_{n2}\frac{di_{n2d}}{dt} + L_{n21}\, i_{n2q}\frac{d\theta_1}{dt} = 0\,; \\ &U_{2d}\sin(\theta_2 - \theta_1) + U_{2q}\cos(\theta_2 - \theta_1) - \\ &- r_{n2}\, i_{n2q} - L_{n21}\frac{di_{n2q}}{dt} - L_{n21}\, i_{n2d}\frac{d\theta_1}{dt} = 0\,; \\ &U_{20} - r_{n2}\, i_{n20} - L_{n20}\frac{di_{n20}}{dt} = 0. \end{aligned} \tag{4}$$

The occurrence of the factor $\cos(\theta_2 - \theta_1)$ and $\sin(\theta_2 - \theta_1)$ is due to the fact that the terminal voltage of *SG*2 is referred to axes rigidly connected to its rotor.

The equations expressing Kirchhoff's first law [9], considering the positive directions of the currents as assumed in Fig. 1 will be:

$$\begin{aligned} &i_{t2d} + i_{2d}\cos(\theta_2 - \theta_1) - i_{2q}\sin(\theta_2 - \theta_1) - \\ &- i_{n2d} = 0\,; \\ &i_{t2q} + i_{2d}\sin(\theta_2 - \theta_1) + i_{2q}\cos(\theta_2 - \theta_1) - \\ &- i_{n2q} = 0\,; \\ &t_{t20} + i_{20} - i_{n20} = 0\,. \end{aligned} \tag{5}$$

It should be noted that if the equations of the static load N2 are referred to axes rigidly connected to the rotor of *SG*2, equations (5) will become complicated to the extent equations (4) will be simplified.

Indeed, if we refer the equations of the static load N2 to axes rigidly connected to the axes of the rotor *SG*2 we get [9 and 10] :

$$U_{2d} - r_{n2}\, i_{n2d} - L_{n21}\frac{di_{n2d}}{dt} + L_{n21}\, i_{n2q}\frac{d\theta_2}{dt} = 0;$$

$$U_{2q} - r_{n2}\, i_{n2q} - L_{n21}\frac{di_{n2q}}{dt} - L_{n21}\, i_{n2d}\frac{d\theta_2}{dt} = 0; \tag{4a}$$

$$U_{20} - r_{n2}\, i_{n20} - L_{n20}\frac{di_{n20}}{dt} = 0.$$

Under the same conditions the equations of Kirchhoff's first law [*cf.* (2)] are written as follows :

$$i_{t2d} + i_{2d}\cos(\theta_2 - \theta_1) - i_{2q}\sin(\theta_2 - \theta_1) - i_{n2d}\cos(\theta_2 - \theta_1) + i_{n2q}\sin(\theta_2 - \theta_1) = 0;$$

$$i_{t2q} + i_{2d}\sin(\theta_2 - \theta_1) + i_{2q}\cos(\theta_2 - \theta_1) - i_{n2d}\sin(\theta_2 - \theta_1) - i_{n2q}\cos(\theta_2 - \theta_1) = 0; \tag{5a}$$

$$i_{t20} + i_{20} - i_{n20} = 0.$$

We will further consider in the equivalent circuit of the transformer $T1$ the branch of the no-load current (Fig. 2). For the branches 1 – 7 of the primary winding we get [9 and 10] :

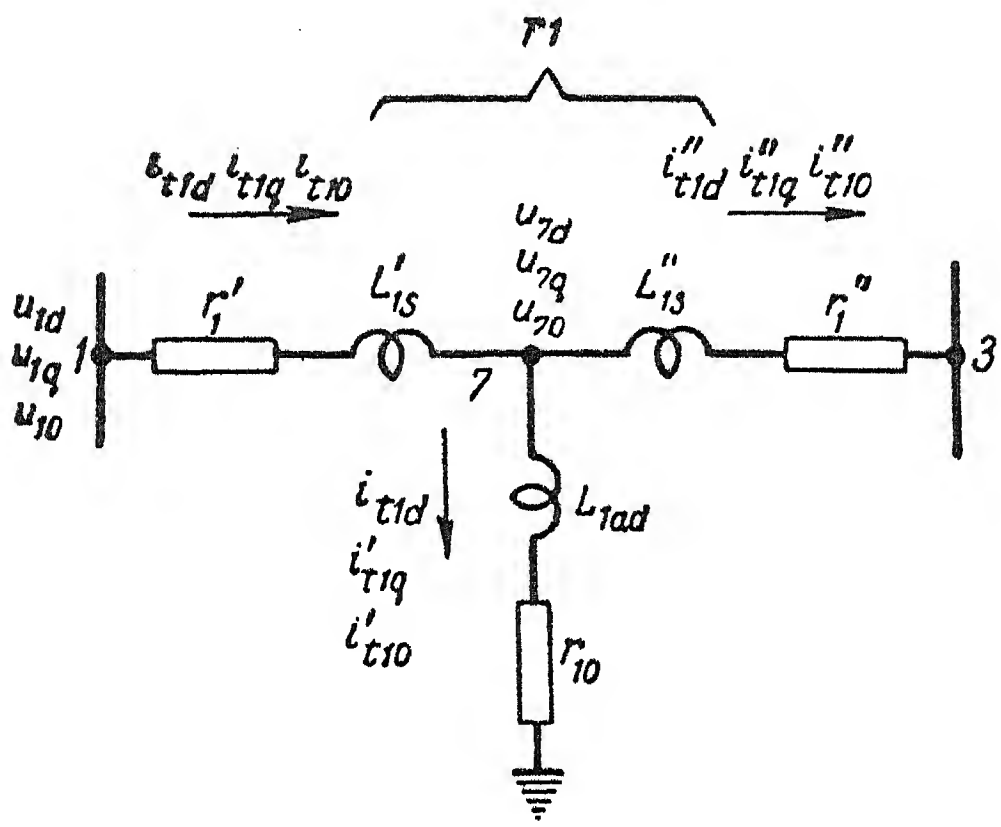

FIG. 2.

$$U_{7d} = U_{1d} - r'_1 i_{t1d} - L'_{1s1} \frac{di_{t1d}}{dt} + L'_{1s1} i_{t1q} \frac{d\theta_1}{dt};$$

$$U_{7q} = U_{1q} - r'_1 i_{t1q} - L'_{1s1} \frac{di_{t1q}}{dt} - L'_{1s1} i_{t1d} \frac{d\theta_1}{dt}; \tag{6}$$

$$U_{70} = U_{10} - r'_1 i_{t10} - L'_{1s0} \frac{di_{t10}}{dt}.$$

Similarly, we get for the branches 7 – 3 of the secondary winding:

$$U_{3d} = U_{7d} - r''_1 i''_{t1d} - L''_{1s1} \frac{di''_{t1d}}{dt} + L''_{1s1} i''_{t1q} \frac{d\theta_1}{dt}; \tag{7}$$

$$U_{3q} = U_{7q} - r''_1 i''_{t1q} - L''_{1s1} \frac{di''_{t1q}}{dt} - L''_{1s1} i''_{t1d} \frac{d\theta_1}{dt} ; \quad (7)$$

$$U_{30} = U_{70} - r''_1 i''_{t10} - L''_{1s0} \frac{di''_{t10}}{dt} .$$

For the no-load branch we get :

$$0 = U_{7d} - r_{10} i'_{t1d} - L_{1ad1} \frac{di'_{t1d}}{dt} + L_{1ad1} i'_{t1q} \frac{d\theta_1}{dt} ;$$

$$0 = U_{7q} - r_{10} i'_{t1q} - L_{1ad1} \frac{di'_{t1q}}{dt} - L_{1ad1} i'_{t1d} \frac{d\theta_1}{dt} ; \quad (8)$$

$$0 = U_{70} - r_{10} i'_{t10} - L_{1ad0} \frac{di'_{t10}}{dt} .$$

Equations of Kirchhoff's first law [*cf*(7)] are :

$$i_{t1d} - i'_{t1d} - i''_{t1d} = 0 ;$$

$$i_{tq} - i'_{tq} - i''_{tq} = 0 ; \quad (9)$$

$$i_{t10} - i'_{t10} - i''_{t10} = 0 ;$$

The equations for the compensating coil $2L_{1k}$:

$$0 = U_{3d} - 2r_{1k} i_{L1d} - 2L_{1k1} \frac{di_{L1d}}{dt} + 2L_{1k1} i_{L1q} \frac{d\theta_1}{dt} ; \quad (10)$$

$$O = U_{2q} - 2r_{1k}\, i_{L\,1q} - 2L_{1k1}\, \frac{di_{L\,1q}}{dt} - 2L_{1k1}\, i_{L\,1d}\, \frac{d\theta_1}{dt}\,;$$

$$O = U_{30} - 2r_{1k}\, i_{L\,10} - 2L_{1k0}\, \frac{di_{L\,10}}{dt}\,. \qquad (10)$$

We consider above the branches of the primary and the secondary windings of transformer $T1$, its no-load branch and the branch of the compensating coil as rL-circuits. If the mutual inductance between the phases of these branches may be neglected, the expressions of the parameters after simplying [10] for example, for the compensating coil $2L_{1k}$ we get :

$$L_{1k} = L_{1k1} = L_{1k0}. \qquad (11)$$

The equations for the capacitance $C_{1l}/2$ may be obtained from the identities (3, 5) . . . . (3, 7), given in [10] if we substitute in them

$$C_3 = C1l/2,\ i_{C\,3d} = i_{C\,1d},\ i_{C\,3q} = i_{C\,1q},\ i_{C\,30} = i_{C\,10}$$

and $\theta_3 = \theta_1$ since at 3 (Fig. 1) the synchronous generator is not connected, and the voltage u_3 is directly referred to axes rigidly connected with the rotor of $SG1$, viz :

$$U_{3d} = \frac{2}{C_{1l}} \int i_{C\,1d}\, dt + \int U_{3q}\, \frac{d\theta_1}{dt}\, dt\,;$$

$$U_{3q} = \frac{2}{C_{1l}} \int i_{C\,1q}\, dt - \int U_{3d}\, \frac{d\theta_1}{dt}\, dt\,; \qquad (12)$$

$$U_{30} = \frac{2}{C_{1l}} \int i_{C\,10}\, dt.$$

The equations of Kirchhoff's first law [cf (3)] are as

$$i''_{t\,1d} - i_{L\,1d} - i_{C\,1d} - i_{ld} = O\,;$$

$$i''_{t\,1q} - i_{L\,1q} - i_{C\,1q} - i_{ld} = O\,; \qquad (13)$$

$$i''_{t10} - i_{l10} - i_{C10} - i_{lo} = 0. \tag{13}$$

We may get the equations for the line (r_l, L_l) with the compensating capacitance C_{com} connected to it, for example, from the identities (7) and (12), viz:

$$U_{4d} = U_{3d} - r_l i_{ld} - L_{ld} \frac{di_{ld}}{dt} +$$

$$+ L_{l1} i_{lq} \frac{d\theta_1}{dt} - \frac{1}{C_k} \int i_{ld}\, dt + \tag{14}$$

$$+ \int (U_{4q} - U_{3q} + r_l i_{lq} + L_{l1} \frac{di_{lq}}{dt} +$$

$$+ L_{l1} i_{ld} \frac{d\theta_1}{dt}) \frac{d\theta_1}{dt}\, dt\,;$$

$$U_{4q} = U_{3q} - r_l i_{lq} - L_{l1} \frac{di_{lq}}{dt} -$$

$$- L_{l1} i_{ld} \frac{d\theta_1}{dt} - \frac{1}{C_k} i_{lq}\, dt - \tag{15}$$

$$- \int (U_{4d} - U_{3d} + r_l i_{ld} + L_{l1} \frac{di_{ld}}{dt} -$$

$$- L_{l1} i_{lq} \frac{d\theta_1}{dt}) \frac{d\theta_1}{dt}\, dt\,;$$

$$U_{40} = U_{30} - r_l i_{l0} - L_{l0} \frac{di_{l0}}{dt} - \frac{1}{C_k} \int i_{l0}\, dt. \tag{16}$$

The equations for the capacitance $C_{2l}/2$ of the line will be analogous to (12), viz :

$$U_{4d} = \frac{2}{C_{2l}} \int i_{C2d} dt + \int U_{4q} \frac{d\theta_1}{dt}\, dt\,; \tag{17}$$

$$U_{4q} = \frac{2}{C_{2l}} \int i_{C2q}\, dt - \int U_{4d} \frac{d\theta_1}{dt}\, dt$$

$$U_{40} = \frac{2}{C_{2l}} \int i_{C20}\, dt. \qquad (17)$$

The equations for the compensating coil $2L_{2\,com}$ will be analogous to (10) viz :

$$0 = U_{4d} - 2r_{2k}\, i_{L2d} - 2L_{2k1} \frac{di_{L2d}}{dt} + 2L_{2k1}\, i_{L2q} \frac{d\theta_1}{dt};$$

$$0 = U_{4q} - 2r_{2k}\, i_{L2q} - 2L_{2k1} \frac{di_{L2q}}{dt} - 2L_{2k1}\, i_{L2d} \frac{d\theta_1}{dt}; \qquad (18)$$

$$0 = U_{40} - 2r_{2k}\, i_{L20} - 2L_{2k0} \frac{di_{L20}}{dt}.$$

The equations of Kirchhoff's first law [*cf* (4)] are

$$i_{ld} - i_{C2d} - i_{L2d} - i_{t2d} = 0;$$

$$i_{1lq} - i_{C2q} - i_{L2q} - i_{lq} = 0; \qquad (19)$$

$$i_{l0} - i_{C20} - i_{l20} - i_{t20} = 0.$$

Since the way of considering the no-load current in the equivalent circuit is shown for transformer $T1$, we will write down the equations for transformer $T2$ without considering this factor. These equations may be obtained from the identities (1, 17) . . . . (1, 19) adduced in [10], if we consider that the voltage [*cf* (4)] is referred directly to coordinate axes rigidly connected with the rotor of $SG1$; we have therefore to assume $\theta_3 = \theta_1$. Also having brought the symbols in Fig. 1, 1 of [10] and Fig. 1 of the present paper into agreement, we get

$$U_{3d} = U_{4d};\ U_{3q} = U_{4q};\ U_{30} = U_{40}; \qquad (20)$$

$$r_{l2} = r_{t2}\ ;\ L_{l2p} = L_{t21}\ ;\ L_{l20} = L_{t20}\ ;$$

$$i_{l2d} = i_{t2d}\ ;\ i_{l2q} = i_{t2q}\ ;\ i_{l20} = i_{t20}\ . \tag{20}$$

We then get the branch of transformer $T2$

$$U_{2d}\cos(\theta_1 - \theta_2) + U_{2q}\sin(\theta_1 - \theta_2) =$$

$$= U_{4d} - r_{t2}\, i_{t2d} - L_{t21}\,\frac{di_{t2d}}{dt} + L_{t21}\, i_{t2q}\,\frac{d\theta_1}{dt}\ ;$$

$$-U_{2d}\sin(\theta_1 - \theta_2) + U_{2q}\cos(\theta_1 - \theta_2) = \tag{21}$$

$$= U_{4q} - r_{t2}\, i_{t2q} - L_{t21}\,\frac{di_{t2q}}{dt} - L_{t21}\, i_{t2d}\,\frac{d\theta_1}{dt}\ ;$$

$$U_{20} = U_{40} - r_{t2}\, i_{t20} - L_{t20}\,\frac{di_{t20}}{dt}\ .$$

Since the equations of the individual circuit elements may be assumed to be known, the whole system of equations can be put together from the individual equations referring to its blocks, which we can immediately write down for each of the circuit elements.

Should it be necessary to consider in any of the synchronous generators or compensating coils the dependence of the inductance on the state of saturation of the steel, this circuit element should be separated and its differential equations be re-written in the proper form, based on the character of the magnetisation curve.

It should be noted that the equations for all the zero-sequence components form a separate system, to be solved independently of the other equations. Their number is 18 in the case of the circuit of Fig. 1.

Determination of the total order of system of non-linear differential equations from structure of circuit

On the above considerations it is possible to determine from the structure of the scheme, without writing down the actual differential equations, the total order to the latter. In doing this we have to bear in mind the following circumstances:

1. For a synchronous machine (generator, synchronous condenser or motor) with in-phase or quadrature damper windings the total order of the equations is

7*, if the circuit contains apart from this at least one more synchronous machine, i.e. a machine of magnetic or electric asymmetry (equations of system (1), except the third).

The order of the equation of motion of the rotor of each of the synchronous machines is 2.

If the circuit contains only one synchronous machine, the total order of the equations for it will be six, because in this case the differential equation of the motion of the rotor will be of the first order and the angle θ will not occur in one of them (by change of the variables $d^2\theta/dt^2 = d\omega/dt$ and $d\theta/dt = \omega$ the order is reduced by one).

2. Neglecting each of the damper windings of the synchronous machine reduces the total order of its defferential equations by one.

3. The total order of the differential equations of an induction machine is 5. This means that each induction machine connected to the system increases the total order of the system of differential equations by 5.

4. The equations of Kirchhoff's first law for the branching points are not differential equations and therefore, do not increase the total order of the equations of the system.

5. The stator circuits of the machines (stationary circuits) must be divided into the simplest independent circuits and their differential equations have to be set up for the in-phase as well as for the quadrature components. This doubles the order of the differential equations for each individual circuit.

6. If a line, system or static load are represented by a coil with resistance and inductance, its series-connexion with the stator of any of the machines does not increase the total order of the differential equations of the system.

7. If the circuit comprises a transformer whose no-load current is not considered, it is represented by a coil. If, however, the no-load current is considered, the equivalent circuit contains a no-load branch (additional circuit), which, together with the necessity of considering the equations of the in-phase and quadrature components, increases the total order of the differential equations of the circuit by 2.

8. If there are no synchronous machines in the circuit (e.g. if one or several induction motors for static loads, etc., are supplied from busbars of infinite power), it is not necessary to set up the equations separately for in-phase and quadrature components. If the complex instantaneous values of currents and voltages are introduced, a static load or transmission line (each of them separately) will be represented by first-order differential equations, and an induction

* This does not take into account the differential equations for the zero-sequence components.

motor by a third-order differential equation. In this case, the connexion of any further induction machine to the circuit increases the total order of the system of differential equations by 3.

Let us determine the total order of the system of differential equations for the circuit of Fig. 3.

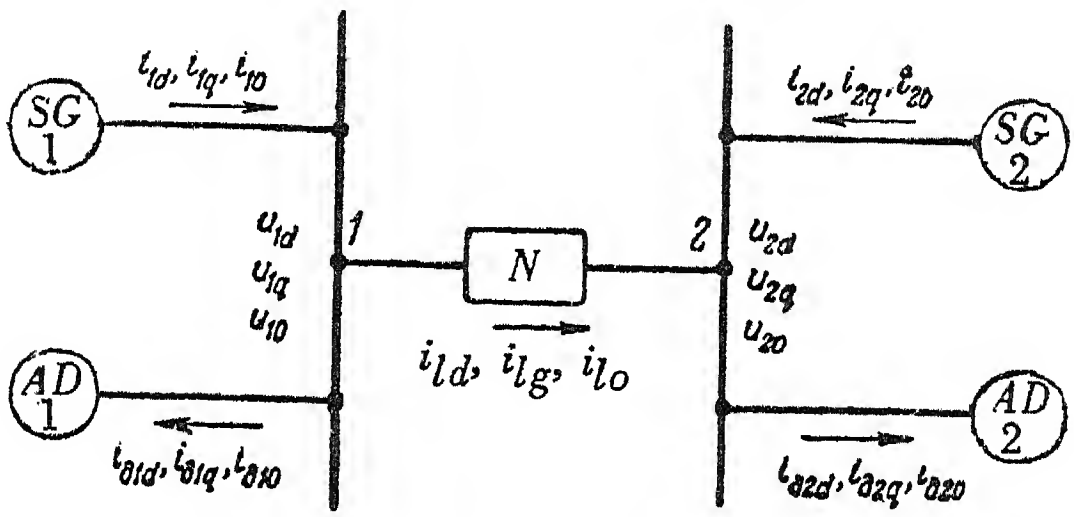

FIG. 3.

In Fig. 3. the stationary part of the circuit is resolved into three circuits, viz:

(a) The stator $SG1$ – stator $IM1$;

(b) Stator $IM1$ – line – stator $IM2$;

(c) Stator $SG2$ – stator $IM2$; for each of which, if the in-phase and quadrature components have to be considered, the differential equation is of the second order, this resulting in the total order of six. Each of the synchronous machines makes a total order of the order of the remaining equations 5, and each of the induction machines involves a total order 3. The total order of the differential equations for the whole circuit will therefore be 22.

In Fig. 1, if the no-load currents of the transformers $T1$ and $T2$ have to be considered, the stationary part of the circuit is resolved into 9 simpler circuits, for example, as follows.

(a) Stator $SG1$ – stator $IM1$ (if it is necessary to consider in-phase and quadrature components, the order of the equations will be 2);

(b) Stator $IM1$ - no - load branch of the equivalent circuit of transformer $T1$ (Fig. 2) (order of the equations-2);

(c) No-load branch of equivalent circuit of transformer $T1$-compensating coil $2L_{1\ com}$ (order of the equations-2);

(d) Compensating coil $2L_{1\ com}$-capacitance of the line $C_{1l}/2$;

(e) Capacitance of the line $C_{1l}/2$ - line - capacitance of the line $C_{2l}/2$ (order of the equations-4).

(f) Capacitance of the line $C_{2l}/2$-compensating coil $2L_{2\ com}$ (order of the equations-4);

(g) Compensating coil $2L_{2\ com}$ - no-load branch of equivalent circuit of transformer $T2$ (order of equations-2);

(h) No-load branch of equivalent circuit of transformer $T2$-static load $SL2$ (order of equations-2);

(i) Stator $SG2$-static load $SL2$ (order of equations-2); this adding up to a total order 24. From this figure the fraction concerning transformers $T1$ and $T2$, lines and loads $SL2$, i.e. the static circuit elements amounts to a total order 18. For the two synchronous generators the total order of the determining equations is 10; for the induction motor, 3.

We see, therefore, that the total order of the differential equations for the whole system will be 37.

If the line is not represented by one member but by several T — or π-type members, the fraction of the line elements (series, connected inductances and shunt-capacitances) in the total order of the system of the differential equations of the circuit will increase still further. This fact is very important in the choice of the method for solving the resulting system of differential equations.

If the in-phase and quadrature damper windings of both synchronous generators are not considered, the total order of the equations will be reduced by 4, i.e. to 33. If, furthermore, we neglect the no-load branches in the equivalent circuits of the 2 transformers, the total order of the equations is again reduced by 4, i.e. to 29. If the two compensating coils $2L_{1\ com}$ and $2L_{2\ com}$ are also neglected, the total order of the equation is again reduced by 4, i.e. to 25.

It is worth noting that in the last case again both synchronous and one induction machine together result in a decrease of the total order of differential equations by 13; the remainder, 12, refers as before to the transmission line.

REFERENCES

1. V.A. Venikov; *The adoption of the theory of similarity and physical modelling in electric technology* Gosenergoizdat (1949).
2. V.A. Venikov and A.V. Ivanov-Smolenskii; A synchronous generator for the dynamic modelling of electrical systems. *Elektrichestvo*, No. 8 (1951).
3. V.A. Venikov *et al.*; *A brief description of dynamic models for electrical systems*, Moscow Power Institute (1955).
4. M.P. Kostenko and E.D. Treivish; Modelling of electrical machinery and transformers in experimental research on the stability of parallel work in power stations. *Transactions of the Leningrad Power Institute* No. 1 (1946).
5. M.P. Kostenko; Electrodynamic model for the study of stability. *Elektrichestvo* No.9 (1951).
6. M.P. Kostenko; The modelling of electrical machinery equipment in the study of stability of parallel work on power systems, linked with long-distance transmission lines *Isz. Akad. Nauk SSSR, Otd. tekh. nauk* No. 12 (1953).

7. V.L. Lossievskii; *The use of the similarity theory and dynamic analogies in problems connected with the modelling of objectives and regulation processes*, Gosenergoizdat (1951).
8. V.A. Trapeznikov; Mathematical modelling of dynamic systems *Elektrichestvo* No. 8 (1955).
9. S.V. Strakhov ; Selection of the co-ordinating systems for calculation of transition processes in chains with synchronous machine *Elektrichestvo* No.6 (1954).
10. S.V. Strakhov; The equating of transition processes in static and rotating elements in electrical chains. *Report on scientific research work. Moscow Power Institute* (1956).
11. R.E. Vowels; Transient Analysis of Synchronous Machines. *Proc. Inst. El. Eng.*, vol. 99 part IV, No. 3 (1952).
12. A.A. Yanko-Trinitskii; The equating of transition electromagnetic processes of an asynchronous motor and their solution. *Elektrichestvo* No. 3 (1951).

THE INDUCTION LAW FOR AN ELECTROSTATIC MACHINE*

A.A. BAL'CHITIS

(Received 19 December 1956)

Introduction

The fundamental equations of the classical theory of electrodynamics, the first and second equations of Maxwell point to two possible methods of conversion of mechanical into electrical energy. For example, by the first equation of Maxwell†

$$\text{curl}\,\bar{H} = \gamma\,\bar{E} + \frac{\partial \bar{D}}{\partial t} \tag{1}$$

such a conversion is possible when an electric field changes with time, i.e. by mechanical action on the electric field it is possible to obtain the magnetic field connected with it in space.

According to the second equation

$$\text{curl}\,\bar{E} = -\frac{\partial \bar{B}}{\partial t} \tag{2}$$

it is possible to obtain an electric field by changing the magnetic field associated with it.

The second equation of Maxwell was the generalized form of Faraday's experimental law of electromagnetic induction, viz.

$$E = B\,l\,v, \tag{3}$$

which was discovered in 1831 and forms the basis of the design of a large variety of electric machines, covered by the general term "electromagnetic machines".

Machines working on the principle of a mechanical change of an electric field (Maxwell's first equation) are not nearly so widely used; they are known as *electrostatic* machines. These machines are used for obtaining high and very high voltages for research purposes.

For a long time electrostatic machines did not find practical uses. The suc-

* *Elektrichestvo* No.7, 11 – 14, 1957 [Reprint Order No.EL33].

† All equations are given in terms of the absolute practical rationalized system of units.

cesses in the development of the electromagnetic machines relegated the electrostatic machines to the background. The development of electrostatic machines was also hampered by the absence of a satisfactory theory, since attempts at providing such a theory were based on the electrostatic theory. The electrostatic machine is a converter of one form of energy into another and to apply to it the laws of electrostatics is useless since the electrostatic field is characterized by the fact that energy conversion is impossible in it.

The electrostatic machine has a number of valuable characteristics. Electromagnetic d.c. machines for voltages over 15 kV are very difficult to produce. However, electrostatic machines of much simpler design for voltages of 5 to 5000 kV and more can be built. Their ratings can reach several hundred MW at a very high efficiency.

Soviet scientists have made important contributions to the research on electrostatic machines. A.F. Ioffe and V.M. Gokhberg developed a lucid theory of the electrostatic generator and designed a number of interesting electrostatic machines which found practical application [1].

A.E. Kaplyanskii presented in 1938 a general analytical theory of electromagnetic and electrostatic machines based on suggestions by Olendorf.

In his paper [2] on a general theory of electric machines A.E. Kaplyanskii started from the equations of Lagrange and proved that the conversion of mechanical into electrical energy and vice versa is only possible by variable inductances or capacitances.

The purpose of the present article is to obtain a fundamental law, the law of induction for the electrostatic machine, on the basis of an analysis of the operation of an existing type of such a machine.

Maxwell's first equation must obviously be a generalization of this law.

Operating principle and the working cycle of electrostatic machines

Nearly all modern electrostatic machines work on the principle suggested by Topler [3]. Let us consider the operation of the simplest electrostatic machine with independent excitation (Fig.1).

The electrostatic machine works on the principle of varying (by rotation of the rotor) capacitances, its main elements are therefore the electrodes 1 and 2 of the stator and the rotor, forming the variable capacitance of the machine. It is possible to design the rotor and the stator electrodes i.e., the active surfaces of the machine, in the form of cylinders, discs or rods [4].

The commutators 3 and 4 are on the rotor shaft with the adjacent brushes 5 and 6.

The voltage $-U_1$ is applied to the rotor for the excitation of the machine.

A.F. Ioffe recommended a working cycle for the electrostatic machine in the co-ordinates C, U or Q, U. Such a cycle is similar to the cycle of the ideal four-stroke steam engine.

The co-ordinate system C, U (Fig.2) provides a clear representation of the potential variations of the conductor system representing the electrostatic machine during the variation of its capacitance.

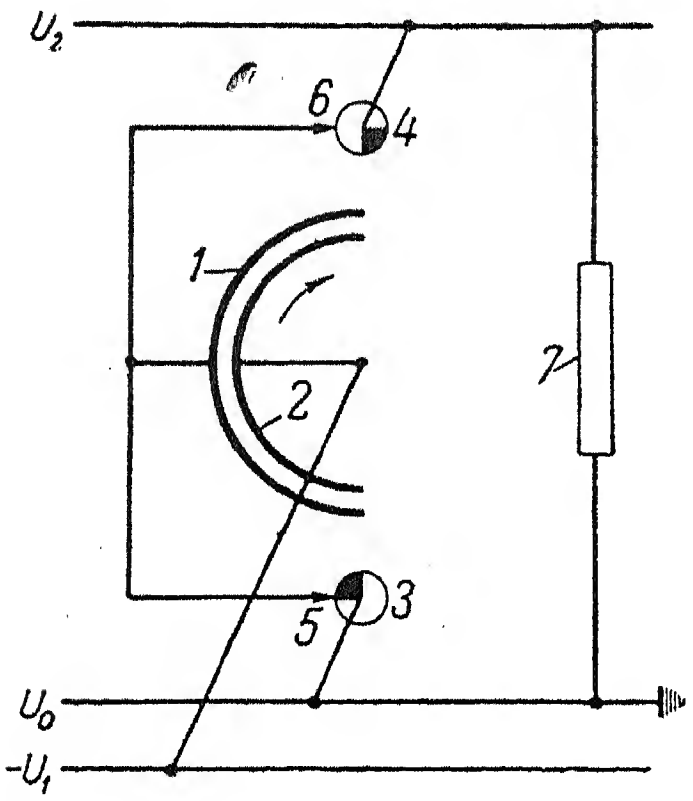

FIG.1. Basic circuit diagram of an electrostatic machine with independent excitation.
1 and 2 stator and rotor electrodes respectively, 3 and 4 commutators, 5 and 6 brushes, 7 load.

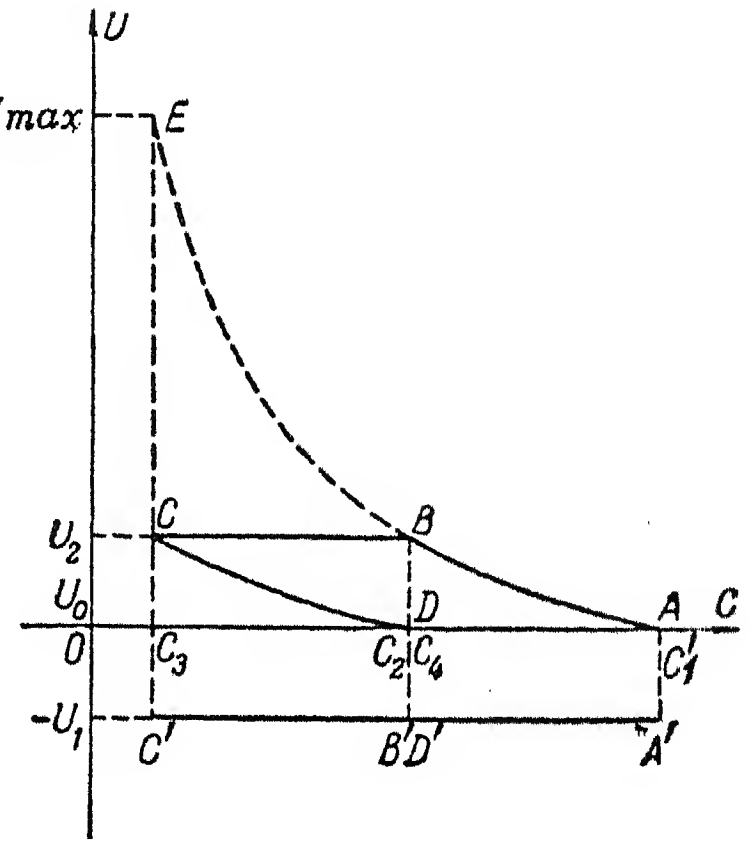

FIG.2. Working cycle of the electrostatic machine in the C, U co-ordinate system.

The co-ordinates Q, U (Fig.3) enable the variations of the magnitude of the charges in the system to be represented in relation to the capacitance of the system.

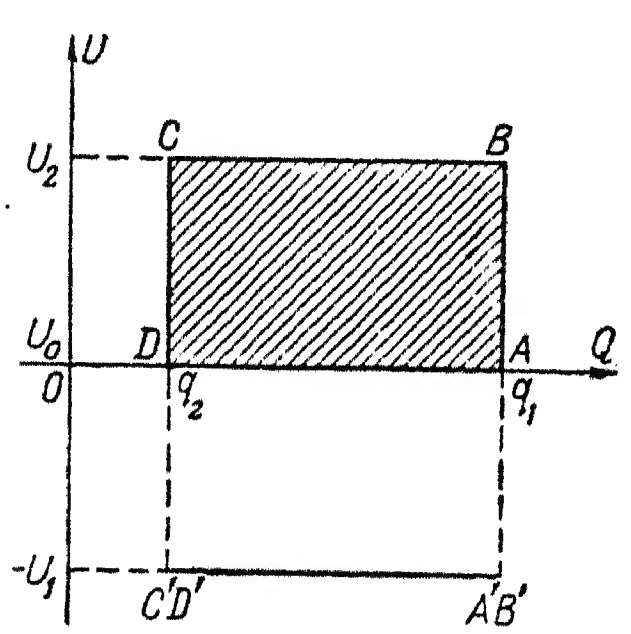

FIG.3. Working cycle of the electrostatic machine in the Q, U co-ordinate system.

In the position of the rotor of the machine shown in Fig.1 the capacitance of the system stator-rotor has its maximum, viz. C_1. The potential of the rotor is $-U_1$ and the potential of the stator U_0. As a result of the electrostatic induction the charge q_1 appears on the stator surface, equal in magnitude to the charge on the rotor surface but opposite in sign. To this position of the machine correspond the points A and A' respectively, of the representations in the C, U and Q, U co-ordinates (Fig.2 and 3). Point A determines the value for the stator surface and point A' the corresponding value for the rotor surface.

Rotation of the rotor in a clockwise direction alters the capacitance of the system. Since

the brushes 5 and 6 are insulated the potential of the stator will rise. During this process the charges on the stator and the rotor remain unchanged, viz. equal to $C_1 U$ to which the part AB of the cycle in the co-ordinates Q, U corresponds. The voltage and capacitance vary, therefore, according to a rectangular hyperbola.

During a ¼ revolution of the rotor the capacitance of the system decreases to

$$C_2 = \frac{C_1}{2},$$

and the potential of the system rises to the value

$$U_2 = \frac{q_1}{C_2} = \frac{2q_1}{C_1} = 2U_1,$$

corresponding to point B of the operating cycle of the machine.

When the rotor continues its revolution, the stator electrode, whose potential is now U_2, is connected through the brush 6 and the commutator 4 to the h.v. terminal. When the capacitance decreases to its minimum value C_3, the charge decreases to

$$q_1 - q_2 = (C_2 - C_3) U_2$$

(point C).

The stator is then disconnected from the terminal. The capacitance of the system with unchanged charge q_2 increases to the value C_4, and simultaneously the potential drops to the value U_0 (point D).

During the last part of the operating cycle of the machine, (section DA) while the capacitance increases from C_4 to C_1, a charge equal to $q_1 - q_2$ is absorbed from the low voltage source.

During a full working cycle a charge equal to $q_1 - q_2$ passes therefore from the source at potential U_0 to the h.v. electrode at potential U_2.

The mechanical energy required for the transfer of charges from the equipotential surface U_0 to the surface U_2 is given by

$$W = (q_1 - q_2)\ (U_2 - U_0).$$

The electrostatic machine is reversible and the whole cycle can be carried out in the reverse direction. In this case the h.v. source gives off its charge and the low voltage terminal receives it. The difference of the energy values of the h.v. and the l.v. sources is converted into mechanical energy.

We have considered the operating cycle of an ideal electrostatic machine. In an actual machine it is necessary to consider the losses determined by friction, ohmic and dielectric losses in the conductors and insulators respectively, etc.

The magnitude of the maximum voltage U_{max} developed by the generator

(point E, Fig.2) is determined by the minimum possible capacitance C_3, while the system is disconnected from the high voltage terminal from the condition:

$$C_1 U_1 = C_3 U_{max} = \text{const.}$$

The current at maximum voltage is zero because then $C_2 = C_3$, whence

$$q_1 - q = (C_2 - C_3) U_2 = 0.$$

Thus, U_{max} is the no-load voltage of the machine.

According to the general theory of electric machines, the equations determining the electrical condition of the machine are the voltage equations for machines based on the principle of electromagnetic induction, and the current equations for electrostatic machines. If the internal losses of the electrostatic generator are neglected, a current is induced in it. Its voltage depends on the load.

Thus, if after one cycle of the electrostatic machine the charge delivered at the high voltage terminal is, a charge equal to nq will have been delivered after q revolutions per 1 second. The load current is calculated from the equation

$$i = nq = (C_2 - C_3) n \cdot U_2. \tag{4}$$

When U_2 and the speed remain constant, the tenerator will supply a mean current of constant magnitude.

Equation (4) can be simplified by putting $C_3 = 0$ which is the case in an ideal machine:

$$i = C_2 \cdot n \cdot U_2. \tag{5}$$

The induction law for the electrostatic machine

Equations (4) and (5) yield the mean value of the current induced by the electrostatic machine. To obtain the instantaneous value of the current, it is necessary to separate section BC from the working cycle (Fig.2) since the current flows into the external circuit load only at this instant. During this part of the working cycle of the machine the instantaneous value of the current is determined by the equation

$$i = U_2 \frac{dC}{dt},$$

or in the general case,

$$i = U \frac{dC}{dt}, \tag{6}$$

which has also to be used as a basis for deriving the induction law for the electrostatic machine.

The working capacitance of the machine is determined by its geometric dimensions and by the value of the dielectric constant, $\epsilon\epsilon_0$, of the insulation which fills the gap, δ, of the machine:

$$C = \frac{\varepsilon\varepsilon_0 s}{\delta} = \varepsilon\varepsilon_0 \frac{a \cdot \Delta b}{\delta},$$

where $s = a.\Delta b$ is the overlap area of stator and rotor electrodes,
a the linear extension of the electrode at right angles to the direction of rotation,
Δb the increment of the linear extension of the electrodes in the direction of rotation.

Substituting the value of C in (6) we obtain:

$$i = U \frac{dC}{dt} = \frac{\varepsilon\varepsilon_0 U}{\delta} a \frac{d(\Delta b)}{dt}$$

or

$$i = \frac{\varepsilon\varepsilon_0 U}{\delta} a \frac{db}{dt}. \tag{7}$$

Equation (7) can be considerably simplified and put into a form analogous to the electromagnetic induction law, viz.

$$i = D \cdot a \cdot v, \tag{8}$$

where $D = \epsilon\epsilon_0 E = \frac{\epsilon\epsilon_0 U}{\delta}$ is the electric displacement (induction) in the working gap of the machine;
$v = \frac{db}{dt}$ the linear velocity of the rotor electrode.

Equation (8) represents the induction law for the electrostatic machine.

The similarity of the law of the electromagnetic induction (3) and the induction law for the electrostatic machine (8), is not incidental since, similarly to Maxwell's first and second equation, they express the same physical electromagnetic process of the field in which the forces of electric and magnetic nature appear.

When the overlap of the stator by the rotor electrodes varies by the amount

$$ds = a\, db$$

the corresponding change of the flux of the electric displacement vector N is

$$dN = D\, ds = D\, a\, db.$$

In unit time the flux of the electric displacement vector varies by

$$\frac{dN}{dt} = D.a\frac{db}{dt} = D.a.v. \tag{9}$$

Comparison of equations (8) and (9) yields a new expression of the induction law for the electrostatic machine

$$i = \frac{dN}{dt}, \tag{10}$$

i.e. the current induced in the machine equals the rate of change of the flux of the electric displacement vector in the working gap of the machine.

Equation (10) is easily related to Maxwell's first equation (1). Therefore Maxwell's first equation is the most general expression of the induction law (current induction) for the electrostatic machine.

In the general case, when the electrode-conductor has an arbitrary shape and moves in a non-uniform electric field we can write the expression for an infinitely small current di induced on the part $d\bar{a}$ of the electrode surface. Let $d\bar{a}$ be a vector at right angles to the conductor axis in the direction defined as positive and of magnitude equal to the width of the surface considered. If the velocity vector makes an angle α with vector $\bar{a}$ (Fig. 4), the area traced out by the conductor section da during the time dt is $ds = v\,dt\,da\sin\alpha$.

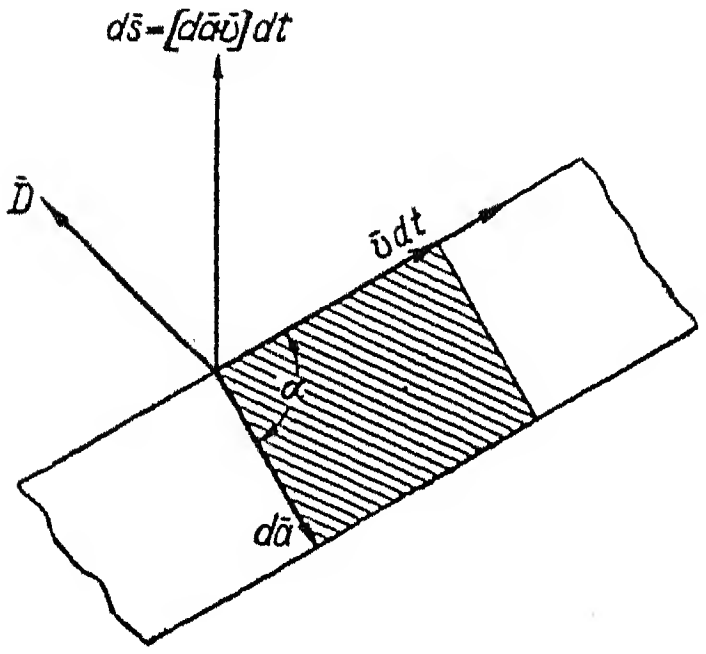

FIG. 4.

Representing this area by the vector $d\bar{s}$ in a direction perpendicular to it, we can write

$$d\bar{s} = [d\bar{a}\ \bar{v}\ dt] = [d\bar{a}\ \ \bar{v}]\,dt,$$

where $[d\bar{a}\ \ \bar{v}]$ is the vector product of $d\bar{a}$ and $\bar{v}$.

The flux of electric displacement

$$dN = \bar{D}\,.\,d\bar{s} = \bar{D}[d\bar{a}\,.\,\bar{v}]\,dt,$$

incident on this area induces in the segment $d\bar{a}$ during the movement of the conductor in time dt the current

$$di = \frac{dN}{dt} = \bar{D}\ [d\bar{a}\ \ \bar{v}]. \qquad (11)$$

Assuming as positive direction of the vector of the electric induction that pointing towards the surface of the conductor, the direction of the induced current in the conductor coincides with the direction of the change of the electric field with respect to the conductor.

The current in the external circuit of the machine is set up as a result of the "displacement" of the stator charge during the decrease of the capacitance of the stator-rotor system; for this reason it makes no sense to ascribe a certain direction to the current in the stator electrode of such a machine.

Conclusions

The electrostatic machine considered, with a working cycle similar to that of a steam engine clearly illustrates the present state of the development of the theory of these machines. Only a small part of the working cycle is used for generating electric current, the rest being taken up by preparatory operations.

Further developments of the theory of electrostatic machines should lead to the

production of new and improved designs of such machines, to be used not only in physical research laboratories but also for industrial purposes, particularly in the field of long-distance d.c. power transmission.

Definition of symbols

$\overline{B}$ vector of the magnetic flux density;
$\overline{D}$ vector of the electric displacement;
$\overline{E}$ vector of the electric field strength;
$\overline{H}$ vector of the magnetic field strength;
W energy;
$\overline{v}$ velocity vector;
γ conductivity.

REFERENCES

1. A.A. Vorob'ev; *Extra high electric voltages. Gosenergoizdat* (1955).
2. A.E. Kaplyanskii; *Introduction to the general theory of electric machines. Gosenergoizdat* (1941).
3. Karel Malek; *Electrostatic generators and their use as h.v. sources for particle accelerators. Elektrotechnický* obzor, 3 (1956).
4. Zdenek Zán; *Design types of modern electrostatic machines. Elektrotechnický* obzor, 7 (1956).

GENERALIZED METHOD OF INVESTIGATING THE TRANSIENT PROCESSES IN ELECTRIC DRIVE SYSTEMS*

D.P. MOROZOV and YU.A. BORTSOV

(Received 28 November 1956)

The investigation of the transient processes in various and complicated systems of electric drives enables the optimum operating conditions of the driven mechanisms as regards the economy and output to be selected. To reduce the differential equations of these processes for circuits with rigid and flexible closed loops is a difficult task which often confronts the designer. It is particularly so where the general differential equation of the transient process of an electric drive has to be written down for different initial conditions. For example, starting, reversal and braking of a motor at a steady speed take place with what is known as "natural" initial conditions. In this case only the initial values of the variable and of one or two of its higher derivatives cannot be zero. However, when the value of a disturbing effect or of any circuit parameter varies at a time at which the system was still in a transient state, all the initial conditions will differ from zero. Examples are to be found in braking before the speed is steady, or the action of "cut-offs", etc.

We will make a few preliminary remarks, viz,

1) The coupling coefficient between control windings placed on a common core in an electric machine is according to experimental findings considerable, viz. of the order 0.85-0.9. The resultant flux then varies with a time constant approximately equal to the sum of the time constants of all the control windings.

2) In an amplidyne the time constant of the first stage may be comparable to the time constant of its short-circuited circuit. It is, therefore, necessary to consider the parameters of both stages of the amplifier in writing down the differential equation.

3) In setting up the basic equations it is not necessary to use the coefficients of mutual inductance between the windings. The derivation becomes simpler and more lucid if the setting up of these equations is based on the resultant magnetic flux [1 and 2].

* *Elektrichestvo* No. 7, 19-24, 1957 [Reprint Order No. EL 34].

4) In setting up the general differential equation of the system for various operating conditions it is recommended to use a method according to which

a) all the variables are written in the form of an algebraic sum of the initial value of the given quantity obtaining at the end of the preceding state of operation, and the increment of this variable quantity during the new stage of the transient process. For example, speed and current of the motor are written as follows: $n = n_0 + n'$; $i_a = I_{a0} + i'_a$, where n_0 and I_{a0} are speed and armature current of the motor, respectively, e.g., at a "cut-off", and n' and i'_a the increments after this instant;

b) the equations of the preceding operating conditions are calculated from equations put together in a similar way. As a result, the system of differential equations for the deviations is obtained; this can then be solved with respect to the required variables (current, e.m.f., speed of the motor, etc.).

The setting-up of the differential equations is based on operating conditions characterised by "natural" initial conditions, i.e. the conditions of "standstill". In the general case they may also be non-zero, for example, for conditions of braking and reversal from steady conditions. This case is the simplest one. The circuit shown in Fig. 1 is used for a number of mechanisms in the metallurgical and mechanical industries. The desired voltage U is supplied by a potentiometer; all the control windings link with the total resultant flux Φ_c.

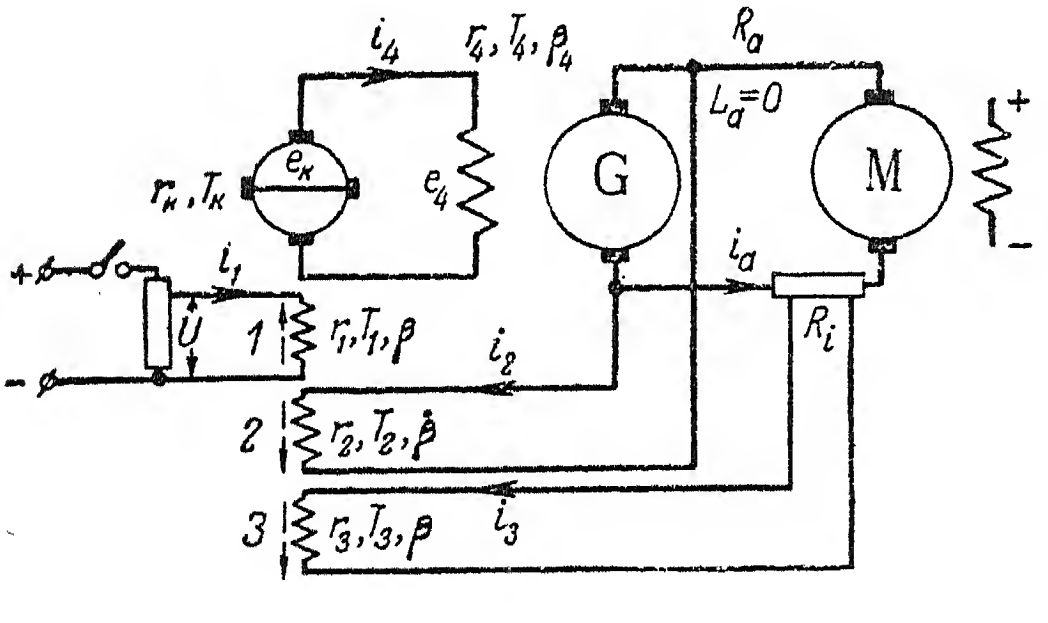

FIG. 1. Circuit generator-motor with negative rigid feedbacks of generator voltage and motor current.

Parameters of the reprint winding: r_1 resistance; b_1 susceptance; w_1 number of turns; L_1 inductance; T_1 time constant; β proportionality factor between ampere-turns of control, winding and e.m.f. of the short-circuited circuit e_{sh}; $k_1 = w_1 \beta$ proportionality factor between control current and e.m.f. of the short-circuited circuit e_{sh}; $m_1 = w_1 \beta / r_1$ voltage amplification factor (gain).

The parameters of the second and all the other windings are denoted similarly. Other symbols used: R_a total resistance of the armature circuit generator-motor; $\theta = GD^2 R_a / 375\, c_e c_m$ electromechanical time constant.

Let us set up the equations for zero initial conditions, characterising no-load starting of the motor ($M_c = 0$). In doing so,

a) we neglect the leakage of all the magnetizing windings;
b) we linearise the magnetization curves of all the machines;

c) we neglect the electromagnetic time constant of the main circuit;

d) we do not consider the active resistance of the generator in setting up the fundamental equations of the feedback circuits.

The equations are as follows:

$$U = i_1 r_1 + w_1 \frac{d\Phi_c}{dt}; \tag{1}$$

$$e_z = i_2 r_2 - w_2 \frac{d\Phi_c}{dt}; \tag{2}$$

. . . . . .

$$i_a = \frac{GD^2}{375\, c_M} \cdot \frac{dn}{dt}. \tag{3}$$

From this system of equations we derive the general differential equation involving the current and the motor speed. Considering that $d\Phi_c/dt = 1/k_c \cdot de_{sh}/dt$, (1) may be written for the first winding in the following form

$$U = i_1 r_1 + \frac{w_1}{k_c} \frac{de_{sh}}{dt}. \tag{4}$$

Divining all the terms of (4) by r_1 and multiplying into $\omega_1 \beta$, and furthermore considering that $w_1^2 \beta / k_c r_1 = L_1/r_1 = T_1$, we get

$$m_1 U = i_1 w_1 \beta + T_1 \frac{de_{sh}}{dt}. \tag{5}$$

For the circuit of winding 2 we get an analogous equation, viz.

$$m_2 e_z = i_2 w_2 \beta - T_2 \frac{de_{sh}}{dt}. \tag{6}$$

Let us note that the negative sign before the second term in (6) and (2) indicates that the e.m.f. induced in the winding 2 by the resultant flux Φ_c sets up a current opposing the flux increase. Consequently, the e.m.f. in winding 2 coincides with the direction of e_g (for rigid negative feedback). The same is the case in the negative current feedback loop.

To complete the setting-up of the general equation it is convenient to cast it in operator form [3], viz.

for the first control winding

$$m_1 \bar{U} = \bar{i_1} w_1 \beta + T_1 p \bar{e}_{sh}; \tag{7}$$

for the second control winding

$$m_2\bar{e}_g = \bar{i}_2 w_2 \beta - T_2 p \bar{e}_{sh}; \tag{8}$$

for the third control winding

$$m_3 \bar{i}_a R_i = \bar{i}_3 w_3 \beta - T_3 p \bar{e}_{sh}. \tag{9}$$

From (7) we subtract (8) and (9) term by term and, considering that $(\bar{i}_1 w' - \bar{i}_2 w_2 - \bar{i}_3 w_3 - \beta = \bar{e}_{sh}$, we get

$$\bar{e}_\kappa = \frac{m_1 \bar{U} - m_2 \bar{e}_g - m_3 \bar{i}_a R_i}{1 + (T_1 + T_2 + T_3) p}. \tag{10}$$

Furthermore, using (1) - (3), we find successively e_4, e_g and, lastly, i_a:

$$\bar{i}_a = \frac{m_1 m_\kappa m_4 \theta b_a p \bar{U}}{(1 + T_c p)(1 + T_{sh} p)(1 + T_4 p)(1 + \theta p) + m_2 m_{sh} m_4 (1 + \theta p) + R_i b_a \theta m_3 m_{sh} m_4 p}. \tag{11}$$

The speed of the motor is found from (3), viz.,

$$\bar{n} = \frac{\bar{i}_a}{\theta b_a c_e p} = \frac{m_1 m_\kappa m_4 \bar{U}/c_e}{(1+T_c p)(1+T_{sh} p)(1+T_4 p)(1+\theta p) + m_2 m_{sh} m_4 (1+\theta p) + R_i b_a \theta m_3 m_{sh} m_4 p}. \tag{12}$$

We will show that (11) and (12) may also be used for considering the transient process on braking the motor from some steady speed n_0. We will not only set up the equations for the same drive system, but also consider the initial conditions; as such we assume constant values of the fluxes (or currents) and e.m.f.'s which existed in the motor circuit when the motor operated at a steady speed.

We get

$$0 = (I_{10} + i'_1) r_1 + w_1 \frac{d(\Phi_{c0} + \Phi'_c)}{dt}; \tag{13}$$

$$E_{g0} + e'_g = (I_{20} + i'_2) r_2 - w_2 \frac{d(\Phi_{c0} + \Phi'_c)}{dt}; \tag{14}$$

. . . . . .

$$I_{a0} + i'_a = \frac{GD^2}{375 c_m} \frac{d(n_0 + n')}{dt}. \tag{15}$$

The equations of the "statics", characterizing the preceding process of braking conditions of the motor ($E_{g0} = I_{20} r_2$, etc.) are subtracted from the corresponding equations of the system (13) - (15). Considering that all the differentials of the constant values $d\Phi_{c0}/dt$, dI_{sh0}/dt.....dn_0/dt vanish, we get the following system of equations for the deviations of the variables:

$$0 = (I_{10} + i'_1)\, r_1 + w_1 \frac{d\Phi'_c}{dt}\,; \tag{16}$$

$$e_2 = i_2 r_2 - w_2 \frac{d\Phi'_c}{dt}\,; \tag{17}$$

. . . . . .

$$i'_a = \frac{GD^2}{375 c_m}\,. \tag{18}$$

Let us denote $I_{10} r_1 = U_0$; equation (16) is then written as follows:

$$-U_0 = i'_1 r_1 + w_1 \frac{d\Phi'_c}{dt}\,.$$

As a result we get the solution of the system of equations (16) - (18) with respect to i'_a:

$$i'_a = \frac{-m_1 m_\kappa m_4 \theta b_a p \bar{U}_0}{(1 + T_c p)(1 + T_{sh} p)(1 + T_4 p)(1 + \theta p) + m_2 m_{sh} m_4 (1 + \theta p) + R i b_a \theta m_3 m_{sh} m_4 p} \tag{19}$$

In substituting the numerical values of the parameters into (19) we have to consider:

a) that in the denominator the time constant of the variation of the direct-axis flux $T_c = T_1 + T_2 + T_3$ assumes a new value, since the constant T_1 increases with decreasing resistance r_1;

b) in the numerator the variation of r_1 during braking acts differently on U_0 and m_1. When r_1 increases, the leap in the effect of U_0 also becomes greater. Simultaneously, the second factor, viz. the voltage amplification factor m_1, decreases in the same ratio. Thus, the value of the numerator as a whole remains unchanged. Only its sign changes, indicating that the armature current in the main machines has now the opposite direction to that during starting.

This method may also be used in investigating processes such as the reversing of a motor from any steady speed to a given speed in the opposite direction and any other analogous cases characterised by "natural" initial conditions.

It is more difficult to investigate processes with non-zero initial conditions throughout. Let us examine one of these cases.

One of the frequently occurring operating conditions of motors driving certain mechanisms (operating train of a reversing rolling mill, traversing mechanism of the table of a planing machine, etc.) is the braking from an unsteady speed, taking place at an instant at which the running-up of the motor is not yet completed and the cutting-out of the reference input voltage or the change of its polarity has occurred.

To set up the general differential equation of the current and the speed of a motor operating in a generator-motor system with closed loops (Fig. 1) we use the

system of equations (13) - (15). Each variable was written as a sum of the initial values and its deviations. However, allowance has now to be made for the fact that in all the circuits containing inductances the voltages (e.m.f.'s) applied are balanced not only by the active voltage drops, but also by the self-induced e.m.f.'s.

The solution of the simultaneous equations (13) - (15) with respect to i'_a leads to the following expression:

$$\bar{i}'_a = \frac{\theta b_a p\,[m_4 (\bar{E}_{40} - \bar{I}_{40} r_4)(1 + T_\kappa p)(1 + T_y p) +}{(1 + T_y p)(1 + T_\kappa p) \times} \rightarrow$$

$$\rightarrow \frac{+ m_\kappa m_4 (\bar{E}_{\kappa 0} - \bar{I}_{\kappa 0} r_\kappa)(1 + T_y p) - m_\kappa m_4 \bar{E}_{\kappa 0} - m_2 m_\kappa m_4 \bar{E}_{z0} - m_3 m_\kappa m_4 \bar{I}_{a0} R_i] -}{\times (1 + T_4 p)(1 + \theta p) + m_2 m_\kappa m_4 (1 + \theta p) +} \rightarrow$$

$$\rightarrow \frac{- I_{a0} [(1 + T_y p)(1 + T_\kappa p)(1 + T_4 p) + m_2 m_\kappa m_4]}{+ R_i b_a \theta m_3 m_\kappa m_4 p}. \qquad (20)$$

Hence, by use of (15), transformed to the form $\bar{I}_{a0} + \bar{i}'_a = \theta b_a c_e p \bar{n}'$, we get the following expression for $\bar{n}'$

$$\bar{n}' = \frac{\bar{I}_{a0} + \bar{i}'_a}{\theta b_a c_e p} = \frac{\bar{i}'_a}{\theta b_a c_e p} + \frac{\bar{I}_{a0}}{\theta b_a c_e p}. \qquad (21)$$

It should be noted that (20) and (21), set up for the special case of braking from an unsteady speed, may be used as general differential equations of a typical control circuit with amplidynes and with current and voltage feedbacks.* It is possible to get from them without derivation the equations describing any desired transient process such as starting, braking, reversal, etc. in circuits

a) with negative or positive current and voltage feedbacks or only one of these);

b) with "cut-off" of voltage, and current feedback;

c) with separate current and voltage "cut-offs";

d) with current "cut-off" and voltage feedback;

e) with an amplidyne working as generator in a generator-motor system;

f) with an ordinary d.c. machine working as an exciter of a generator.

From the general differential equation it is easy to obtain the equations for operating conditions with zero initial conditions, which were set up above for

* For this purpose it is only necessary to add the term $m_1 m_{sh} m_4 \theta b_a p U$ in the numerator of (20); this expresses the presence of the reference quantity U at the input of the control system.

starting and braking from steady-speed operation; *Cf.* (11), (12) and (19). The setting-up of the equation of the transient processes in circuits with "cut-offs" must be carried out by stages according to whether the circuit elements are connected up or not. The initial conditions have to be determined separately for each stage.

Starting a motor in a generator-motor system with negative current feedback and voltage "cut-off"

Let us set up the differential equation and represent the transient processes $n(t)$ and $i_a(t)$ for the circuit of the drive shown in Fig. 2. In this case the whole starting period has to be divided into two stages.

First stage, i.e. up to the establishment of the voltage feedback, when the opposing voltage ΔU of the potentiometer is greater than the rising generator voltage e ; we have zero initial conditions, viz., $E_{g0} = E_{40} = E_{sh0} = 0$, $I_{a0} = I_{40} = I_{sho} = 0$; there is no voltage feedback ($m_2 = 0$); the time constant of the first amplifier circuit $T_c = T_1 + T_3$; the reference (input) voltage is U..

Under these conditions we obtain from (20) and (21)

$$\bar{i}_a = \frac{m_1 m_\kappa m_4 \theta b_a p \bar{U}}{(1 + T_y p)(1 + T_\kappa p)(1 + T_4 p)(1 + \theta p) + R_i b_a \theta m_3 m_\kappa m_4 p} \tag{22}$$

$$\bar{n} = \frac{\bar{i}_a}{\theta b_a c_e p} = \frac{m_\partial \bar{i}_a}{\theta b_a p} =$$

$$= \frac{m_\partial m_1 m_\kappa m_4 \bar{U}}{(1 + T_y p)(1 + T_\kappa p)(1 + T_4 p)(1 + \theta p) + R_i b_a \theta m_3 m_\kappa m_4 p}. \tag{23}$$

The second stage, i.e. after the "cut-off" has begun to act, when e_g is greater than ΔU, and their difference $(e_g - \Delta U)$ begins to supply the demagnetizing ampere-turns of the voltage feedback (winding 2). The initial conditions (E_{g0}, E_{40}, ..., I_{sh0}) will be non-zero. When the effect of the "cut-off" begins, $E_{g0} - \Delta U = 0$, and the term $\bar{E}_{g0} m_2 m_{sh} m_4$ in (20) is zero; the time constant $T_c = T_1 + T_2 + T_3$; the input voltage U remains as before.

Under these conditions we get from (20) and (21)

$$\bar{i}'_a = \frac{\theta b_a p [m_4 (\bar{E}_{40} - \bar{I}_{40} r_4)(1 + T_{sh} p)(1 + T_c p) + \rightarrow}{(1 + T_c p)(1 + T_{sh} p) \times}$$

$$\rightarrow \frac{+ m_\kappa m_4 (\bar{E}_{\kappa 0} - \bar{I}_{sh0} r_{sh})(1 + T_y p) + m_1 m_{sh} m_4 \bar{U} - \rightarrow}{\times (1 + T_4 p)(1 + \theta p) +}$$

$$\rightarrow \frac{-m_\kappa m_4 \bar{E}_{sh0} - m_3 m_{sh} m_4 I_{a0} R_i] -}{+ m_2 m_{sh} m_4 (1 + \theta p) +} \rightarrow$$

$$\rightarrow \frac{-\bar{I}_{a0}[(1 + T_y p)(1 + T_\kappa p)(1 + T_4 p) + m_2 m_\kappa m_4]}{+ R_i b_a \theta m_3 m_{sh} m_4}; \quad (24)$$

$$\bar{n}' = \frac{\bar{I}_{a0} + \bar{i}'_a}{c_e \theta b_a p} = \frac{m_m \bar{i}'_a}{\theta b_a p} + \frac{\bar{I}_{a0}}{\theta b_a c_e p}. \quad (25)$$

Determination of the initial conditions. To determine the initial conditions it is necessary to know the values of the variables involved at $t = t_0$, i.e. the time of the "cut-off". This requires the functions $e_g(t)$, $e_4(t)$ and $e_{sh}(t)$ to be calculated. We use the system of equations (1) - (3), thus,

$$\bar{e}'_z = \frac{\bar{i}'_a (1 + \theta p)}{\theta b_a p} = \frac{m_1 m_{sh} m_4 \bar{U} (1 + \theta p)}{\theta_1 (p)}; \quad (26)$$

$$\bar{e}'_4 = \frac{\bar{i}'_4}{b_4} (1 + T_4 p) =$$

$$= \frac{\bar{e}'_z}{m_4} (1 + T_4 p) = \frac{m_1 m_{sh} \bar{U} (1 + T_4 p)(1 + \theta p)}{\theta_1 (p)}; \quad (27)$$

$$\bar{e}'_\kappa = \frac{\bar{i}'_\kappa}{b_\kappa} (1 + T_\kappa p) = \frac{m_1 \bar{U} (1 + T_{sh} p)(1 + T_4 p)(1 + \theta p)}{\theta_1 (p)}, \quad (28)$$

where $\theta_1 (p)$ is the characteristic equation of the system during the first stage of the start.

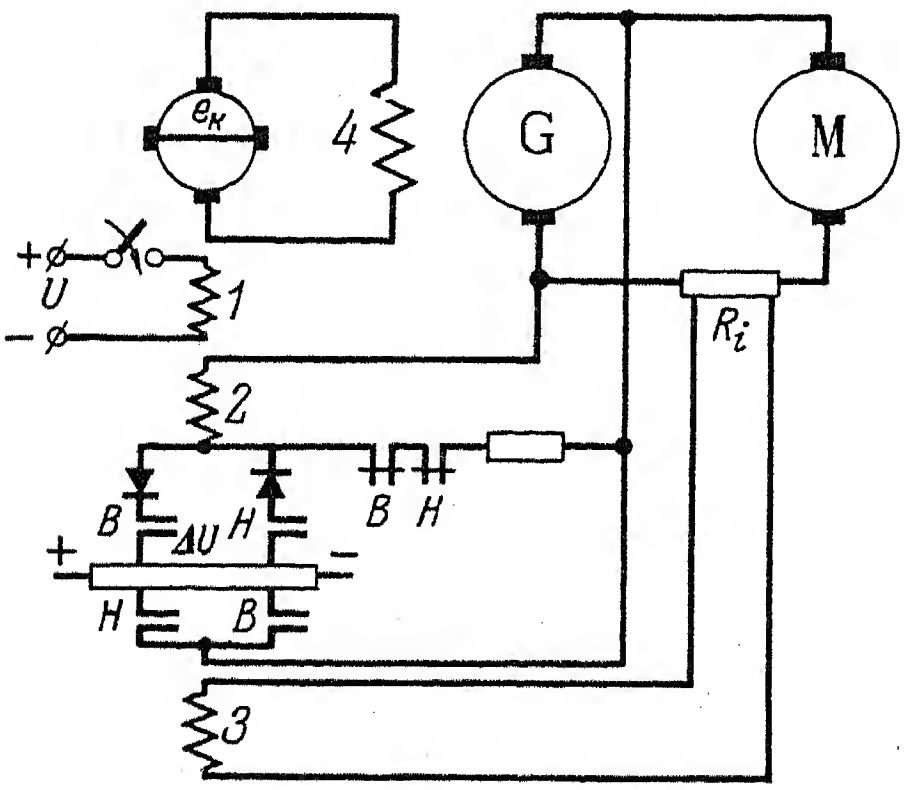

FIG. 2. Generator-motor system with negative current feedback and voltage "cut-off".

The variation of the individual variables in a closed automatic control system

follows the same characteristic equation. This fact also exists in the case considered, and simplifies the calculation of the roots on determining the initial conditions.

We find the initial conditions from (26) - (28) for $t = 0$, viz.,

$$E_{g0} = [e'_g]_{t=t_0}; \quad E_{40} = [e'_4]_{t=t_0}; \quad E_{sh0} = [e'_{sh}]_{t=t_0}; \tag{29}$$

$$I_{40} = \frac{E_{c0}}{k_4} = \frac{E_{c0}}{m_4 r_4}; \quad I_{sh0} = \frac{E_{40}}{k_{sh}} = \frac{E_{40}}{m_{sh} r_{sh}}. \tag{30}$$

Example. It is required to determine the transient speed and current processes on starting a roll-train driving motor in a generator-motor system with negative feedback and voltage "cut-off" (Fig. 2).

Data of the electric machines: two series-connected separately-excited motors of type MP-82, $P_n = 100$ kW, $U_n = 220$ V, $n_n = 475$ rev/min., $I_n = 500$ A; generator rating $P_n = 320$ kW, $U_n = 460$ V, $n_n = 485$ rev/min; $I_n = 700$ A; amplidyne rating $P_n = 4.5$ kW, $U_n = 230$ V, $n_n = 2935$ rev/min, $I_n = 19.6$ A, $I_{sh} = 5.9$ A, $r_{sh} = 0.85\ \Omega$.

The basic data of the static calculation are collected in the table.

We will assume that the static torque, only due to the friction losses, is zero, this being a characteristic feature of the drive of a rolling train and enabling equations (22) - (25) to be used without any change.

First stage. $T_c = T_1 + T_3 = 0.0214 + 0.0143 = 0.0357$ sec; $m_2 = 0$.

Substituting the values of the parameters into (23) we get:

$$\bar{n} = \frac{1\,010}{p\,(0{,}00092p^4 + 0{,}0417p^3 + 0{,}51p^2 + 3{,}37p + 1)} = \frac{A(p)}{pB(p)}.$$

The roots of the characteristic equation: $p_1 = -0.305$; $p_2 = -30.5$; $p_{3,4} = -7.25 \pm j8.04$.

Using a well-known expansion theorem, we find the original, viz.,

$$n(t) = \frac{A(0)}{B(0)} + \sum_{i=1}^{i=4} \frac{A(p_i)\, e^{p_i t}}{[B'(p)]_{p=p_i}} =$$

$$= 1\,010 - 1\,055e^{-0.305t} + 2.18e^{-30.5t} +$$

$$+ 45.1e^{-7.25t} \cos 8.04t + 12.85e^{-7.25t} \sin 8.04t.$$

Considering that $i_a = GD^2/375c_m \times dn/dt$, we find the expression for the current during the first stage of starting, viz.,

$$i(t) = 885e^{-0,305t} - 260e^{-30,5t} - 530e^{-7,25t}\cos 8,04t - \\ - 1\,280e^{-7,25t}\sin 8,04t.$$

The expressions $n(t)$ and $i(t)$ are represented in Fig. 3.

Determination of the initial conditions. We will assume that the "cut-off" becomes effective at the motor speed $n = 0.8n_n = 380$ rev/min., this corresponding to the time $t = t_0 = 1.78$ sec, when the current $I_{a0} = 520$ A, and the generator e.m.f. $E_{g0} = I_{a0}R_a + c_e n_0 = 365$ V. To solve the equation for the start at the second stage, it is still necessary to know the initial values of E_{40} and E_{sh0}. Their determination is carried out by finding the originals of expressions (27) and (28). For $t = t_0 = 1.78$ sec, $E_{40} = 161$ V, $E_{sh0} = 3.6$ V.

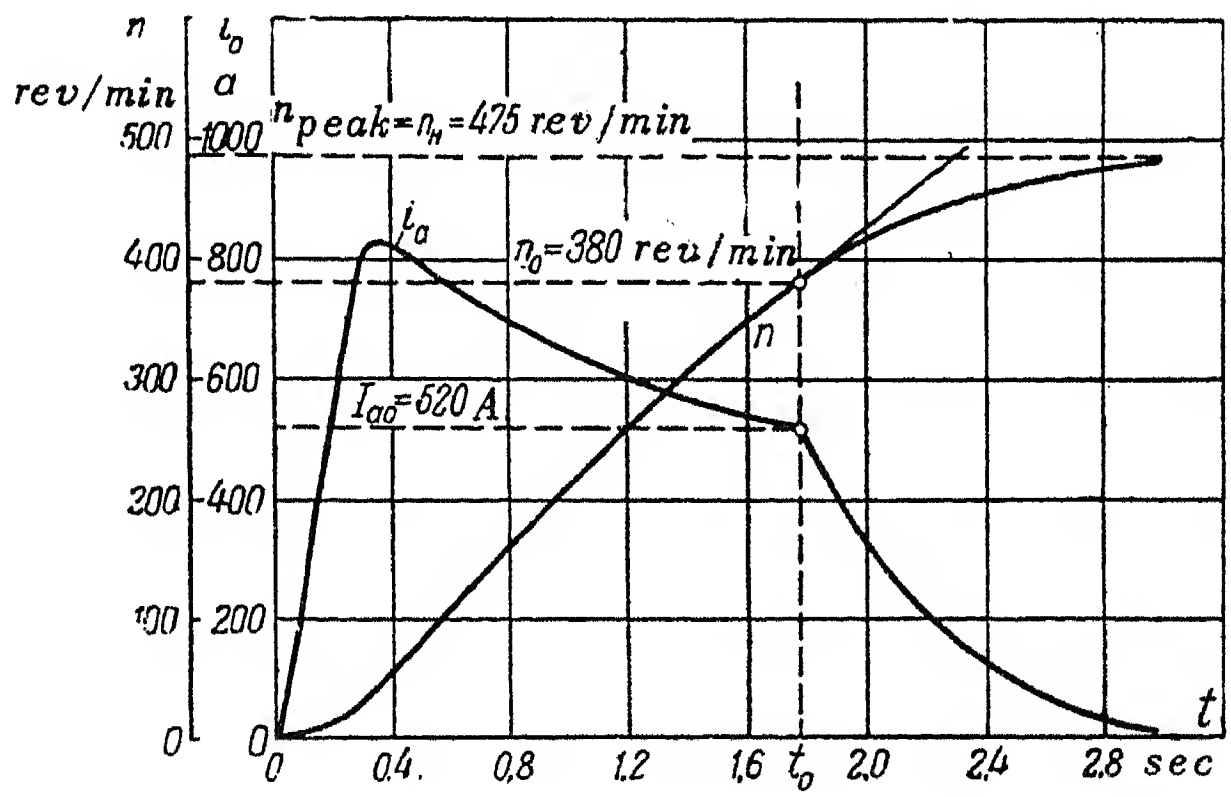

FIG. 3. Curves of the transient process on starting the motor in a generator-motor system with current feedback and voltage "cut-off".

From (30) we get

$$I_{40} = E_{g0}/m_4 r_4 = 365/3.83 \times 6 = 16 \text{ A},$$
$$I_{sh0} = E_{40}/m_{sh} r_{sh} = 3.95 \text{ A}.$$

Second stage. We use (24) and substitute the numerical values of the parameters into it. We consider also the value $T_c = T_1 + T_2 + T_3 = 0.0477$ sec.

The solution of this equation furnishes an expression for the current of the motor during the second stage of the start, viz.,

$$i_a(t) = I_{a0} + i'_a(t) = 489e^{-2.3t} + 30.8e^{-31.3t} - \\ - 10.7e^{-5.85t}\cos 7.54t + 6.2e^{-5,85t}\sin 7.54t.$$

$n(t)$ can also be obtained by graphical integration of the curve of $i_a(t)$ (Fig. 3).

It is possible to draw some conclusions as to the nature of the circuit and the correct values of the parameters from the plotted curves of current and speed of the motor. For example, the duration of the transient process is, without any doubt, excessively long. To obviate this shortcoming, the forcing must be considerably increased and the voltage amplification and other parameters of the control circuit altered accordingly. It is advisable to use separate current and voltage "cut-offs" instead of the basic circuit considered.

The method discussed was investigated experimentally on several variants of the control circuit. Comparison of the theoretical and experimental results revealed differences of the order of 10 - 20 per cent.

Conclusions

1. A method of setting up the differential equations of controlled electric drive circuits for operational conditions characterized by various initial conditions is presented.

2. The differential equation is derived for a number of types of electric drives with rigid feedbacks and "cut-offs" of voltages and current. The equation is suitable for the case of a constant load at the motor shaft.

3. It is proposed to extend the investigation to setting up the equations for circuits with flexible feedbacks.

TABLE 1.

Time constants (sec)	$T_1 = 0.0214$	$T_2 = 0.012$	$T_3 = 0.0143$	$T_{sh} = 0.2$	$T_4 = 1.5$	$\theta = 0.086$
Amplification factors	$m_1 = 0.0455$	$m_2 = 0.0272$	$m_3 = 0.24$	$m_{sh} = 48$	$m_4 = 3.83$	$m_q = 1.1$
Other parameters	$R_a = 0.0396\ \Omega$	$b_a = 25.2$	$R_i = 0.016\ \Omega$	$U = 110$ V	–	–

REFERENCES

1. A.G. Iosifyan, *et al; Theory of an amplidyne-selsyn synchronous follower system, Elektrichestvo,* No. 3, (1946).
2. D.P. Morozov; *Excitation of electric machines in automatic circuits with amplidynes, Elektrichestvo,* No. 9, (1948).
3. D.P. Morozov; *Method of setting up the differential equations of complicated circuits of electric drives of mechanisms, Trans. Molotov., Institute of Power Engineering.,* No. 22, *Gosenergoizdat,* (1956).

CORONA LOSSES ON LIVE TRANSMISSION LINES*

V.D. KRAVCHENKO, V.I. LEVITOV and V.I. POPKOV

(Received 7 February 1957)

The corona loss on an energized transmission line constitutes only a small fraction of the transmitted energy and is commensurable with or sometimes even smaller than the heat loss. Therefore, it is practically impossible to determine this loss by separating the current component which corresponds to the corona loss from the total line current as measured by conventional methods.

The corona loss is due to the cross currents, that is, the currents that flow between the conductors and between the conductors and earth. If it were possible to measure quantities which are proportional to these currents, or to their corresponding charges this would be the best solution of the problem of measuring the corona losses on energized lines.

Fig. 1 shows an arrangement consisting of a single phase-conductor, 1, and an aerial, 2, which is earthed through a measuring element Z connected to the middle of the aerial.

The e.m.f. induced electromagnetically in an aerial isolated from earth is so distributed that it is zero at the middle of the aerial [1]. Therefore, if this point is earthed through a measuring element Z, no current can flow in the element owing to the magnetic field of the line. The current which flows in the element is determined only by the electrostatic coupling between the line and the aerial.

The minimum height at which conductors are suspended on conventional lines is 7–8 m. At this height the space charge in the region G (Fig. 1) is distributed practically symmetrically with respect to the conductor axis, i.e. the space charge density depends only on the distance from the axis of the conductor of the element of charge considered. Consequently, the integrated electrostatic effect of the space charge on the aerial is the same as that of a linear charge of equal magnitude placed at the axis of the conductor.

For sufficiently small values of the impedance Z the relation between the charge on the aerial and the total charge of the conductor is given by:

$$\alpha_{12}q_1 + \alpha_{22}q_2 = 0 \qquad (1)$$

* *Elektrichestvo* No. 7, 31 – 34, 1957 [Reprint Order No. EL 35].

or

$$q_2 = -\frac{\alpha_{12}}{\alpha_{22}} q_1, \tag{2}$$

where $\alpha_{12} = \frac{1}{2\pi\varepsilon_0} \ln \frac{r'}{r}$ - mutual potential coefficient of the aerial and conductor; $\alpha_{22} = \frac{1}{2\pi\varepsilon_0} \ln \frac{2h}{a_0}$ - self potential coefficient of the aerial (a_0 is the radius of the aerial wire); $q_1 = q_c + q_s$ - total charge of conductor per unit length (q_c is the charge on conductor surface and q_s is the integrated space charge); q_2 - charge per unit length of aerial.

Thus, the charge on the aerial which is earthed at its middle point is proportional to the total charge enclosed in the region G, i.e. is determined by both the charge on the conductor surface and the space charge due to corona.

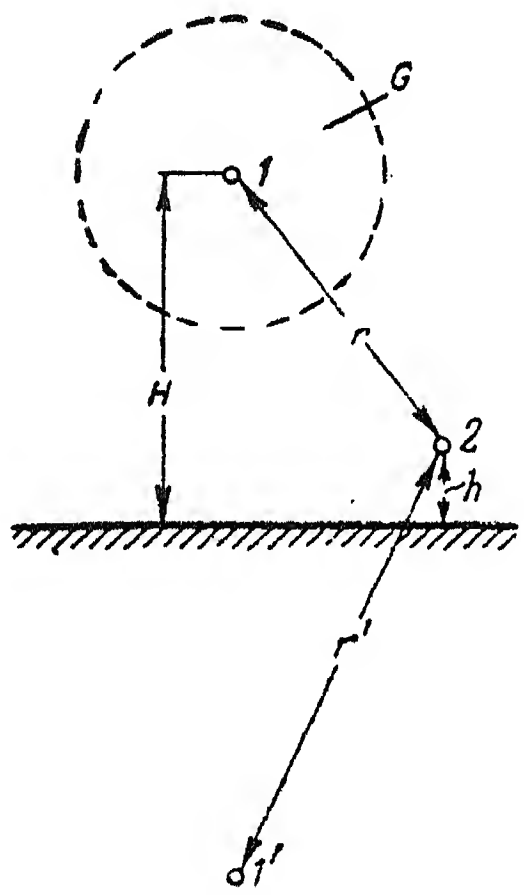

FIG. 1.

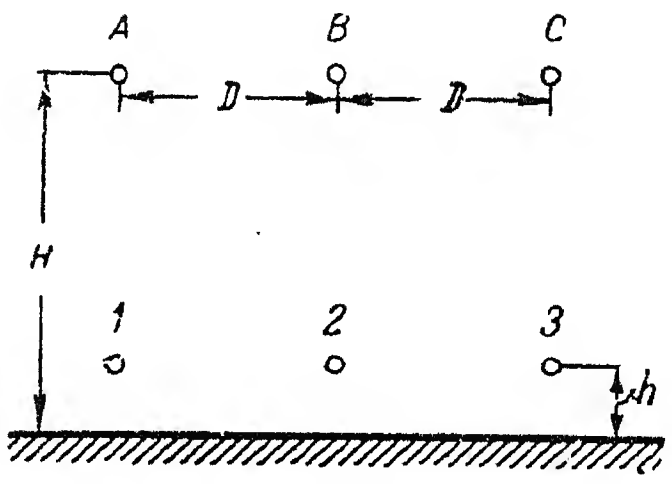

FIG. 2.

Also, the coefficient of proportionality α_{12}/α_{22} is a constant quality depending only on geometrical dimensions of the conductor-aerial arrangement. These circumstances make it possible to use aerials for corona loss measurements.

Three aerials are necessary for measurement on three-phase lines. Fig. 2 shows a possible arrangement of aerials placed directly under the three phase conductors. In this case the relation between the total charges on phase conductors q_A, q_B and q_C and the charges on earthed aerials q_1, q_2 and q_3 is given by the following system of equations:

$$\left.\begin{aligned} -(\alpha_1 q_1 + \alpha_2 q_2 + \alpha_3 q_3) &= \alpha_I q_A + \alpha_{II} q_B + \alpha_{III} q_C; \\ -(\alpha_2 q_1 + \alpha_1 q_2 + \alpha_2 q_3) &= \alpha_{II} q_A + \alpha_I q_B + \alpha_{II} q_C; \\ -(\alpha_3 q_1' + \alpha_2 q_2 + \alpha_1 q_3) &= \alpha_{III} q_A + \alpha_{II} q_B + \alpha_I q_C, \end{aligned}\right\} \tag{3}$$

where $a_1 = a_{11} = a_{22} = a_{33}$; $a_2 = a_{12} = a_{21} = a_{23} = a_{32}$; $a_3 = a_{13} = a_{31}$; $a_1 = a_{1A} = a_{2B} = a_{3C}$; $a_{11} = a_{1B} = a_{2C} = a_{3B} = a_{2A}$; $a_{111} = a_{1C} = a_{3A}$ are self and mutual potential coefficients determined from the geometrical dimensions.

By solving the system of equations (3) with respect to conductor charges q_A, q_B and q_C, we get

$$\left.\begin{aligned} q_A &= A_1' q_1 + A_2' q_2 + A_3' q_3; \\ q_B &= B_1' q_1 + B_2' q_2 + B_3' q_3; \\ q_C &= C_1' q_1 + C_2' q_2 + C_3' q_3. \end{aligned}\right\} \qquad (4)$$

The coefficients A'_i, B'_i and C'_i are composed of potential coefficients a_i which appear in (3). For example,

$$A_1' = \frac{A_1}{\Delta}; \quad A_2' = \frac{A_2}{\Delta}; \quad A_3' = \frac{A_3}{\Delta},$$

where $\Delta = a_I(a_I^2 - a_{III}^2) - 2a_{II}^2(a_I - a_{III})$ - the determinant of the system of equations (3);

$$A_1 = -a_1(a_I^2 - a_{II}^2) + a_2(a_I a_{II} - a_{II} a_{III}) - a_3(a_{II}^2 - a_I a_{III});$$

$$A_2 = -a_2(a_I^2 - a_{II}^2) + a_1(a_I a_{II} - a_{II} a_{III}) - a_2(a_{II}^2 - a_I a_{III});$$

$$A_3 = -a_3(a_I^2 - a_{II}^2) + a_2(a_I a_{II} - a_{II} a_{III}) - a_1(a_{II}^2 - a_I a_{III}).$$

It follows from (4) that the sum of the products of charges on the three aerials, q_1, q_2 and q_3, into their corresponding coefficients A'_i, B'_i and C'_i give the total charges on the phase conductors, q_A, q_B and q_C.

Either capacitors or resistors can be used as the measuring elements. In the first case, the voltages across the elements are proportional to the total charges of phase conductors and in the second case, to their time derivatives, that is to the cross-currents of the line. However, it is preferable to choose capacitors since in this case the measurement will be practically unaffected by the possible h.f. pick-ups of the aerial.

The voltages on the measuring capacitors are given by:

$$U_i = \frac{q_i l}{C} \qquad (5)$$

where U_i - voltages on the aerials; q_i - charges per unit length of the aerials; l - lengths of aerials; C - measuring capacitances.

If follows from (5) that the input voltage to the measuring circuit depends not

only on the coefficients a_i (which are determined by the geometry of the conductor-aerial arrangement) but also on the lengths of aerials and on the values of the me measuring capacitors. The choice of the ratio l/c is governed by the magnitude of the voltage required at the input to the measuring circuit, i.e. it depends on the sensitivity of the measuring device.

The length of the aerial should be such that the part of the conductor catenary which is above the aerial can be taken as being parallel to the ground.* For example, for 220 and 400 kV lines with spans of 450 m this condition is satisfied by an aerial 50 m long placed at mid-span. With this aerial suspended at a height of 0.5 m and with measuring capacitances of the order of 0.1 μF the voltage on the aerial is about 8 to 15 volts.

From the above, a block circuit diagram may be drawn for a device for measuring the corona loss on energized lines. Such a diagram is shown in Fig. 3; A, B and C are line con ductors; 1, 2 and 3 aerials; C_u measuring capacitances; $1A$, $1B$ and $1C$ voltage transformers or voltage dividers;

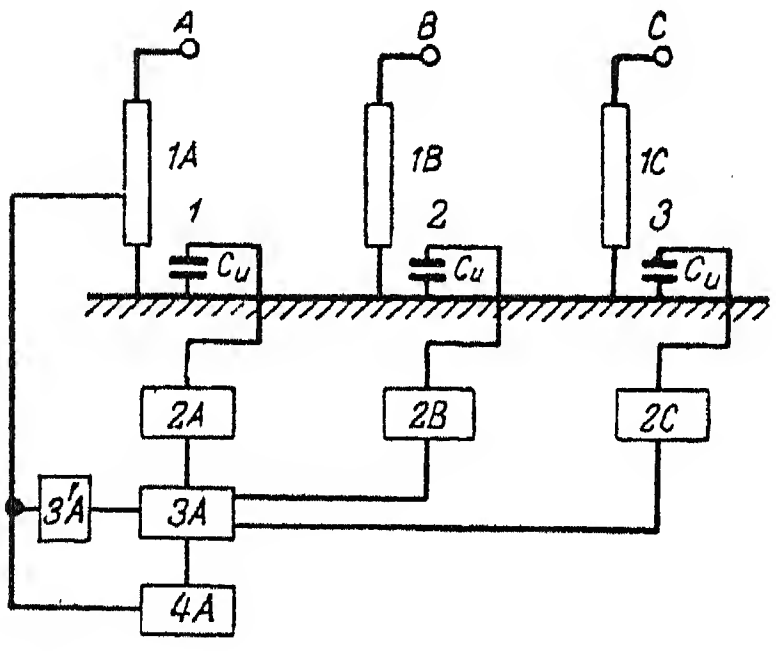

FIG. 3.

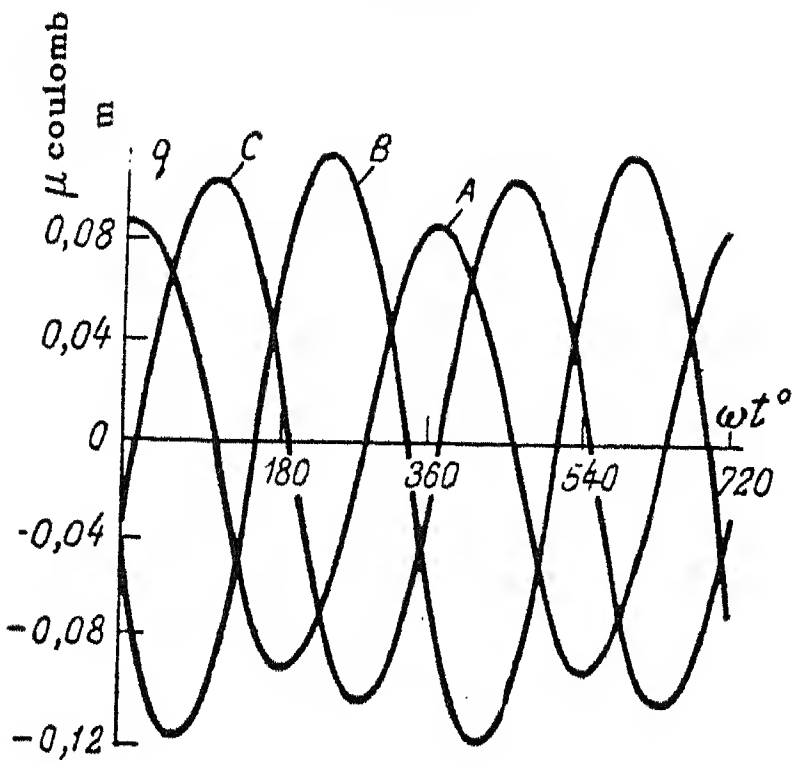

FIG. 5.

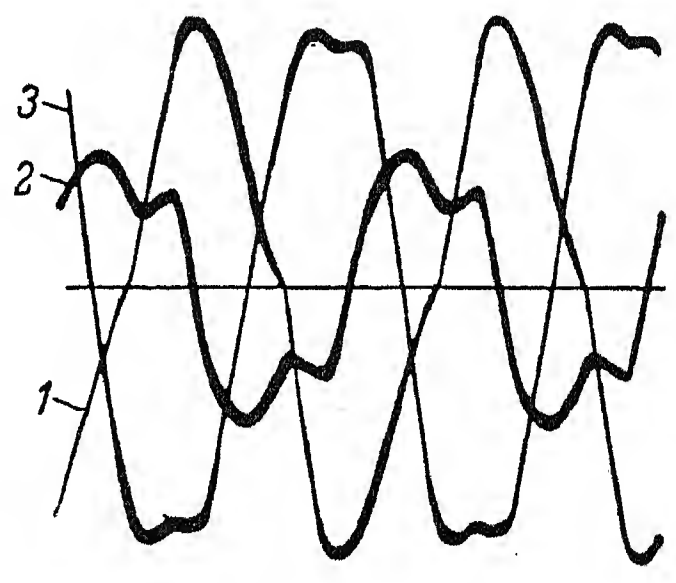

FIG. 4.

$2A$, $2B$ and $2C$ are elements multiplying the voltages corresponding to aerial charges q_1, q_2 and q_3 by their corresponding coefficients A'_i, B'_i and C'_i; $3A$ is an element carrying out the summation of the above products. As a result of this summation we get a voltage (or current) out put proportional to the total charge of phase conductor A; $4A$ is a wattmeter of some sort.

To increase the accuracy of corona loss measurements, particularly at small values of loss, it may be necessary to compensate for the reactive component of the charge q_A.

* In general this condition is not essential, since the effect of the caternary can be taken into account, when calculating potential coefficients. However, it simplifies calculation, if this condition is fulfilled.

Such a compensating voltage may be applied to the integrating element $3A$ bv a suitable device indicated by $3'A$.

For simplicity the measuring circuit is drawn for one phase only, the circuits for the remaining two phases are identical.

The assumption made above about the symmetrical distribution of the space charge due to corona with respect to the conductor axis was varified experimentally in the laboratory. A three-phase transmission line model having the following dimensions was set-up: viz. line length - 14.5m; height of conductor suspension 2m; interphase clearances - 1.3m; diameter of polished steel conductors - 1mm. As aerials copper conductors of 0.83mm dia, having the same length as the model line were used. One aerial was placed under each phase conductor at a height of 0.27m above the ground and was earthed through a capacitor. The voltages on the capacitors which are proportional to the charges on the respective aerials were applied in turn (using a special synchronizing device) to the deflecting plates of the CRO and photographed on the same plate. Each oscillogram contains therefore three voltage records. A sample oscillogram obtained with a phase-to-earth voltage of $U = 64\ \mathrm{kV}_{max}$ is shown in Fig. 4.

It is seen from this oscillogram that the curves of the charges on the aerials are irregular and differ from each other. The amplitudes of the charges on the external aerials are approximately the same, but the amplitude of the charge on the middle aerial is about one-half of that of each of the outer aerials. By multiplying the ordinates of the curves by their respective coefficients A'_i, B'_i and C'_i, and adding, we get curves corresponding to equations (4) which are shown on Fig. 5.

It follows from the above that the curves of Fig. 5 should be identical with the curves of the total charges of the experimental conductors in corona conditions. To compare these two sets of curves, an oscillographic record of the volt-coulomb characteristic was obtained for each of the three line conductors. The recording circuit for one phase only is shown in Fig. 6. In this figure the voltage across the capacitor C_q, which is proportional to the total conductor charge, was applied to one pair of deflecting plates of the CRO and the voltage across one arm (C_1) of the capacitance potential divider which is proportional to the voltage of the h.v. transformer T, was applied to the other pair of deflecting plates of the CRO.

With such a circuit the trace on the CRO screen has the form of a closed loop which is known as the volt-coulomb characteristic. The area enclosed by the loop is proportional to the energy loss due to corona for one cycle of the alternating voltage [2].

The volt-coulomb characteristics obtained for the conductors of the experimental line by direct measurement at a phase-to-earth voltage of $U_{ph} = \mathrm{kV}_{max}$ are shown in Fig. 7 (curves drawn in continuous lines). The curves drawn in broken lines represent volt-coulomb characteristics constructed from the data obtained from the aerial measurements (the curves of Fig. 5 and oscillograms of phase-to-earth voltages on the conductors recorded simultaneously with the records of the charges on the aerials), using the same voltage applied to the line.

A good measure of agreement is shown between the volt-coulomb characteristics obtained by the two methods considering the amount of error introduced by the intermediate calculations and constructions in deriving the final curve from the experimental data. The two sets of characteristics agree well as regards the amplitude of the

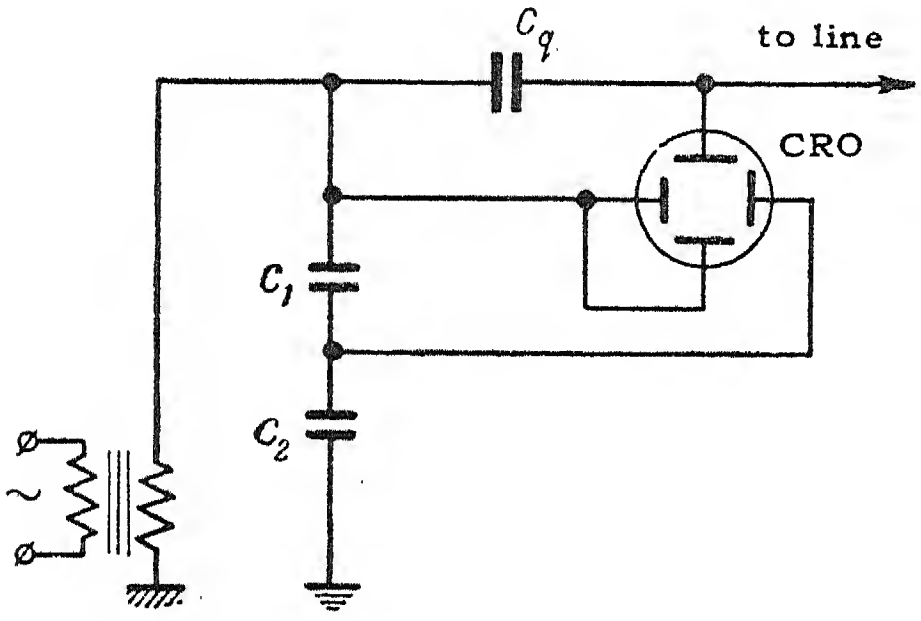

FIG. 6.

charge, the shape of the curve, and the area enclosed by the curve (the last factor being of importance from the point of view of corona loss measurement by means of aerials).

The construction of total charge and volt-coulomb curves was performed for different phase voltages up to a value exceeding three times the critical corona inception voltage. In this way values of corona loss were obtained for the experimental line for a wide range of voltages. These losses are indicated by crosses on Fig. 8 on which are also plotted corona losses derived from the volt-coulomb characteristics obtained by direct measurement. It is seen from this figure that the losses obtained by both methods are practically identical.

Thus, experimental investigations confirm the possibility of measurement of corona loss on live lines by means of aerials and also of verifying the correctness of the assumptions made.

In conclusion it should be mentioned that apart from its application to corona loss measurement the method presented can also be used for investigating other problems; for

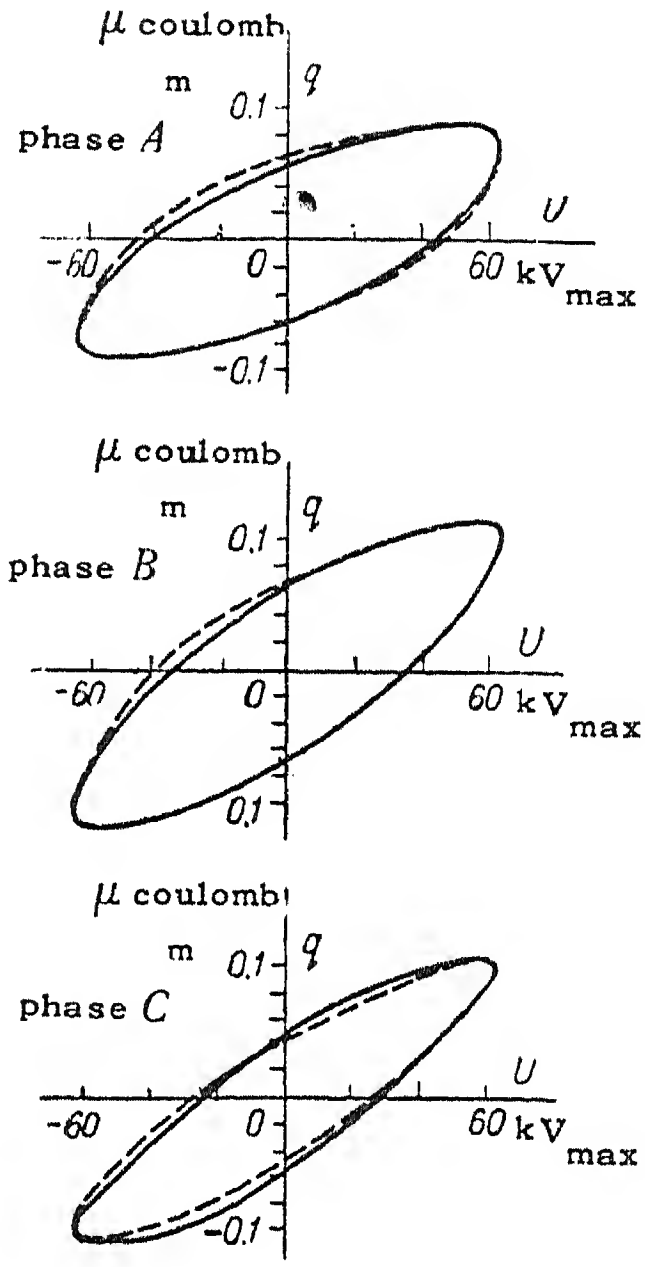

FIG. 7.

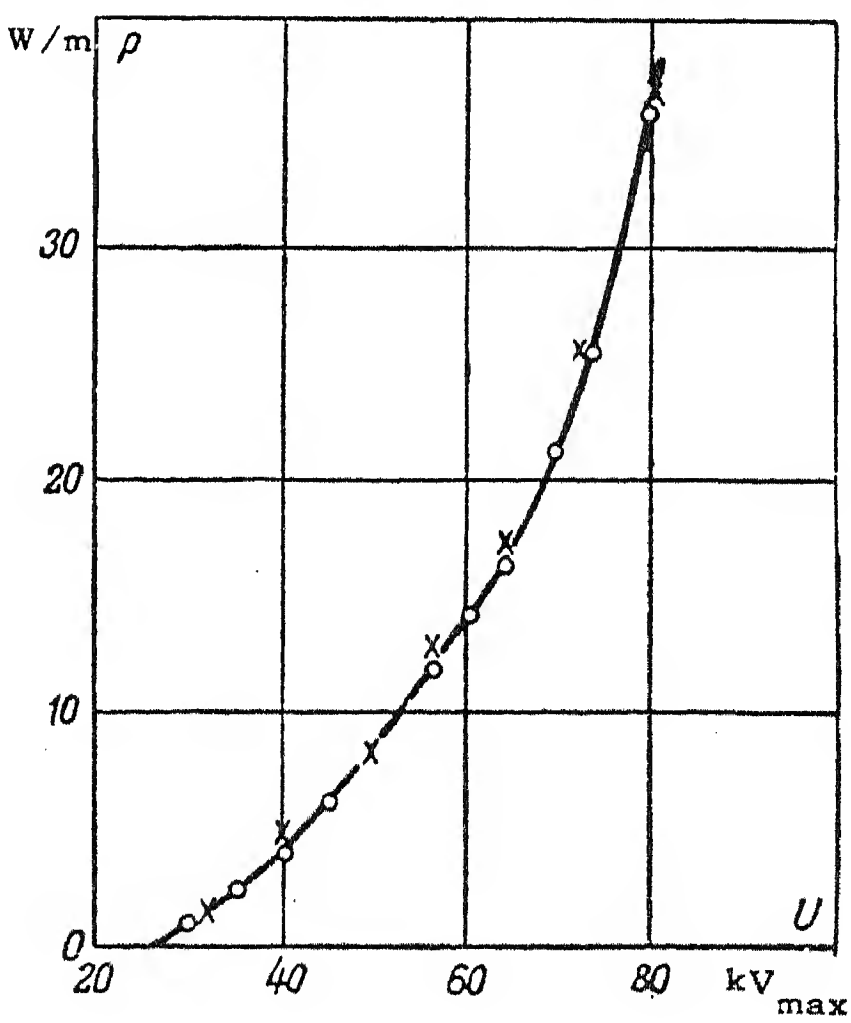

FIG. 8.

example, the distribution of losses along the conductor span, the measurement of charges, etc.

REFERENCES

1. M.I. Mikhailov; *The protection of communication lines. Svyaz'izdat* (1939).
2. H.I. Ryan and H.H. Henline; *The hysteresis character of corona formation. Trans. Amer. Inst. Elect. Engrs.* 43 (1924).

ANALYSIS OF THE STATIC STABILITY OF COMPLEX POWER SYSTEMS BY ELECTRONIC COMPUTERS*

L.V. TSUKERNIK and N.A. KACHANOVA

(Received 7 January 1957)

In the lay-out of installations for the automatic control of the operating conditions of power systems, particularly having regard to their interconnection and the erection of long-distance transmission systems, stability investigations have to be carried out very thoroughly; this refers particularly to the methods of preventing "hunting" under certain operating conditions of the system and as an effect of a possible variation of the system parameters. For such an analysis electronic computers can be used with great advantage.

It is obvious that this has not to be understood in the sense of a preference of electronic digital computers to network analysers which are very suitable indeed for the solution of such problems.

Principles of programming stability calculations

The problem of analysing the steady-state stability of a complex, automatically regulated power system may be divided into the following main stages:

1) Calculation of the coefficients of the characteristic equation of the system;

2) Calculation of the stability criteria;

3) Determination of the limits of the stability range in the space of the given parameters.

The calculation of the coefficients of the characteristic equation is preparatory, but a very significant and a difficult part of the work. It is convenient to represent the equations of the disturbed movement of the power system in matrix form, after which it is easy to obtain an algorithm for programming. The elements of the initial matrices are determined directly from the data of the usual electrical calculation of the initial conditions of the power system and from the parameters of the machines and automatic regulators.

The writing-down of the equations of the disturbed movement of the power

* *Elektrichestvo* No.7, 39–45, 1957 [Reprint Order No.EL 36].

system, the transformation into matrix form and the method of finding an algorithm for programming were described in detail in special papers [1 and 2]. We only note here that the programme of the calculations on an electronic digital computer comprises the development of the characteristic determinant, whose order equals the number of stations in the equivalent circuit used and whose elements are operator polynominals with real coefficients.

The calculation of the stability criteria will preferably follow a programme corresponding to Routh's well-known algorithm [3] because having thus obtained a sequence (recurrence) of simple arithmatical operations remaining equal for characteristic equations of any order. In this respect stability criteria in the form of Hurwitz determinants [3] are less suitable for programming.

However, in analysing the stability of systems with automatic regulation it is desirable not only to test the stability under given conditions but above all, to clarify the effect of various factors (the parameters of the automatic regulators, parameters of the main equipment, etc), for which it is necessary to determine the limits of the stability range in the space of the parameters of interest for the analysis. It is most convenient to use for the solution of this problem two-dimensional representation as functions of two selected parameters. Series of such diagrams obtained by varying the other parameters, the influence of which we want to investigate, may be collected to form an "album of stability ranges".

The determination of the limits of a stability range in the plane of the given parameters is programmed by using "logical" operations to be carried out on an electronic digital computer, with systematic use of the calculation of Routh's criterion as a "sub-programme". The scheme of the programme is as follows.

We feed into the machine as initial data the coefficients of the characteristic equation, represented as function of two parameters, for example the coefficients of the regulation of the excitation of the generators of the power system. In the automatic mechanical calculation process these parameters are given successive number of numerical values with a fairly small numerical difference (step). For each pair of values Routh's criterion is calculated continuously. Simultaneously the change of sign of Routh's criterion is automatically checked. As a result we obtain from the machine pairs of values of the parameters varied for the beginning and end of the interval in which the criterion changes sign. These values are the limiting coordinates between which the required boundary or limit of the stability range exists. The determination of the distribution of the stability and instability ranges with respect to this limit is also carried out on the basis of the calculations of Routh's criterion mentioned above.

This method of determining the limit of the stability range is much more convenient for programming than the well-known method of D-resolution [3]. For a non-linear relation between the coefficients of the characteristic equation and the parameters in the plane of which the *D*-resolution is carried out, the use of the method of *D*-resolution meets, in some cases, very great difficulties. The

calculation of the points of the limit of the stability range in the plane of two parameters (k' and k'') for one of the existing varients of the programme is made clear (Fig.1). We mark up first the extreme values of the parameters k' and k'', determining the sides of the rectangle $ABCD$ inside which we require to find the limit of the stability range. In general, we have a fair idea of the sign and order of the quantity or of realisable values k_a', k_b' and k_a'', k_b'' (Fig.1); if not, they are marked arbitrarily. Also we consider possible limitations of the values k', k'', related to the condition that all the coefficients of the characteristic equation should be positive. The magnitude of the computing interval along the axes k', k'' is then chosen.

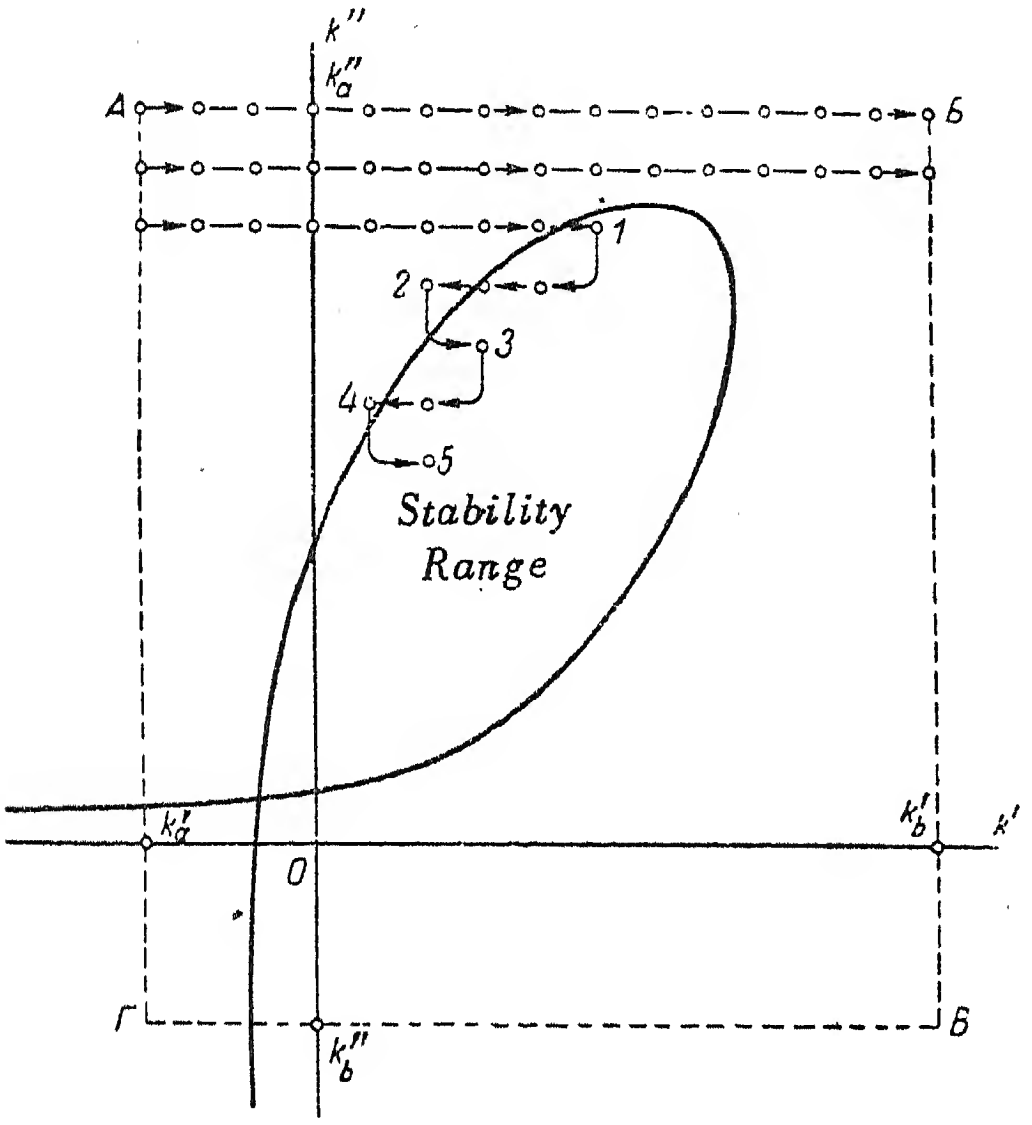

FIG.1. Scheme of the programme of tracing the boundary of the stability range (only the points indicated by the numbers in order are printed).

The calculation may be started at any point, e.g. at A. For this point the machine computes Routh's criterion storing (memorising) the result, without issuing (printing) it from the machine. Then a computing step is made in the direction of k', Routh's criterion computed again, and the result compared with the preceding one. If the sign of the criterion did not change a new computing step is made, etc., not if the sign of the criterion changed, i.e. if the limit of the stability range was over stepped, the machine prints the coordinates of the point considered (k', k''). This fixes point *1* (Fig.1).

Hereafter, the machine begins to follow the limit automatically. For this purpose, it makes twice a computing step in the direction perpendicular to the previous one, and calculations of Routh's criterion in the inverse direction of the original one, so long as the sign of the criterion changes. The coordinates of point 2 are then printed, this fixing the first interval $1-2$ through which the required limit passes. The calculation then proceeds similarly.

If the extreme values of k' are reached in the calculation without change of sign of Routh's criterion, the machine begins to calculate again in the same direction of k', moving through the computing interval along the side AD of the rectangle (Fig.1). If the limit of the range is not found within the rectangle $ABCD$, the computing interval may be reduced sufficiently to verify whether or not the stability range may not be found within a rectangle with sides equal to the original computing interval (for sake of clarity the computing interval was made very large in Fig.1).

The described scheme of a "tracking" programme was evolved by the Mathematical Institute of the USSR Academy of Science [4] for the purpose of providing a possibility of continuous outlining of the boundaries of a stability range of closed configuration.

By grouping the parameters in the plane of which the limit of the stability range is tracked, in pairs, and also by successful variation of other initial data we can obtain the "album of stability ranges" mentioned above.

Calculation of the steady-state stability of a power system

In 1954–1956 the Institute of Electrical Engineering and Mathematics of the Ukrainian Federal Republic Academy of Science carried out a number of calculations of the stability and electro-mechanical transient process of the transmission system Kuibyshev GES – Moscow (on instructions of the technical administration of the Ministry of Power Stations) with an electronic computer. The present communication will give a brief outline of the content of the calculations of the steady-state stability*.

Three types of automatic regulation of the excitation of the generators of the Kuibyshev GES were considered (*Cf.* Appendix):-

1) According to deviations of voltage and current and also according to the first and second derivatives of the current;

2) According to deviations of voltage and current, and also to slip and acceleration relative to an axis rotating at the synchronous speed of normal operation;

3) According to deviations of voltage and current, viz. compounding ($T_I = 0$), and delaying electromagnetic voltage corrector ($T_U = 3$ sec), connected to the main or booster exciter.

In considering the first type of regulation the time-lag of the generator ($T_{go} = 5.5$ sec), of the booster exciter ($T_{ex} = 0.12$ sec), the regulator ($T_{reg} = 0.1$ sec) and the presence of a rigid negative feedback of the exciter voltage was considered in the structural diagram. This type of automatic excitation control corresponds basically to a strong-action regulator with which the majority of the generators of the Kuibyshev GES is to be provided.

The second type of excitation control is analogous to the first and differs from the "strong action" regulator responding to angle and first and second

* All the calculations were carried out in relative units ($U_{bas} = 400$ kV, $P_{bas} = 1150$ MW, time in radians). The computer calculates with six and prints the results in five significant digits. Consequently the accuracy of the calculation depends on the accuracy of the data fed to the computer. All the calculations on the computer were duplicated, control variance being calculated after recording the programme. The programming of typical problems took about 10–20 hr and the calculation of one curve 15–45 mins.

derivatives of the angle, designed by the Central Electrical Research Laboratory of the Ministry of Power Stations by the fact that there is no necessity of telemetering the angle in this regulator. The slip and acceleration relative to an axis rotating at a synchronous speed of the initial operating conditions may be measured by a special instrument with a memory-element.

The automatic control of the third type was installed on the first generator of the Kuibyshev GES as main regulation, and on the following generators as stand-by. by. The possibility of a control according to individual generator currents was investigated. The Kuibyshev GES was in this investigation represented by two equivalent controlled generators (Fig.2, circuit 1). The characteristic of the system according to this circuit is of the tenth order. The parameters of the regulation according to current (k) or to voltage shown, or to the first and second derivatives (k', k''), in the plane of which the limit of the stability range was determined, are contained in most of the coefficients of the characteristic equation in a higher than the first degree, viz. as squares and products. In such cases a D-decomposition by the ordinary method involves very laborious calculations.

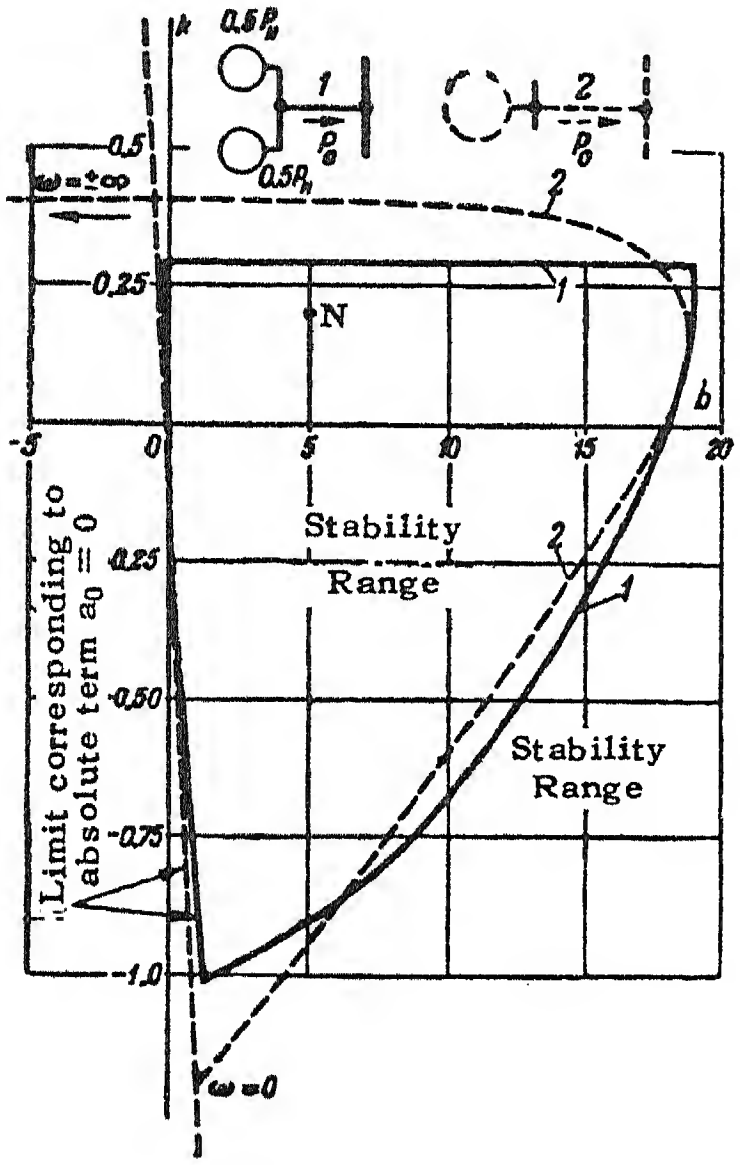

FIG.2. Stability ranges ($P_0 = 1.0$). For representations of the Kuibyshev GES by two equivalent generators (1) and one equivalent generator (group control) (2).

The calculations on the electronic computer showed that there is no stability range for the first type of automatic excitation control, which was also confirmed by analytic calculation and agrees with the results of tests on the electro-dynamic model of the Molotov Institute for Electrical Engineering [5]. It follows that for this type group regulation is required, for example, based on the mean current of generators working in parallel. The stability ranges for group regulation are shown in Fig.3 a and 4 a below.

For an automatic control of the third type a stability range exists, as is shown in Fig. 2 (curve 1). The same figure shows the stability range for group regulation (circuit 2, curve 2). Point N corresponds to the normal setting of the regulator. A comparison shows that group regulation increases the stability margin. The calculations did not consider the mechanical damping of the machine and, consequently, the actual stability margin will be slightly larger.

The margin of stability according to power transmitted was determined and the possibility of cumulative hunting in various loadings of the transmission

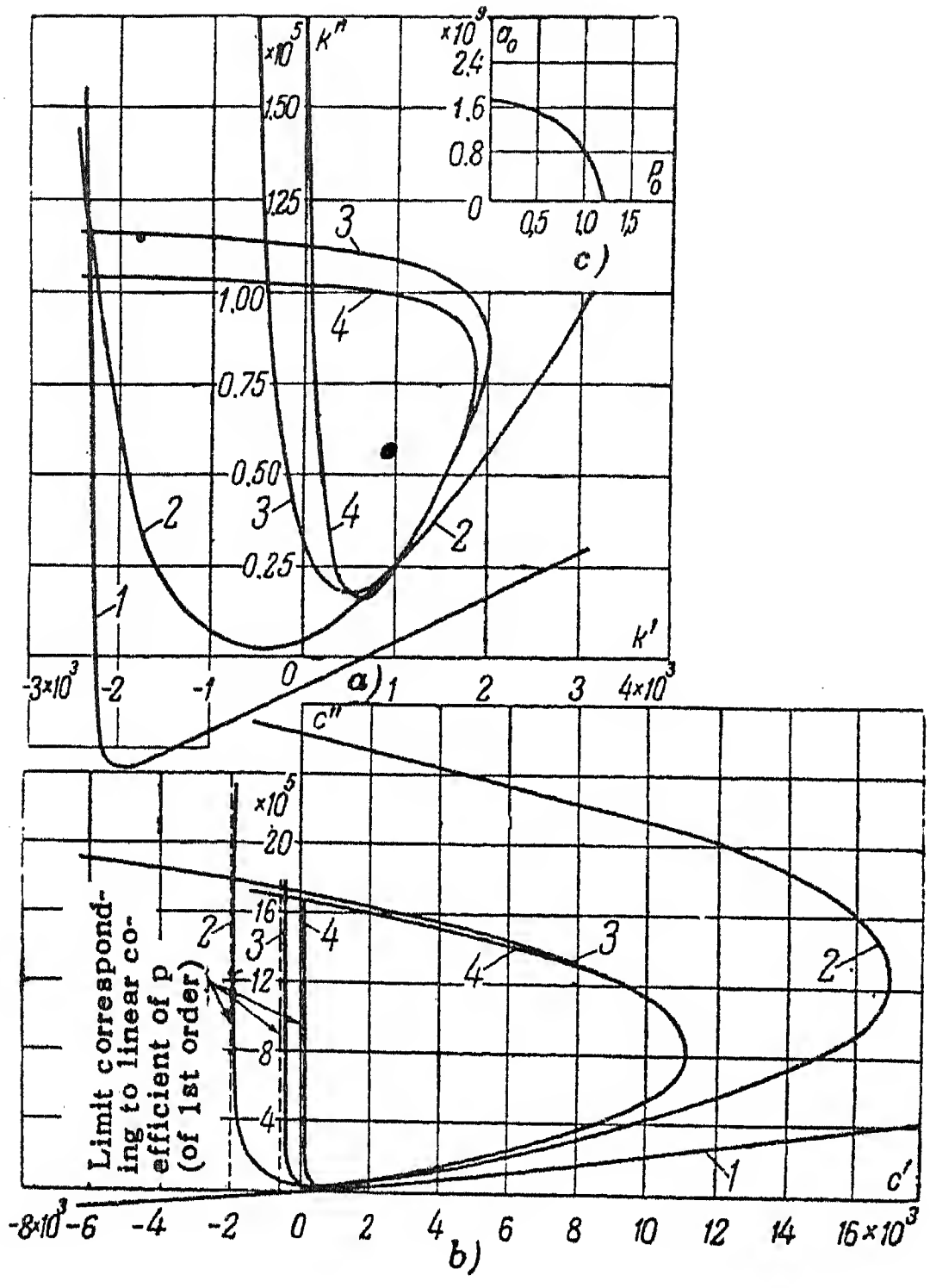

FIG.3. Stability ranges ($k = 0.2$, $b = 5.0$). a) Automatic excitation control of first type; b) Automatic excitation control of second type; c) Graph of the variation of a_0 vs. P. $1 - P_0 = 0$; $2 - P_0 = 0.5$; $3 - P_0 = 1.0$; $4 - P_0 = 1.1$

system was considered.*

For this purpose series of stability ranges were calculated for automatic excitation control of the first and second types (group regulation according to current) and a variation of a power transmitted from 0 to 1.1 for the case that there is no series compensation and the transmitting capacity of the line (ideal power limit), 1.15.

For comparison we entered in Fig.3 the results of the stability ranges in the plane of the coefficients of regulation according to slip and acceleration c', c''. The graph of Fig.3 shows that in both cases the power transmitted may be raised to the value of the transmitted capacity of the line, if the coefficients of the regulations are within the limits of the common stability ranges.

We may suppose that for equal regulation coefficients (in relative units) the design parameters of regulators of the first and second types may be approximately equal. The difference will consist only in the input elements, viz. in the case of a regulator of the second type an angle-measuring element in a memory-element. We may, therefore, conclude that an automatic regulation of the second type has, according to the operating characteristics determined by the graphs of Fig.3 advantages over a regulation of the first type because in the latter type the ranges of the permissible regulation coefficients are considerably increased. Also for load changes of the transmission systems the common part of the stability ranges for regulation by slip and acceleration becomes greater than for regulation according to derivatives of the current; for example, Fig.3 shows that in the first case for the transition from $P_0 = 1.0$ to P_0 1.1 the common part of the stability range 4

* The calculation relating to the measures to be taken to prevent self-excitation and cumulative hunting on no-load and at small loads of the transmission system are not included in the present, because they are not essential where two limiting power transmitted is concerned and mostly to be carried out by simpler methods.

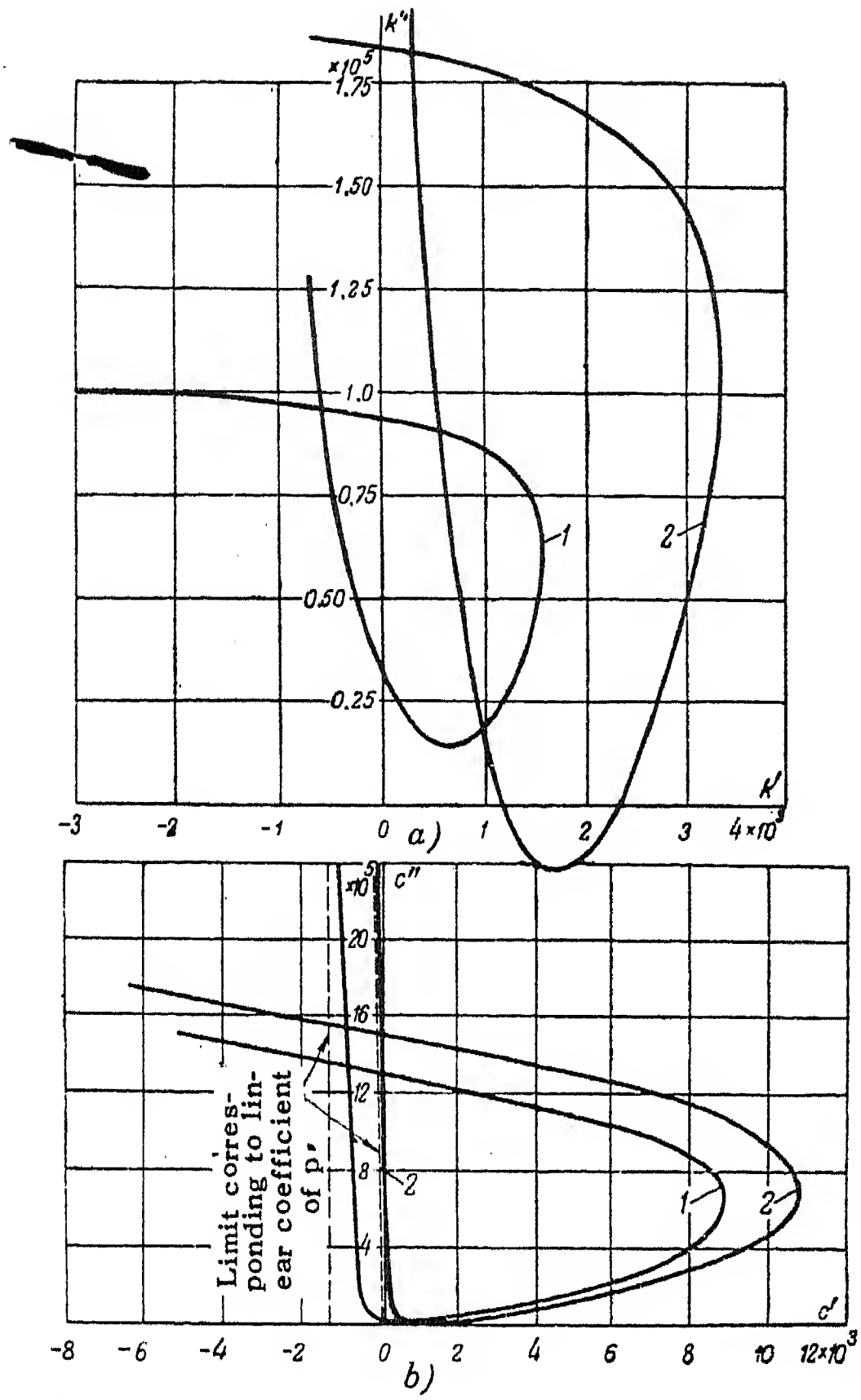

FIG.4. Stability ranges of: double-circuit transmission system ($P_0 = 1.0$; $k = 0.2$; $b = 25.0$). a) Automatic control of the first type: b) Automatic control of the second type. 1 – All the sections of both circuits of the line and series and parallel compensation gears are connected; 2 – One circuit of the head section of the line and parallel compensation gears are connected.

amounts to about 95 per cent of range 3, but in the second only to about 70 per cent.

From the position of the origin of the coordinates relative to the stability ranges (Fig.3) we may draw the conclusion that $P_0 > 0.4$ and in regulation without derivates of the operational parameters no stability can be achieved.

The possibility of cumulative hunting subsequent to alteration of the circuit of the transmission system was assessed. Fig.4 represents the stability ranges for a double-circuit line, calculated for $P_0 = 1.0$ and the same types of automatic excitation control as the stability ranges in Fig.3. The curves *1* refer to the case where all the sections of both circuits are connected as well as series and parallel compensation gears, and the curves 2 to the case where the circuit of the head section of the transmission and compensating gear are disconnected. In Fig.4 we see that with the regulation of the second type the coinciding part of the stability ranges is greater than for the regulation of the first type. Therefore, it is much easier to assure steady operation of the transmission system for possible changes in its circuits with regulation by slip and acceleration without readjustment of the regulation. This agrees very well with the results of tests on the dynamic model of the Molotov Institute of Electrical Engineering [5].

The curves of Fig.4 also show that the stability ranges of the compensated line (curves 1) are under otherwise equal conditions much smaller than the stability ranges of the uncompensated line. This indicates that in the presence of compensation the danger of cumulative hunting is greater. This fact must be considered in a project design and an actual operation.

However, we have to bear in mind not only a margin of stability with respect to cumulative hunting, but also as regards the "aperiodic limit". It is quite obvious that in the example considered the transmitting capacity and the aperiodic limit of the system stability are much higher for a compensated than for an uncompensated line. In the first case, the transmitted capacity of the line including the transformers at the far end, is $P_{max} = 1.87$, in the second $P_{max} = 1.03$. Consequently, when analysing the variation of the stability ranges for different configurations, we must extend our analysis to the character of the variation of the absolute term a_0 of the characteristic equation of the system (Fig.3 c) or else compare the values of the transmitting capacity of the line.

The analysis of the effect of the coefficient of the regulation according to the voltage and current deviations on the stability when "strong-action" is used, was carried out by direct comparison of a series of calculations, as shown, e.g. in Fig.5. We conclude that a variation of the coefficient k within wide limits has but a small influence on the stability ranges in the plane of k' and k'' (Fig.5 a) whereas a variation of the coefficient b has a more marked effect (Fig.5 b). If we bear in mind that a minor instability of the coefficients k and b is still possible after the adjustment of the regulator, there is no reason to assume that this instability may lead to hunting of the system. A simultaneous increase of the coefficients k and b (Fig.5 c) will slightly reduce the variation of the stability range due to an increase of the coefficient b only.

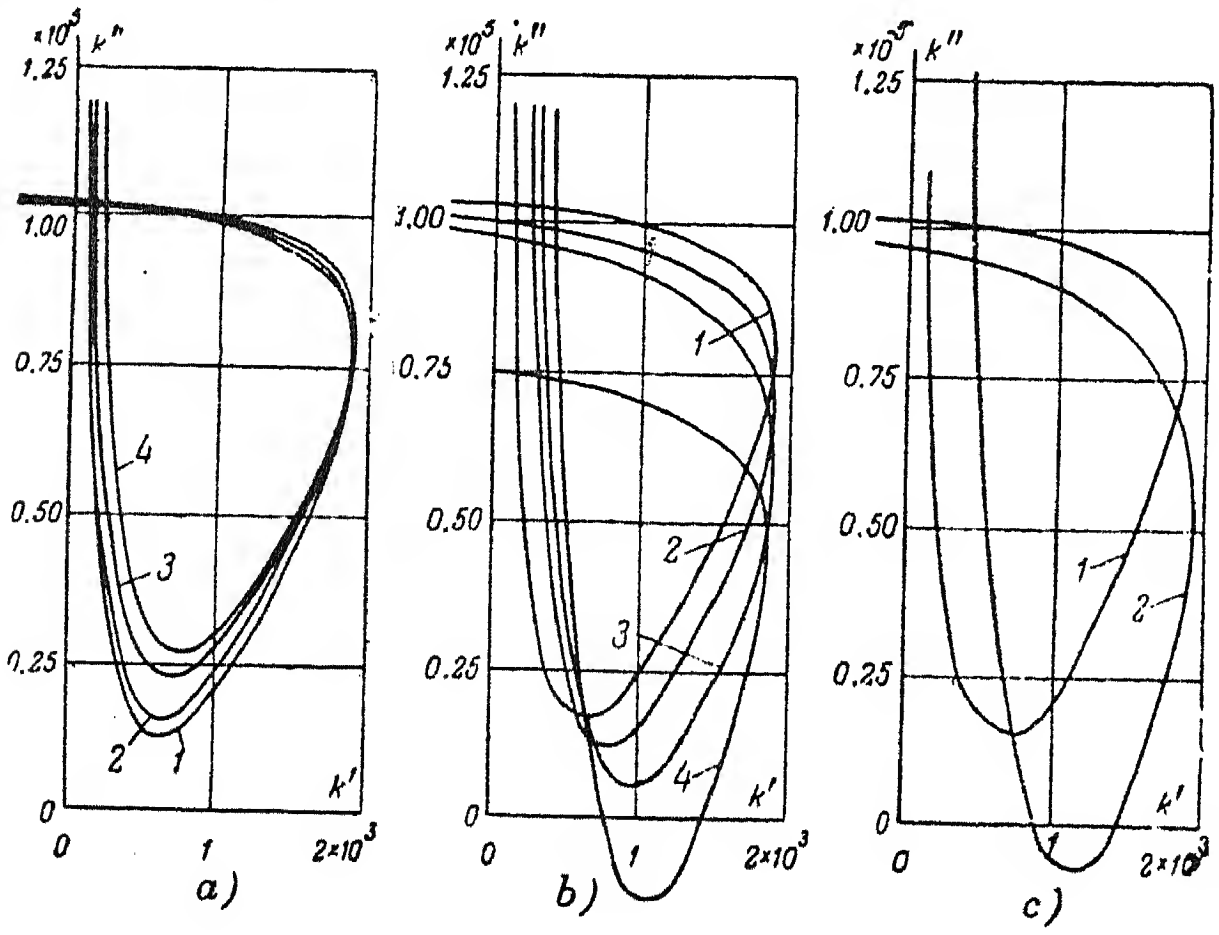

FIG.5. Stability ranges ($P_0 = 1.1$). a) When coefficient of regulation varies with the current ($b = 5$): $1 - k = 0.1$; $2 - k = 0.2$; $3 - k = 0.6$; $4 - k = 1.0$. b) When coefficient of regulation varies with the voltage ($k = 0.2$); $1 - b = 5$; $2 - b = 10$; $3 - b = 15$; c) When coefficients k and b vary simultaneously: $1 - k = 0.2$, $b = 5$; $2 - k = 1.0$, $b = 2.5$.

An increase of the coefficients k and b entails an increase of the absolute term of the characteristic equation and, consequently, an increase of the margin of stability with respect to the aperiodic limit.

The stability ranges in the plane of the coefficients of regulation according to deviations of voltage and current, were calculated, e.g. for $k' =$ var and $k'' =$ const. as shown in Fig.6. Two straight lines correspond to each of the ranges, viz. the line $a_0 = f(b, k) = 0$ and the line which with increasing k' turns anticlockwise from position *1* into position 5; during this rotation the point of inter-

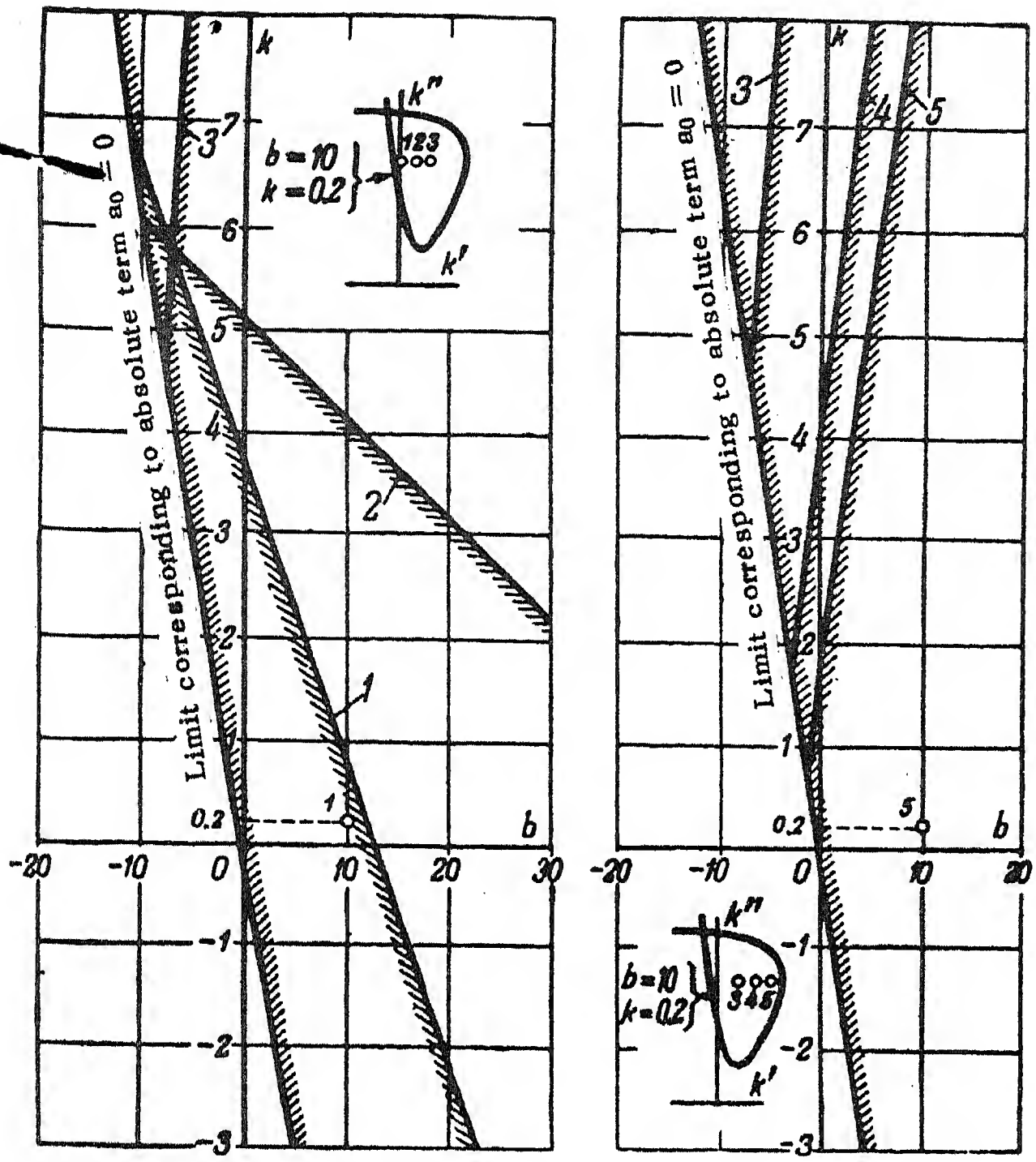

FIG.6. Stability ranges ($P_0 = 1.0$, $k'' = 0.75 \times 10^5$). $1 - k' = 0$; $2 - k' = 0.4 \times 10^5$; $3 - k' = 0.75 \times 10^5$; $4 - k' = 1.6 \times 10^5$; $5 - k' = 1.8 \times 10^5$.

section with the straight line $a_0 = 0$ moves downwards.

For a clear demonstration we entered in Fig.6 the stability range in the plane of k' and k'' on a reduced scale (for $b = 10$ and $k = 0.2$), in which we indicated the intersection studied. Considering for example, point 5 near the limit of the stability range plotted in the plane of the parameters k' and k'', we find that on the graph plotted in the plane of the parameters b and k the proximity of the limit of the stability range is not noticeable. This is as could be expected, for the reason that the stability ranges vary only slightly with a variation of the parameters b and k within fairly wide limits (Fig. 5).

We may, therefore, conclude that the fundamental analysis is better carried out by plotting the stability ranges in the plane of the parameters of regulation according to derivatives than in the plane of parameters of regulation according to deviations.

Stability calculations were carried out for transmission systems with intermediate synchronous condenser, on the assumption that the synchronous condenser of 375 MVA rating is erected in the sectionalizing substation of the transmission system Kuibyshev GES - Moscow and that the line has no series compensation. When the excitation of the synchronous condenser was controlled by a regulator of the first type, no stability range was found even in the presence of a considerable mechanical damping torque ($D = 2$). With a regulation of the third type, supplemented by regulation according to slip and acceleration, stability ranges were obtained (Fig.7) for three cases, viz. $D = 0$; 1; 2. The curves of Fig.7 show the favourable influence of the mechanical damping torque, which is often neglected in calculations, in the stability.

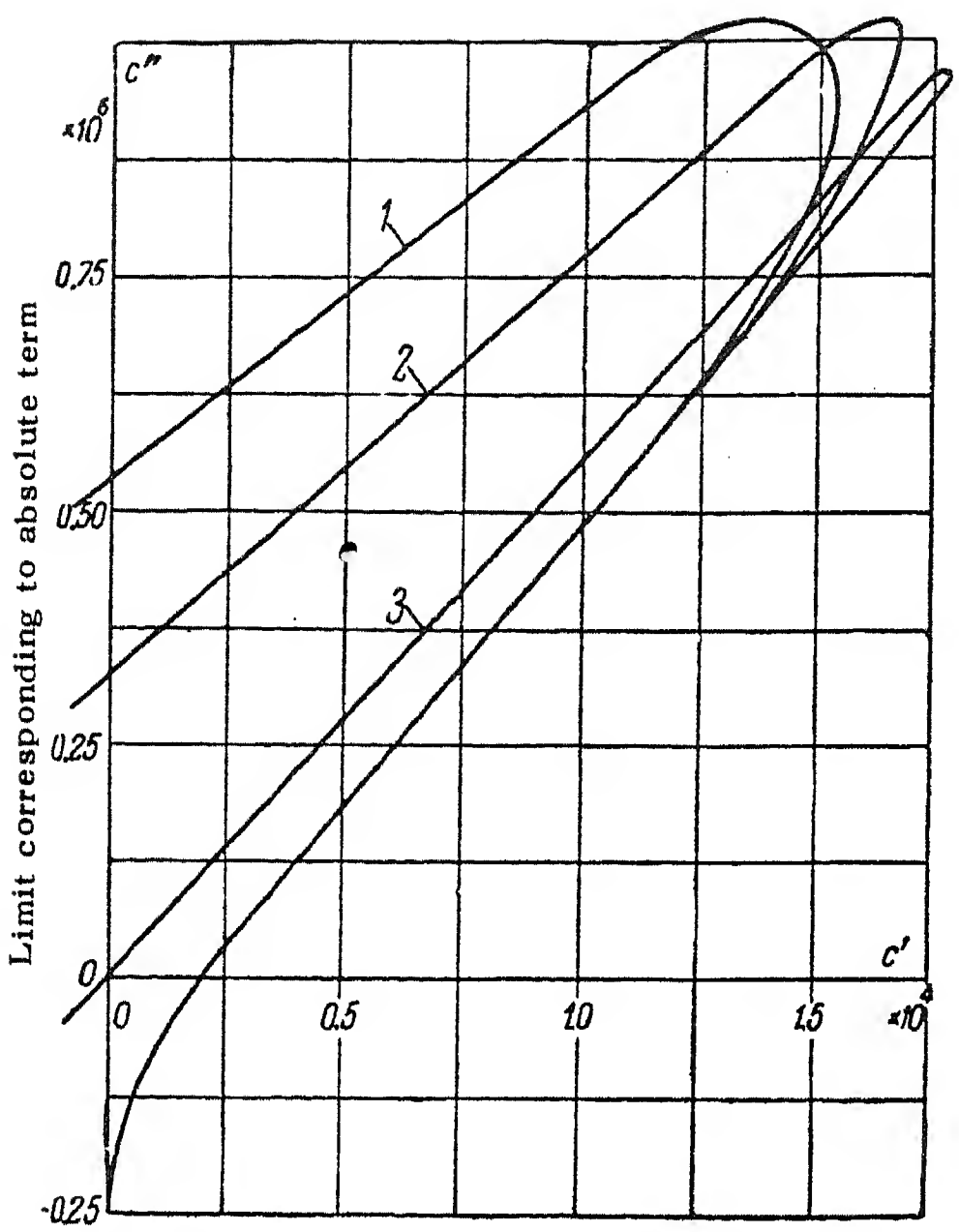

FIG.7. Stability ranges for a transmission system with intermediate synchronous condenser: ($P_0 = 1.0$, $k = 0.12$, $b = 25.0$). Damping torque of condenser: $1 - D = 2.0$; $2 - D = 1.0$; $3 - D = 0$. Stability range bounded by each of the curves 1,2 and 3.

Direct comparison of the results of calculations of typical variants enables us to examine the permissibility of some simplifications in the stability calculations.

With automatic excitation control of the generator groups of the Kuibyshev GES we may neglect the salient-pole character of the generators (Fig.8 a).

The replacement of the receiving system by infinitely powerful busbars does not alter the stability ranges substantially (within the range of positive values of the coefficients of regulation according to derivatives) by comparison with its replacement by an equivalent power state and load (Fig.8 b). In all the cases investigated the stability ranges were inside those obtained for a system with fixed angle coordinates. That means that the fixing of the angles corresponds to necessary, but not sufficient, conditions of stability [1 and 2]. These simplified calculations may sometimes by useful for preliminary assessment of the schemes (rectangle *ABCD*), and for the elimination of definitely unsatisfactory variants. In comparative calculations, we may neglect the time constant of the booster exciter. When the negative feedback of the exciter voltage is weakened in the calculations, we assumed a weakening by a factor (Fig.8). However, it should be borne in mind that for operating conditions near the limit of the stability range this simplification may introduce a considerable error whether by exaggerating or by unduly reducing the stability range (Fig.8 c).

Appendix

Generalised Structural Diagram of a Composite System Considering Automatic Excitation Control of the Synchronous Machines

The transmission functions: of the exciter $\overset{*}{F}_{ex}$, of its feedback $\overset{*}{F}_{fb}$, of the regulation according to angle deviation $\overset{*}{F}_{\delta}$, of the regulation according to deviation of voltage F_v and according to deviation of current F_I [3];

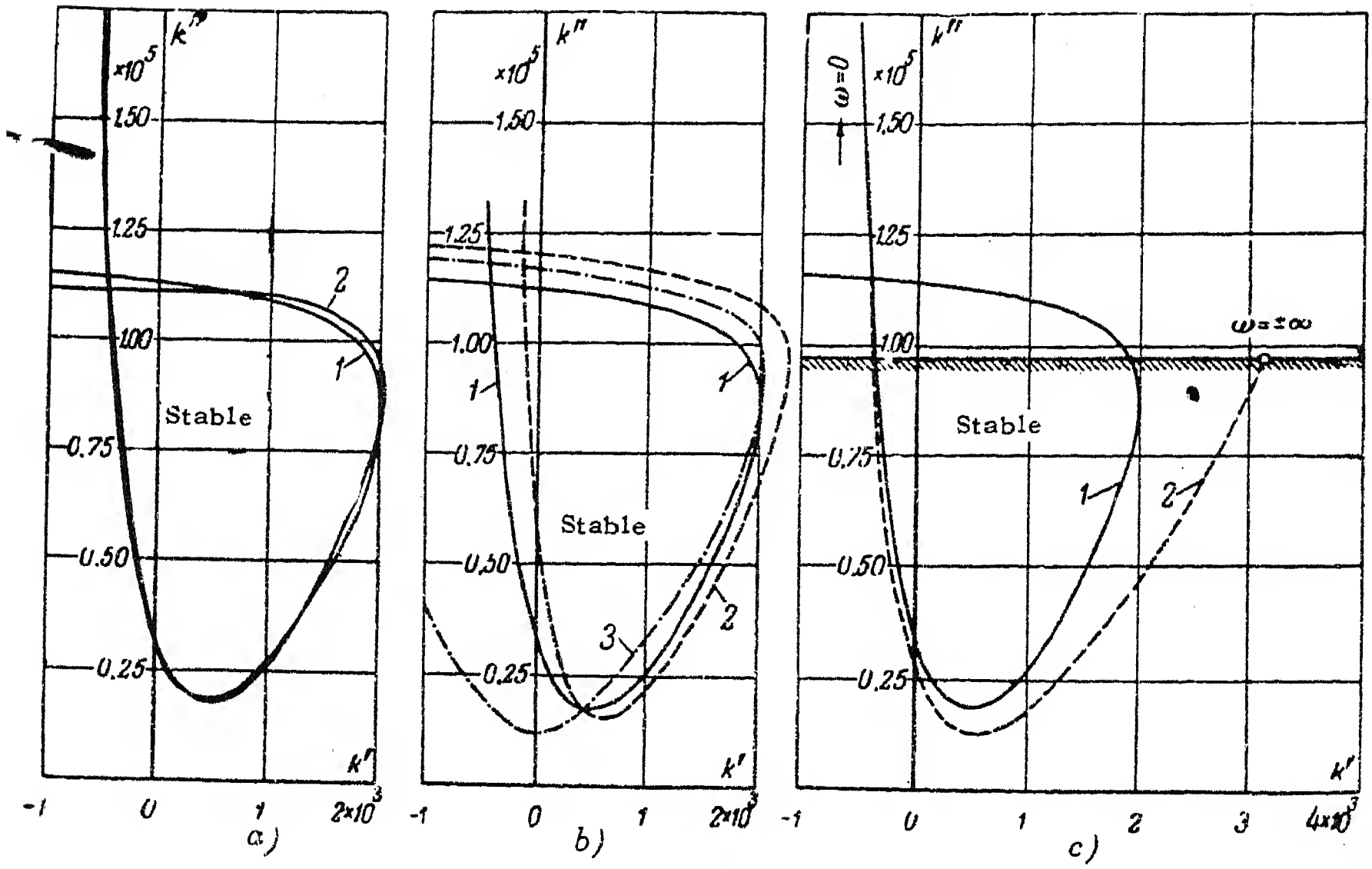

FIG.8, Stability range ($P_0 = 1.0$, automatic control of the first type: $k = 1.2$; $b = 5$). a) 1 – Considering the salient-pole generators of the Kuibyshev GES; 2 – Without considering the salient-pole character. b) 1 – At the end of the line busbars of infinite power; 2 – Receiving system represented by a load and an equivalent station for which $E' = \text{const}$ and $M = \infty$. 3 – The receiving system is represented by a load and an equivalent station for which $E' = \text{const}$ $M \neq \infty$. c) 1 – $T_{ex} = 0.12$ sec; 2 – $T_{ex} = 0$.

For automatic regulation of the excitation of the first type,

$$\overset{*}{F}_{ex} = \frac{1}{1 + T_{ex}\, p}; \quad \overset{*}{F}_{fb} = -\, d; \quad \overset{*}{F}_{\delta} = 0;$$

$$\overset{*}{F}_{v} = \frac{-\, b}{1 + T_p p}; \qquad \overset{*}{F}_{I} = \frac{k + k' p + k'' p^2}{1 + T_p\, p}.$$

For automatic regulation of the excitation of the second type,

$$\overset{*}{F}_{ex} = \frac{1}{1 + T_{ex}\, p}; \quad \overset{*}{F}_{fb} = -\, d; \quad \overset{*}{F}_{\delta} = \frac{c' p + c'' p^2}{T_p\, p};$$

$$\overset{*}{F}_{U} = \frac{-\, b}{1 + T_p\, p}; \quad \overset{*}{F}_{I} = \frac{k}{1 + T_p\, p}.$$

For automatic regulation of the excitation of the third type,

$$\overset{*}{F}_{ex} = \frac{1}{1 + T_{ex}\, p}; \quad \overset{*}{F}_{fb} = 0; \quad \overset{*}{F}_{\delta} = 0;$$

$$\overset{*}{F}_u = \frac{-b}{1 + T_u p}; \quad \overset{*}{F}_I = k.$$

For the synchronous machines, the number of which may be in general n, we considered additionally to the equations of the electro-magnetic transient process in the field winding, represented in Fig.9, the equation of the mechanical movement,

$$(Mp^2 + Dp)\,\Delta\delta = -\Delta p\,.$$

The system connecting the synchronous machines is represented by self and mutual impedances.

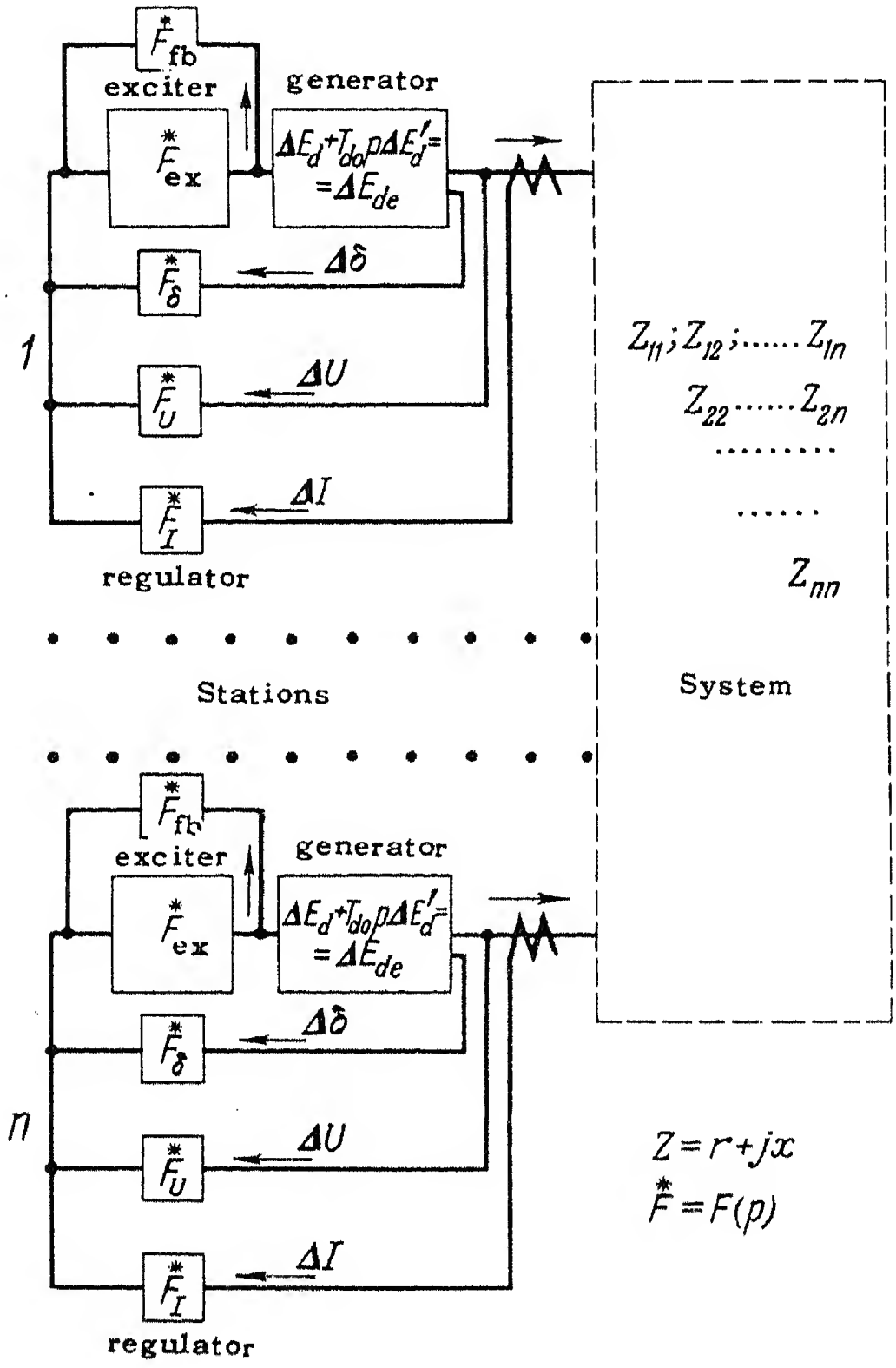

FIG.9. Generalised structural diagram of a power system, considering the automatic excitation control of the synchronous machines.

REFERENCES

1. L.V. Tsukernik; *Differential equations of Disturbed Operation of a Composite Power System for Analysing its Steady-State Stability.* I zv. Otn. A.N.S.S.S.R., 3 (1956).
2. L.V. Tsukernik; *Generalised Equations of Dynamics of a Composite Power System and Use of Electronic Computer for Analysing its Stability. Automatika i Telemekhanika,* 1 (1957).
3. A.A. Voronov; *Elements of the Theory of Automatic Regulation.* 2nd Ed., *Voengiz* (1954).
4. V.S. Korolyuk and D.L. Yushchenko; *Determination of Equipotential Lines of Functions of Two Variables on High-Speed Electronic Computers. Monograph Problems of the Design of High-Speed Computers,* 2, *Akad. Nauk Ukr. SSR* (1955).
5. V.A. Venikov and I.V. Litkens; *The effect of the Excitation Control on the Transmitting Capacity of Long Transmission Systems. Elektrichestvo,* No.11 (1955).

A PRACTICAL METHOD FOR DESIGNING RELAYS WITH RECTIFIERS*

G.G. GIMOYAN

(Received 3 December 1956)

Recent developments in relay engineering are characterized by rapid spreading of the use of semiconductor-type rectifiers in protection and automatic control systems. Design and construction of relays so equipped are still complicated by the fact that they constitute non-linear dipoles for the a.c. circuit. For example, single-coil relays or relays with two magnetically decoupled relays (such as balance relays) are represented in Fig. 1; relays with two inductively coupled and mutually opposing coils in Fig. 5b. There are still other circuits which, however, will not be considered in the present communication.

An analytical determination of the relations of the electrical quantities at input and output of the rectifiers used in these circuits requires involved transcendental equations to be solved. For this reason it is preferable to represent them for practical calculations by linear dipoles (Fig. 7a), obeying Ohm's law.

The determination of the correction factors required for such a transformation is the object of the present paper.

This determination is carried out by the method of linearization [1]; assuming the voltage at the rectifier input as linear,† its current is resolved into harmonic components for each of which a separate equivalent circuit is drawn and the correction factors are found.

For practical calculations it is sufficient to consider the equivalent circuit for the first harmonic only, since the accuracy is sufficiently high and the error does not exceed 5-10 per cent [1-3].

Operation of rectifiers with single-coil relays

For ideal rectifier units and with an input voltage

$$u = \sqrt{2}\, U_1 \sin \theta$$
$$\theta = \omega t \qquad (1)$$

* *Elektrichestvo* No. 7, 50 – 53, 1957 [Reprint Order No. EL 37].

† Structure and parameters of the equivalent circuit depend on whether the rectifier works in conditions of sinusoidal current or voltage. The operation of the circuits in Fig. 1 and 4b is considered only for sinusoidal voltage, because in relay circuits the resistance of the supply is assumed small [3], to reduce consumption and increase the sensitivity of the arrangement.

where U_1 is the effective value of the fundamental (there being no other harmonic in this case) of the rectifier input, ω the angular frequency of the fundamental. The operation of the rectifier of the circuit of Fig. 1 may be in two different modes, for each of which the relationships between the instantaneous values of currents and voltages are different.

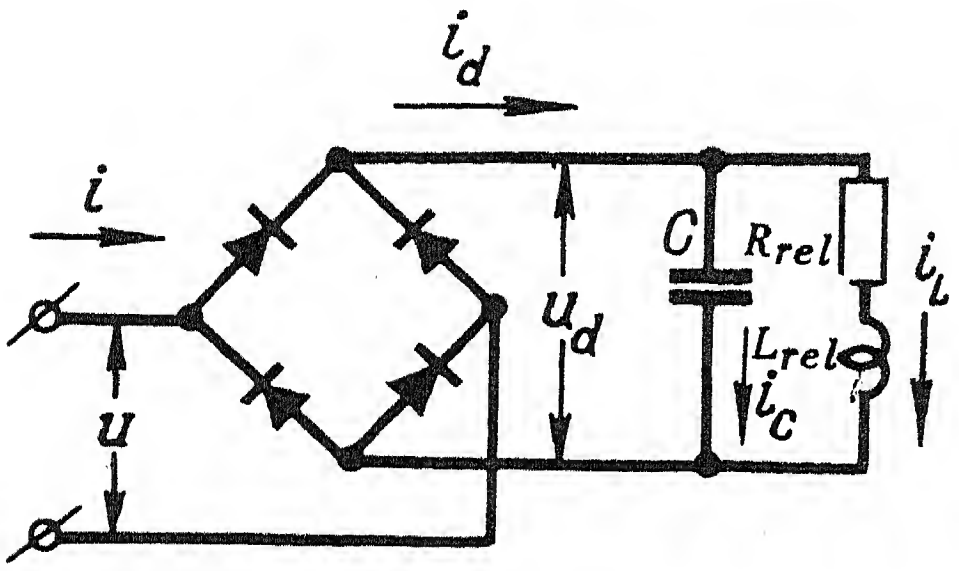

FIG. 1. Equivalent circuit or single-coil relay.

Since a capacitor is connected to the output of the rectifier, the rectified voltage never drops to zero owing to the charge of the capacitor. At the input side of the rectifier, however, the voltage varies sinusoidally and during certain fractions of the period it becomes very small (when changing its direction). During these fractions of the period the following relations hold

$$u_d > |u|;\ i = 0;\ i_d = 0 \qquad (2)$$

where u, i and u_d, i_d are the instantaneous values of voltage and current at input and output of the rectifier.

The mode of operation to which condition (2) applies is known in the literature as the R-state (in the absence of current) [1]. In this state the a.c. and d.c. circuits appear to be absolutely independent because they are separated by the rectifier bridge. According to the line-diagram of voltages and currents (Fig. 2) the circuit operates in the R-state when

$$\begin{aligned} &0 < \theta < \theta_1; \\ &\theta_2 < \theta < \pi + \theta_1; \\ &\pi + \theta_2 < \theta < 2\pi \end{aligned} \qquad (3)$$

When the absolute instantaneous value of the voltage at the rectifier input has reached the value of output voltage, the rectifier begins to conduct, this state being known in the literature as N-state, instead of the R-state.

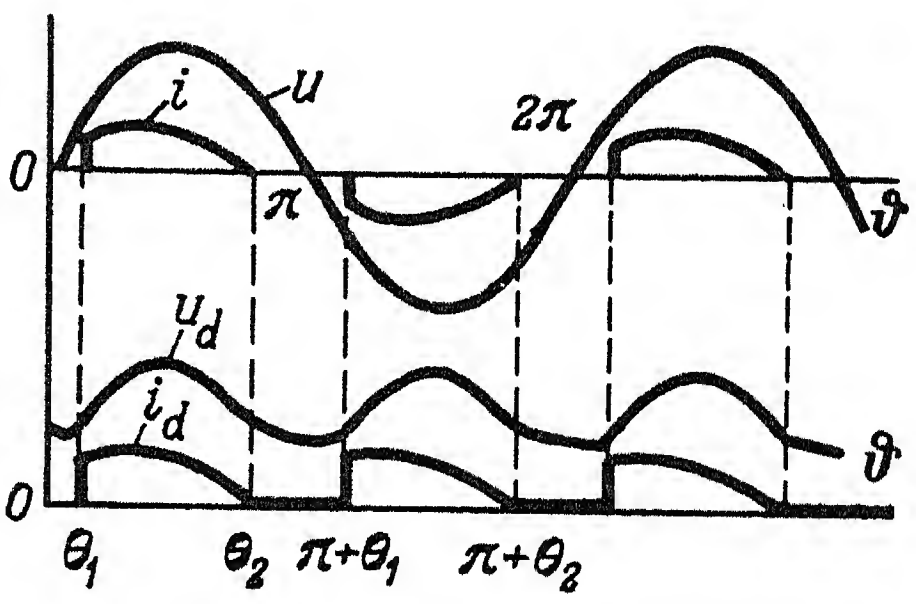

FIG. 2. Line diagrams of voltages and currents at rectifier input (u,i) and output (u_d, i_d).

In the N-state the following identities apply:

$$u_d = |u|\ ;\ i_d = |i|. \qquad (4)$$

The fractions of the period during which the rectifier operates in the N-state correspond to the time intervals

$$\theta_1 < \theta < \theta_2;\ \pi + \theta_1 < \theta < \pi + \theta_2 \qquad (5)$$

The coefficients of equivalent conductance and susceptance are determined by

the formulae

$$\gamma_1 = \frac{\sqrt{2}\,R_p}{2\pi U_1}\int_0^{2\pi} i \sin\vartheta d\vartheta; \tag{6}$$

$$\beta_1 = \frac{\sqrt{2}\,R_p}{2\pi U_1}\int_0^{2\pi} i \cos\vartheta d\vartheta. \tag{7}$$

The expressions under the integral sign in (6) and (7) are the instantaneous values of the input current of the rectifier, i, where the input voltage U_1 is given. The relation between the given quantities depends on the circuit parameters. Owing to the large number of unknowns (R_{rel}, L_{rel}, C) it is difficult to determine this relationship by the usual methods of circuit theory. To facilitate the solution of this problem it is useful to carry it out at first for the boundary conditions $R_{rel}/\omega L_{rel} = \infty$ and $R_{rel}/\omega L_{rel} = 0$, and then to find the required solution by comparing the results for the two limiting cases, so that we get an approximate solution for $0 > R_{rel}/\omega R_{rel}$.

The operation of the rectifier of Fig. 1 in the limiting case $R_{rel}/\omega L_{rel} = \infty$ is analysed in [1].

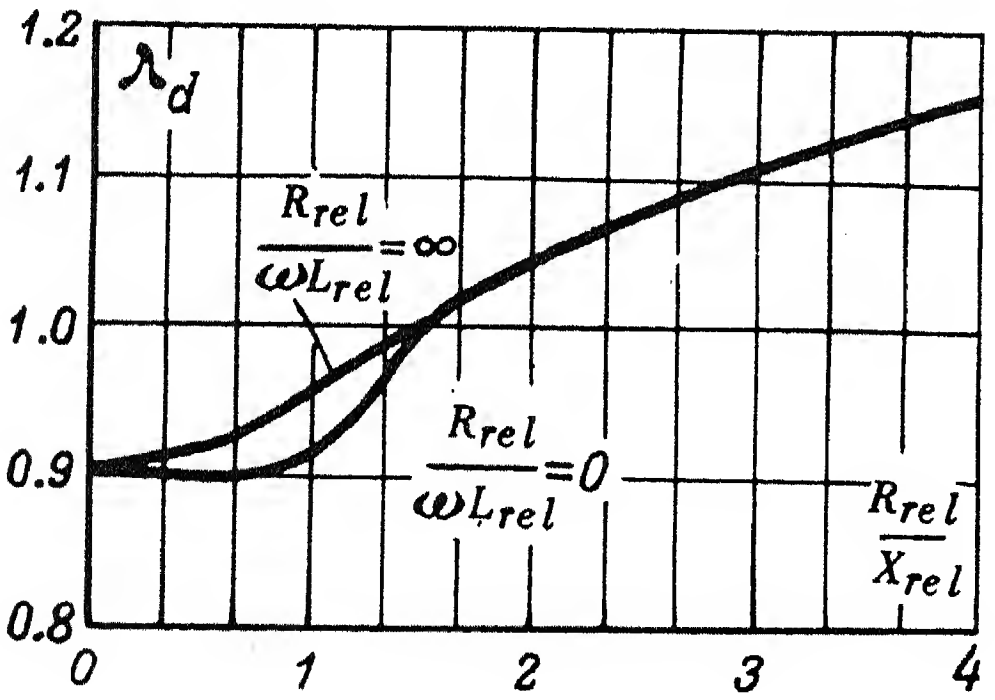

FIG. 3. Values of coefficients determining mean value of rectified voltage.

In the limiting case $R_{rel}/\omega L_{rel} = 0$ the steady-state current passing through the branch with resistance and inductance, i_L, practically remains constant during the period. Since under these conditions the current passing through the capacitive branch has no steady (d.c.) component, the current i_L is practically equal to the mean value of the current at the rectifier output, I_d. The instantaneous values of the output current of the rectifier are therefore determined by the following differential equations:-

in the R-state

$$\frac{1}{X_c}\cdot\frac{dU_d}{d\theta} + I_d = 0 \tag{8}$$

in the N-state

$$i_d = \frac{1}{X_c}\cdot\frac{dU_d}{d\theta} + I_d = \frac{\sqrt{2}\,U_1\cos\theta}{X_c} + \frac{U_d}{R_{rel}} \tag{9}$$

The commutation angles θ_1 and θ_2 and the coefficient of the constant voltage component may be found from (1), (8) and (9) as follows:

$$\theta_2 = \cos^{-1}(U_d X_c / \sqrt{2}\, U_1 R_{rel}); \tag{10}$$

$$\sin\theta_1 = \sin\theta_2 - (U_d X_c / \sqrt{2}\, U_1 R_{rel})\,(\pi + \theta_1 - \theta_2) \tag{11}$$

$$\lambda_d = U_d/U_1 = \frac{\sqrt{2}}{\pi}\{\cos\theta_1 - \cos\theta_2 + \sin(\pi + \theta_1 - \theta_2) - \\ - \frac{U_d}{\sqrt{2}\,U_1} \cdot \frac{X}{R_{rel}}\left[\frac{(\pi + \theta_1)^2 - \theta_2^2}{2} - \theta_2(\pi + \theta_1 - \theta_2)\right]\} \tag{12}$$

The quantities θ_1, θ_2 and λ_d as functions of the ratio X_c/R_{rel} are determined rapho-analytic solution of the last three equations [3].

The coefficients of the equivalent conductance γ, and susceptance β_1, respecy, are found from (6) and (7), when (9) is considered, thus,

$$\gamma_1 = \frac{1}{\pi}\left[\lambda_d(\cos\theta_1 - \cos\theta_2) + \left(\frac{R_{rel}}{X_c}\left(\frac{\cos 2\theta_1 - \cos 2\theta_2}{2}\right)\right]\right; \tag{13}$$

$$\beta_1 = \frac{1}{\pi}\left[\lambda_d(\sin\theta_2 - \sin\theta_1) + \frac{R_{rel}}{X_c}\left(\theta_2 - \theta_1 + \frac{\sin 2\theta_2 - \sin 2\theta_1}{2}\right)\right] \tag{14}$$

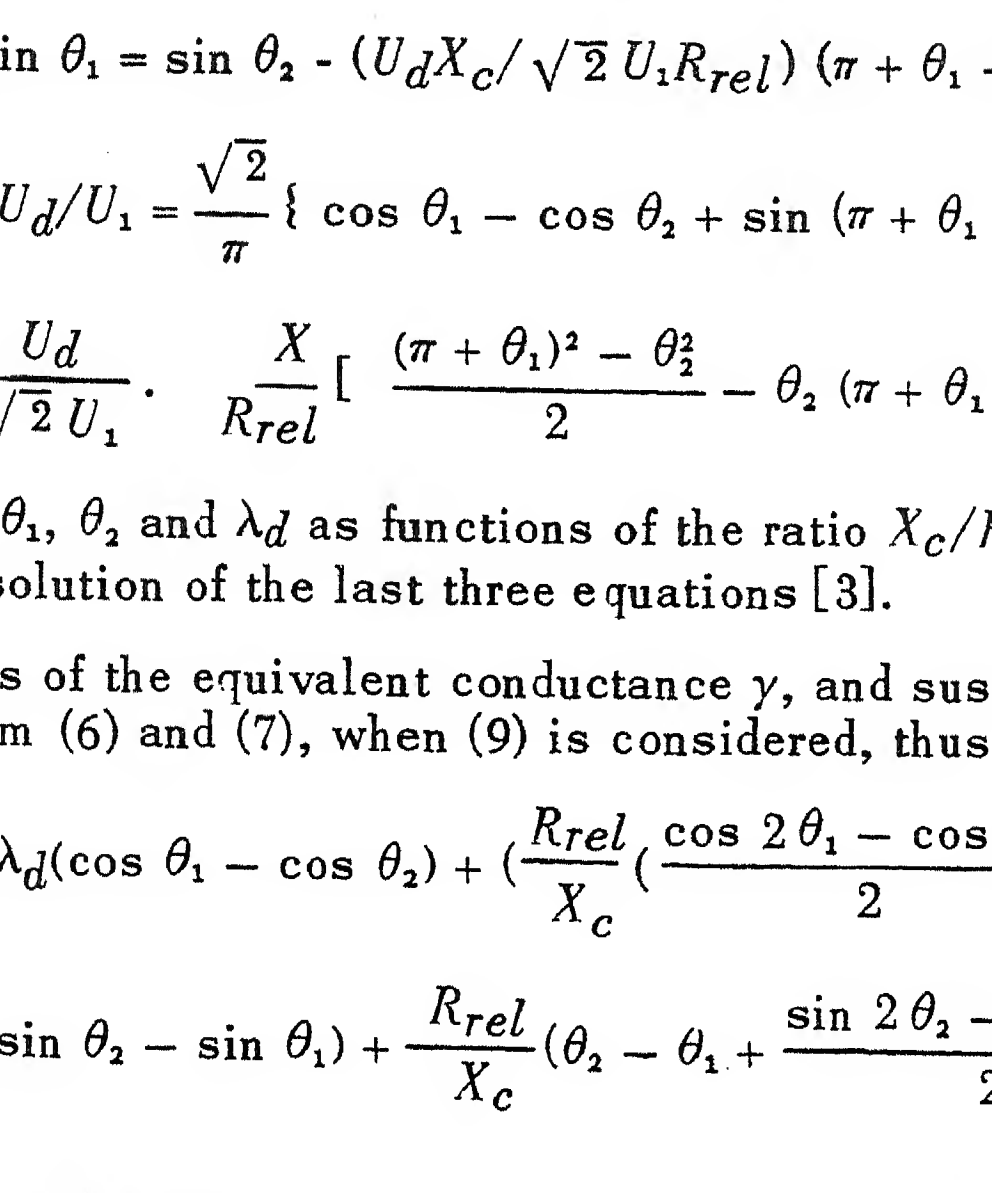

FIG. 4. Theoretical coefficients for the design of automatic control and protection gear using single-coil relays.

The relationships $\lambda_d = f(X_c/R_{rel})$; $\gamma_1 = f(X_c/R_{rel})$ and $\beta_1 = f(X_c/R_{rel})$ for wo mentioned limiting cases are drawn in Fig. 3 and 4. The curves show that resence of the inductance affects the values of λ_d, γ_1 and β_1 at small values $:/R_{rel}$.

Operation of rectifiers having relays with two coils

We will consider the operation of rectifiers having a relay with two magnetically coupled coils on the example of a distance relay for h.v. transmission lines [3]. According to the diagram of Fig. 5a the operating (OP) and restraining (OT) coils of this relay are supplied by the rectifiers BP and BT, the input voltages of which are U_p and U_T, respectively. Considering that in any real relay the coupling coefficient of the coils varies, viz. $0 < M_{rel}/L_{rel} < 1$ (where L_{rel} and M_{rel} are self- and mutual-inductances of the relay winding), it will be convenient to examine the operation of the circuit of Fig. 5a for the two limiting cases, viz.

$$M_{rel}/L_{rel} = 0 \text{ and } M_{rel}/L_{rel} = 1.$$

In the limiting case $M_{rel}/L_{rel} = 0$ each relay winding may be imitated by the circuit of Fig. 1 analysed above.

In the limiting case $M_{rel}/L_{rel} = 1$ and under the condition that the ratio X_C/R_{rel} is such as to permit an operation of both rectifiers only in the N-state, the relay circuit may be represented by the linear four-terminal network of Fig. 5c, the input and output voltages of which are U_p and U_T, respectively.

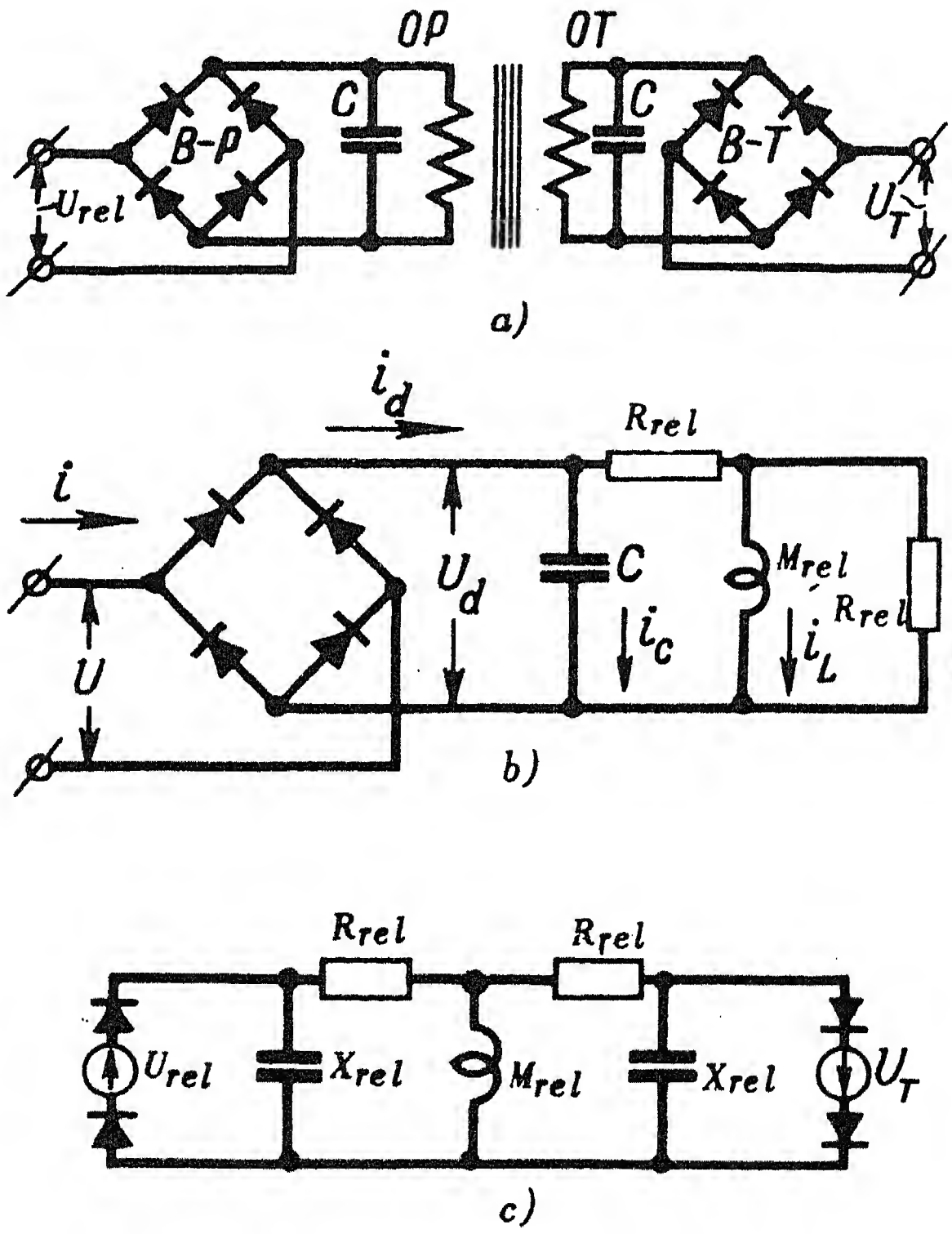

FIG. 5. a) Basic circuit of a distance relay; b) Equivalent circuit of two-coil relays; c) Equivalent circuit of this relay for ideal magnetic coupling of the coils.

The calculation for such a four-terminal network is more conveniently carried out by the method of superposition, i.e. by representing it in the form of two dipoles (Fig. 5b), the rectifiers* of which operate in the N-state.

If we take into account that in reality the inductive reactance of the relay windings is considerably larger than their resistance, it is fairly easy to find by Kirchhoff's laws an expression for the output current of the rectifier [3]:

$$i_d = \sqrt{2}\, U_1 \cos \theta / X_c + \sqrt{2}\, U_1 \sin \theta / 2 R_{rel} + U_d / 2 R_{rel} \qquad (15)$$

The critical value of $(X_c/R_{rel})_{crit}$ at which the rectifier operates in the N-state, can be found from the last equation by the substitutions

$$i_d = 0;\ \theta = \pi \text{ and } U_d / \sqrt{2}\, U_1 = 2/\pi;$$

Hence $$(X_c / R_{rel})_{crit} > \pi.$$

We note that in the limiting case $M_{rel}/L_{rel} = 0$, $(X_{rel}/R_{rel})_{crit} \geq \pi/2$.

The values of the equivalent coefficients γ_1 and β_1 are plotted against X_c/R_{rel} for both limiting cases in Fig. 6.

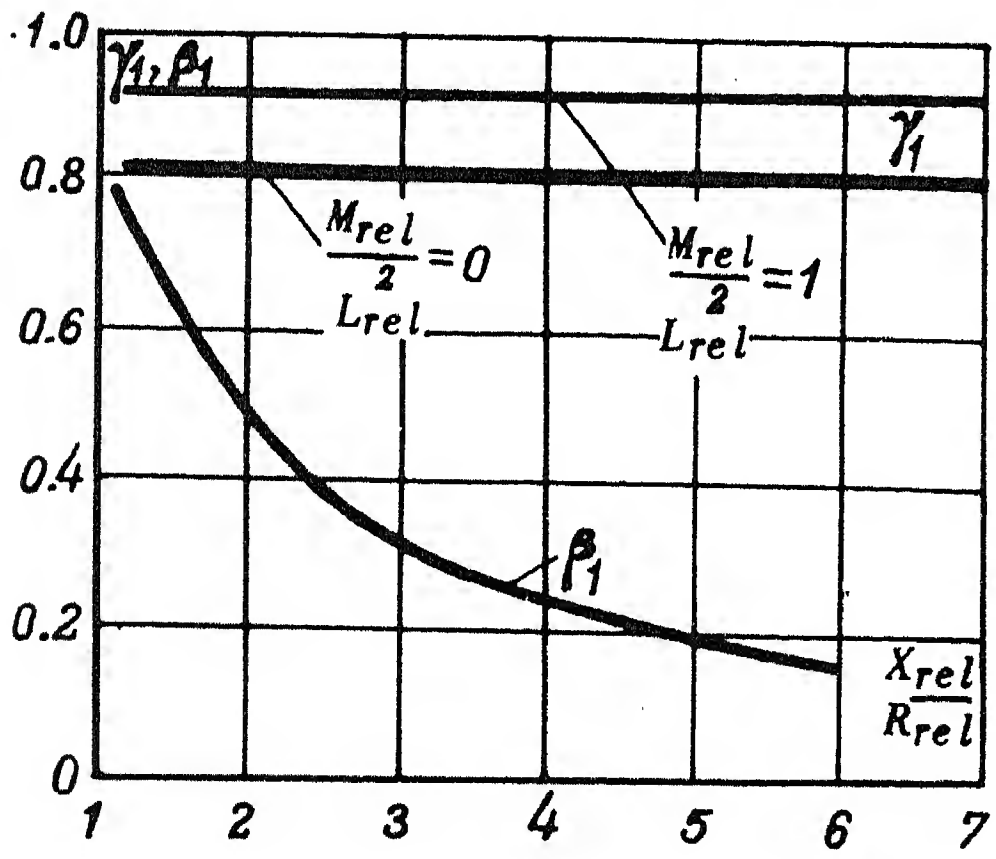

FIG. 6. Design factors for automatic control and protective gear using two-coil relays.

For the limiting case $M_{rel}/L_{rel} = 1$ they were determined from (6), (7) and (15).

The curves indicate that when the mutual inductance is considered, the conductance is slightly reduced, whereas the susceptance remains unchanged.

Appendix

The design of protective and automatic control relays with semiconductor rectifiers centres on the determination of the optimum circuit parameters resulting in the maximum sensitivity and minimum power consumption of the relays, and also in their reliable operation and compact construction.

It is clear that the purpose and the sequence of the calculations will differ according to the type and use of the relay [1-3]. We will solve, by way of example, the following problem. To find the parameters of the other circuit elements (rectifier, supply transformer, etc) when the relay parameters (P_{mean}, R_{rel}, I_{mean}) and the reactance of the capacitive filter X_c are given.

* The rectifier of Fig. 5b may in general operate, analogously to the rectifier of Fig. 1, in the R- and N-states. We use the superposition method only when the N-state exists.

1. As first approximation, viz. assuming ideal rectifier units according to the curves $\gamma_1 = f(R_{rel}/X_c)$ and $\beta_1 = f(R_{rel}/X_c)$, we determine γ_1 and β_1, and from these the resistances and reactances of the equivalent circuit:

$$R_{eq} = \frac{\gamma_1}{\gamma_1^2 + \beta_1^2} R_{rel} \text{ and } X_{eq} = \frac{\beta_1}{\gamma_1^2 + \beta_1^2} R_{rel}.$$

2. From the given value of I_{mean} we determine the mean values of the output current and voltage of the rectifier, viz. $I_d = K_{ser} I_{mean}$ (K_{ser} being the coefficient of reliability of service) and $U_d = I_d R_{rel}$.

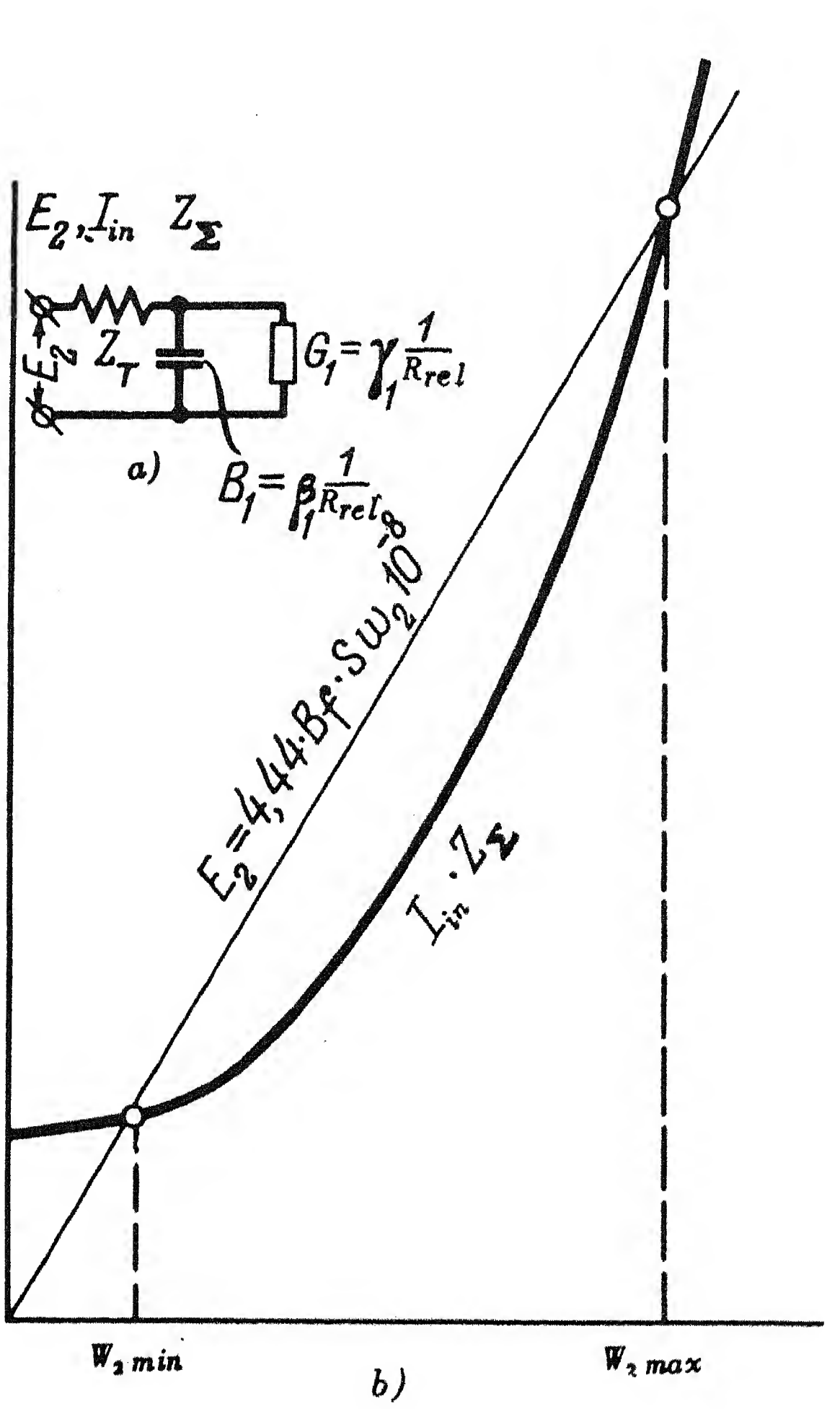

FIG. 7. a) Equivalent circuit of the relay considering internal resistance of supply; b) Graphical solution of the equation of the relay operation.

3. From the value of U_d we find the input voltage U_{in} and current I_{in} of the rectifier, viz.

$$U_{in} = U_d/\lambda_d ; I_{in} = U_{in}/\sqrt{R_{eq}^2 + X_{eq}^2}$$

(λ_d being found from the curve of Fig. 4).

4. From I_d, U_d, I_{in} and U_{in} we determine the number of rectifier elements to be connected in parallel (a) and series (n) into a bridge arm [1 and 2], and with these resultant resistance of the elements of the rectifier $R_a = 2nr_u/a$ (r_u being the resistance of a single rectifier unit).

5. Adding R_a to the resistance R_{rel}, we repeat the calculation for the actual rectifier units, i.e. assume the load resistance to be $R_d = R_{rel} + R_a$.

6. The minimum turns number of the interposing transformer assuring reliable relay operation is found from the condition of equality of the e.m.f. E_2 induced in the secondary winding of the transformer and the voltage drop in the equivalent circuit (Fig. 7a).

$$E_2 = I_{in} Z_{\Sigma} \tag{I.1}$$

where Z_{Σ} is the total impedance of the equivalent circuit

$$E_2 = 4.44\, B.S.f.w_2\, 10^{-8} \tag{I.2}$$

$$Z_{\Sigma} = \sqrt{(C_R\omega_2^2 + R'_{eq})^2 + (C_X\omega_2^2 = X'_{eq})^2} \tag{I.3}$$

In the last equation $C_R\omega_2^2$ and $C_X\omega_2^2$ are the resistance and reactance, respectively, of the secondary winding of the interposing transformer; for a given type of core stampings of the transformer they depend only on ω_2 [3]; R'_{eq} and X'_{eq} are resistance and reactance, respectively, of the equivalent circuit of the rectifier, considering the self-resistance of the latter.

The value of ω_{2min} is determined by the bi-quadratic equation obtained from (I.1), when (I.2) and (I.3) are considered, or by solving equation (I.1) graphically (Fig. 7b).

REFERENCES

1. V.G. Komar; *Operation of Semiconductor Rectifiers in Control Circuits, Gosenergoizdat* (1952).
2. I.L. Kaganov; *Electronic and Ionic apparatus, Gosenergoizdat* (1950).
3. G.G. Gimoyan; *Distance Protection using Semiconductor Rectifiers, Dissertation. Moscow Electrotechnical Institute* (1954).

THE USE OF LOAD DISTRIBUTION DIAGRAMS FOR THE DESIGN OF URBAN SYSTEMS*

YU. A. GLANTS

(Received 12 October 1956)

The character of the distribution of the loads in a system has a great influence on its design and operation. This factor becomes very important for the design of low-voltage systems especially in urban areas.

The choice of the system arrangement for one or other type of distribution of loads must be made on the basis of technical and economical considerations. The proposed method of plotting the load distribution diagrams facilitates these calculations and the derivation of the economic optimum design of the system. We owe the idea of plotting these diagrams to V.P. Khashchinskii [1].

Let us first consider a radial line feeding the loads distributed along its route. The diagram of the distribution of these loads along the line may be presented as shown in Fig. 1.

The area of the diagram, Fig. 1, can be determined by the sum of the load moments:

$$\Sigma P_i l_i = P_1 l_1 + P_2 l_2 + P_3 l_3 + P_4 l_4$$

of

$$\Sigma p_i l'_i = p_1 l'_1 + p_2 l'_2 + p_3 l'_3 + p_4 l'_4,$$

where

P_1, P_2, P_3 and P_4 are the values of power sent through the line sections;
l_1, l_2, l_3 and l_4 are the lengths of the line sections;
p_1, p_2, p_3 and p_4 are the loads connected to the line;
l'_1, l'_2, l'_3 and l'_4 are the distances of the connected loads from the supply source.

Since each of the sums of the load moments represents the same area it can be written:

* *Elektrichestvo* No. 7, 45-50, 1957 [Reprint Order No. EL 38].

$$\sum P_i l_i = p_1 l'_1 \qquad (1)$$

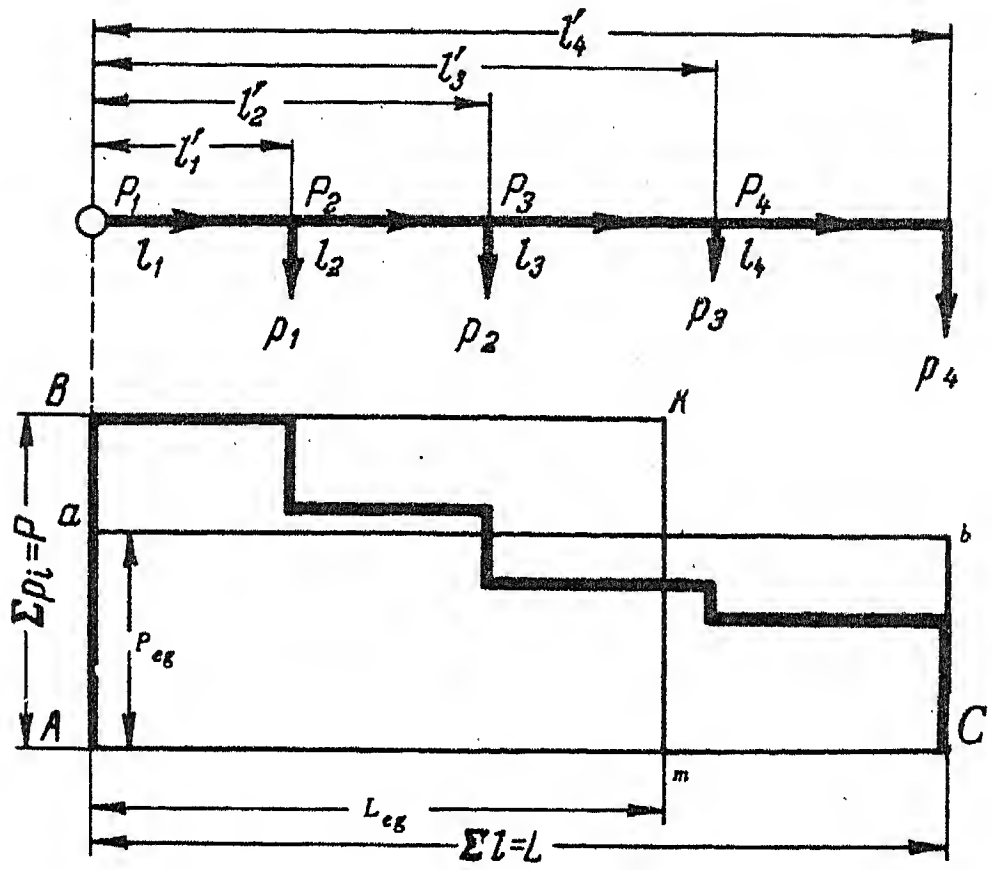

FIG. 1.

The stepped diagram shown in Fig. 1 can be replaced by an equivalent rectangular diagram. There are two alternative methods of such a replacement: 1) The stepped diagram is replaced by the rectangle $AabB$ with the base of the rectangle equal to the length of the line $\Sigma\ l_i = L$; 2) the stepped diagram is replaced by the rectangle $ACkm$ with the height of the rectangle equal to the total load of the line $\Sigma\ p_i = P$.

In the first case we obtain the possibility of replacing the total load by one equivalent load connected to the end of the line. The equivalent load is

$$P_{eq} = \frac{\Sigma p_i l'_i}{L} \qquad (2)$$

In the second case we also obtain the possibility of replacing the distributed load by a concentrated one, but in contrast to the preceding case, the latter although equal to the total load, is at an equivalent distance from the supply point given by

$$L_{eq} = \frac{\Sigma p_i l'_i}{P} \qquad (3)$$

We now change to relative values of equivalent load P^*_{eq} and of equivalent distance L^*_{eq}, of which the first is considered to be a fraction of the total load and the second a fraction of the line length. It is not difficult to see that

$$P^*_{eq} = L^*_{eq} = \frac{\Sigma\ p_i l'_i}{P L} = \alpha \qquad (4)$$

V.M. Khrushchov [2] was the first to introduce this coefficient α. He called it the coefficient describing the distribution of the load and derived this formula for its determination.

The value of the coefficient α may vary between 0 and 1, where the upper limit refers to the case that power is transmitted through the line to a load concentrated at its end, and the lower limit to the case that the load is directly at the supply point.

The coefficient α can be determined graphically if the load distribution diagram is plotted in relative units with unity load being the total load and unity distance the total line length. The coefficient α is determined by the ordinate $Aa = Bb$, or by the abscissa $Am = Ck$ (Fig. 1).

In a similar manner a diagram can be plotted for the squares of the loads, which can be replaced by an equivalent rectangle in the same way as it was done above. The height of this equivalent rectangle plotted on the same base, the line length, is equal to the equivalent square load. The base of the equivalent rectangle whose height is the square of the total load equals the equivalent distance of the connection point of this load from the supply point.

In a similar way as the coefficient α was determined for the load distribution diagram, a coefficient β can be found as follows

$$\beta = \frac{\Sigma\ P_i^2\, l_i}{p^2 L}\ . \tag{5}$$

If the diagram is plotted in relative units,

$$\beta = \Sigma\ P_i^2\, l_i$$

It should be noted, that, if the line has the same conductor size along its entire length, for purely active power the coefficient β will be proportional to the power loss of the line and the coefficient α proportional to the voltage regulation.

Having the values of the coefficients α and β, one can replace the distributed loads by the concentrated loads and thus simplify the design calculations.

It follows from (4), (5) and (1) that the sum of the moments of the distributed loads is

$$\Sigma\ P_i l_i = \quad \Sigma\ p_i l_i' = \quad \alpha\ P\, L \tag{6}$$

and the sum of the moments of the square loads

$$\Sigma\ P_i^2 l_i = \quad \beta\ P^2\, L \tag{7}$$

With the change from the system with distributed loads to the system with concentrated loads it is necessary for the determination of the voltage regulation to arrange at the end of the line a load equivalent to αP or for determination of the power loss a load equivalent to $\sqrt{\beta}\, P$.

Diagrams with the same value of α can have different values of the coefficient β. With diagrams of the same coefficient α it is possible to have two extreme cases: 1) the diagram has the shape of a rectangle wi th unit base but a height of α 2) the diagram has the shape of a rectangle with the base α but unit height. In the first case $\beta = \alpha^2$ and in the second $\beta = \alpha$.

The diagram of the load distribution along a ring line is obtained from two conjugated diagrams, of which one is obtained by considering the line as a radial feeder supplied from one end. One of the diagrams would correspond to the feeding in the direction 0-1-2-3-4, and the other in the direction 0-4-3-2-1 (Fig. 2). The area of the first diagram is shaded and that of the second one is not shaded. The areas of the two diagrams supplement each other to the rectangle $ACDB$ with the base equal to the line length and the height equal to the total load of the line.

Ring feeders supplied from both ends can be divided at the point of current reversal into two branches. The point of current reversal on the line can be determined graphically from the following conditions: 1) the voltage regulation in each of the branches must be equal, that means the areas of the two load distribution diagrams must be the same; 2) the sum of the loads at the supply point must be equal to the total line load.

For the determination of the point of current reversal it is necessary in the diagram of Fig. 2 to lay a line ab parallel to the abscissa so that the areas $aBbdef$ and $cCmkighf$ cut out by it from the two conjugated diagrams are equal to each other. These diagrams are then also the load distribution diagrams of the two branches of the ring feeder.

The line ac divides the rectangle $ACDB$ into two parts: The area of the lower part $AacC$ is equal to the shaded area of the conjugated diagram, and the upper part $BacD$ is equal to the unshaded part of that diagram. Therefore, the rectangle $AacC$ is equivalent to the shaded diagram, and the rectangle $BacD$ is equivalent to the unshaded diagram.

The maximum ordinates of the branch diagrams aB and cC represent the magnitude of the power flow at the point of supply in each of the branches of the ring feeder. Each load power flow is

$$P_b = \alpha' P \tag{8}$$

where

α' is the coefficient of the load distribution determined for each branch from its conjugated diagram (for the left branch from the unshaded

diagram, and for the right branch from the shaded diagram);
P is the total load of the ring feeder.

It is possible to plot diagrams of the distribution of the square of the loads from the diagram of the load distribution of the branches of the ring feeder by using the square of the ordinates. The one permits the determination of the voltage regulation and the other that of the power losses of the ring feeder.

The area of the load distribution diagram of the branches of the ring feeder will be designated in the following by M_r and the sum of the areas of the diagrams of the distribution of the squares of the loads in both branches by N_r.

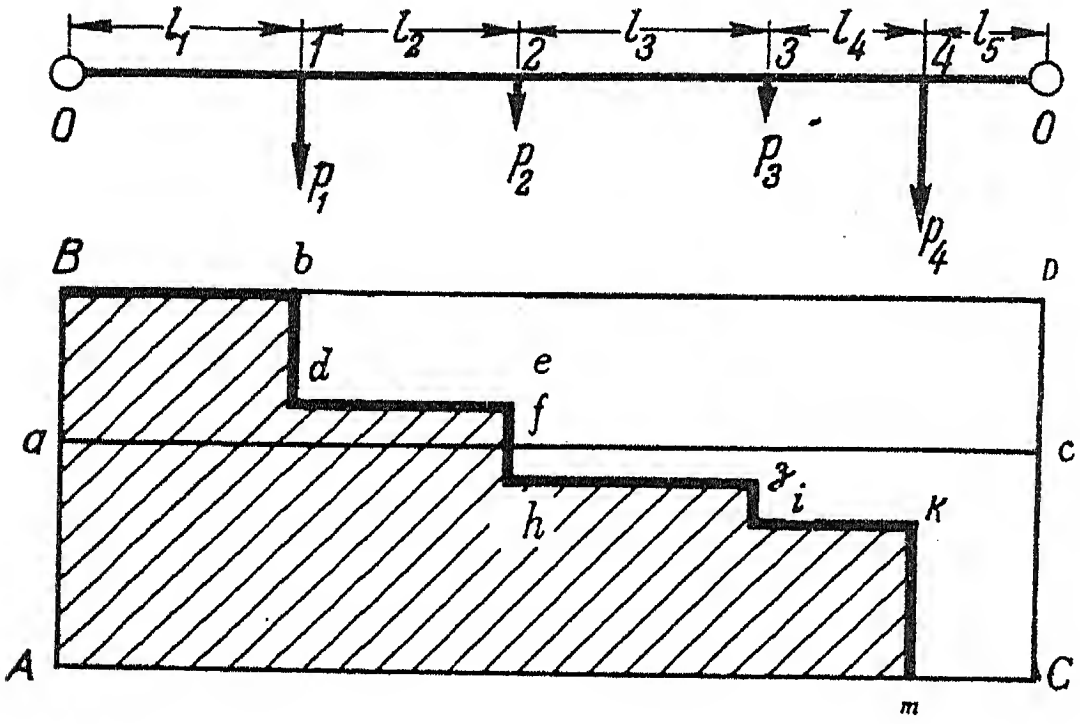

FIG. 2.

The value of N_r can be determined in another way. For this purpose we consider two diagrams, Fig. 3a and 3b which have a different configuration but whose coefficients α and β are respectively equal.

Considering any of the load distribution diagrams Fig. 3a or 3b we transform it into a two-stepped diagram whose first step is unity and whose second is α (Fig. 3c, diagram $Bbcdef$).

If one changes from that equivalent diagram to the square one, then the first step of the latter is also unity, but the second is α^2.

The length of the first step of the equivalent diagram (Fig. 3c), whose ordinate is unity, is designated by x, and the length of the second step, whose ordinate is α, by y. Then, as follows from Fig. 3c, the area of the equivalent diagram, plotted in relative units, is

$$\alpha = x + \alpha y,$$

and the area of the square diagram

$$\beta = x + \alpha^2 y.$$

Solving jointly these two equations we obtain

$$x = \frac{\beta - \alpha^2}{1 - \alpha} \tag{9}$$

$$y = \frac{\alpha - \beta}{\alpha - \alpha^2} \tag{10}$$

The area of the part $aCcd$ of the equivalent diagram (Fig. 3c) is $x(1-\alpha)$. Consequently, on the basis of (9) it is $(\beta - \alpha^2)$. This area changes with a change in the shape of the equivalent diagram. It goes towards zero, if the equivalent diagram approaches the single-stepped diagram $AacC$ with the ordinate α. This corresponds to the extreme case when the total load is supplied directly from the source. It will go towards its maximum value, if the equivalent diagram adopts the shape of the single-stepped diagram $ABkm$ with unity value of the ordinate. The area $aBbd$ has in that case the value $\alpha(1-\alpha) = \alpha - \alpha^2$. This corresponds to the extreme case that the concentrated load is supplied through the ring feeder.

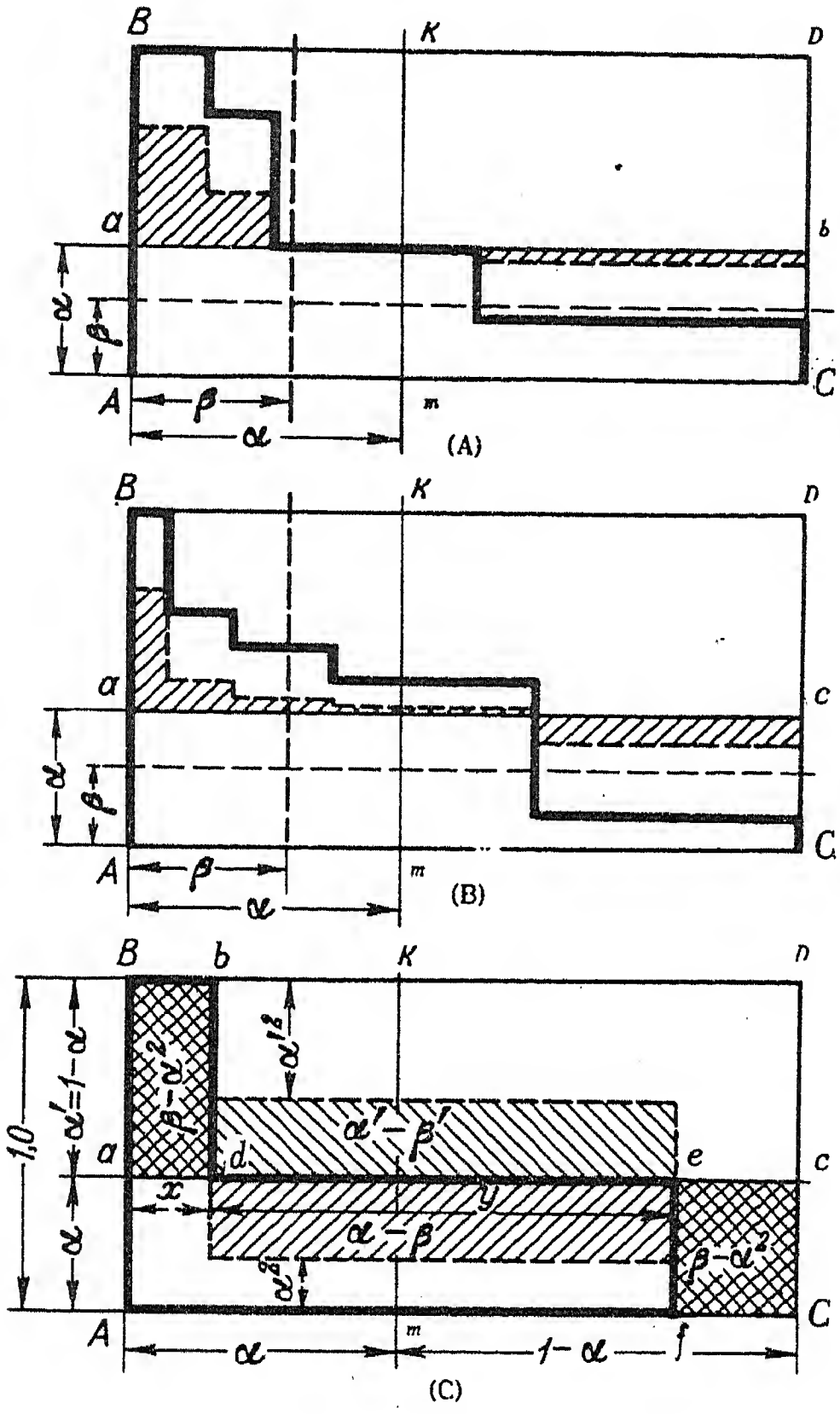

FIG. 3.

In the latter extreme case the area of the square diagram of one branch of the ring feeder is $(1-\alpha)^2\alpha$, and that of the other branch $\alpha^2(1-\alpha)$. The sum of the areas of the square diagrams of the branches is

$$N_r = (1-\alpha)^2\alpha + \alpha^2(1-\alpha) = \alpha - \alpha^2.$$

Since in the considered case $\beta = \alpha$

$$N_r = \beta - \alpha^2 \qquad (11)$$

i.e. the sum of the areas of the square diagrams of the branches equals the area $aCcd$.

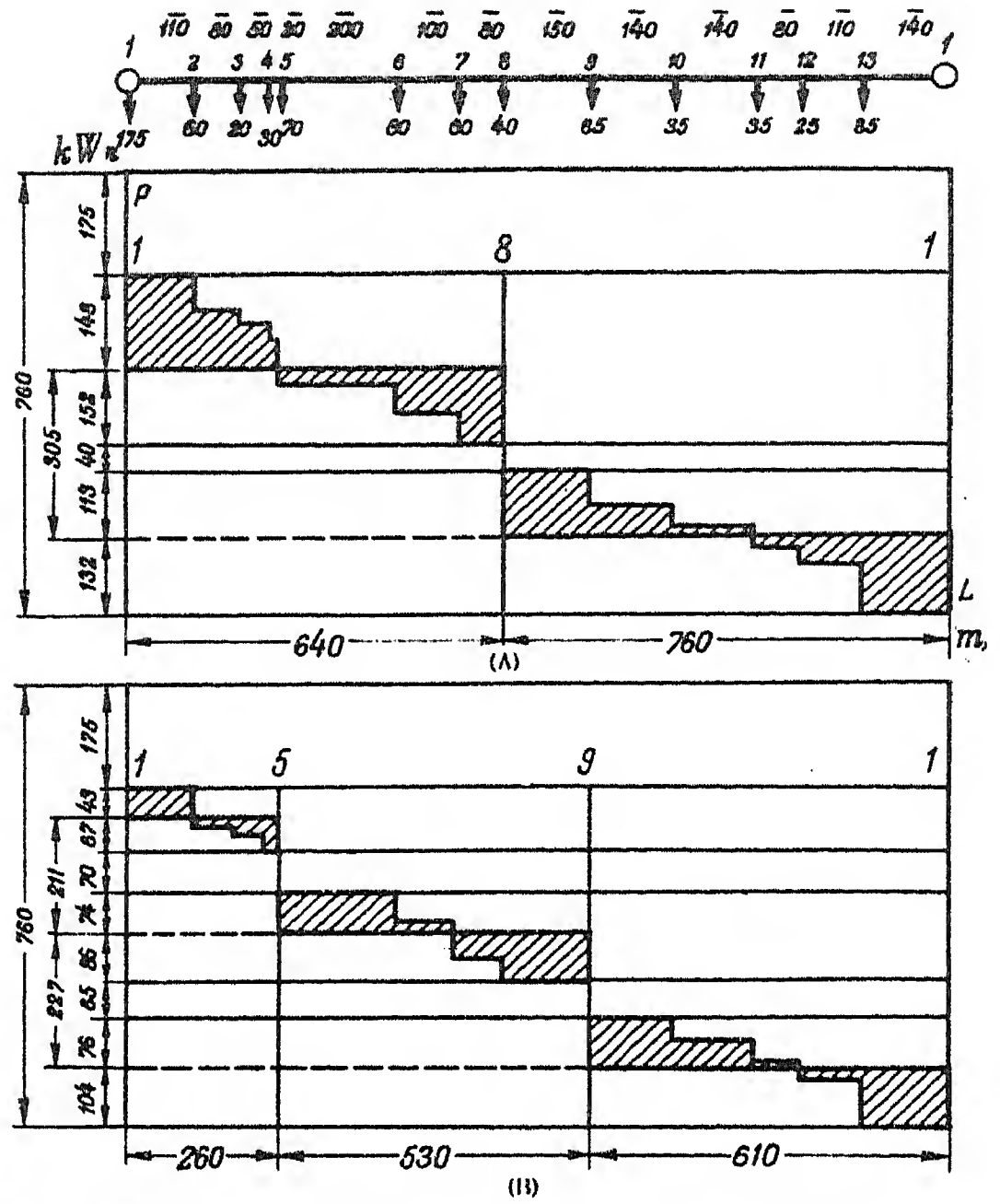

FIG. 4.

Analysis of a large number of diagrams shows that the sum of the areas of the square diagrams of the branches of ring feeder is always equal to the area $aBbd$. Thus, the value of N proportional to the power losses in the ring system can be determined from the magnitude of the area $aBbd$ or the equal area $fecC$. This permits the determination of N_r from (11), i.e. without plotting the diagram, if the coefficients α and β are known for one of the conjugate diagrams of the ring system.

It follows from (11) that the power losses in a feeder for feeding from both ends differ from the losses with feeding from one end by α^2. The ratio of these losses is

$$\frac{\beta - \alpha^2}{\beta} = 1 - \frac{\alpha^2}{\beta}; \qquad (12)$$

that means the change to feeding from both ends is the more effective in reducing the losses, the larger is the term (α^2/β).

The above derived relationship of the coefficients of the diagram of the ring system is interesting, because it facilitates the determination of the power losses for feeding from both ends, if the losses for feeding from one end are known. Besides, it is not necessary to calculate both conditions of single-end feeding and it is sufficient to calculate only one of these conditions since one diagram of load distribution also determines the conjugate diagram. Thus one calculation is sufficient for all three supply conditions of the ring feeder.

It follows from the determination of the conjugate diagram that

$$\alpha' = (1 - \alpha) \tag{13}$$

and, since both shaded areas in Fig. 3c are equal:

$$\alpha - \beta = \alpha' - \beta'.$$

Consequently, the coefficient for the conjugate diagram is

$$\beta' = \beta + (1 - 2\alpha) \tag{14}$$

The above conclusions are to be applied to a concrete example.

The coefficients for the case of a ring feeder supplied from one end may be $\alpha = 0.4$ and $\beta = 0.3$, and the power losses $\Delta P = 2.15$ kW. Then

$$\beta' = 0.3 + (1 - 2\times 0.4) = 0.5$$

Consequently, for feeding the line from the other end the losses are

$$\Delta P = 2.15\frac{0.5}{0.3} = 3.58 \text{ kW}.$$

For feeding from both ends

$$N_r = 0.3 - 0.4^2 = 0.14$$

and the power losses

$$\Delta P_r = 2.15\ \frac{0.14}{0.3} = 1 \text{ kW}.$$

An urban ring system often comprises one or several districts and is supplied from several sources. The calculations for the determination of the voltage regulation and especially of the power losses in such systems with a large number of loads are complicated and laborious. The use of load distribution diagrams in a given case can considerably shorten the calculations and make them clearer.

Consider, for example, a ring system connecting a group of consumers, e.g. houses. Fig. 4 shows three diagrams of the load distribution in such a system: the first, Fig. 4a, for the case of two; the second, Fig. 4b, for three, and the third, Fig. 4c, for four supply points.

The supply points can be located in such a manner that the areas cut out of the conjugate diagrams of the sections of the system and representing the load

TABLE 1.

Items	Sections of system with three supply points (Fig. 4b)				Sections of system with four supply points (Fig. 4c)				
	1-5	5-9	9-1	Total	1-5	5-8	8-11	11-1	Total
Total load (kW)	110	160	180	450	110	120	100	110	440
Total length (m)	260	530	610	1 400	260	380	430	330	1 400
Load moment ($kW-m\times10^3$)	28.6	84.8	110	—	28.6	45.5	43	36.3	—
Square moment ($kW^2-m\times10^6$)	3.14	13.6	19.7	—	3.14	5.46	4.3	4.0	—
Load moment of the diagram ($kW-m\times10^3$)	17.6	45.2	63.7	—	17.6	30	19.95	18.2	—
Square moment ($kW^2m\times10^6$)	1.58	6.25	9.23	—	1.58	3.24	1.67	1.77	—
Coefficient α	0.615	0.534	0.578	—	0.615	0.66	0.464	0.5	—
Coefficient β	0.503	0.458	0.468	—	0.503	0.594	0.388	0.442	—
Coefficient N_T	0.126	0.174	0.135	—	0.126	0.16	0.173	0.19	—
Coefficient M_T	0.163	0.195	0.152	—	0.163	0.18	0.187	0.212	—
Cable size (mm^2)	50	95	120	—	50	70	50	50	—
Resistance (Ω)	0.109	0.118	0.107	—	0.109	0.114	0.18	0.139	—
Equivalent load for determining the power losses (kW')	39	67	66.2	—	39	48	41.7	48	—
Equivalent load for determining the voltage regulation (kW)	17.9	31.2	27.4	—	17.9	21.6	28.2	23.3	—
Power losses (kW)	1.14	3.65	3.2	7.99	1.14	1.82	2.16	2.2	7.32
Voltage regulation (V)	5.12	9.7	7.7	—	5.12	6.45	8.8	8.5	—
Copper volume (dm^3)	39	151	219	409	39	80	65	50	234

distribution diagrams for the individual branches are as small as possible. After that the load flow from the supply points can be determined, the conductor size of the individual sections of the system chosen, the voltage regulation and the power losses determined. Such calculations are given below for the system with three (Fig. 4b) and four (Fig. 4c) supply points. The basic data and the results of the calculations are entered in the table.

The load, distributed along the branches of the sections of the ring system between the supply points was replaced by a concentrated load at the end of the branch. For the determination of the voltage regulation the concentrated load at the end of the branch used in the calculation is $P_v = M_r P$, and for the determination of the power losses $P_p = \sqrt{N_r P}$.

The voltage at all supply points of the system was assumed to be 380 V.

The cable sizes were checked with respect to the thermal ratings corresponding to the maximum permissible load with consideration of the conditions of laying and of the ambient soil temperature. The possibility of feeding each section from one end in emergency conditions was taken into account for the choice of the cable size.

It can be seen from the table that with the change from three to four supply points the copper volume of cables is reduced by 175 dm^3 and the power losses by 0.67 kW. The maximum voltage regulation on all sections of the system with three and four supply points is very reasonable at about 2.5 per cent.

The transformer loads with three supply points are:
322; 211 and 227 kW; and with four supply points 273; 178; 173 and 136 kW.

As the above example shows the method of plotting load distribution diagrams permits a clear and simple determination of the approximate load flow in the system, of the voltage regulation and power losses. Thus it reduces the labour of calculations for the purpose of technical and economical considerations.

In cases where it is not suitable to use the same cable size on a section of the system and where at the supply end twin cables are used, the calculation with the graphical method becomes somewhat more complicated. The twin cable section in that case is to be represented by equivalent data of the basic cable size between the two supply points.

REFERENCES

1. V.P. Khashchinskii; *Distribution of electric energy. Commission for improving living conditions of students, Leningrad* (1926).
2. V.M. Khrushchov; *Electric systems and lines*, Part 1. *Gosenergoizdat* (1932).

THE NOMOGRAM FOR DETERMINING PROTECTIVE ZONES OF LIGHTNING CONDUCTORS*

L.M. LOPSHITS

(Received 24 April 1956)

This nomogram supersedes an earlier one (*Elektrichestvo*, No. 10, 1947) and is deemed necessary because of the distinction made in the latest instruction book on overvoltage protection of electrical installations for 3 - 220 kV (Gosenergoizdat, 1954) between the formulae for lightning conductors up to and above 30 m.

The nomogram is constructed for single and double lightning conductors up to 150 m using an emphirical formula based on laboratory test results and on the assumption that orientation of the lightning stroke onto the lightning conductor takes place at the height of H = 600 m (for an open country).

The use of the nomogram is explained with three examples.

That part of the latest Code of Practice on protection against overvoltages [1] which deals with protection against direct lightning strokes is based on laboratory investigations carried out at the V.I. Lenin All Union Electro-technical Institute, and differs from the earlier edition of the Code [3] in that in it a distinction has been introduced between the formulae for rod lightning conductors up to 30 m high and above 30 m high. Thus, the earlier nomogram for determining protective zones, constructed for lightning conductors up to 60 m has become obsolete and now may be used only for lightning conductors up to 30 m.

Figs. 1 and 2 give curves constructed from the data included in [2] which describe protective zones of single and double lightning conductors respectively. The geometrical sense of the parameters of the protective zone a, h, ha, h_x, b_x, and r_x is clear from Fig. 4; by H is denoted the height at which orientation of the lightning channel onto the lightning conductor takes place for open country.

For taller lightning conductors, $h > 30$ m, H was taken as 600 m, and for shorter lightning conductors, $h < 30$ m, the constant ratio of $H/h = 600/30 = 20$ was taken. It should be mentioned here that the Code of Practice does not set definite limits within which its recommendations are valid but merely states that the value of $H = 600$ m can be used for "very tall lightning conductors".

The curves given in Figs. 1 and 2 can be applied in these cases when the height of the lightning conductor does not exceed 150 m ($H/h = 4$), which corres-

* *Elektrichestvo* No. 7, 76 – 78, 1957 [Reprint Order No. EL 39].

ponds to the greatest height of chimneys built in power stations.

With the above value assumed for the height at which orientation of the lightning channel takes place, the following empirical expressions can be written for the relations represented on Figs. 1 and 2.

$$\frac{r_x}{h_a} = \frac{1.6}{1+\frac{h_x}{h}} \cdot p_1(h); \tag{1}$$

$$\frac{a}{h_a} = 7\sqrt[1.3]{1-\left(\frac{b_x}{r_x}\right)^{1.4}} \cdot p_2(h), \tag{2}$$

where $p_1(h)$ and $p_2(h)$ are coefficients depending on the height of the lightning conductor (Fig. 3).

It should be noted that in order to simplify calculations the following assumption is made in the Code of Practice*; $p_1(h) = p_2(h) = p(h)$,

where $$p(h) = \sqrt{\frac{30}{h}} \quad (\text{for} \quad h \geqslant 30 \text{ m}).$$

The relation $p(h)$ is shown in Fig. 3 by the curve drawn in a broken line.

Eliminating r_x from (1) and (2) one gets the following formula for the double lightning conductor:

$$\left(\frac{b_x}{1.6h_a \cdot p_1(h)}\right)^{1.4} \times \left(1+\frac{h_x}{h}\right)^{1.4} + \left(\frac{a}{7h_a \cdot p_2(h)}\right)^{1.3} - 1 = 0$$

which if $a = 0$, becomes also valid for the single lightning conductor.

The calculation of the lightning conductor height using this formula is lengthy and tedious; the present nomogram (Fig. 4) removes this disadvantage. The following examples explain the use of the nomogram and illustrate its scope.

Example 1. The given object has the shape of a parallelepiped with the base 48×48 m^2 ($b_x = 24$ m) and the height 15 m. It is located between two lightning rods 49 m high in such a way that a line drawn through the centres of the lightning rods coincides with the axis of symmetry of the object. It is required to verify that the object is protected if the distance between the lightning rods is 60 m.

Place one point of a pair of dividers at the point $a = 60$ m on the abscissa (the scale of centres). Bring the other point to $b_x = 24$ m on the ordinate. Keeping the first point unmoved and without altering the distance between the two points place the second point on the curve $h_x = 15$ m.

Through this point of the nomogram the curve $h_a = 32$ m also passes. Thus, the necessary height of the lightning conductor is $h = h_x + h_a = 15 + 32 = 47$ m. Therefore, with $h = 49$ m the object lies within the protective zone of the lightning conductor.

* There are errors in Figs. 4 and 5 of the Code. Instead of $h_x = 0.7h$ and $h_x = 0.9h$ it should be $h_x \approx 0.6h$ and $h_x \approx 0.7h$ respectively.

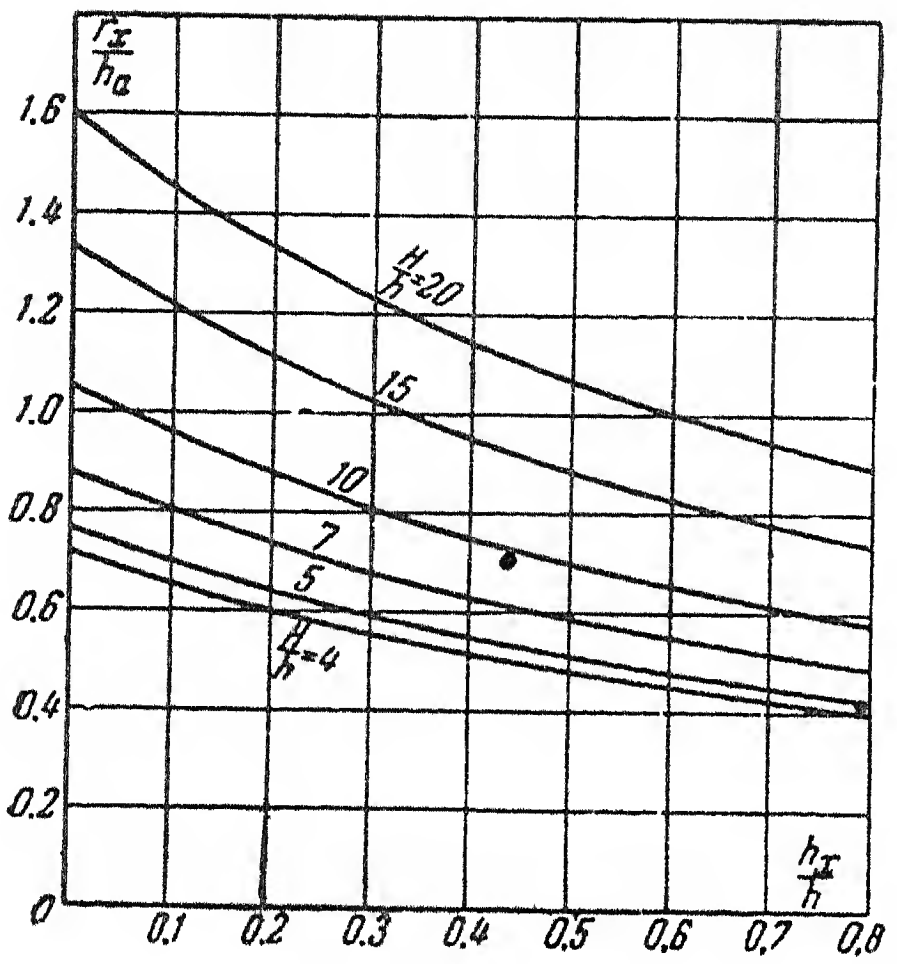

FIG. 1.

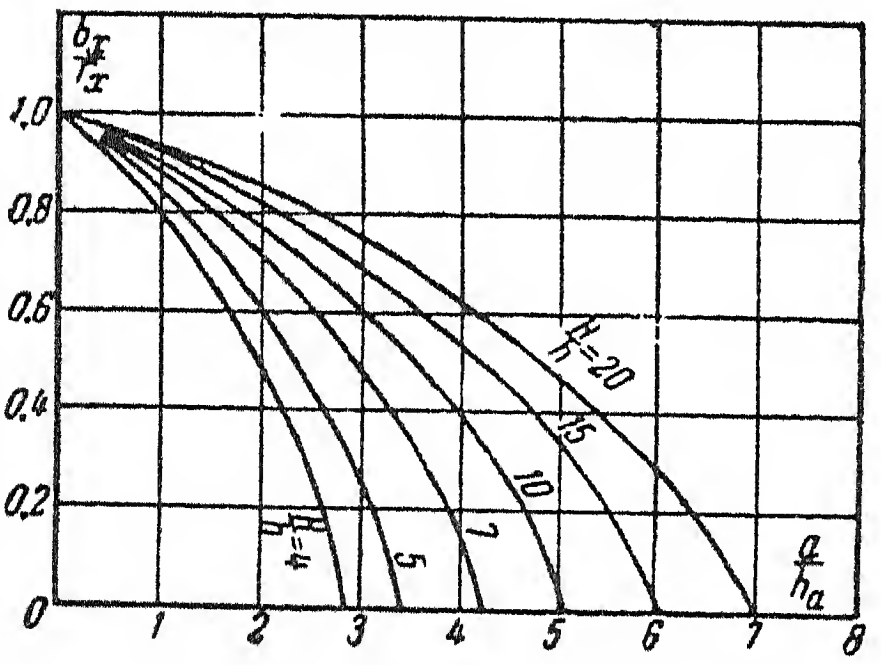

FIG. 2.

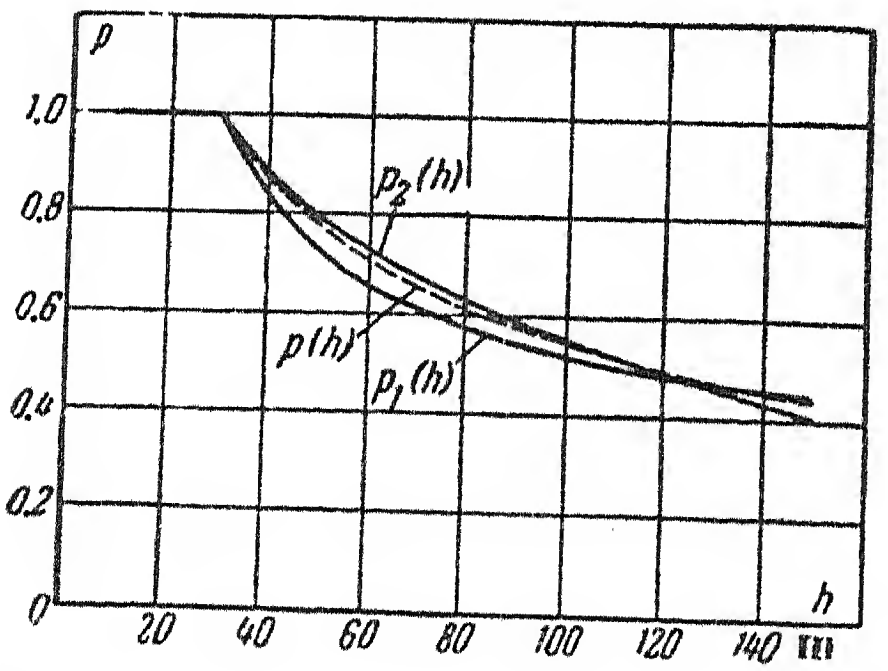

FIG. 3.

The nomogram can also be used in a different way. Set the dividers to the distance between the point $a = 60$ m and the point of intersection of the curves $h_x = 15$ m and $h_a = 49 - 15 = 34$ m. With this distance as radius and with point $a = 60$ m as the centre determine the point at which the ordinate is intersected; this is seen to be at $b_x = 25$ m. It follows then that the given lightning conductor would protect an object for which $b_x = 25$ m.

Example 2. Determine the necessary active height of a single lightning conductor placed in the centre of a structure having a cylindrical form with the diameter 40 m and the height 6 m.

With radius equal to the distance from the origin ($a = 0$) to the point $r_x = b_x = 20$m, determine the point of intersection with the curve $h_x = 6$ m. The curve $h_a = 16$ m which also passes through this point gives the desired value for the active height of the conductor.

Example 3. Find the radius of the protective zone at the level of $h_x = 26$ m for a single lightning conductor 120 m high placed on the chimney of a power station.

With origin as centre and radius equal to the distance from the origin to the point $h_x = 26$ m on the curve for $h = 120$ m, determine the point of intersection with the ordinate; this is found to be $b_x = r_x = 59.5$ m, which is the required value for the radius of protection.

The nomogram has been constructed on the assumption that the distance a between two lightning rods is given, which is normally the case in practice. In these exceptional cases when the distance is to be determined, it may be quickly found using a simple geometrical construction.

From the middle of the line joining the given points b_x (on the ordinate) and h_a

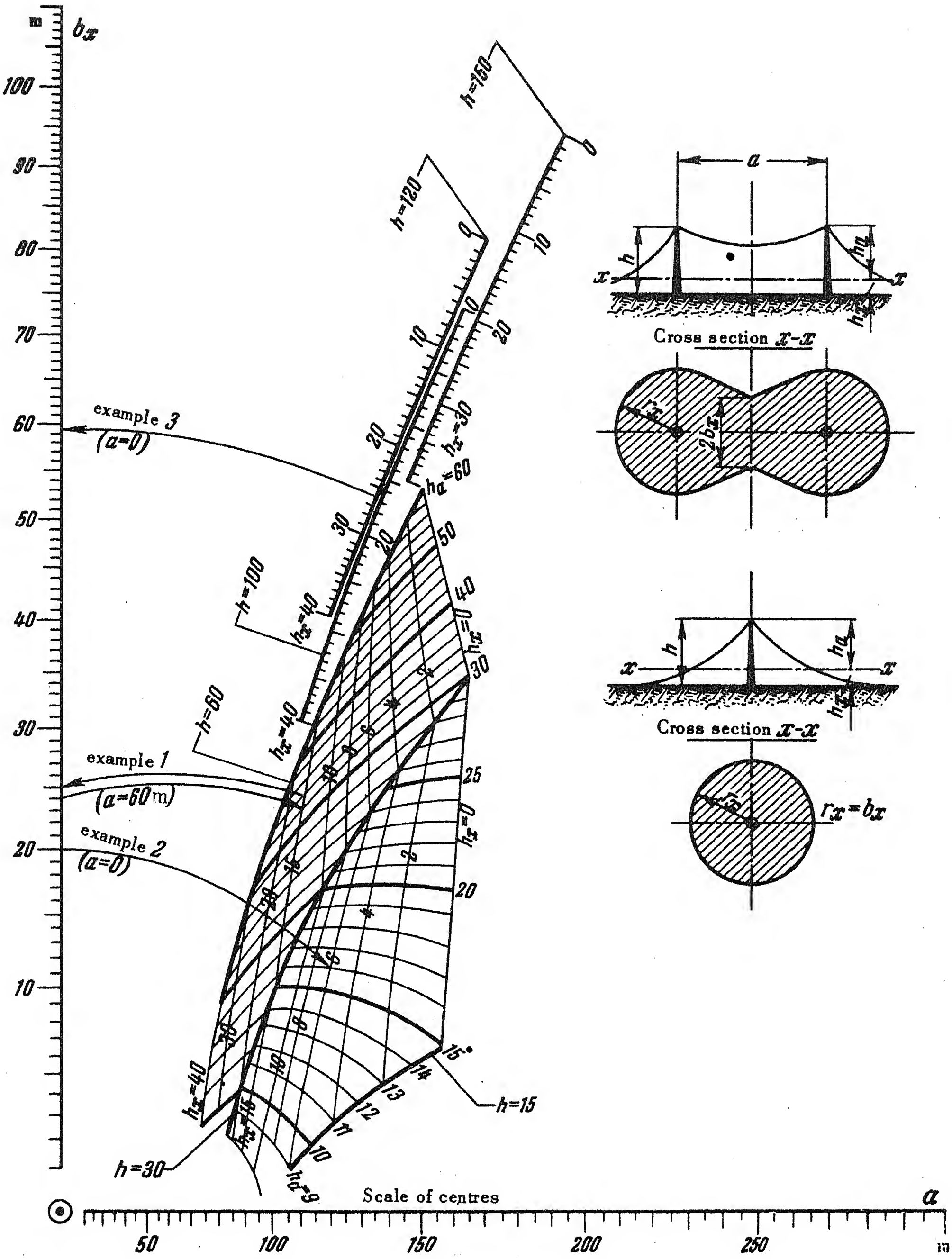

FIG. 4. The nomogram for determining protective zones of rod lightning conductors.

and h_x (the intersection of the corresponding curves) drop the perpendicular on the scale of centres. The point of intersection with this scale gives the required distance between the two lightning rods.

In conclusion it should be mentioned that the Code of Practice considers but in a small degree the critical observations regarding simplification of the contour of the protective zone [5]. In the present edition of the Code it would be desirable to approximate the curvilinear generatrix of the "cone" of the protective zone by a number of straight lines. This should considerably simplify graphical constructions.

REFERENCES

1. *The Code of practice on protection from overvoltages of a.c. electrical installations for* 3 - 220 *kV. Gosenergoizdat* (1954).
2. A.A. Akopyan; *Proceedings All-Union Electrotechnical Institute* VOL. 36, *Gosenergoizdat* (1940).
3. *The code of practice on protection from overvoltages of a.c. electrical installations for* 3 - 220 *kV. Gosenergoizdat* (1946).
4. L.M. Lopshits; *A Nomogram for determining protective zones of lightning conductors up to* 60 *m high. Elektrichestvo,* No. 10 (1947).
5. I.S. Stekol'nikov *et al; Lightning protection of industrial structures and buildings. Izd. Akad. Nauk SSSR* (1951).

INTERNATIONAL SERIES OF MONOGRAPHS ON ELECTRONICS AND INSTRUMENTATION

Editors: **D. W. Fry** (*Harwell*) *and* **W. Higinbotham** (*Brookhaven*)

WITH the applications of electronics and instrumentation expanding more rapidly every year the need increases for authoritative up-to-date accounts of recent advances. It is to meet such a need that the Pergamon International Series of Monographs on Electronics and Instrumentation was started a few years ago. The authors who contribute are all specialists actively engaged in research and in close touch with the most recent developments in their respective fields.

Of the monographs already published Dr. J. B. Birks' *Scintillation Counters*, Mr. A. B. Gillespie's *Signal, Noise and Resolution in Nuclear Counter Amplifiers* and the one by Mr. I. A. D. Lewis and Mr. F. H. Wells on *Millimicrosecond Pulse Techniques* will be of particular interest to everyone interested in nucleonics. The physics of secondary electron emission and its applications in many electronic devices is discussed in the monograph *Physics and Applications of Secondary Electron Emission* by Dr. H. Bruining; whilst the theory of probability as applied to electronics, communication and radar has been dealt with elegantly by Mr. P. M. Woodward in *Probability and Information Theory with Applications to Radar.*

Others in the series are Professor J. R. Mentzer's *Scattering and Diffraction of Radio Waves* and *An Introduction to Electronic Anologue Computers* by Mr. C. A. A. Wass. With the rapidly increasing use of electronic calculating machines in many branches of applied science, Mr. Wass's monograph is likely to be of considerable interest to everyone with problems in dynamics and kinematics.

A further addition to the series to be published shortly is Mr. A. H. W. Beck's monograph entitled *Space Charge Waves.* A strong need exists for a book which reviews the many advances made in microwave valves using distributed circuits during the last few years; Mr. Beck's book does this.

The ready sale which these monographs have is convincing evidence of the wide interest with which they are received. It is the intention of the editors and publishers to maintain in the future the high standard which has already been set, both in merit and quality of production.

Titles in this series:

Vol. 1. **Signal Noise and Resolution in Nuclear Counter Amplifiers** by A. B. GILLESPIE. *Price 25s. ($4.50)*

Vol. 2. **Scintillation Counters** by J. B. BIRKS. *Price 25s. ($4.50)*

Vol. 3. **Probability and Information Theory With Applications to Radar** by P. M. WOODWARD. *Price 25s. ($5.00)*

Vol. 4. **Physics and Applications of Secondary Electron Emission** by H. BRUINING. *Price 25s. ($5.50)*

Vol. 5. **Millimicrosecond Pulse Techniques** by I. A. D. LEWIS and F. H. WELLS. *Price 50s. ($7.50)*

Vol. 6. **Introduction to Electronic Analogue Computers** by C. A. A. WASS. *Price 40s. ($6.50)*

Vol. 7. **Scattering and Diffraction of Radio Waves** by J. R. MENTZER. *Price 30s. ($4.50)*

Vol. 8. **Space-charge Waves** by A. H. W. BECK. *Price 90s. ($15.00)*

PERGAMON PRESS

LONDON NEW YORK PARIS LOS ANGELES

4 & 5 Fitzroy Square, London, W. 1

122 East 55th Street, New York 22, N.Y.

Lubrication Science and Technology

***Edited by* JOHN BOYD**

With this volume, The American Society of Lubrication Engineers initiates a publication devoted to all aspects of the science and technology of lubrication. This is the outgrowth of the expanding number of lubrication papers which has been the result of an increasing appreciation of the benefits to be gained by a scientific approach to the lubrication problems of industry.

LUBRICATION SCIENCE AND TECHNOLOGY complements the Society's Journal, *Lubrication Engineering*, and encourages the pursuit and dissemination of the basic technical information necessary for solving industry's problems.

Price £5. 5s. net ($15.00)

PERGAMON PRESS

London New York Paris Los Angeles

4 & 5 Fitzroy Square, London W. 1

122 East 55th Street, New York 22, N.Y.

ELEKTRICHESTVO

Editor-in-Chief: N. G. DROZDOV

Deputy Editor-in-Chief: I. A. SYROMIATNIKOV

EDITORIAL BOARD

K. A. ANDRIANOV, N. I. BORISENKO, G. V. BUTKEVICH, M. G. CHILIKIN, A. A. GLAZUNOV, V. A. GOLUBTSOVA, E. G. KOMAR, M. P. KOSTENKO, L. R. NEIMAN, I. I. PETROV, V. I. POPKOV, A. M. FEDOSEEV

IMPORTANT EDITORIAL NOTICE

To assist readers, reprints of any article appearing in *Electrical Technology, U.S.S.R.* can be obtained on application at a price of $2 (10s.) per reprint, to cover the overhead costs involved in production. The Reprint No. of each article (which appears on the foot of the first page of the article) must be quoted on every order. Orders should be accompanied by the correct remittance.

All orders of reprints of Russian articles should be addressed to The Administrative Secretary of the Pergamon Institute at either 122 East 55th Street, New York 22, or 4 and 5 Fitzroy Square, London W.1, whichever is more convenient.

Pergamon Press are also the publishers of the following journals:

JOURNAL OF NUCLEAR ENERGY (*including* THE SOVIET JOURNAL OF ATOMIC ENERGY *on behalf of the Pergamon Institute, a non-profit-making foundation*)
REACTOR TECHNOLOGY (*Journal of Nuclear Energy, Part B*)
HEALTH PHYSICS (*The Official Journal of the Health Physics Society*)
JOURNAL OF INORGANIC AND NUCLEAR CHEMISTRY
TETRAHEDRON (*The International Journal of Organic Chemistry*)
TALANTA (*An International Journal of Analytical Chemistry*)
INTERNATIONAL JOURNAL OF APPLIED RADIATION AND ISOTOPES
BIOCHEMICAL PHARMACOLOGY
*BIOPHYSICS
*JOURNAL OF MICROBIOLOGY, EPIDEMIOLOGY AND IMMUNOBIOLOGY
*PROBLEMS OF HEMATOLOGY AND BLOOD TRANSFUSION
*PROBLEMS OF VIROLOGY
*PROBLEMS OF ONCOLOGY
*SECHENOV PHYSIOLOGICAL JOURNAL OF THE U.S.S.R.
*BULLETIN OF THE ACADEMY OF SCIENCES OF THE U.S.S.R.: GEOPHYSICS SERIES
*RADIO ENGINEERING
*RADIO ENGINEERING AND ELECTRONICS
*TELECOMMUNICATIONS
*PHYSICS OF METALS AND METALLOGRAPHY
*THE ABSTRACTS JOURNAL OF METALLURGY
*APPLIED MATHEMATICS AND MECHANICS
CHEMICAL ENGINEERING SCIENCE
JOURNAL OF ATMOSPHERIC AND TERRESTRIAL PHYSICS
PLANETARY AND SPACE PHYSICS
GEOCHIMICA ET COSMOCHIMICA ACTA
BULLETIN GÉODÉSIQUE
ANNALS OF THE INTERNATIONAL GEOPHYSICAL YEAR
SPECTROCHIMICA ACTA
JOURNAL OF THE MECHANICS AND PHYSICS OF SOLIDS
ACTA METALLURGICA (*for the Board of Governors of Acta Metallurgica*)
INTERNATIONAL JOURNAL OF THE PHYSICS AND CHEMISTRY OF SOLIDS
DEEP-SEA RESEARCH
JOURNAL OF NEUROCHEMISTRY
JOURNAL OF PSYCHOSOMATIC RESEARCH
JOURNAL OF INSECT PHYSIOLOGY
JOURNAL OF AIR POLLUTION
INTERNATIONAL ABSTRACTS OF BIOLOGICAL SCIENCES (*for Biological and Medical Abstracts Ltd.*)
RHEOLOGY ABSTRACTS
VACUUM
OPERATIONAL RESEARCH QUARTERLY
ANNALS OF OCCUPATIONAL HYGIENE

*Translations of the Russian journals published on behalf of the Pergamon Institute, a non-profit-making foundation.

Leaflets giving further details and subscription rates of each of these journals are available on request.

ELECTRIC TECHNOLOGY, U.S.S.R.

1958 VOLUMES 2 and 3 NOVEMBER

CONTENTS

[This issue completes the papers selected from *Elektrichestvo*, 1957]

Made and printed in Great Britain by The Campfield Press, St. Albans